6-28-2019

Protection of Active Distribution Networks and Their Cyber Physical Infrastructure

Hany Fawzy Kamel Habib
hhabi003@fiu.edu

FLORIDA INTERNATIONAL UNIVERSITY

Miami, Florida

PROTECTION OF ACTIVE DISTRIBUTION NETWORKS AND THEIR CYBER PHYSICAL INFRASTRUCTURE

A dissertation submitted in partial fulfillment of

the requirements for the degree of

DOCTOR OF PHILOSOPHY

in

ELECTRICAL AND COMPUTER ENGINEERING

by

Hany Fawzy Habib

2019

To: Dean John Volakis
College of Engineering and Computing

This dissertation, written by Hany Fawzy Habib, and entitled Protection of Active Distribution Networks and Their Cyber Physical Infrastructure, having been approved in respect to style and intellectual content, is referred to you for judgment.

We have read this dissertation and recommend that it be approved.

_____
Kemal Akkaya

_____
Mohammed Hadi

_____
Sakhrat Khizrorv

_____
Mark J. Roberts

_____
Osama Mohammed, Major Professor

Date of Defense: June 28, 2019

The dissertation of Hany Fawzy Habib is approved.

_____
Dean John Volakis
College of Engineering and Computing

_____
Andrés G. Gil
Vice President for Research and Economic Development
and Dean of the university Graduate School

Florida International University, 2019

DEDICATION

This dissertation is dedicated to the soul of my father, my mother, my family. Without their support, encouragement, and most importantly their everlasting love, the completion of this work would never have been possible.

ACKNOWLEDGMENTS

I would like to express my sincere gratitude to my principal advisor, Professor Osama Mohammed, for his guidance, support, encouragement, and thought-provoking discussions during my doctoral research. This dissertation would not have been possible without his help, support, resolute dedication, and patience. His passion for success has inspired me to come up with new ideas. His expert advice and unsurpassed knowledge of the various fields of electrical energy systems has always provided me an endless supply of idea to move to the next step and complete this dissertation. I am also grateful for the chance he gave me to work under his supervision at his excellent research group at the Energy Systems Research Laboratory. In addition, this atmosphere enabled me to develop professionally in an environment where research work and engineering ethics are highly respected.

I highly acknowledge the support I received as a research assistant under my major professor research grants received from the Office of Naval Research and the US Department of Energy throughout my research at the energy systems research laboratory. I thank the university graduate school for awarding me the Dissertation Year Fellowship (DYF) which significantly helped me complete this dissertation.

I would like to also thank my dissertation committee members for their insightful comments and constructive suggestions in the review of my dissertation.

Also, I am thankful to all my colleagues at the Energy Systems Research Laboratory. Many graduate and undergraduate student scholars have helped me with discussions, contributions, and assistance contributing to achieving my research goals.

Finally, I would like to give a special thanks to my mother and father for their unconditional support and love. I also extend my gratitude to for their encouragement and assistance.

ABSTRACT OF THE DISSERTATION

PROTECTION OF ACTIVE DISTRIBUTION NETWORKS AND THEIR CYBER PHYSICAL INFRASTRUCTURE

by

Hany Fawzy Habib

Florida International University, 2019

Miami, Florida

Professor Osama Mohammed, Major Professor

The Smart Grid constitutes several smaller interconnected microgrids. The integration of converter-interfaced distributed generation (DG) in microgrids has raised several issues including the fact that fault currents in these systems in the islanded mode are much less, than in grid-connected systems. Therefore, microgrid protection schemes require a fast, reliable and robust communication system, with backup, to automatically adjust relay settings for the appropriate current levels according to the microgrid's operation mode. The risk of communication link failures, cyber security threats and the high cost involved to avoid them are major challenges for the implementation of an economic adaptive protection scheme. This dissertation develops an adaptive protection scheme for AC microgrids, which is capable of surviving communication failures. The idea is the use of an energy storage system as the main contributor to fault currents in the microgrid's islanded mode when the communication link fails to detect the shift to the islanded mode. The design of an autonomous control algorithm for the energy storage's AC/DC converter capable of operating when the microgrid is in both grid-connected and islanded mode.

Utilizing a single mode of operation for the converter will eliminate the reliance on communicated control command signals to shift the controller between different modes. Also, the ability of the overall system to keep stable voltage and frequency levels during extreme cases such as the occurrence of a fault during a peak pulse load period. The results of the developed protection scheme showed that the energy storage -inverter system is able to contribute enough fault current for a sufficient duration to cause the system protection devices to clear the fault in the event of communication loss. The developed method was investigated under different fault types and showed excellent results of the developed protection scheme. In addition, it was demonstrated in a case study that, whenever possible, the temporary disconnection of the pulse load during the fault period will allow the utilization of smaller energy storage device capacity to feed fault currents and thus reduce the overall expenditures.

Furthermore, in this dissertation we utilized a hybrid framework to verify our protection algorithm. We simulated the microgrid on MATLAB/Simulink SimPowerSystems to model the physical system dynamics, whereas all control logic was implemented on embedded microcontrollers communicating over a real network. This work suggested a protection methodology utilizing contemporary communication technologies between multi-agents to protect the microgrid.

.

TABLE OF CONTENTS

CHAPTER PAGE

LIST OF TABLES

LIST OF FIGURES

FIGURE PAGE

LIST OF ACRONYMS

DER	Distributed Energy Resource
DG	Distributed Generation
ESDs	Energy Storage Devices
SMV	Sampled Measured Values
GOOSE	Generic Object Oriented Substation Event
IED	Intelligent Electronic Device
PCC	Point of Common Coupling
ES	Energy Storage
HESS	Hybrid Energy Storage Solutions
OC	Over Current
CBs	Circuit Breakers
FRT	Fault Ride Through
FCL	Fault Current Limiter
DOCR	Directional Overcurrent Relays
PLC	Power Line Currier
LA	Lead Acid
LI	Lithium Ion
EVs	Electric Vehicles
UPS	Uninterruptible Power Supplies
FW	Flywheel
SC	Supercapacitor

PMU	Phasor Measurement Unit
MAS	Multi-Agent System
DDS	Data Distribution Service
MCU	Main Control Center
BMS	Battery Management System
PDC	Phasor Data Concentrator
IRIG-B	Inter-Range Instrumentation Group
DoS	Denial of Service
LAN	Local Area Network
ARP	Address Resolution Protocol
CAM	Content Addressable Memory
PSO	Particle Swarm Optimization
LB	Lower Bounds
UB	Upper Bounds
OMG	Object Management Group
ACL	Agent Communication Language
SGIP	Smart Grid Interoperability Panel
Open FMB	Open Field Message Bus
RTPS	Real Time Publisher-Subscriber
QoS	Quality of Service
RTI	Real Time Innovation
MPPT	Maximum Power Point Tracking
SBC	Single Board Computers

MCPU	Microgrid Central Protection Unit
FLISR	Fault Location, Isolation and Service Restoration
JADE	Java Agent Development Framework
OPC UA	Open Connectivity Unified Architecture
FIPA	Foundation of Intelligent Physical Agents
AVR	Automatic Voltage Regulation
TD	Time Dial
CTI	Coordination Time Interval
MA	Main Agent
SCA	Supercapacitor Agent
DERA	Distributed Energy Resource Agent
GA	Generator Agent
UA	Utility Agent
TL	Transmission Line
PI	Proportional Integral
PLL	Phase Locked Loop
R	Relay
API	Application Programming Interface
IDL	Interface Definition Language
MCU	Main Control Center

Chapter 1 Introduction and Literature Review

1.1 Introduction

Distributed energy resources connected to a microgrid and their integration with the main grid are the targets in achieving optimum operation of electric power system networks [1]. Reducing greenhouse gases generated by conventional energy resources while increasing the reliability and power quality for consumers who require uninterruptible power supplies are some of its main advantages [2], [3]. However, along with these benefits, microgrids introduce some major technical challenges in terms of protection schemes. Microgrids are dynamic entities where Distributed Generators (DG), loads, and Energy Storage Devices (ESDs) are constantly connected and disconnected [4], [5]. Operating conditions vary rapidly, since the inertia of the system is much less than that of conventional networks. Weather conditions, resource availability and consumption affect the operating conditions of the equipment. In order to ensure safe operation, all elements must be monitored and necessary changes must be made to their settings as the operating conditions of the microgrid change. Since conventional protection schemes that rely on large inertia and long transient periods are insufficient, new schemes are necessary [6].

Communication with relays is necessary in order to update operating currents of the relays and detect the direction of fault currents to properly isolate the faults. DGs, on the other hand, are monitored to follow their status and include or disregard their fault contribution if they are on or off [7], [8]. It is therefore evident that incorporation of communication technologies into microgrids has become inevitable to provide contemporary adaptive protection schemes.

However, the complex interdependencies between the cyber and physical components of such systems increase the difficulty of devising control algorithms for them. The challenge is in the fact that in a closely interconnected cyber-physical system, such as in a microgrid with adaptive protection, minor malfunctions in the cyber domain can have catastrophic impacts in the physical domain [9].

In order to address this, extensive efforts have been placed to devise data communication standards for power transmission. Acknowledging their criticality in power transmission, communication requirements for protection algorithms are viewed in extensive detail in the IEC 61850 international standard. The IEC 61850 standard was developed by the IEC Technical Committee Number 57 Working Group 10 and IEEE for Ethernet (IEEE 802.3)-based communication in electrical substations and is currently being extended for use tele protection (IEC 61850-90-1) [10]. IEC 61850 is also mentioned in recent literature for microgrid applications [11]. The IEC 61850 poses stringent restrictions on messages that communicate fault-related signals, such as the 4 ms time limitation imposed on SMV and GOOSE messages. Consequently, designing control algorithms for a protection system is a delicate and complex procedure.

This complexity is further leveraged when dealing with an adaptive protection algorithm design in which the collaboration between multiple agents, namely Intelligent Electronic Devices (IEDs), for detecting and isolating faults is time-critical. Clearly, the robustness and availability of the communication infrastructure is an important prerequisite for the success of contemporary adaptive protection algorithms [12]. Therefore, communication failures in such applications is a high priced risk with serious consequences.

The goal of a resilient adaptive protection algorithm is to ride through communication failures without causing serious damage to hardware assets, financial reparations, or productivity costs. Considering the above factors, in this work, an adaptive protection scheme for AC microgrids, which is capable of surviving communication failures by the aid of Energy Storage Devices (ESDs), was developed as shown in Figure 1.1.

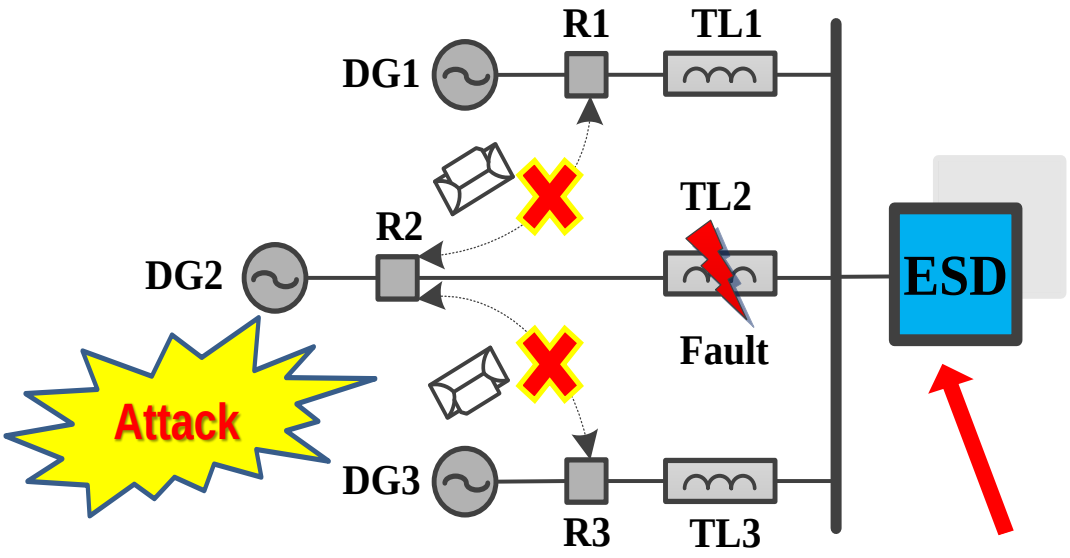

Figure 1.1 The configuration of microgrid during islanded mode of operation.

1.2 Main Protection Challenges in Microgrids

There are several challenges that should be taken into consideration in designing a proper protection scheme for a microgrid. The following subsections discuss some of the major issues one may face in the proper operation of a microgrid protection scheme.

1.2.1 Selectivity and Sensitivity Issues

Two main characteristics that should be found in microgrid system protection devices are selectivity and sensitivity features. First, selectivity refers to the ability of the protection system to locate and classify a fault correctly. Over Current (OC) relays should determine

whether the fault is internal or external to its zone. The protection algorithm should be able to distinguish between the main grid and local microgrid faults [14]. During main grid faults, the microgrid needs to be capable of islanding to protect equipment in the system [15], [16]. During microgrid faults, the function of the protection scheme becomes more complicated as it is required to disconnect the smallest part of the faulty section from the system [17], [18]. It should be noted that the importance of the selectivity feature of the relays is to operate under various faults while isolating the faulty part.

Secondly, sensitivity refers to the fact that OC relays should be able to detect the fault conditions in the system. The fault should be cleared as quickly as possible to maximize safety while minimizing system instability and damage to equipment [19]. The OC relay should quickly arrive at a decision and CBs must function rapidly [20]. The sensitivity of the relays must be adjusted such that a high redundancy can be achieved without affecting selectivity of the protection system [21]-[23].

1.2.2 The Direction of Power Flow

Distribution systems become active systems due to the integration of DERs in the system [24]. The microgrid feeds local loads and can also support power to the grid in the case of excess generation. This operation changes the flow of the power from unidirectional to bidirectional. Bi-directional power flow has effects on the amplitude and direction of the fault current thereby affecting coordination of the protective relays [25], [26]. In this case, the protection system in a typical distribution system is designed according to a time or current coordination principle, in which the relay closest to the fault operates first and in the event of a failure, a backup protective relay operates after a delay time.

However, the effectiveness of this protection requires a radial grid connection, which is no longer the case when DGs are connected to the network. This results in either changing or completely losing coordination between protective devices [27], [28]. The different adverse effects of DG connections on the distribution network protection include false tripping of feeders, blinding of protection, increase or decrease in the fault level with the connection or interruption of DERs affecting the reach of the OC relay settings [29], [30].

1.2.3 Dynamic Changes in the Microgrid Architecture

Dynamic changes of the microgrid configuration should be taken into consideration when designing the protection scheme. Some changes include the disconnection of generation units, shutting down some loads during peak hours, or exporting of power to the main grid during excess generation periods for optimum and economic operations [24]. Adaptive protection is required to change the relay settings according to the current microgrid configuration. Prior knowledge of every state in the microgrid as well as online monitoring and calculation of the short circuit fault current is needed for proper operation. As previously discussed, this requires the application of a fast, reliable, and robust communication system [31], [32].

1.2.4 Faults in Grid-Connected Mode.

For a fault on the main grid during normal operation, the response of the protection devices of individual DERs should not trip before the protection device at the Point of Common Coupling (PCC) trips, while DERs should continue operation during sensing and switching of the PCC device. To allow this, all DERs should have a Fault Ride Through (FRT) capability [33]. For a fault within the microgrid during normal operation, the

response of line and feeder protection must be to disconnect the faulty portion from the rest of the system as quickly as possible and how it is done depends on the features and complexity of the microgrid and the protection strategy used. There may be some non-fault cases resulting in low voltage at the PCC such as voltage unbalances and non-fault open phases that are difficult to detect and may potentially create hazards for sensitive loads, micro sources, etc. Therefore, some protection mechanisms are needed to avoid such situations [34].

1.2.5 Faults in Islanded Mode.

The high penetration of DERs based on power electronic inverters interfaced with the microgrid as shown in Figure 1.2 has a great impact on the protection scheme. These systems limit the short circuit current during islanded mode of operation, as they are equipped with a Fault Current Limiter (FCL) that prevents high OC levels to flow during the fault period [25], [35], [36]. A significant difference exists in the amount of short circuit current that occurs when in grid connected and islanded modes of operation. In grid connected, fault currents of a much higher magnitude (5-10 times the full load current) are available to help conventional OC relays to activate under abnormal operations. However, in islanded mode, the fault current reduces to only about 3 times the full load current [17]. Furthermore, a large integration of connected converter-based DERs further reduces the fault current to only 1.2-1.5 times the full load current [37], [38]. Usually, conventional OC relays are set to operate at 1.2-8 times full load current. Accordingly, the time-current coordination of OC relays and OC devices with extremely inverse characteristics are disturbed.

1.3 Existing Techniques for Protection of Microgrids

One can conclude from the previous section that protection of a microgrid is complex and desires a reliable, smart technique to reduce impacts from the previous problems that mentioned in section 1.2. Adaptive protection, with the aid of a communication link, can offer a solution for a protection scheme in the microgrid to handle its multiple modes of operation.

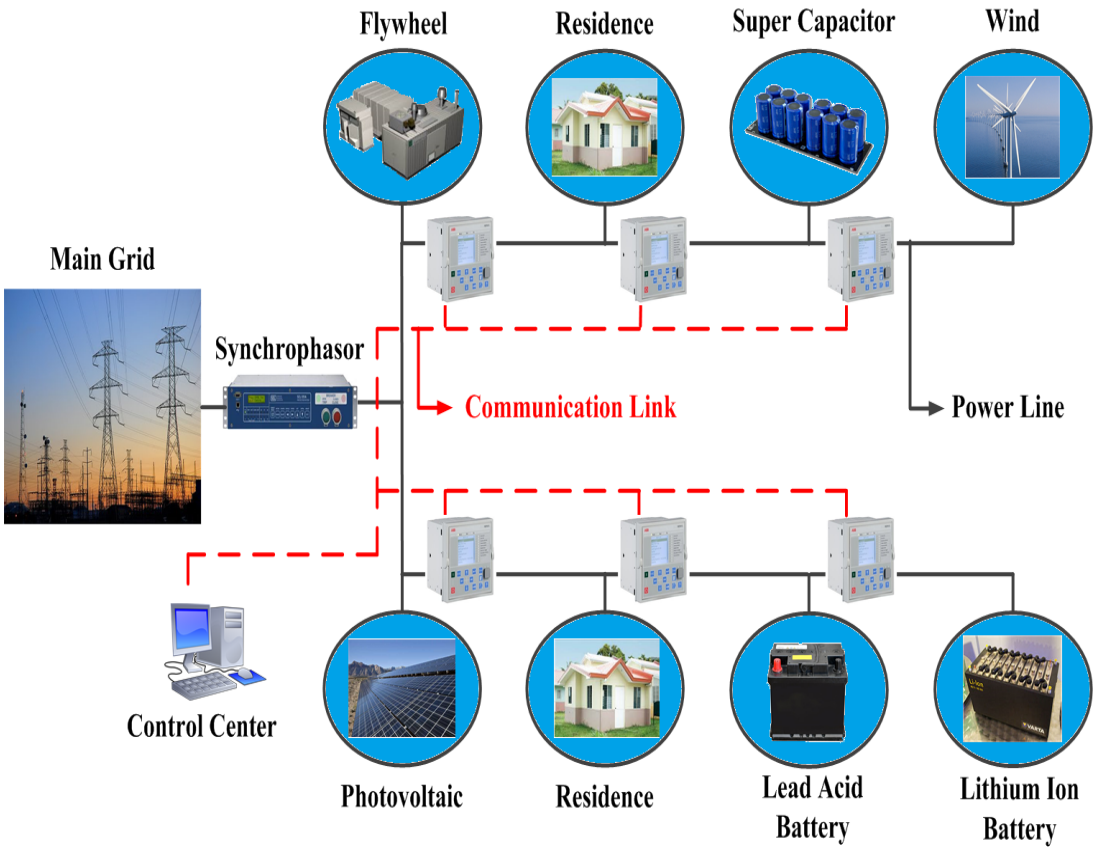

Figure 1.2 The configuration of a typical microgrid.

Adaptive protection refers to an online process which modifies the preferred protective responses and correlates them to a change in system conditions or requirements in a timely manner through control or signaling [13]. Adaptive protection consists of a smart control unit that monitors the grid parameters including a smart fault diagnostic system to detect

the fault, the fault type, identify the faulted zone, and a smart relaying system which protects the system against faults. Adaptive protection of the microgrid can be realized with the use of microprocessor-based Directional Overcurrent Relays (DOCR). DOCR have the possibility to choose different tripping curves to suit a particular system. An adaptive protection scheme can be implemented with centralized or decentralized control approaches, but each requires a different communication architecture [39].

The centralized control architecture communicates with each IED and adjusts their settings accordance with the configuration of the present microgrid as shown in Figure 1.2. Centralized communication architecture is supported by various communication protocols including Modbus, DNP3, IEC 60870-5-101/104, IEC 61850 and can be implemented with a serial/bus communication over a PLC or via an Ethernet network [40].

The decentralized control architecture depends on sending and receiving data between IEDs. Each IED can change its settings according to the data that it receives from other IEDs. Presently, the industry is focused on the IEC 61850 standard as the protocol for decentralized communication [41], [42]. The microgrid protection scheme requires an adaptive, smart, and upgradable protection algorithm. A survey of existing key adaptive protection schemes are presented in this section.

In [21], a novel adaptive protection technique is developed using extensive communication and digital relays. Settings of the relays are changed according to the microgrid configuration. The technique is further extended by using numerical directional relays with a directional interlock capability for selective operation. Additional adaptive protection schemes were introduced in [43], [44] with advanced communication technologies for updating the relay settings in accordance with the microgrid configuration.

The authors developed a central protection unit to be equipped with the microgrid to change the tripping characteristics of the relays with every interruption call for the connection and disconnection of DGs. The author in [22] studied the fault current of an inverter-based microgrid and developed an adaptive protection algorithm for the fault current. This technique depended on comparing the impedance of the grid and microgrid using the voltage and current fault components in a real time manner. In this way, the relay updated its settings by observing the changing impedance of the utility and microgrid. Reference [34] suggested a system with a high penetration of DGs that loosened the coordination of the protective relays due to bidirectional power flow in the system. A centralized control center communicated online with modern CBs in the system to send a trip signal under the fault condition. Fault contribution from the sources was obtained online through a Thevenin equivalent impedance. Under abnormal conditions, a change in the Thevenin impedance of the adjoining fault bus source was detected. Thus, the relay determined the fault and tripped the appropriate CBs. In [45], the authors used numerical relays to detect the fault current under grid connected and islanded modes. Different trip characteristics settings were calculated in both modes and saved in the relays.

When the microgrid switched into islanded mode, the relay automatically changed a group of settings that matched this mode.

Previously in [9], a supercapacitor with a DC-DC converter was added to each DER with the same rated power that would add to the cost of the protection system, especially given supercapacitors were not originally used during normal operation. In [28], a technique is presented to protect the microgrid based on a voltage measurement of the fault detection

modules, but it may not be accurate to determine the faulty part of the system and may also require time.

This would have direct impacts on selective protection of the microgrid. Authors in [46] introduces communication failures as a critical issue which is now being widely presented in literature.

The operation of the relay depends on the voltage drop during the fault that may require many loads to disconnect from the system. Finally, in [47] different techniques that could be used to protect the microgrid are reviewed. In [47], a direction relation to our work is identified as it highlights the importance of communication in protection schemes which cannot be carried out in a cyber-attack and identifies the need for a solution to solve the problems of communication failures.

1.4 Energy Storage as a Contingency

The previous section revealed the need for the communication networks to implement a suitable protection scheme for the microgrid. However, the communication outage as it will be discussed in chapter 3 may be effect on the operation of the protective devices. The loss of adequate communication to a relay can be catastrophic to a microgrid protection scheme, where the most difficult aspect is handling a dramatically increased fault current magnitude when moving from grid to islanded mode.

In the event of a cyber-physical attack or loss of communication, a protection scheme would be paralyzed, where relays would no longer be capable in adjusting OC limits.

Assuming a cyber-physical attack or communication loss has taken place, relays will now require 5-10 times the full load current to trip in islanded mode. In this case, ESDs

already present in the system for other purposes could now also be tasked in assisting to increase the fault current magnitude.

First, four types of common grid ESDs are reviewed, compared, and discussed for their suitability to inject the required fault current as well as the concept of a HESS.

Next, a summary of grid applications and capabilities that installed ESDs can serve on the network is presented. Finally, some potential single ES and HESS solutions are developed to aid in supplying the fault current as well as considerations and trade-offs in deploying them in the system.

In this case, it is assumed that the microgrid under study already has one or multiple ES devices connected to the network due to their strength in filling one of the previous applications, hence no cost is intended to be added to the system.

Their participation in supporting the required fault current would be classified as another capability

Table 1.1 Comparison of Four Prominent Energy Storage Resources

Energy Storage Type	**Energy Density (Wh/L)**	**Power Density (W/kg)**	**Energy Cost ($/kWh)**	**Response Time**	**Self Discharge Rate**	**Lifespan**	
						Max. Cycles	**Service (years)**
Lead Acid Battery	85	180	8.50	Slow	3-20%/mo	1,500	3-12
Lithium Ion Battery	463	295	250.00	Medium	6-8%/mo	4,200	5-20
Supercapacitor	10	3,500	1,000.00	Very Fast	1-2%/day	1,000,000	10-35
Flywheel	8	5,000	500.00	Fast	3-40%/hr	10,000,000	20-35

1.4.1 Common Grid Energy Storage Types

The following subsections will review the operation of four common grid ES types' devices: LA batteries, LI batteries, Supercapacitors, and Flywheel ES. Table 1.1 depicts a comparison of each ES type as well as the categories considered, while Figure 1.3 provides a 6-point performance snapshot for each. The operation of each type, their strengths and weaknesses, and examples of previous grid applications are discussed.

1) Lead Acid Batteries

The LA battery has maintained a strong hold in the market as a result of its simplicity in design and inexpensive materials [48]. Despite the fact that emerging EVs have moved onto LI types, the LA market remains strong as it is still the most common starter battery and battery in UPS [49]. Furthermore, some of the drawbacks in deploying them in EVs are relieved when placing them in a stationary grid application. While real estate may still remain a premium, concerns with weight can be alleviated. The LA battery has been demonstrated as a dependable resource in stationary grid applications to smoothen the energy harvested by renewables, but has been more universally accepted in restoring system frequency and voltage following an outage [50]-[52]. This is covered in more detail later. Despite its strengths in reliability and low cost, LA has a relatively low energy and power density and suffers from a number of drawbacks. LA are not ideal in sourcing high frequency pulsed loads as a result of their large double layer capacitance, a weakness which would also reduce their suitability to solely supply a fault current [53].

Pulsed loads are defined as a load that requires a high instantaneous power demand for a relatively short period of time and are discussed in detail in the following section.

Its operation utilizes a sulfuric acid electrolyte as a fuel primarily governed by changes in the concentration, an inefficient process that leads to a number of lifespan concerns. First, their operational current is severely limited, as an increase from a conservative 20-hour discharge rate (C/20) would result in reduced usable capacity and increased ageing. Ergo, in order to fill a fault current, the size of the LA array should be sufficiently large to limit the peak array current. Finally, their shelf and cycle life are highly limited.

2) Lithium Ion Batteries

LI battery usage has surged in recent years not only in portable electronics, but also in large scale EVs and even grid storage [54]. Advanced LI battery management systems have been demonstrated in microgrid applications for both islanded and grid-connected modes to provide voltage and frequency support [55], [56].

Since LI battery management is more complex than that of LA, studies have looked at the best method to control these schemes [57], [58].

LI operation is significantly different from that of LA, where energy is stored inside its electrodes utilizing the electrolyte as simply a transfer layer [59]. This combined with a smaller cell construction allow them to respond faster to a pulsed load that in turn, would also make them suitable in feeding a fault current [60].

LI batteries offer a significant improvement in their capability to source high current without the same trade-offs in lifespan as seen with the LA battery.

Their lifespans are much longer, but similar to the LA battery, are still limited by excessive operational currents and particularly temperature [61]. Battery management system cost for LI batteries is increased as a result of required crucial cell balancing and thermal control for safety.

Finally, a number of companies have been working to reduce the cost of grid-scale LI battery arrays, as their cost is still at a premium as compared to LA.

3) Supercapacitors

The SC provides a significant increase in the speed of response versus any electrochemical battery. Although their construction is chemical in nature, no reaction takes place. This enables them to respond extremely fast to a demand, while even under heavy current, their lifetime is virtually unaffected [62]. Composed of two porous electrodes divided by a separator soaked in a solvent electrolyte, their construction enables a much higher charge density versus the traditional capacitor as a result of an increased surface area [63]. Their usage has been studied in mobile shipboard applications where weight is a concern, but also in some grid applications with multiple renewable energy resources where they provide short term storage to supply the deficiency power [64], [65]. Unfortunately, their low energy density can require an enormous capacitance, which may not prove to be practical as a sole ES device.

Although their response time in feeding the required power would be superb, sourcing the total energy to fill a fault current would come at a massive cost [66]. Its energy density is only around 10% of that of the LA battery and 2% of a LI battery while their self-discharge rate is relatively high.

4) Flywheel Energy Storage

Like the LA battery, FW ES has been synonymous with industrial UPS systems, but for a very different purpose. FW ES provides some of the highest power density in our study and are primarily purposed to support to pulsed loads which would initially make them

appear to be a great candidate to inject a fault current [67]. Analogous to an electromechanical battery, the FW stores kinetic energy in a high inertia rotating mass, where an electric machine operates simultaneously as a motor during charging and generator during discharging. The power output is a function of a square of the speed, allowing them to provide extremely high power density. This has made them an excellent solution for maintaining power quality [68], [69]. They have also been tested for their usage in both wind and solar applications as a mechanism to quickly store and expend energy [70]. FW also carry a unique capability unlike other ES: the ability to supply inertia to the system [71]. Unfortunately, the FW has a very high self-discharge rate as a result of friction losses and like the SC, have a very low energy density [72]. Although their cost is half that of the SC, their response time is still very fast, limited only by the initial inertia required to start moving the rotating mass. However, their energy density is very low, some 20% below the SC, which would further reduce their capability in solely injecting the fault current.

5) Hybrid Energy Storage Systems

Although some ES devices, such as the LI or LA battery, can provide a rather balanced contribution of energy versus power density, cost and lifetime aspects could jeopardize their sole integration with the grid. Similarly, the integration of a SC or FW alone could provide excellent voltage and frequency support for a small outage, but would fail to fill energy demands over longer periods without a huge array. For this reason, HESS could provide a more balanced solution in terms of not only power and energy density, but also cost, lifespan, and self-discharge. HESS have emerged in an effort to utilize the strengths of multiple ES devices in a way that is not only more efficient, but potentially cost and lifetime effective.

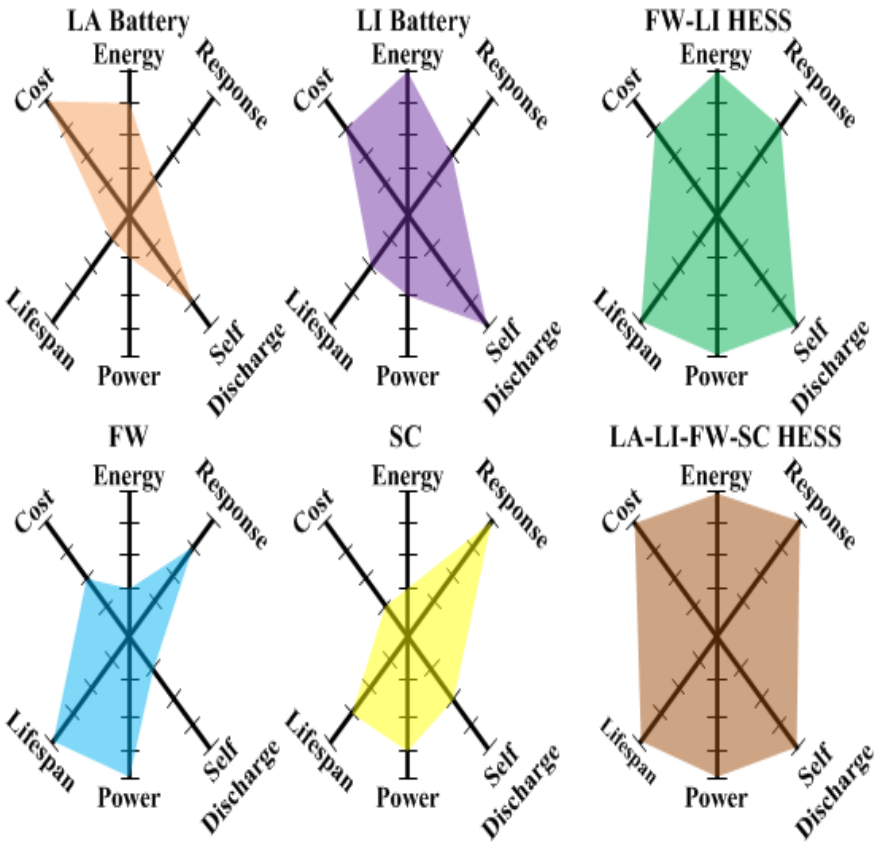

Figure 1.3. Energy Storage and Hybrid Energy Storage Performance Snapshot [32]

Recent HESS for microgrid applications have focused on the collaboration of batteries with SCs, evaluating their combination with both LA and LI [73], [74]. Minimizing losses while ensuring an optimum power split between the two sources has spawned research in this topic [75]. A great deal of work has focused specifically on pulsed load management through the deployment of HESS systems [76], [77].

Unfortunately, reaching the required level of power and filling the energy demand over such a short period of time can be challenging. Examples can be found in a number of Naval platforms, the starter current for a vehicle, and the case addressed in this paper: a fault current.

1.4.2 Grid Applications for Energy Storage Devices.

ESDs can be utilized for a variety of major applications on the utility grid. In this section, these purposes are categorized into network applications, supplying critical loads, and feeding pulsed loads.

The importance level of these storage devices to improve the performance of these different applications are shown in Figure 1.4. According to different characteristics including but not limited to power density, energy density, cycle life, cost and self-discharge, an optimal selection of ESDs can be identified to increase the efficiency for each application .

Figure 1.4 (a) shows the main requirements of the ESDs for network services and the overall importance of each requirement. As can be seen, since there are less space and weight limitations for an ESD plant, a low cost per unit power and energy plays a more important role for the selection of the storage technology.

Having a long lifespan and life cycle as well as high efficiency are other important factors that need to be considered. Thus, based on the characteristics of the storage technologies discussed before and presented in Table 1.1, the FW and SC can be more optimally used for the high-power grid services. Moreover, the capability of this technology to provide very high-power makes them distinctive for power grid applications. In the case of the LI battery, although it has a relatively low cost per unit energy and long discharge capability, its high cost per unit power is its main limitation for high-power grid services.

1. Network Applications

Utility grid network applications are commonly broken into three categories: frequency regulation, voltage control, and voltage ride-through.

A) Frequency Regulation: As a result of their faster response time versus DGs, ESDs are considered a suitable technique to improve frequency regulation in the system. Reference [78], shows commercial uses of ESDs to sustain frequency regulation on the grid. Some other studies were performed, with a particular focus on the FW in conjunction with the assistance of power monitoring software, to demonstrate its effectiveness [79]-[81]. In addition, some research has demonstrated that most batteries and SCs are suitable for frequency control applications as well [82]-[87].

B) Voltage Control: ESDs can be utilized to maintain the voltage level of the transmission system within an acceptable range [88]-[93]. Bidirectional converters are connected with ESDs to inject or reject reactive power for voltage stability purpose. Batteries beside other ESDs technologies are a suitable alternative, as they can respond instantaneously to changes in the voltage [94], [95].

C) Voltage Ride Through: The voltage level decreases during major faults in the AC grid at the PCC between the plant and the grid [96]. Thus, the power that can be transferred from the DC to the AC side is reduced. As a result, trapped energy on the DC side can cause severe overvoltage on the converter. ESDs, such as the FW and SC, can be used to maintain the voltage level at the DC-link and ride through the fault by injecting reactive power to grid [97]-[103].

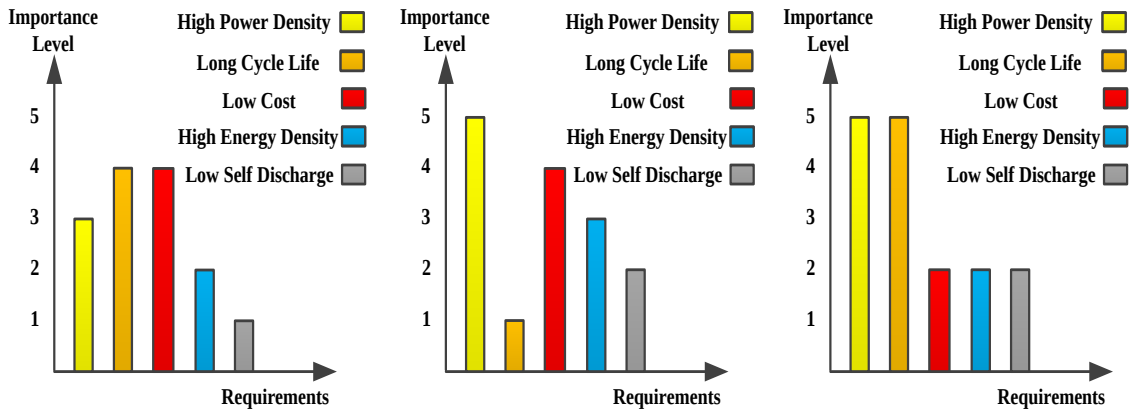

(a) Network Applications (b) Critical load (c) Pulsed load

Figure 1.4 Importance Level (changing from level (1) less important to level (5) very important) of the energy storage characteristics for various applications

2. Critical Loads

Short-duration ESDs can be utilized to provide a bridge to startup and synchronize standby generators. The main requirements of ESDs for critical loads with a short-time failure are depicted in Figure 1.4 (b). The overall importance of the storage requirements and the characteristics of FW ES showed that they can be effectively used for an immediate power availability to a critical load during a power disturbance, such as power outage dips, or surges in the voltage and/or current.

Compared to batteries, FW are excellent to deliver short-time, high-power to UPS, offering a lower cost per unit power with lower operating cost due to lower maintenance and replacement costs. Also, the SC has a high-power density and low cost per unit power. As a result, it is well-suited for a system that suffers from short-time failures. Typical SC UPS sizes can range from mill watts to tens of kilowatts with modular solution systems. In addition to being very compact, SC UPS also offers very low maintenance and standby power costs [104]-[107].

3. Pulsed Loads

Figure 1.4(c) shows the requirements of ESDs for pulsed load applications and the overall importance of each requirement. The high instantaneous power demand of a pulsed load can produce power disturbances and thermal issues in the system [108], [109]. Using a SC or FW as a power density storage device with a low cost per unit power would improve the performance of the system.

In this case, the system will have several advantages, including less weight and volume as well as mitigation of thermal issues, frequency disturbances, and voltage variations [110].

1.4.3 Potential Solutions to Source the Fault Current

As previously discussed, each ES device has its own respective strengths and weaknesses and few would be suitable to solely source a fault current. A general example of a fault current is shown in Figure 1.5, where a high in-rush current is needed for approximately 80 ms to reach 5 to 10 times the base load current (Ipu).

A multitude of solutions could assist in injecting the required fault current, however, they are limited by both the available infrastructure as well as the proximity of each ES device from the CB. A multitude of solutions can assist in injecting the required fault current, however, are limited by the available infrastructure.

For this reason, in this section 3 scenarios are presented representing microgrids with the capability to select: 1) a single ES element, 2) a HESS with 2 devices, or 3) the availability of all sources in Table 1.1.

1) Single Source Solutions

For a microgrid with only one type of ES, tasking it to assist in feeding the fault is more complicated. First, a system which only contains a LA or LI would be limited to their lifespans. In addition, these batteries are limited by excessive operational currents and particularly temperature. The two most suitable devices, if adequately sized, are the SC and FW, as they provide the greatest balance which can be visualized in Figure 1.5. The FW ES provides the highest power density in our study and are used to feed the pulsed loads, but has a very high self-discharge rate as a result of friction losses and low energy density. The response time is very fast, limited only by the initial inertia required to start moving the rotating mass.

The SC has the best response time of the ES types and their construction is chemical in nature, no reaction takes place. This helps to respond extremely fast to a demand heavy current [111].

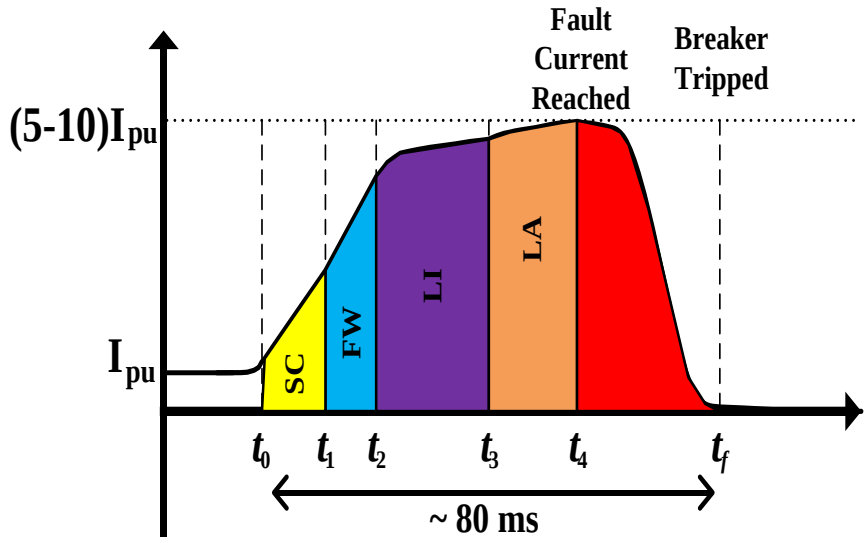

Figure 1.5 Controlled Hybrid Energy Storage to Feed the Fault [60]

2) Multiple Source Solutions

With the inclusion of a secondary ES source, a basic HESS can be designed. In this case, a combination of an ES type with high energy density and battery ES can help to provide a more balanced system. This leaves the selection of either the SC or FW and a battery. The FW features the highest power density in our study while at the same time, the lowest energy density.

As a result of this deficit, the LI battery would find itself most suitable for a FW HESS combination. Though the cost would be exceedingly higher for the LI array, the cost of the FW is half of that of the SC providing a strong balance for the FW-LI HESS. Its performance distribution is depicted in Figure 1.5, revealing only weaknesses in terms of cost and response time.

3) Availability of all Energy Storage Devices

In the event that all resources in Table 1.1 are available on the network, a combination of the strengths from all ES devices could be used to feed the fault current in a dynamically switched SC-FW-LI-LA HESS. Figure 1.5 breaks down the initial concept, which involves contribution from each ES to the surge pulse broken into four switching steps. An ES type is first connected at the start of the fault (t_0), where each of the remaining three devices are sequentially added in parallel until the final required fault current level has been reached at t_4, tripping the breaker (t_f).

The developed sequence begins with the deployment of the SC at t_0 as it responds quickest to the demand initially injecting high power until reaching t_1, where the FW assists in increasing the power even faster to get within the range of the fault current level, while concurrently contributing inertia to the system.

Since the SC and FW have a low susceptibility to lifespan issues, the selection of t_1 would primarily rely upon the availability of each to provide the energy to reach t_2. Since the energy stored in both is relatively small, the LI battery would be added at t_2 to assist in maintaining the energy required to fill the pulse. Since the LI battery provides a good balance of both power and energy, it can assist in feeding the required energy, while simultaneously increasing the power until the LA battery is added at t_4 to reach the fault current level. A trade-off can once again be made between the availability of LA and LI capacities, but now involving lifespan as well. The cost of a LI array may force the operator to require more support from LA, shifting the location of t_3. However, the severe consequences in overusing LA should be considered, as their lifespans would take the highest toll.

1.5 Problem Statement

The future power network will feature many microgrids especially at the electric distribution level, and deliver clean renewable energy close to the end user [120]. Along with these benefits, microgrids introduce many challenges for power system operations and protection strategies. Legacy protection schemes designed for passive distribution networks are not suitable for use in microgrids [112].

This is because, besides feeding local load, a microgrid is also expected to export power to the main grid and other microgrids, thus requiring a bi-directional power flow. The bi-directional power flow affects the amplitude of the fault currents [113]. Also, the short circuit fault current capacity of the system may get affected by any change in the microgrid configuration either due to the integration or the interruption of DGs in the

existing grid. In grid connected mode, the main grid will provide enough high fault current to activate fault protection devices (typically 3-6 times normal rated current is required).

However, an islanded microgrid is dominated by power electronic interfaces and these inverters will have a maximum current rating of perhaps 1.5-2 times normal rated current [114]. At the very least, a system that is designed to protect a microgrid should take the following into account; (a) bidirectional power flow in feeders; (b) reduced fault levels in islanded operation [115]. In order to protect AC microgrids in both grid-connected and islanded modes of operation, an adaptive protection scheme is required [116].

A major issue related to the smooth operation of adaptive microgrid protection scheme in a smart grid scenario is the prior knowledge of every state of the grid and the online monitoring and calculation of the short circuit fault current level for every small change in the grid configuration.

This requires application of a communication system with a backup and fast data acquisition system between generators, the protective devices and loads etc., so that shifting between high and low relay settings can be done automatically. In [117]-[118], central protection approaches were developed to calculate the fault current of the distributed energy resources (DERs). This system can be used to monitor a microgrid over communication lines and react to dynamic changes of the system.

Authors in [119] calculate both the system's and the microgrid's impedances by measuring the voltage and current fault in a real-time manner, the protection device will send a trip signal to circuit breakers according to the value of impedance that changes simultaneously with the system topology. The authors in [120] change the time-current

characteristics for short circuit and overload conditions by observing the difference in voltage drops during these two events, respectively.

Most of the developed adaptive protection methods are completely dependent on exchange or transfer of data/information in the shape of measured system parameters and direction and interlocking signals between different protection devices via some kind of communication link [121]. The existing adaptive protection schemes are improved at different modes of operation with the help of the communication networks [122]. On the other hand, by using supercapacitor bank in the system when the communication is not available, the supercapacitor can inject current immediately and help the relay that should work to isolate the fault from the system without disconnecting large parts in the system. Standards addressing protection applications realize their criticality and thus pose stringent restrictions on messages that communicate fault-related signals such as the 4 ms time limitation imposed on Sampled Measurement Values (SMV) and Generic Object Oriented Substation Event (GOOSE) messages by IEC 61850. Therefore, designing control algorithms for a protection system is a delicate and complex procedure. This complexity is further leveraged when dealing with adaptive protection algorithm design in which the collaboration between multiple agents, namely Intelligent Electronic Devices (IEDs), for detecting and isolating faults is time-critical.

Here again, the robustness and availability of the communication infrastructure is an important prerequisite for the success of contemporary adaptive protection algorithms. Therefore, communication failure in such applications is a high priced risk with serious consequences.

Therefore, the goal of a resilient adaptive protection algorithm is to ride through communication failures without serious damage to hardware assets (transmission lines in this case), financial, or productivity costs. Considering the above factors, in this work, an adaptive protection scheme for AC microgrids, which is capable of surviving communication failures by the aid of energy storage systems, is developed. The microgrid under study comprises an AC side feeding various resistive loads with different ratings and a DC side having a supercapacitor supplying a pulse. The power flow between the two sides is achieved by using three-phase AC/DC voltage source converter (VSC). A fuel cell is also used as a DC source in the system studied to assist the AC generators in supplying their loads. The microgrid operates in a grid connected and in an islanded mode of operation and thus the developed protection scheme adjusts the protection relays' settings in order to detect and isolate faults in both modes of operation. That is, as long as the microgrid is connected to the main grid, the relays' settings are adjusted to their High Settings since the main grid will have the main contribution for the fault current in order for the relays to detect it.

However, in the islanded mode, there won't be enough resources to contribute to the fault current and thus the relays' settings must be reduced to the Lower Settings. The shift between the two settings comes from a command signal issued by the point of common coupling (PCC) to all relays according to the current mode of operation. In the event of communication failure during the islanded operation, relays' settings will not be adjusted to the lower setting and thus faults will not be detected. This above sections reviewed the various different challenges in microgrid protection schemes and the need for adaptive protection to deal with these problems. An analysis of various protection schemes, based

on an adaptive protection technique deployed with communication links between IEDs is presented. Different types of attacks that may impact the communication network are described and the need to solve the issue of the Denial of Service attack that was not covered by the literature works, This dissertation introduces a solution of this issue by discussing how various ES and HESS could be used as a secondary measure to assist the system in filling the required fault current in the event of a communication failure. The developed solution does not intend to incur additional costs to the system studied, as the ESDs are already utilized for different applications in the system, as will be explained later.

1.6 Research Objective

Microgrids will play a major role in enhancing the resiliency and robustness of power delivery to end users. The protection of microgrids' assets is of utmost importance to ensure continuous operation of the grid. Microgrids are dynamic in nature, therefore, to account for that, new protection schemes need to be established for microgrid infrastructures.

The aim of this doctoral research is to; 1) develop a new protection infrastructure for decentralized active distribution networks that can be implemented in a practical way manner, taking into account the different various challenges that arises from the dynamic nature of the microgrid, which is different than the classical protection techniques used in the current bulk grid infrastructure.

2) The developed selectivity schemes must avoid disconnection of different large sources in the system. For instance, power flow is bidirectional in modern microgrids,

therefore, when dealing with selectivity issues one should take into account the operation of distributed energy resources in the microgrid.

3) Another important factor to account for is the different modes of operation of modern microgrids. This research develops the utilization of energy storage devices to compensate for low short circuit currents in microgrids' during the different modes of operation.

4) Another objective of this dissertation is to ensure the maximum utilization of these resources, an optimal value of the capacity of the energy resources and the cost of these devices will be developed. Finally, the communication link between IEDs can be used to account for the dynamic changes in the microgrid and changing relays' settings according to the present architecture of the microgrid.

The Research Problem has the following focus areas:

1. Developed a solution to the denial-of-service cyber-attack on adaptive Microgrid protective schemes.

2. Tested a new controller with only one autonomous mode of operation for both grid-connected and islanded modes of operation to inject current from supercapacitors and other energy storage schemes without the need for needing communication infrastructure.

3. Verified the impact of energy flow on the stability and protection of the distribution architectures during normal, pulsed and resource outage conditions. Varying optimized distribution architectures will need to be achieved based on prevailing conditions.

4. Created a proper sizing of the energy storage devices which is important in order to maintain a stable system operation and also to regulate the protection scheme's cost. A complete study on the effects of developed solutions on size and cost.

5. Developed, designed and experimentally verified a protection schemes for the active distribution of networks in response to different operational scenarios and the developed practical solutions.

6. Techniques and algorithms developed during this research were verified experimentally through practical operation of a descriptive system implemented in a laboratory scale power system test-bed with hardware in the loop in the Energy Systems Research Laboratory, Department of Electrical and Computer Engineering, Florida International University (FIU).

1.7 Original Contributions and significance of the dissertation

One main challenge in the practical implementation of a microgrid is the design of an adequate protection scheme in both grid connected and islanded modes. Conventional overcurrent protection schemes face selectivity and sensitivity issues during grid and microgrid faults since the fault current level is different in both cases for the same relay. Various approaches have been implemented in the past to deal with this problem, yet the most promising ones are the implementation of adaptive protection techniques abiding by the IEC 61850 communication standard. However, the risk of communication link failures and cyber security threats still remain a challenge in implementing a reliable adaptive protection scheme. A contingency is needed where a communication issue prevents the relay from adjusting to a lower current level during islanded mode. An adaptive protection

scheme is developed that utilizes energy storage (ES) already available in the network as a mechanism to source the higher fault current.

1- Developed a new controller of the energy storage device to inject high current at the islanded mode operation.
2- Tested the developed protection technique in the Energy Systems Research Laboratory at FIU.
3- Improved the sizing and the cost of the supercapacitor to avoid add cost to the protection scheme.
4- Created several protection schemes based on MAS to integrate between the cyber and physical parts for active distribution systems.
5- Verified the system stability in terms of frequency and voltages at AC and DC sides to ensure that the system performance became healthy after isolating the fault

1.8 Dissertation organization

This dissertation is organized in eleven chapters, including the current chapter, which presents the introduction of this dissertation following by the problem statement and the significant contribution. Chapter 2 discusses the Hybrid AC/CD microgrid that is used to verify the developed protection schemes. The main components that are used in the system including the different sources at AC/DC sides such as the synchronous generator, programming loads, distributed energy resources, energy storage devices, pulsed, steady state loads and the power converters. Also, this chapter introduces several industrial equipment's such as PMUs, IEDs and PLC.

Chapter 3 describes the structure of GOOSE and SV messages and discuss the different types of physical attacks that may impact the adaptive protection scheme and prevent communication networks from dealing with the dynamic changes of microgrid. Security attacks in microgrid communication networks are intended to interrupt messages that are exchanged between IEDs. The attacks can be implemented using common network security attacks or by exploiting GOOSE and SV messages.

Chapter 4 develops an adaptive protection scheme which utilize super capacitive energy storage to enhance resiliency against communication outages. This chapter also introduces an autonomous control algorithm developed for the super-capacitor's AC/DC converter. The developed control is capable of deciding upon charging, discharging of the super-capacitor, and whether or not to feed fault currents on the AC side, based on direct voltage and frequency measurements from its connection point with the microgrid. This eliminates the need for a control command to be sent from the point of common coupling of the microgrid with the main grid to adjust the controller's mode of operation and thus reduce the risk of controller failure due to cyber-attacks or other communication issues. Simulation tests of the developed protection scheme are presented at different modes of operation.

Chapter 5 presents two solutions to reduce the size of the supercapacitor that used to feed the fault and the pulsed load simultaneously when the communication is not available in the system during islanded mode operation. The first method presents two-level optimization scheme for minimizing the supercapacitor size along with optimizing its controllers' parameters. The second method will lead to a reduction of the supercapacitor fault current contribution and an increase in that of other AC resources in the microgrid in

the extreme case of having a fault occurring simultaneously with a pulsed load. It was also shown that the size of the supercapacitor can be reduced if the pulsed load is temporary disconnected during the transient fault period. Simulation results showed that the resulting supercapacitor size and the optimized controller parameters were feeding enough fault currents for several types of faults in different locations and minimizing the cost of the protection scheme.

Chapter 6 presents a co-simulation platform for microgrid based on MAS when the communication is available in the system. IEC 61850 was used to emulate the developed protection scheme. DDS middleware is used to link between the hardware and software environments. During islanded mode, the system is capable of riding-through communication failures by the aid of a lithium ion battery. When the communication is attacked, the battery plays an important role and contribute to the fault current for helping the circuit breaker to trip during islanded mode. The design of the control algorithm for the battery's AC/DC converter is developed with single mode operation to eliminate the reliance on communicated control command signals to shift the controller between different modes. Simulation and experimental results were investigated to test the developed technique.

Chapter 7 develops a communication-assisted fault localization, isolation and restoration method for microgrids based on MAS. The developed system comprises distributed agents, located in the middle and at the two ends of a protection section, which will detect a fault through phase angle comparison of current signals at both sides of a given distribution line. The agents then send a trip signal to the corresponding circuit breakers accordingly. The importance of the developed protection technique is twofold:

first, it eliminates the use of voltage transformers and thus reduces costs. Second, it does not require transfer of data along long distances which decreases the delay time for fault isolation. Power restoration processes following the fault clearance considering voltage, frequency and power flow constraints in the microgrid under study was also performed. The simulation of the developed protection methodology was presented,

Chapter 8 presents a co-simulation platform for a microgrid based on MAS utilizing a supercapacitor bank to enhance the resiliency of the protection scheme. The simulation software, embedded microcontrollers, and a real communication architecture collectively perform the protection scheme platform. The DDS middleware is used to link the hardware and software environments. This method does not need to change the relay settings at different configurations of the microgrid. The developed solution does not incur additional costs to the system studied, as the supercapacitor is already used to feed a pulsed load. The chapter also develops a coordination process between the relays with the help of the supercapacitor. Primary and back-up protection were studied according to IEEE Std C37.112 to isolate the fault properly. This chapter details the fault current that supplied by any DG to any point inside the network. The results showed that the co-simulation infrastructure introduces a high dependability design, analysis, and testing environment for cyber and physical data flow in the system.

Chapter 9 presents the hardware setup that used to test the control and protection operations for the microgrid system. The hybrid AC/DC microgrid, used for experimental verification, consists of several types of sources that supply loads with different characteristics, including: AC load, a normal steady-state load, and a heavy pulsed load at

DC side. The experimental results showed excellent agreement with the simulated protection scheme

Chapter 10 presents a centralized control approach to monitor the modes of the microgrid and helping the relays to define the fault location and clear it from the system. The developed technique helps to identify the shortest path from the source to the fault location. The MCU is responsible for adjusting the relays settings based on the current topology and the shortest path to the fault point. This technique is investigated on IEEE 14 bus microgrid system for all the possible fault paths. The developed scheme is able to clear the fault by isolating the minimum part of the system and certifying the endurance of the power to supply the different loads in the system.

Chapter 11 provides conclusion the discussing the test results of the dissertation. Besides that, some recommendations are provided for the future work to improve the protection schemes for the microgrids.

Chapter 2 Configuration of The Microgrid to Investigate the Protection Schemes

2.1 Introduction

This chapter presents the construction of the developed hybrid AC/DC microgrid. The microgrid is implemented to investigate the developed techniques for protection, control and energy management operations of the microgrid at the Energy Systems Research Laboratory, Florida International University. The main construction of the microgrid includes synchronous generator, inverter-based energy resources and programming control loads, energy storage devices such as supercapacitor bank and batteries. Other equipment's are used to help in monitoring and measurements processes such as PMU, PLC, IEDs and PDC. The next section will present the components of the microgrid that contains the generation units and the different load types.

In order to increase the resiliency of the system, cyber physical architecture is required to facilitate the operation of sending and receiving the information between the devices. The data should be send via communication links to perform the protection and control operations. One of the main devices used to measure frequency and voltage and current vector quantity is PMU device. Standard IEEE std. c37.118 is used to formulate the data from PMU to other devices.

The main challenge of the Hybrid AC/DC microgrid architecture is to design the system at different modes of operation. During the grid connected mode, the system is stable and the frequency is not changed above or below the accepted limits due to the large support from the utility. At islanded mode operation, the frequency fluctuates and needs to

be adjusted using the distributed energy resources that are connected based on inverter interface.

The developed improvements in microgrid architecture provide a synchronous generator and several renewable resources that are connected through AC/DC and DC/DC converters to provide the regulation of the voltage at both sides, improve the stability of the system and increase the efficiency by achieving MPPT for the solar stations.

One of the issues involved in designing a suitable architecture for the microgrid is the protection scheme against the communication outages. Different types of attacks can be effect on the communication signals that used to trip the circuit breakers at AC side of the microgrid system. One of the contribution of this dissertation is to use the energy storage devices at DC side to help the relays to reach its settings at the AC side and isolate the fault from the system. Also, there are different challenges that should be taken into our consideration to adjust the settings of the relays at different modes of operation as it will be discussed in the following sections.

2.2 Main Components of the Microgrid

The microgrid contains different components that are used to test the different protection schemes that developed for the microgrid configuration

2.2.1 Synchronous Generator

A 13.8-kVA, 60-Hz, 208-V, and 1800 Rpm AC are representing the specification of the synchronous generator generation unit. The generator is equipped with a half-wave phase-controlled thyristor-type automatic voltage regulator. The generating station has 5 different types of motor drives acting as 5 different prime movers to enable the implementation of various generation control strategies. The frequency drive part follows

"vector speed control" that serves to maintain the frequency stable. In order to keep the power-voltage buses, the prime mover of the generator is operated by a torque-controlled frequency drive, which adjusts the active power of the generation station to keep the voltage signal within the accepted value. The speed reference and the torque of the frequency machine is controlled by a PLC. The specifications of the synchronous generator are shown in Table 2.1. Figure 2.1 indicates the synchronous generator set for the frequency machine and the voltage regulator.

Table 2.1 Synchronous generator parameters.

Component	Parameter	Specification
Synchronous Generator	S_N	3 kVA
	V_N	208 V
	F_N	60 Hz
	X_L, R_S	6.87 *mH*, 1.45 Ω

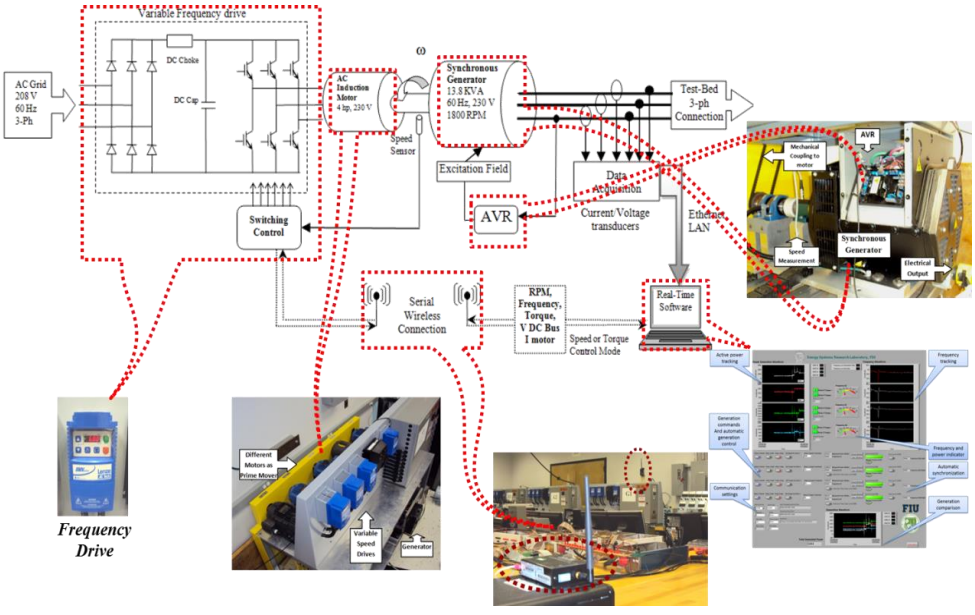

Figure 2.1 Synchronous generator at the ESRL Smart Grid Testbed

2.2.2 Distribution Lines and Load Models

The transmission line models are composed of series inductors and parallel capacitors and arranged in medium length π-type. The load module is consists of ten steps changes between 0-3 KW in step of 300 W at normal voltage. These resistances can be controlled by PLC which represented [2 x 72 Ω + 4 x 144 Ω]. In order to maintain the frequency within the accepted range, the inductance loads are implemented based on constant inductance to avoid the derivation in the frequency signal. A solid state relays are used with the ratings of 530 V and 25 Amps. The operation of On/Off status can be controlled by PLC with 3-32 DC voltage. Figure 2.2 shows the transmission line resistive and inductive loads models.

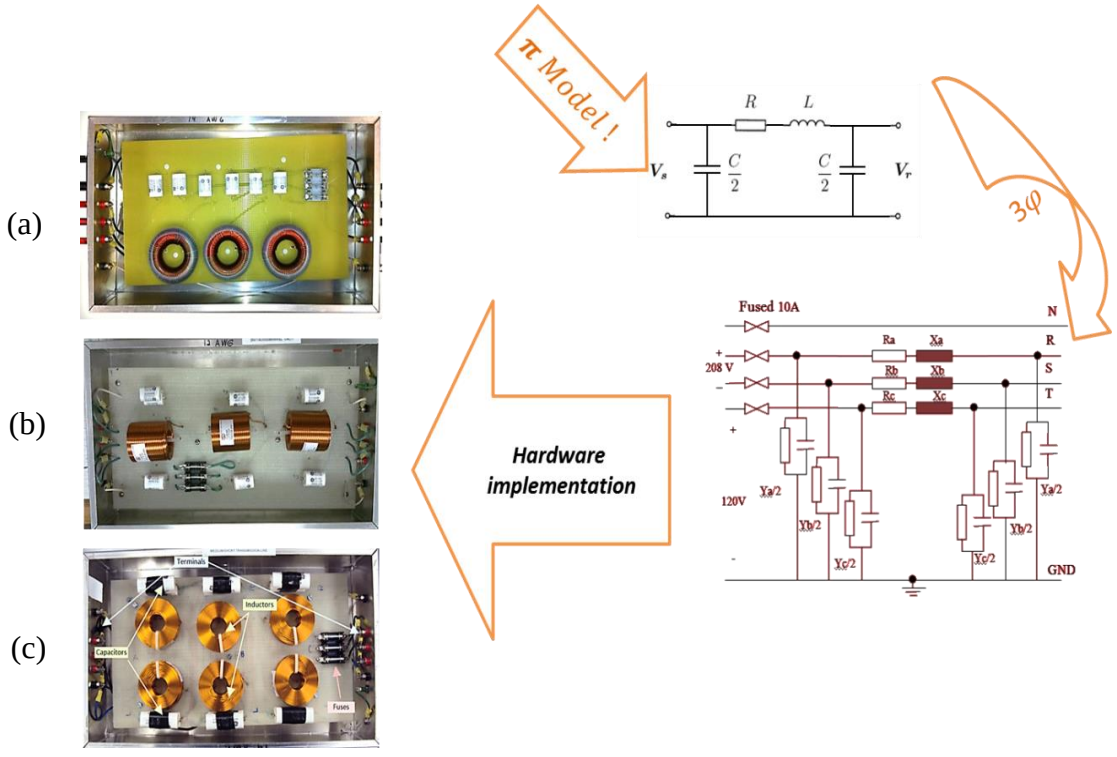

Figure 2.2 Line and load models: (a) medium length line; (b) resistive load; (c) inductive load.

2.2.3 Bus Models

The test-bed setup has 14 bus model emulator to control the switching action and emulate real power system dynamics. These modules can switch up to 15 amps per phase. The hardware implementation of the bus model is shown in Figure 2.3.

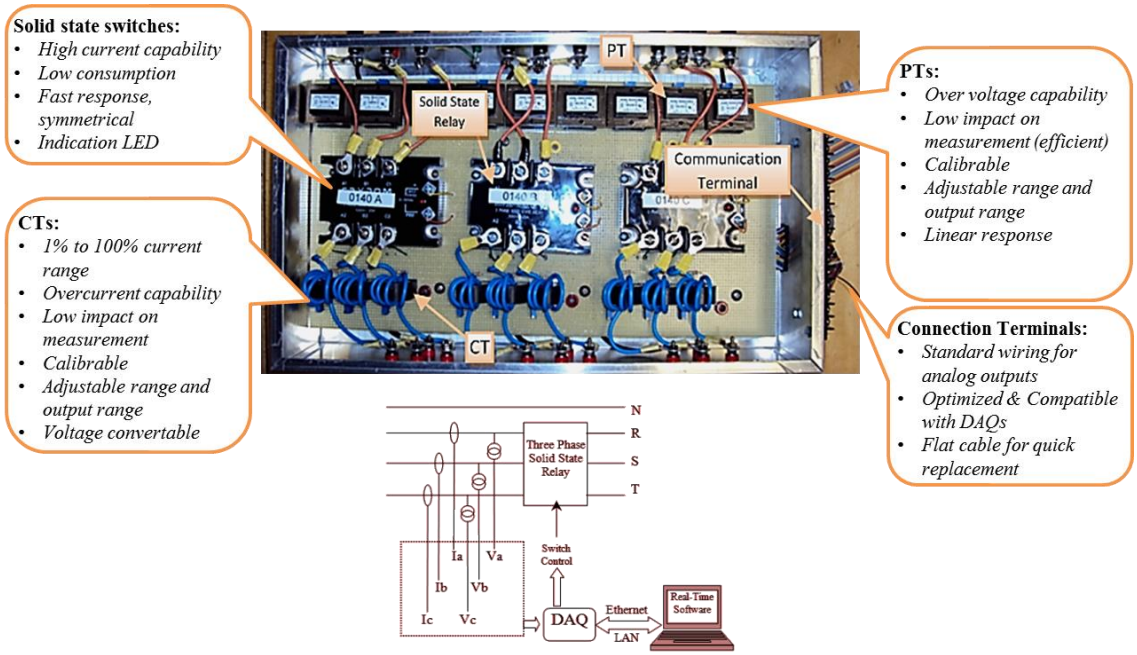

Figure 2.3 Bus Model Hardware Implementation.

2.2.4 Bi-Directional AC/DC and DC/DC Converters

This converter can be controlled from AC/DC sides. The frequency and the voltage signals are fed the control circuits of the converter. For the DC side, the voltage is controlled by adjusting the charging and discharging periods of the energy storage devices such as supercapacitor. The voltage of these devices can be controlled through DC/DC converter. The PWM circuit of the inverter can be adjusted through different types of dSpace such as 1103 and 1104 based on the measured and the control signals as shown in Figure 2.4. Matlab/Simulink software is used to program the active/reactive power

generation of the IGBT circuit. RS232 serial port is used for the communication and the PLC control purpose.

Figure 2.4 dSpace system for developing embedded controller

2.2.5 Bi-Directional DC/DC Converter

This converter is used to regulate the DC voltage of the supercapacitor bank. During the grid connected mode operation, the main function of the converter is to regulate the charging rate of the supercapacitor. At the islanded mode of operation, this converter plays an important role to charge/discharge the supercapitor bank based on the suggested control to maintain the voltage within the accepted limits of the standard.

2.2.6 Bi-Directional AC/DC Converter

The bi-directional AC/DC converter can take control of the AC side frequency and voltage amplitude. The DC bus voltage is regulated by controlling the charging and discharging of the battery banks, which also means controlling the current flow through the bidirectional DC/DC converter. The DSP-based embedded dSpace control platform is used to control the inverter-based DER model. The internal active/reactive power generation of the IGBT-based inverter is programmed using the Matlab/Simulink platform as shown in Figure 2.5.

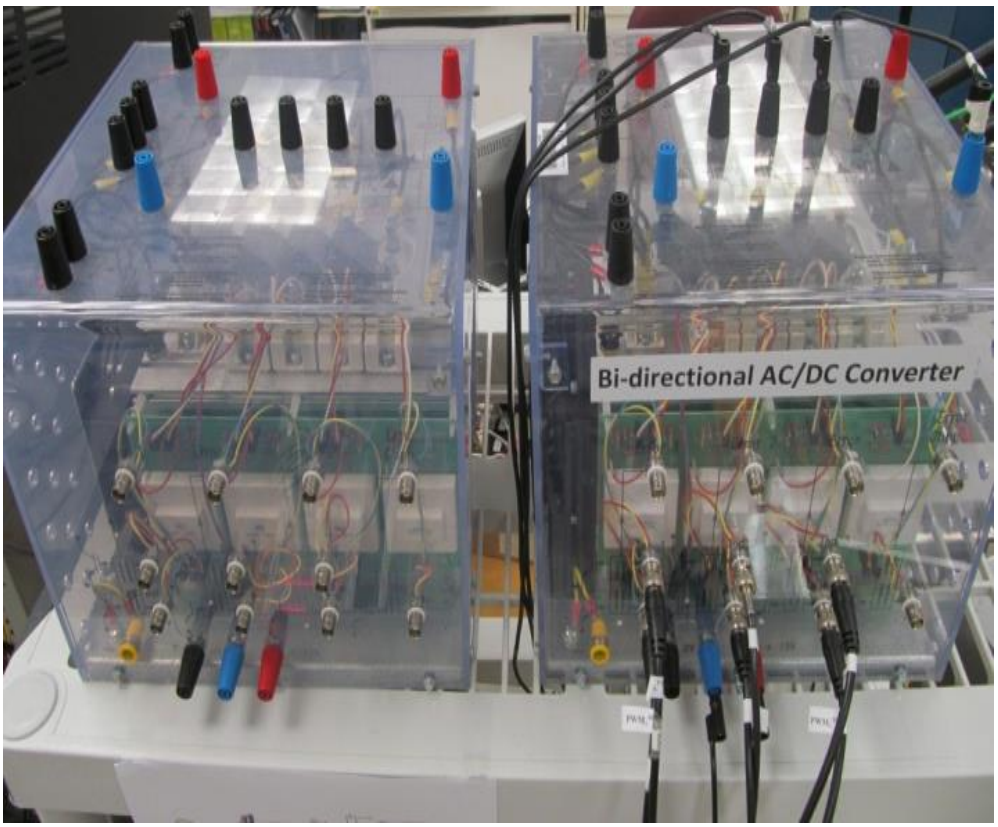

Figure 2.5 Converter Systems Hardware Setup.

2.3 Energy Storage

A wide variety of energy storage technologies and ratings are used in the testbed. There is a lead acid battery bank that can store energy up to 12 kWh. Also, there are other lead-acid batteries with different ratings to be used as distributed energy storage. There are 5x1000 Wh Lithium-ion batteries. In addition, there is a 40 module super-capacitor bank and a flywheel system implemented with its driving converter.

2.3.1 Battery storage system

The lead acid battery bank storage, shown in Figure 2.6, has a 10-110 Ah capacity (approximately 13.2 KW) and is equipped with a unique BMS which individually manages, balances and conducts diagnostics on each battery module using hall-effect sensors of

voltage and current. The BMS not only monitors the batteries, but also extracts the defective battery and compensate its loss through the distribution of the load on other resources using power electronic converters (e.g. buck/boost converter). This system is expandable to any chemistry and quantity of batteries based on its modular characteristics. This system is capable of data logging and advanced protection to limit the current and voltage of each battery. The system also controls the charging profile with independent frequency, duty cycle, and magnitude.

Figure 2.6 Battery Bank Stored Safely in a Closed Cabinet.

2.3.2 Super Capacitor bank

An energy management system improves the performance and efficiency of unpredictable renewable energy resources through integration of super capacitor energy storage systems in the testbed with two 2.9 F super capacitors in series or parallel architecture rated at 1.45F-650V or 5.8F-320V. A super capacitor at the DC bus will stabilize all the converters to work in current control mode, and one will be used to stabilize the voltage and power quality indices on the DC bus, especially in the presence of pulse loads.

The supercapacitor bank, is built using 350 F, 2.7 V cells of Maxwell Technologies supercapacitors cells connected in series to form a 58 F, 16.2 V module. Twenty supercapacitor modules were connected in series to configure a 2.9 F, 320 V supercapacitor bank. Figure 2.7 shows the supercapacitor bank implemented in the test setup.

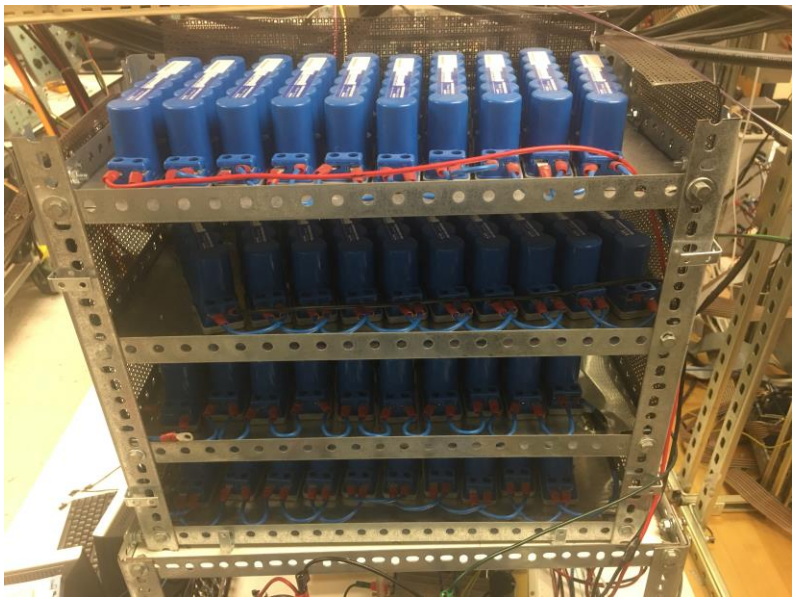

Figure 2.7 Supercapacitor Hardware Setup.

2.3.3 Flywheel storage system

A large rotating mass coupled to a DC machine constitutes a Flywheel Energy Storage System which works under 3 operating modes: charging mode, stand-by mode, and discharging mode. This setup is used to perform several studies. To name some: the power failures and outages, mitigation of pulse loads, power quality improvements, and design and performance of flywheel systems.

2.4 Phasor Measurement Units

The testbed includes 2 Phasor Measurement Units (PMUs) from SEL, shown in Figure 2.8, with a total input of 5 voltage and current measurements, which are time-stamped with a real-time GPS clock. PMU measurements are published and available in PDC through c37.118 Synchrophasors protocol. A real-time automation controller from SEL integrated to exchange information in DNP3, Modbus, IEC 61850 GOOSE, IEC 60870-5-101/104, LG 8979, SES-92, IEEE C37.118 protocols.

Figure 2.8 SEL Phasor Measurement Units.

2.5 Vector Processing Unit and GPS Clock

As mentioned earlier, the deployed PMUs in the system send their acquired data with time-stamp information to the Vector Processing Unit shown in Figure 2.9. The collected data from several PMUs are sorted and correlated per the time-stamp value. This enables comparable real-time monitoring of the system with high precision sampling. The collected data is also stored in a large database system for accurate post mortem applications such as fault event monitoring, loss-of-mains and blackout analysis. Synchro phasor measurement and time-referenced critical applications, such as fault event analysis and protection relays, require highly reliable satellite clocks. Inaccurate time-stamps can cause misdiagnosing of the network and degrade the controllability of distribution network. The IRIG-B time code is widely accepted for time distribution in substations. We use a GPS clock with IRIG-B, shown in Figure 2.10, outputs in our test bed to perform time stamping.

Figure 2.9 The Phasor Data Concentrator.

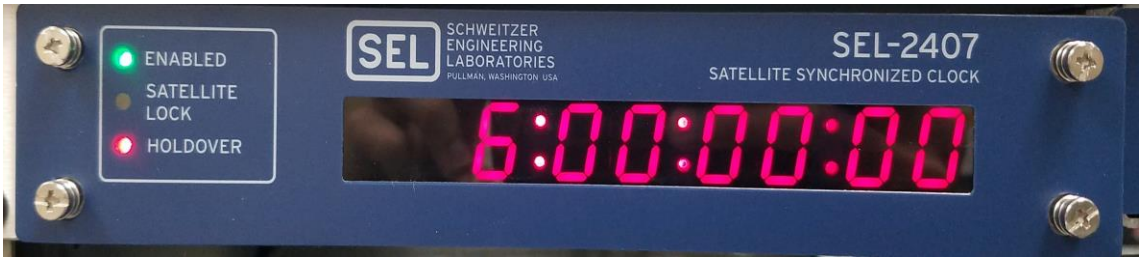

Figure 2.10 The GPS Clock.

2.6 Intelligent Electronic Devices (IEDs)

Figure 2.11 ABB IEDs Hardware Setup.

Intelligent Electronic Devices constituting 5 ABB 615 Relion series protection relays with IEC 61850 capability are integrated into the system to form a distribution or substation network, as shown in Figure 2.11. The setup also covers Modbus protocol to provide industrial communication and control features. The above-mentioned protocols are merged through an OPC server as a middleware and the gateway for interconnection within the protocols to interface measured data and issued commands with external organizations, such as computational intelligence, HMI, SCADA, etc.

The IEDs are located on system buses to enable monitoring, control and protection. The agent platform controlling these IEDs was implemented on a single personal computer, however, since the information is accessible through the network, the computation can be easily distributed. An off-the-shelf OPC UA server was implemented to acquire IEC 61850 logical node measurements. An OPC UA client was embedded in the Java platform to enable JADE to access mapped IEC 61850 measurements, and c37.118 Synchrophasors protocol.

Chapter 3 Cyber Physical Threats on Microgrid Operation

3.1 Introduction

This chapter explains the structure of the messages that can be transmitted between the different IEDs in the system to protect the active distribution system. The main messages that can be used to determine the statues of the system are GOOSE and SMV messages. One of the main features of these messages is the critical time that should not be exceed a certain period to trip and control the circuit breaker. The main function of the GOOSE message is to trip the circuit breaker and isolate the fault from the system. While, the main purpose of SMV messages is to measure the voltages and currents signals from the measurement devices.

Also, this chapter introduces the different types of attacks that can be threaten the network and prevent the authorized devices to perform their functions. We can divided the attacks into two main types, the first one is the attack on the networks, which can be categorized into Denial of service, Password cracking, and Eavesdropping attacks. Secondly, the attacks on the GOOSE and SV messages.

The main study in this dissertation is the Denial of service attack which collapse the whole communication signals that can be transmitted between the relays in the system. We introduced different solutions as it will be explained later in the next chapters of how to overcome this famous type of attacks.

3.2 Goose Message structure

GOOSE and SMV messages are sent directly to multicast MAC address on layer 2. Since the layer 2 message doesn't use The IP protocol for message routing, it's not prone to ARP poisoning attack. However, the attacker can still perform some types of attack based on the message anatomy and transmission method. Figure 3.1 shows the structure of the GOOSE message.

Table 3.1 Structure of GOOSE Message.

Destination MAC address		Source MAC Address	Priority Tagging/ VLAN ID		
Ethertype (88B8)		APPID	Length		
Reserved 1		Reserved 2	Tag	Length	goosePDU
Tag	Length	gocbRef	Tag	Length	timeAllowedtoLive
Tag	Length	datSet	Tag	Length	goID
Tag	Length	T	Tag	Length	stNum
Tag	Length	sqNum	Tag	Length	test
Tag	Length	confRev	Tag	Length	ndsCom
Tag	Length	numDatSetEntries	Tag	Length	allData
Tag	Length	Data 1(Boolean)	Tag	Length	Data 2 (Float)
••••• •••••			Tag	Length	Data N

All GOOSE messages start with the destination's MAC address, followed by source MAC address, Priority Tagging/VLAN ID, Ethernet type, APP ID, Length and two reserved fields. These fields are described as the following:

• Destination MAC address: GOOSE messages use multicast MAC address as the destination address. The GOOSE multicast address must start with 01-0C CD-01-xx-xx. The first three octets are (01-0C-CD) reserved for IEC 61850 protocol. The fourth octet is set to (01) for GOOSE messages.

• Source MAC address: this field contains the MAC address for the publisher IED.

• Priority Tagging/VLAN ID: GOOSE messages contain IEEE 802.1Q VLAN ID. The IEEE 802.1Q standard supports virtual LANs on an Ethernet network. The IEEE 802.1Q VLAN ID consists of Tag Protocol Identifier (TPID) and Tag control Identifier (TID). The TID is divided to Priority code point (PCP), 1-bit Drop eligible indicator (DEI). This indicator specifies if the message can be dropped in the case of congestion and 12-bit VLAN identifier field.

• Ether type: all GOOSE messages have a unique ether type field equal to 88B8.

• APPID: this field is used by the subscriber IEDs to identify the messages they are subscribing to.

• Length field: The Length field represents the length of the datagram minus eight bytes.

• Two reserved fields: these fields are reserved by the standard for future use.

A GOOSE message also has an IEEE 802.1Q VLAN ID, a unique Ethernet type, and an APPID field which subscribing IEDs use to identify the messages they are subscribing to. The Length field represents the length of the datagram minus eight bytes; the length field is followed by two reserved fields, which the standard leaves for future use.

• gocbRef: GOOSE control block reference

• timeAllowedtoLive: The time a receiver waits before receiving a re-transmitted message

• datSet: Name of the dataset.

• goID: ID of publishing IED.

• t: Timestamp indicating a new GOOSE event.

• stNum: Counter that increments with every GOOSE event.

• sqNum: Counter that increments with every repeated GOOSE message.

• test: Specifies if a message is intended for testing or not.

• confRev: Number of times the data set has changed.

• ndsCom: Needs commissioning field.

• numDataEntires: Number of data elements in allData.

• allData: Actual data being sent (bool, integer, float, etc.).

3.3 Samples Measured Values Message structure

Table 3.2Structue of SV Message

Destination Address			Source MAC Address		Priority Tagging/ VLAN ID
Ethertype (88BA)			APPID		Length
Reserved 1			Reserved 2		APDU
Tag	Length	noASDU	Tag	Length	svID
Tag	Length	SmpCnt	Tag	Length	ConfRev
Tag	Length	SmpSynch	Tag	Length	Sample 1
Tag	Length	Sample 2	Tag	Length	Sample 2
••••• •••••			Tag	Length	Sample N

SMV datagram follows a modified Abstract Syntax Notation One (ASN.1) Basic Encoding Rules (BER) Tag/Length pair encoding scheme. An SMV datagram is composed of two distinct fields: the packet header and the packet data. In the header, the SMV packet is constructed first with a destination MAC address followed by the source MAC address, as well as several fields related to the IEC 61850 protocol that will determine which multicast messages to accept and reject based on the subscriptions of the individual subscribing devices.

In the SMV datagram data field as shown in Figure 3.2, there can be several application protocol data units (ASDU), which are objects that contain relevant information for an individual node. Using several ASDUs allows a single device to send or receive physical sensor data from several nodes in the same datagram.

3.4 Cyber Physical Attacks

This chapter describes the different types of physical attacks that may impact the adaptive protection scheme and prevent communication networks from dealing with the dynamic changes of microgrid. Security attacks in microgrid communication networks are intended to interrupt messages that are exchanged between IEDs. The attacks can be implemented using common network security attacks or by exploiting GOOSE and SV messages as shown in Figure 3.1.

3.4.1 Network Security Attacks

This attack is performed through the communication network to damage, change, or access user data without permission [123]. The following are several types of network security attacks:

1) Denial of Service

DoS is the process of preventing the authorized user of a service to access that service [123]. Main types of DoS that may affect the communication between protective devices include SYN (synchronization) floods and buffer overflow. For the first type, the attacker sends a continuously spoofed SYN request to the target IED to distort the connection between the authorized user and IEDs [124]. This type of attack can be orchestrated by running several protocol services like FTP, HTTP and Telnet on the IED at the same time [125], [126]. For the second type, the attacker may transmit malicious code to an IED and write oversized data to cause a buffer overflow. This attack is possible as a result of the vulnerability of IEDs and the unavailability of security measures for IEDs to detect the malicious code [124].

2) Password Cracking Attempts

This type of attack is defined as an attempt to gain access to an IED, another device, or a system by guessing the password [127]. Attackers who are able to access an IED can send a false tripping signal to the CB that can cause it to disconnect a healthy part in the system. This can be accomplished in two ways: a brute force attack and a dictionary attack. A brute force is performed by arranging all possible combinations of passwords and trying these combinations one-by-one to achieve the correct password but may take a long time. In a dictionary attack, the password is simply guessed.

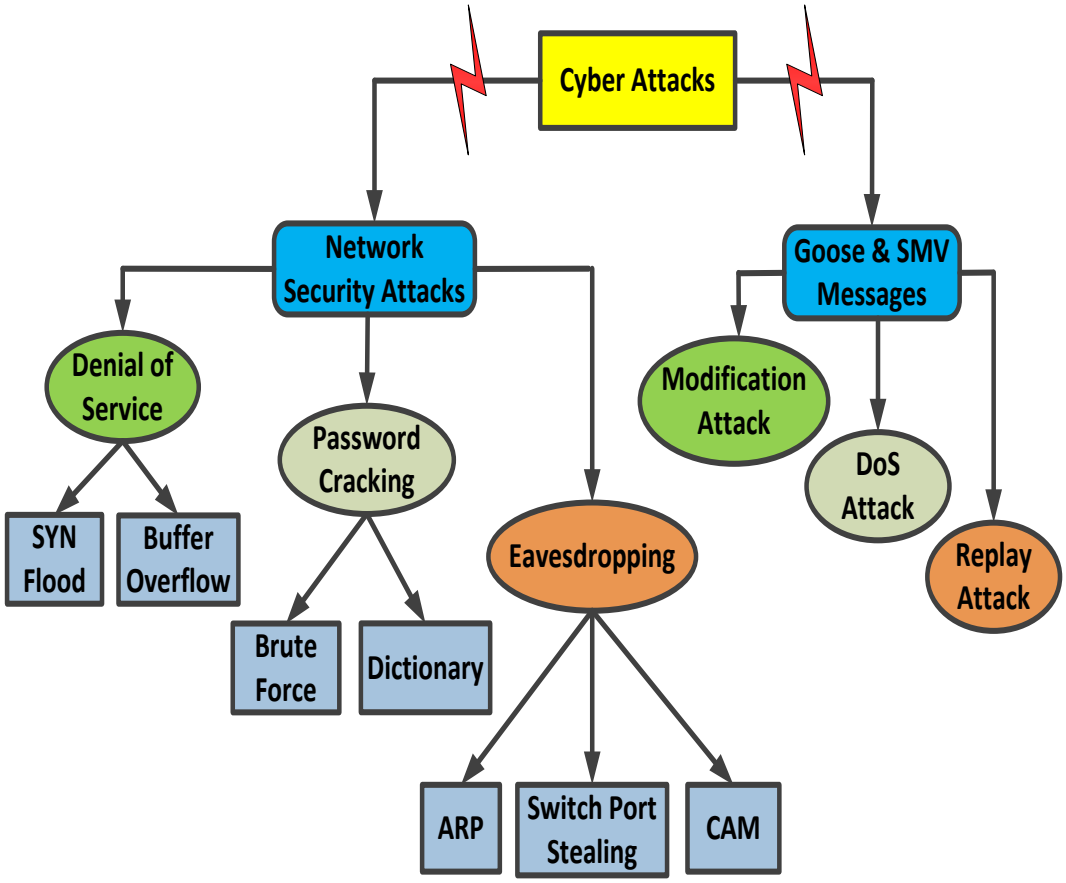

Figure 3.1 Types of Cyber Attacks.

This type may take less time than the latter. In [125] and [126], hackers were able to utilize FTP, HTTP and Telnet services already running on the IED to crack the password.

3) Eavesdropping Attacks

Eavesdropping attack is an attempt to steal packets that are being transmitted through the system. This type of attack is launched from within the LAN and can target FTP, HTTP and Telnet services because messages for these protocols are not encrypted [125]. There are three types of this attack.

The first is known as ARP cache poisoning. ARP is a communication protocol that converts an IP address into incorrect MAC address (i.e. the MAC address of the attacker), the switch will end up forwarding all packets addressed to the attacker and enables the attacker to capture those packets.

The second type is to cause CAM table flooding. This is done by filling in the CAM table of the switch with fake entries. When it is full, packets addressed to a MAC address that are not in the CAM table will be broadcasted to the whole network allowing attackers to capture them.

Finally, the third type is switch port stealing where fake frames are sent to the switch that contain the target host MAC address causing the switch to modify the CAM table. This allows the MAC address to connect to the interface that leads to the attacker [127].

3.4.2 Attacks on GOOSE and SV Messages

There are two multicast message protocols used in IEC 61850 which include GOOSE and SMV messages. The main function of the GOOSE message is to send a trip signal to

the CB to isolate the faulty part from the system. SV messages are used to send voltage and current values from merging units to the protective devices. Both messages use a switched Ethernet network for communication purposes. These messages must be transmitted within 4 ms. The following section discusses several attacks that exploit GOOSE and SMV messages.

1) GOOSE and SV Modification Attacks

In this type, the attacker changes the message that is exchanged between the protective devices without allowing the publisher (the sender of GOOSE messages) or subscriber (the receiver of GOOSE messages) to notice.

Two types can be found in this attack. For the first type, the attacker captures the GOOSE message and modifies it with another message that enables the attacker to control a CB. For a SV packet, an attacker sends a fabricated analog value to a control center in the system that leads to gain control of IEDs and cause a power outage [116]. The second type of attack is performed using a malware script [128].

The malware can capture the message that is exchanged between IEDs altering and re-injecting GOOSE message packets into the IEC 61850 network. In order to enable the malware to perform its job, it must be installed on a computer inside the network. Attackers exploit the weakness in GOOSE where encryption and digital signatures cannot be applied due an IEC 61850 requirement that any operation, which is communicated using a GOOSE message, must take effect within 4 ms. Without encryption and digital signatures, a transmitted packet can be easily captured, modified, and retransmitted into the network.

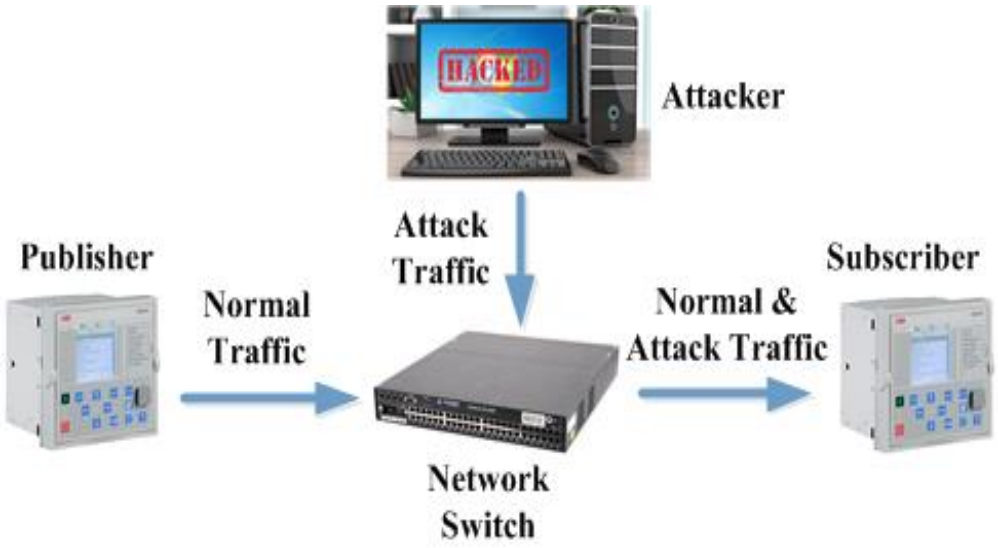

Figure 3.2 GOOSE Poisoning Attack.

2) GOOSE and SV Denial of Service Attacks

These attacks prevent IEDs to respond to legitimate messages made by other IEDs. This can be done by sending a large number of messages to the target IED, where it becomes overwhelmed and is unable to respond to a legitimate request. GOOSE poisoning attacks are another way to perform DoS as shown in Figure 3.2.

The aim of these attacks is to get the subscriber to accept GOOSE messages with a higher sequence number than those sent by the publisher. As a result, all GOOSE messages from the publisher will be considered invalid by the subscribers leaving the subscribers to only accept GOOSE messages from the attacker.

There are three variables of GOOSE poisoning attacks including high status number attacks, high rate flooding attacks, and semantic attacks. For the high status number attack, the attacker sends a single spoofed GOOSE frame with a very high status number to a GOOSE subscriber by the attacker.

Secondly, in a high rate flooding attack, the attacker multicasts a range of spoofed GOOSE messages with higher status numbers. The spoofed GOOSE frames employ a status number higher than the expected status number of a GOOSE subscriber.

In a semantic attack, the attacker will fix the status number in the GOOSE message and determine the rate of status change. Then, the attacker will spoof GOOSE messages that are higher than the detected rate of status change [129].

3) GOOSE and SV Replay Attacks

In this attack, GOOSE messages are captured and kept by the attacker. Then, the attacker sends a message to trip the CB under normal operation which may result in an undesirable action.

For a SV message replay attack, the attacker can also capture a SV packet containing certain values of power and current and send it to another protective device in the substation several times. SV packets with the same power and voltage values circulating inside the system can lead to an unplanned outage [130].

3.5 Summary

Most adaptive protection methods depend on exchanging information amongst intelligent electronic devices by way of a communication link. Therefore, protection against cyber-attacks is crucial to ensure a safe message exchange. Different types of cyber-attacks were introduced that may impact the communication network, keeping in mind these as well as a total loss of communication could be catastrophic to a microgrid protection scheme. In this chapter we introduced the main messages that can be used to protect the electric power system.

The main challenge to perform the protection scheme is to publish and subscribe these message with 4 ms and isolate the fault from the system. Another contribution of this chapter was presented the different types of attacks that can be effect on the communication system and prevent the authorized devices to send a GOOSE message to trip the circuit breaker.

Chapter 4 Utilizing Supercapacitors for Resiliency Enhancements and Adaptive Microgrid Protection against Communication Failures

4.1 Introduction

Islanded microgrids do not have sufficient resources to contribute enough fault current to legacy protection devices to continue operation. Therefore, when a fault occurs in an islanded microgrid, relays with high fault current setting will fail to detect and clear the fault due to the limited sources in the system at this mode of operation. Contemporary adaptive protection schemes rely on communication technologies to adjust the relay settings to adapt to the microgrids' modes of operation; grid-connected or islanded. However, the risk of communication link failures and cyber security threats such as denial-of-service represent major challenges in implementing a reliable adaptive protection scheme. In order to address this issue, this chapter develops an adaptive protection scheme, which utilize super capacitive energy storage to enhance resiliency against communication outages. This chapter also introduces an autonomous control algorithm developed for the super-capacitor's AC/DC converter to allow the supercapacitor to inject current at islanded mode operation. The developed control is capable of deciding upon charging, discharging of the super-capacitor, and whether or not to feed fault currents on the AC side, based on direct voltage and frequency measurements from its connection point with the microgrid. This eliminates the need for a control command to be sent from the point of common coupling of the microgrid with the main grid to adjust the controller's mode of operation and thus reduce the risk of controller failure due to cyber-attacks or other communication issues. Additionally, the chapter develops a solution to avoid installing a larger super-

capacitor by temporarily disconnecting the uncritical pulsed load during the fault instant. The developed protection scheme was investigated through simulation for various fault types and showed successful results, using the developed scheme, in eliminating the aforementioned faults when the communication was available or attacked.

The developed solution takes benefit from the installed supercapacitor in the system with the bidirectional VSC to contribute for the fault current and raise this current value to level which is sensed by the High relay settings. The developed solution does not incur additional costs to the system studied as the supercapacitor is already used to feed the pulse load.

It is also worth noting here that the design of the developed controller for the supercapacitor's AC/DC converter is capable of operating when the microgrid is in both grid-connected and islanded mode.

Utilizing a single mode of operation for the converter will eliminate the reliance on communication control command signals to shift the controller between different modes. The system, as will be detailed later in the chapter, is also designed to maintain stable voltage and frequency levels even during extreme cases such as the occurrence of a fault during a peak pulse load period.

4.2 Hybrid DC/AC Microgrid Description

Figure 4.1 shows the topology of the hybrid AC/DC microgrid under study with grid connection capabilities. The system contains three types of sources: two distributed generators in the AC part of the microgrid, a super capacitor bank to supply a DC pulse load, and a fuel cell. A three phase transformer is implemented to feed the AC microgrid with the required rated voltage.

The system has a filter located between the transformer and the AC microgrid to filter out the harmonics of the AC grid. Another AC filter is added between the AC and DC parts of the microgrid to improve the performance of the bidirectional and unidirectional converters and reduce the harmonics of the AC microgrid as well. The bidirectional converter that is connected between the supercapacitor and the AC side is used for charging the supercapacitor in the normal operation. During islanded operation, and when there is a communication failure, the bidirectional converter allows the supercapacitor to contribute to the fault current during the occurrence of a fault in AC side. The unidirectional converter is present to allow DC sources to support AC sources in feeding various loads in the microgrid. A relay and a circuit breaker is connected to each end of all transmission lines. CB11 and CB12 are connected at the terminals of the DC sources and provide the ability to connect and disconnect these sources.

F1 is applied to the system in order to isolate the microgrid from the grid, then another fault, F2, is applied on the islanded microgrid to investigate its performance with and without communication.

The super capacitor in Figure 4.1, which is connected through a bidirectional VSC to the AC microgrid, is of paramount importance for the role it plays in contributing to the fault current when the communication medium fails as will be explained in details later in this chapter. The super capacitor is of 2.9 F capacitance and it delivers high instantaneous power to the pulse load during the normal operation.

The AC side also feeds the pulse load in normal operation when the super capacitor bank is out of service. Finally, a fuel cell supplies different loads in the AC side using a unidirectional AC/DC converter in cases where the grid is disconnected from the system

and a fault is applied at the AC microgrid resulting in the disconnection of one or more generation units. Specifications of the system components are summarized in Table 4.1.

Table 4.1 System Component Parameters

Component	Parameter	Specification
Generator	S_N	7.5 KVA
	V_N	208 V
	F_N	60 Hz
	$X_{L(pu)}$	1.305
Transformer	Connection	Δ/Y_g
	S_N	7.5 KVA
	V_N	208 V
	$R_{eq,}\ X_{eq}$	0.72 Ω, 2.29 mH
Supercapacitor bank	Number of cells	20
	Rated voltage	320
	Rated capacity	2.9 F
	Surge voltage	340
	Leakage current	5.2 mA
AC filter 1	L_{AF}	4 mH
AC filter 2	L_{AF}	3 mH
AC filter 3	L_{AF}	0.4 mH
Transmission Line	$r_{1,}\ r_0$	0.0015 Ω/Km, 0.03 Ω/Km
	$l_{1,}\ l_0$	0.03 mH/Km, 0.1 mH/Km
	$c_{1,}\ c_0$	3 nF/Km, 2nF/Km

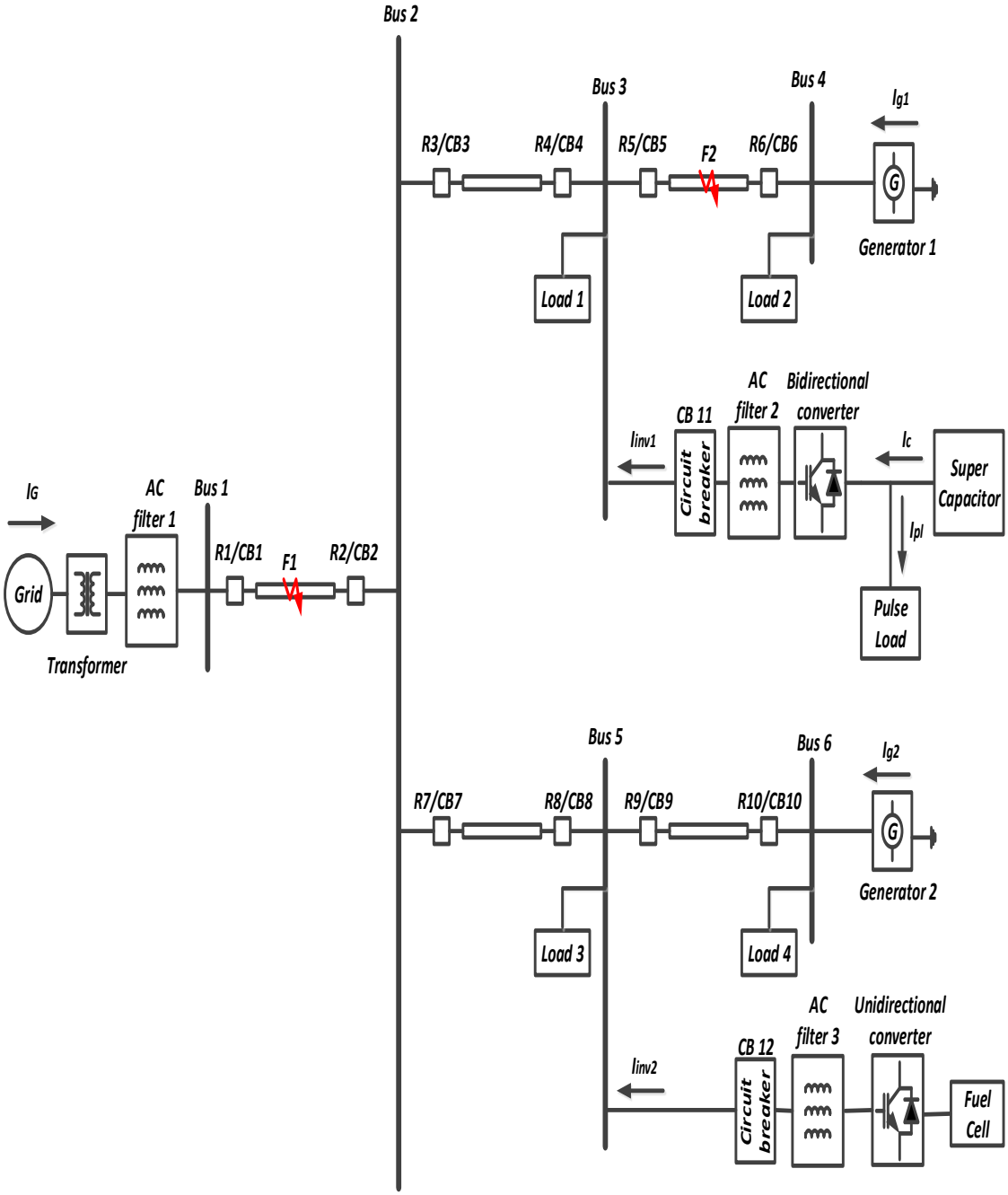

Figure 4.1 Microgrid under Study

4.3 Developed Protection Algorithm

This section describes the logic algorithm of the relays during the different modes of operation under study namely grid connected mode, islanded mode with communication, and islanded mode with loss of communication. As can be seen in Figure 4.2, the logic embedded into the relays in order to sense several of types of faults contains two settings of operation one corresponding to the Higher Setting and another corresponding to the Lower Setting. The higher setting operates at grid and islanded mode with loss of communication, while the lower setting is activated during the islanded mode with communication. Shifting between these two settings occurs as a result of a command signal coming from the point of common coupling (PCC) of the microgrid with the main grid through communication link which is referred to as "Islanded" in Figure 4.2. In the Higher Setting, the relay is configured to trip the circuit breaker at a high group of measured currents, whereas in the Lower Setting the relay is configured to trip the circuit breaker at a lower group of input currents.

For a viable practical implementation of the developed protection scheme, the commonly accepted IEC 61850 communication framework could be applied. This emerging international standard provides an efficient and reliable interoperability framework between different field devices in protection applications.

For that, the Generic Object Oriented Substation Event (GOOSE) messaging protocol will be utilized to send control messages from the PCC to the system's IEDs in order to shift their settings accordingly. IEC 61850 GOOSE messages are broadcast layer 2 messages of the OSI model that enable fast publish/subscribe message exchange between end devices within a quarter cycle. It is also important to realize the presence of Merging Units (MUs) at both ends of a transmission lines. These merging units will digitize current measurements

at the source and broadcast them over the designated network in the form of IEC 61850 Sampled Measured Values (SMV) messages. In this study, we are assuming that all IEDs and MUs are on the same local area network (LAN), however, special router configuration can be applied to exchange messages over wide area networks (WANs) [131].

The mathematical equations that can describe the developed protection technique is explained in the following part. Equation (4.1) gives the operation of the logic circuit of the relay at trigger high (I_{TH}) that represented higher settings, when the system operates at grid connected or at islanded mode when the communication fails.

$$I_{TH} = \begin{cases} 1 & (I_f \geq I_G + I_m) + (I_f \geq I_{SC} + I_m) \\ 0 & otherwise \end{cases} \quad (4.1)$$

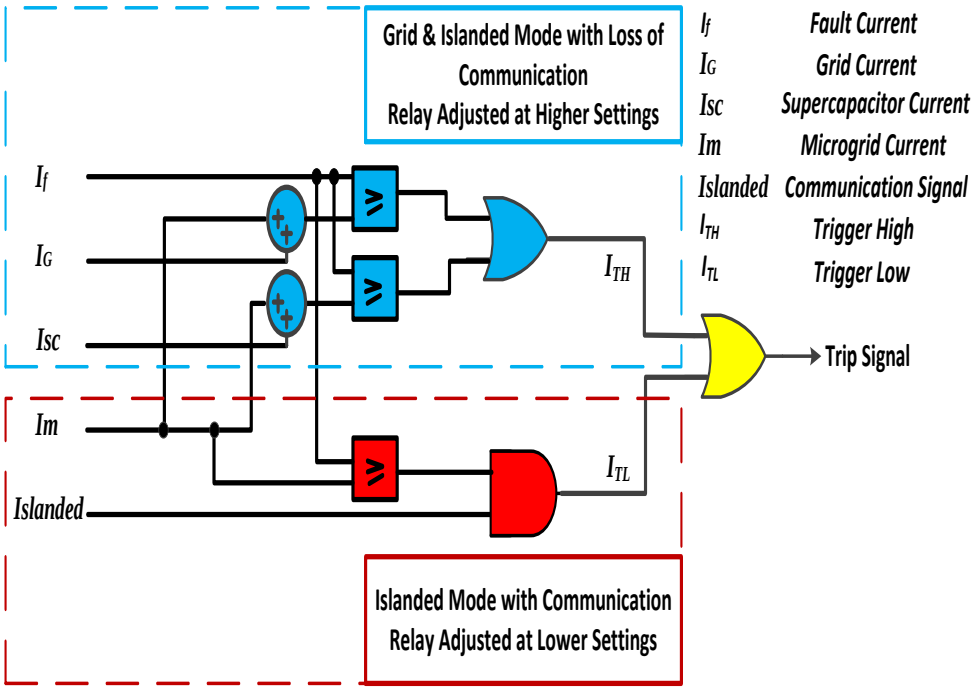

Figure 4.2 Logic Diagram of the High and Low Relay Settings

Equation (4.2) describes the logic of the relay at islanded mode of operation when the communication is available in the system. At this case, the relay will produce (I_{TL}) and adjusted at lower settings.

$$I_{TL} = \begin{cases} 1 & (I_f \geq I_m)\,.Islanded \\ 0 & otherwise \end{cases} \quad (4.2)$$

The relay will send a trip signal to the circuit breaker whether (I_{TH}) or (I_{TL}) achieved as indicated in equation (4.3):-

$$Trip\ signal = I_{TH} + I_{TL} \quad (4.3)$$

Figure 4.3 shows the flowchart of the developed protection algorithm. At grid connected mode, the current at each terminal of the transmission lines is measured. When the fault takes place at the microgrid, the fault can be cleared whether the relay settings is adjusted at high or low settings since the fault will be fed mainly from grid. If the fault occurred at the point of common coupling (PCC) with microgrid, the relay will a trip signal to the circuit breaker when ($I_f \geq I_G + I_m$) and isolate the fault zone. After that, the mode of operation changes to islanded, and the communication plays an important role to determine the relay settings level. When the communication is available, the relay can update its settings to lower settings and at fault clearing condition ($I_f \geq I_m$), the circuit breaker isolates the faulted part from the system. When the communication is lost, due to a cyber-attack for example, the relay remains at high settings and the previous condition is not satisfied. For this case and when the fault occurs, according to the type of fault, the current can be fed and relay reach to the setting value. If the applied fault was single line to ground fault, the microgrid can contribute to the fault current and the faulted zone is isolated from the system

In order to detect three or double phase to ground fault, the supercapacitor can compensate the required current to the relay and isolate the fault. Whether the supercapacitor's state is charging or discharging, it can feed the relay with the current and trip circuit breaker when ($I_f \geq I_m + I_{sc}$). The stability of the overall system is checked to ensure that the frequency and voltages at AC and DC sides are stable especially when the fault happened and pulsed load is turned on.

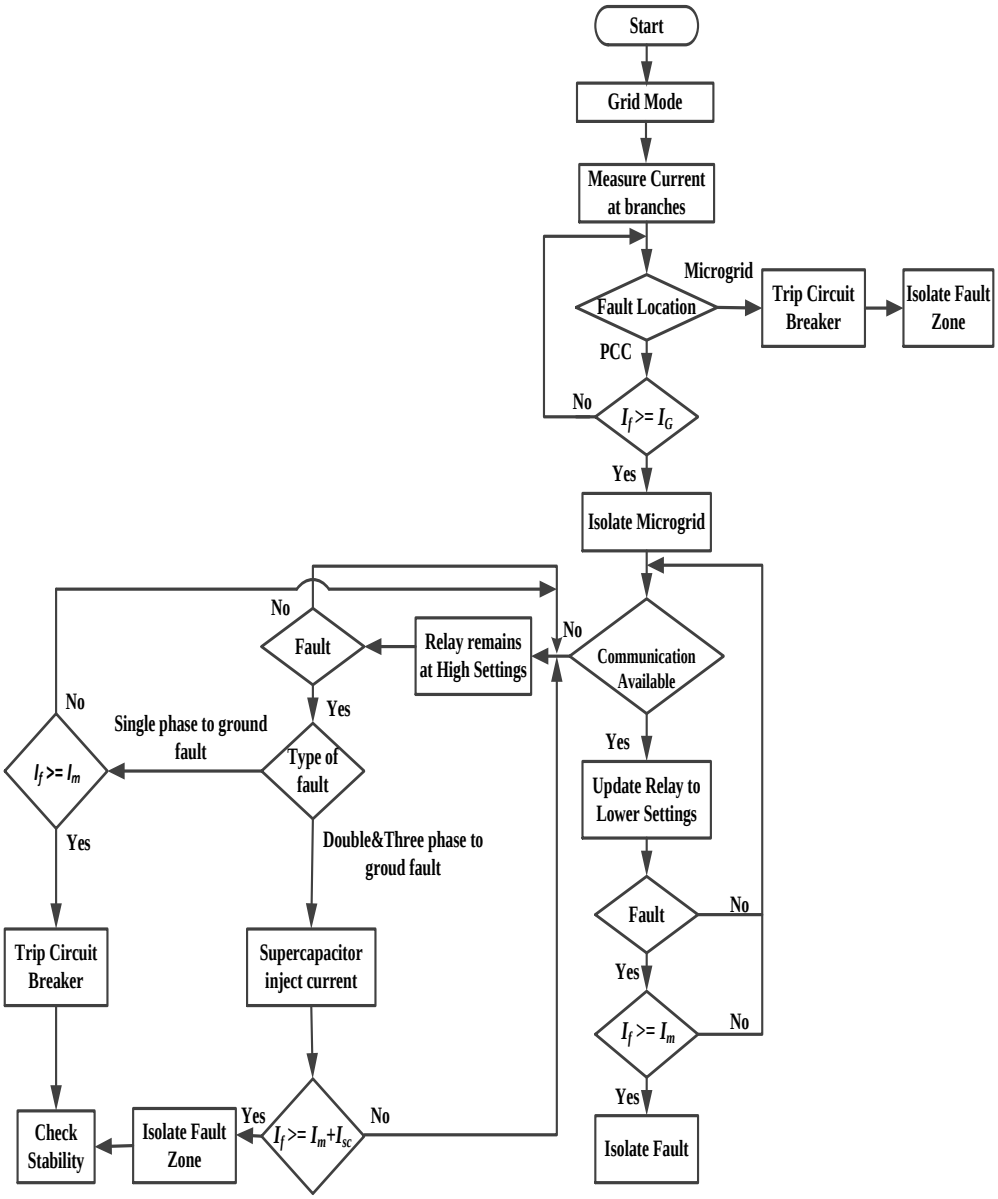

Figure 4.3 Flowchart of the Developed Protection Algorithm

4.3.1 Grid Connected Mode of Operation

The microgrid in this case is assumed to be operating in the grid connected mode. When a fault occurs in any of the transmission lines within the AC microgrid, high short-circuit currents are expected to flow in the place of the fault reaching values between 6-7 times of the rated current value. In this case, the relays are adjusted to the Higher Setting.

4.3.2 Islanded Mode of Operation

It is assumed here that the microgrid has been disconnected from the main grid due to a fault F1 shown in Figure 4.1. The microgrid is thus operating in islanded mode. The relay at the PCC senses this shift and issues a control signal to all relays to shift to the Lower Setting. The setting of the relays are therefore adjusted to be between 1.5-2 times of the rated current at this mode.

This is due to the fact that the microgrid cannot feed the fault with the same capacity as the main grid. Also the power electronic devices that are used for the fuel cell reduce the amount of the short circuit current.

Changing from the grid setting to the microgrid setting can be performed using the Islanded signal shown in Figure 4.2. Reliable communication between the PCC and the relays in the microgrid is therefore critical for shifting between relay settings for proper location and isolation of the fault.

4.3.3 Islanded Mode of Operation with Loss of Communication

The system configuration here is the same as that in B, however, it is assumed that communication is lost between the PCC and the microgrid's relays. Therefore, the settings of the relays will not shift to the proper setting (Lower Setting) and will render them unable

of sensing faults. In this event, energy storage devices can be added to solve the problem of communication failure.

Loss of communication in a system is when a system's components that act control commands stop responding to commands or behave in unconventional ways due to a system malfunction or a malicious cyber-attack [132].

In fact, as explained in [132], loss of communication may be due to several reasons like failure of communication equipment, such as a network switch, or noise on a communication channel causing transmission errors or data unavailability. Communication might also be lost due to a failure in of central systems (e.g. servers) at substations and microgrids control centers causing unreliable sending and reception of control signals.

Last but not least, loss of communication might be due to malicious efforts such as cyber-attacks. A denial of service (DoS) attack is when the attacker attempts to prevent authorized users or machines from accessing a service. One way of doing this is to disrupt or exploit the services of the relay.

In adaptive protection operations, a DoS attack might disrupt the operation of IEDs by transmitting malicious code to the targeted IED or IEDs that writes over-sized data to cause a buffer overflow [133]-[134].

The attacker can choose to exploit common services on a relay. They can do this by opening multiple sessions on either the File Transfer Protocol (FTP), or Telnet services and keeping them idle all the time preventing the relay from responding to critical grid events such as protection. It is also explained in [134] that DoS could be the result of a

flooding attack to delay message delivery past the critical flooding rate by congesting the channel and exhausting the computation resources of the communicating nodes.

When the communication fails in the islanded mode of operation, the setting of the relay is not adjusted to the lower setting and the relay is adjusted to trip at higher setting. The capability of the islanded microgrid is not enough to reach to this setting.

A supercapacitor bank is used to solve this problem. This supercapacitor bank can compensate for the difference between the grid and islanded mode and will contribute to the fault current raising it to a value which is sensed by the high relay setting detect and isolate the fault. Therefore, the developed protection algorithm will be able to survive communication failures.

4.4 Control of Supercapacitor-Based Microgrid

4.4.1 Supercapacitor-Pulse Load Microgrid

A supercapacitor is a storage device which is capable of storing electrical energy directly between two conducting electrodes. The capacitance and energy density of a supercapacitor are thousands of times larger than a conventional electrolytic capacitor. A supercapacitor is also known as a double-layer capacitor since it can store energy across the double layers formed at the interface between an electronically conducting carbon and the electrolyte. A supercapacitor is known to have high power density, low internal resistance, and high life cycle [135]-[137]. In order to increase the energy density of a supercapacitor, high surface-area materials such as activated carbon are used. High power energy storage is commonly used in many systems such as telecommunications, shipboard and spacecraft power systems. In these applications, there are various types of loads that

show high instantaneous power requirement but require a relatively low average power. These types of loads are referred to as pulse loads. The duration of such loads ranges typically from hundreds of milliseconds to seconds with different power levels. In microgrid applications, the high instantaneous power of a pulse load can cause considerable power disturbances and thermal problems. Introducing a fast response high power storage system, such as a supercapacitor bank, with the appropriate power electronic and control, will improve the performance of the system drastically [138]-[141].

Besides the function of the supercapacitor in the normal operation for supplying the pulse load, it has been used in this chapter to enhance the protection system resiliency to communication failures. The control scheme of the microgrid has been modified to allow the supercapacitor to contribute the fault current while there are no enough resources to feed the fault current, which is the case of the microgrid's islanded mode of operation. This is useful in case the protection algorithm is unable update relays' setting due to communication failure as discussed earlier.

4.4.2 Autonomous Control of Supercapacitor AC/DC Converter

The supercapacitor is typically designed to supply a periodic pulse load in a system. This supercapacitor is coupled with the AC side through a bidirectional AC-DC voltage source converter (VSC) as indicated in Figure 4.4 An improved control algorithm with only one mode of operation has been developed in this chapter to allow the microgrid to work properly during the normal and faulty operations whether in grid-connected on islanded mode of operation. Thus the controller needs not to rely on any communication signal to detect the mode of operation of the microgrid as it is autonomous in nature. In the normal operation, the supercapacitor will charge from the AC side during the off-time pulse load,

and then discharge during the on-time pulse load to supply the load demand. Moreover, the controller is designed to allow the DC microgrid to regulate the AC side frequency and voltage during the islanded mode of operation.

During the faulty operation, the controller will direct the microgrid to enhance the system stability and will help the system restore after isolating the fault. This is the controller's role if either the system has enough resources to supply the fault current such as grid-connected operation, or the protection relays were able to update their settings based on data communication. In case of the system does not have enough resources and the communication was unavailable, the controller will force the microgrid to compensate the fault current and achieve fault isolation. This function will enhance the protection system resiliency against communication failures.

The details of the control scheme are indicated in Figure 4.4 Two control loops are implemented for active and reactive power flow control to achieve both frequency and voltage regulation. The supercapacitor reactive power is controlled, based on I_{q_r}, to keep the AC side voltage at a specified value using a PI controller. The active power reference component (I_{d_r}) is generated using two PI controllers. The first is responsible for regulating the AC side frequency to be within the acceptable limit, whereas the second is used to keep the supercapacitor DC voltage within the specified level. Using the AC side frequency as a signature to the active power flow allows the supercapacitor to supply large currents during the fault and contribute to the fault current during loss of communication situations.

Based on the inverse Park transformation the reference three phase currents (I_{a_r}, I_{b_r}, and I_{c_r}) are estimated from the *dq0* rotating reference frame currents. The angle between the two reference frames and the system frequency are estimated from three-phase Phase Locked Loop block (PLL). The *abc* reference currents are compared with the actual measured currents and applied to the pulse width modulation (PWM) scheme to generate the switching signals of the inverter. The hysteresis band current control is considered in this work because of its simplicity of implementation and fast response current loop. It also doesn't need any knowledge of the load parameters [142]-[143].

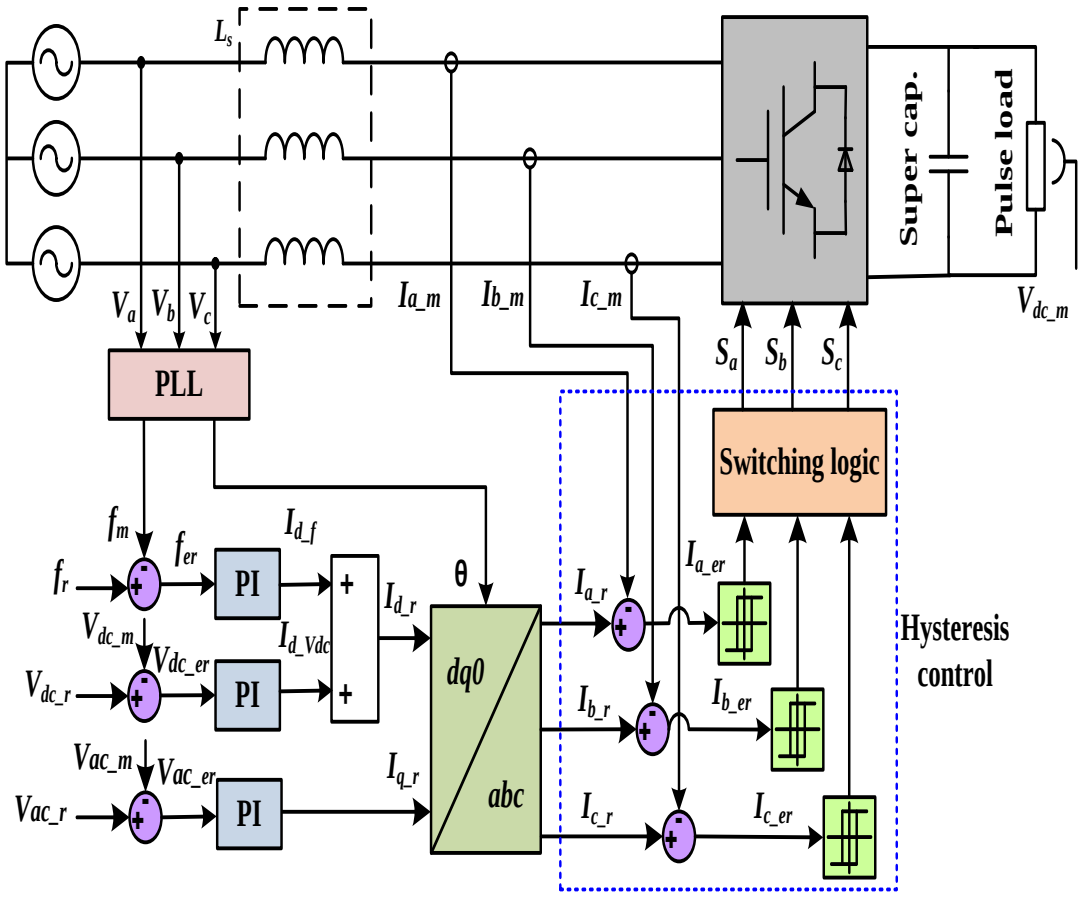

Figure 4.4 Autonomous AC/DC Converter Controller

Mathematical formulation of the suggested control to achieve the protection scheme can be explained in the following formulas:-

Frequency error (f_{er}) is the difference between the reference (f_r) and measured frequency (f_m):-

$$f_{er} = f_r - f_m \tag{4.4}$$

Equations (5), (6) described the AC and DC voltage errors.

$$V_{dc\_er} = V_{dc_r} - V_{dc_m} \tag{4.5}$$

$$V_{ac\_er} = V_{ac\_r} - V_{ac\_m} \tag{4.6}$$

The frequency error introduced to PI controller with k_{p_f} and k_{i_f} parameters and produced direct current component for regulating the system frequency.

$$I_{d\_f} = f_{er} \times \frac{k_{p\_f}s + k_{i\_f}}{s} \tag{4.7}$$

The error in DC and AC voltages controlled by PI controller and produced the required direct current component to regulate them as shown in equations (4.8), (4.9):-

$$I_{d\_Vdc} = V_{dc_{er}} \times \frac{k_{p\_Vdc}s + k_{i\_Vdc}}{s} \tag{4.8}$$

$$I_{q\_r} = V_{ac\_er} \times \frac{k_{p\_Vac}s + k_{i\_Vac}}{s} \tag{4.9}$$

The output of the controller of frequency and DC voltage are combined together and produce the reference of direct current (I_{d_r}):-

$$I_{d\_r} = I_{d\_f} + I_{d\_Vdc} \tag{4.10}$$

Equation (4.11) described the transformation from dq to abc frames:-

$$\begin{bmatrix} I_{a\_r} \\ I_{b\_r} \\ I_{c\_r} \end{bmatrix} = \begin{bmatrix} \cos\theta & \sin\theta & 1 \\ \cos(\theta - 120) & \sin(\theta - 120) & 1 \\ \cos(\theta + 120) & \sin(\theta + 120) & 1 \end{bmatrix} \begin{bmatrix} I_{q\_r} \\ I_{d\_r} \\ I_0 \end{bmatrix} \tag{4.11}$$

The error of the current signals in three phase current (I_{abc_er})is the difference between the reference (I_{abc_r}) and the measured values (I_{abc_m}).

$$I_{abc\_er} = I_{abc\_r} - I_{abc\_m} \tag{4.12}$$

I_{abc_er} is feed to Hysterises current controler to track the current reference I_{abc_r}

4.5 Results and Discussion

This part introduces the results of the developed protection technique at grid connected mode when the communication is available in the system. Also, several cases at the islanded mode operation is disuses when the communication is healthy or attacked in the system.

4.5.1 Simulated Cases

Case 1:- Grid Connected Mode of Operation

In this case a three-phase to ground fault (F2 in Figure 4.1) has been applied in the transmission line between busses 3 and 4 while the microgrid was in grid connected mode of operation. The system performance during this fault is indicated in Figure 4.5.

As it can be noticed, the fault occurred at t = 6 seconds and cleared instantaneously. In this case, the utility helped to maintain the system's frequency stable during and after the fault, as shown in Figure 4.5(a).

Figure 4.5(b) shows the pulse load (I_{pl}), supercapacitor (I_c), and inverter (I_{inv1}) currents. During the off-time pulse load, the capacitor will be charging from the AC side, whereas during the on-time pulse load the supercapacitor will be the major feeder to the pulse load, as indicated in Figure 4.5(c).

The AC side will still be present to feed the pulse load in case the supercapacitor went out of service. Figure 4.5(d) and (e) show the high fault current values of 32 Amps which is mainly being contributed to by the grid.

As anticipated for the grid connected mode, the fault current is almost more than 6 times the rated AC current and thus the protection devices where able to detect and isolate the faults successfully.

Case 2:- Islanded Mode of Operation with Communication

In this situation, a three-phase-to-ground fault (fault F1 in Figure 4.1) occurred at time t = 1.5 seconds, in the transmission line connecting the main grid to the microgrid under study. As a result, relay R1 will send a trip signal to circuit breaker CB1 to isolate the microgrid.

The microgrid successfully shifted to a stable islanded mode by adjusting its overall frequency back to the normal condition after fault, as shown in Figure 4.6(a).

A small disturbance, within acceptable limits, in the output voltages of the sources (V_G, V_{g1}, V_{g2}, V_{inv1} and V_{inv2} representing the voltages at busses 1, 4, 6, 3 and 5, respectively), is noticed in Figure 4.6(b).

Figure 4.6(c) shows a spike in I_G due to the fault and this current drops to zero after clearing the fault by disconnecting the microgrid. An increase in the generator's currents (I_{g1} and I_{g2}) is noticed in order to compensate for the current which was previously supplied mainly by the grid.

Figure 4.6(d) and (e) show the supercapacitor-pulse load microgrid performance parameters which exhibit stable performance during the islanding instant.

Finally, Figure 4.6(f) and (g) indicate the minor change in the AC current at transmission line connecting busses 3 and 4 after the fault.

During the islanded operation, another three-phase-to-ground fault occurred at t = 6 seconds, in the middle of transmission line connecting buses 3 and 4.

Based on the available communication infrastructure in the system, relay R5 settings is adjusted to the lower setting and thus was capable of detecting the fault and tripping CB5 accordingly. Figure 4.6(a) shows the microgrid frequency recovery after the fault incident.

As can be noticed the system is showing stable performance during and after the fault with disturbances within the specified limits of microgrids operation.

The sources voltages V_{g2}, V_{inv1} and V_{inv2} dropped at the fault incident and recovered after clearing the fault, as shown in Figure 4.6(b).

After the fault was cleared, Figure 4.6(c) shows that I_{g1} dropped to zero since generator G1 was isolated from the system. Current I_{g2} increased to feed the loads accordingly.

It can be noticed in Figure 4.6(d) and (e) that the supercapacitor was not used to feed the fault current due to the adaptation process for R5 setting to its lower setting.

Figure 4.6(f) and (g) show that the AC current in transmission line where fault F2 occurred increased significantly from 5 to 12 A during the fault instance.

It can be noticed also, that the fault current level is less than that appeared in the grid connected mode (32 A) as was discussed earlier.

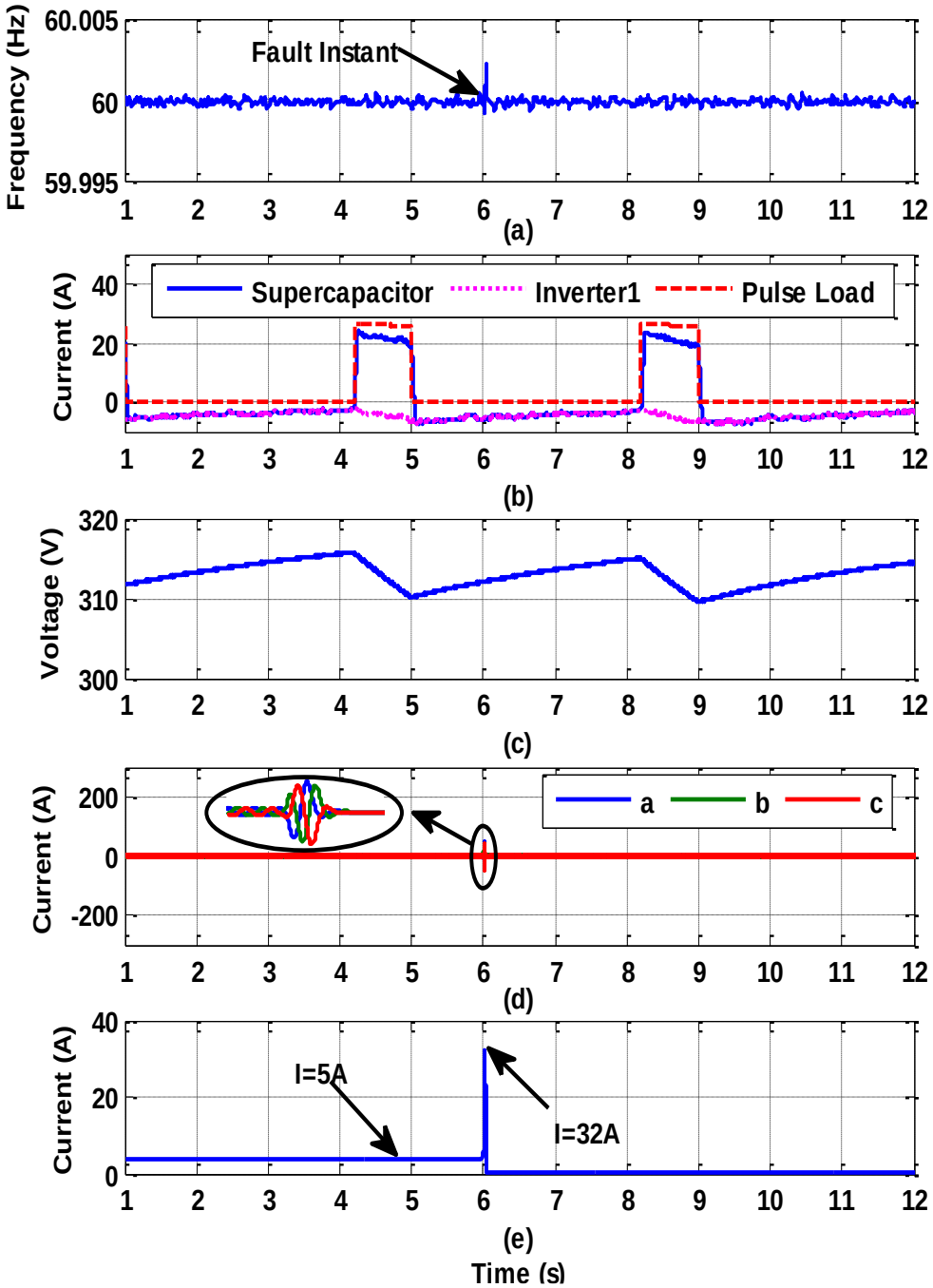

Figure 4.5 System performance during fault at grid connected mode of operation: (a) frequency, (b) supercapacitor current, inverter current, and pulse load current, (c) supercapacitor DC voltage (d) three-phase currents in the faulted transmission line, and (e) RMS current in the faulted transmission line

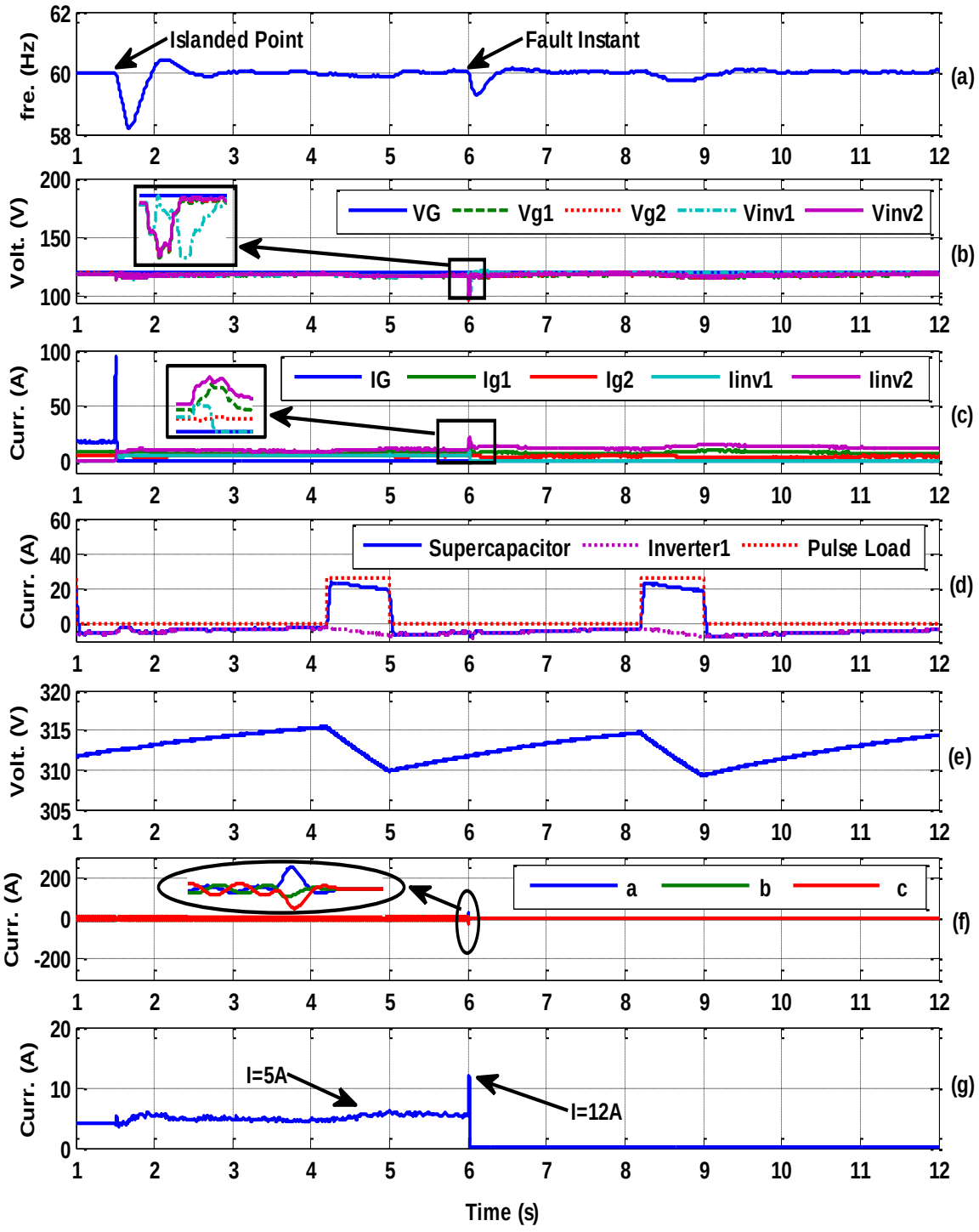

Figure 4.6 System performance during fault at microgrid operation with communication (a) frequency, (b) output voltage of each source, (c) output current of each source, (d) supercapacitor current, inverter1 current, and pulse load current,, (e) supercapacitor DC voltage, (f) three-phase current in the faulted transmission line, and (g) RMS current in the faulted transmission line

Case 3:- Islanded Mode of Operation without Communication during Supercapacitor Charging

In this case, fault F2 occurred during the off-time of the pulse load (i.e. charging of the supercapacitor). Due to the assumption of the communication failure, relay R5 will not be able to switch to the lower settings. In this case, as shown in Figure 4.7(b), the supercapacitor compensate the fault current until it reach to the higher setting of the relay (32 A) as indicated in Figure 4.7(c). This resulted in relay R5 sensing the fault and thus isolating it accordingly. After clearing the faulted region the system restored and shows stable performance.

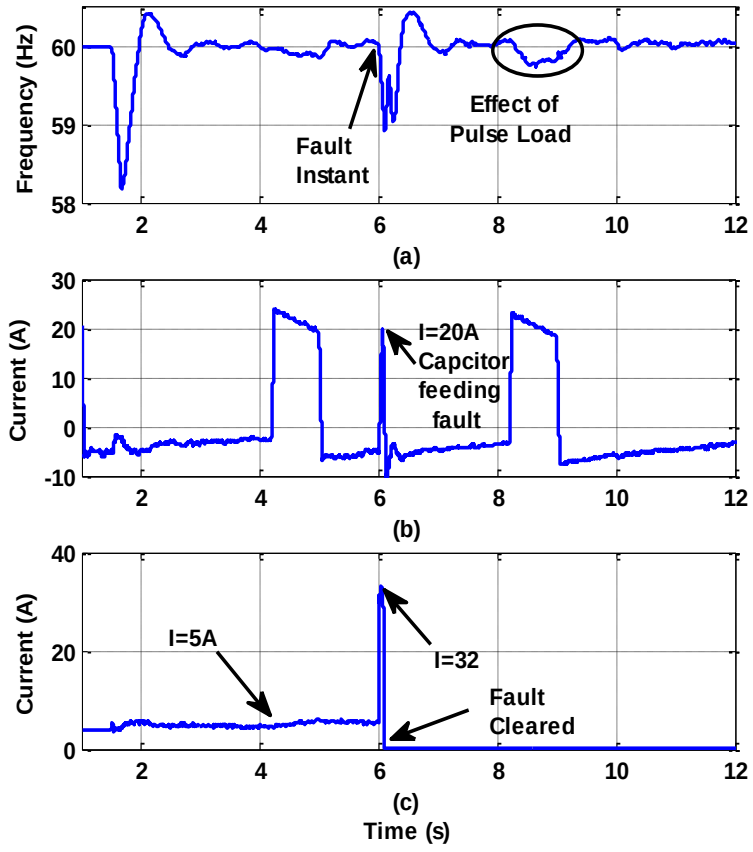

Figure 4.7 System performance during fault at microgrid operation without communication (a) frequency, (b) supercapacitor current, and (c) RMS current in the faulted transmission line

Case 4:- Islanded Mode of Operation without Communication during Supercapacitor Discharging

4.1 Oversized Supercapacitor to Feed the Fault and Pulse Load Currents

This solution is recommended in case of critical pulse loads that cannot accept any instantaneous supply interruption. In this case, the supercapacitor needs to be designed to supply both the pulse load and the fault current requirements. The system performance during a fault F2 at this circumstances is described in Figure 4.8. As indicated in Figure 4.8(b), the fault occurred during the discharging of the supercapacitor phase of the pulse load period. It is noted that due to communication failure, relay R5 will not switch to the lower settings and the supercapacitor quickly contributed to the fault current while still covering the pulse load as reflected on the pulse load current in Figure 4.8(c). The maximum current drawn from the supercapacitor in this case is 45 Amps which is required to feed the fault and the pulse load simultaneously. Figure 4.8(d) shows that the fault current drastically increased from 5 Amps to 32 Amps. This resulted in relay R5 sensing the fault and thus isolating it accordingly as explained in the normal condition.

4.2 Disconnecting the Pulse load during the Fault

This section presents the cheap solution of this problem which is useful in case of the pulse load can accept the instantaneous power interruption. Similar to the previous case, fault F2 occurred during the on-time period of the pulse load. It is noticed in Figure 4.9(b) that, due to communication failure relay R5 will not switch to the lower settings and the supercapacitor quickly contributed to the fault current. However, in this case, the pulse load

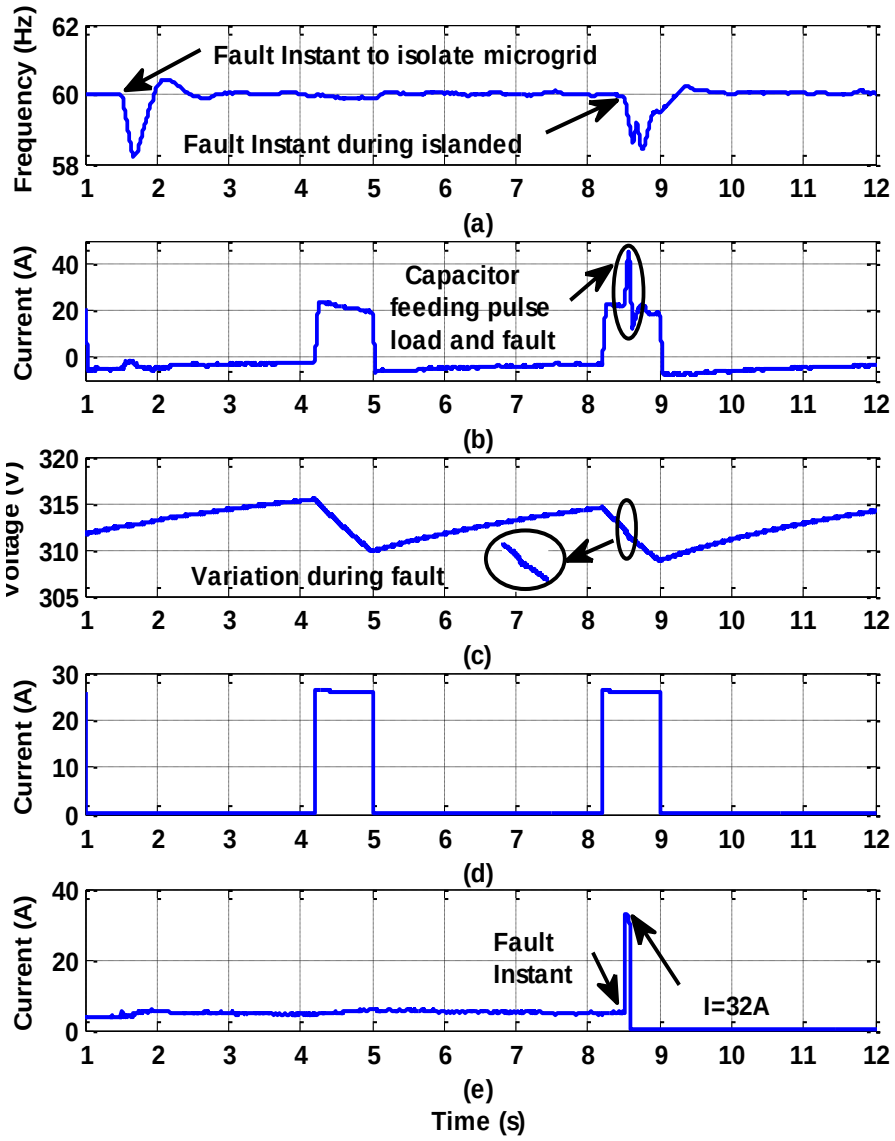

Figure 4.8 System performance during fault at microgrid operation without communication (a) frequency, (b) supercapacitor current, (c) supercapacitor DC voltage, (d) pulse load current, and (e) RMS current in the faulted transmission line

was disconnected for a short period of time during the fault in order to reduce the amount of current drawn from the supercapacitor which reached a maximum of 27 Amps in this case. To disconnect the pulse load, the rate of change of the supercapacitor's voltage was monitored to detect a small notch in the DC voltage indicating the fault as shown in Figure 4.9(c). This in fact does not depend on any communication command or any conventional

change in frequency or AC voltage signature. The pulse load interruption is described in Figure 4.9(d). Figure 4.9 (e) shows that the fault current drastically increased from 5 Amps to 32 Amps. It is worth to mention that this solution is applicable to some types of uncritical loads. However, critical pulse loads, that cannot be disconnected and thus will fall into the category explained in section D.1.

These pulsed loads could be present on ship power systems, which can be electrically treated as islanded microgrids as indicated in [144]. Additionally, pulsed loads do exist in regular power system microgrids (other than ships).

These pulsed loads could be large cranes, radar systems, welding machines or an electric vehicle park with simultaneous fast charging of large number of vehicles [145].

4.5.2 Performance Evaluation of the Developed Protection Schemes under Different Types and Magnitudes of Fault Currents.

The numerical figures in the first row of Table 4.2 represent the results of different case studies discussed earlier at three phase to ground fault (ABCG) with 2 Ω fault resistance. The results of the various modes of operation of the microgrid with and without communication discussed above for different types of faults with varying fault resistances at the transmission line that connecting between buses 3 and 4 (F2) are then shown in the subsequent rows.

For the case of a three- phase-to-ground fault, a significant decrease in the current drawn from the supercapacitor was observed when the pulse load was disconnected during the fault period (from 95.65% to 17.39% in the 2Ω fault resistance case and from 43.47% to 8.69% in the 4Ω fault resistance case).

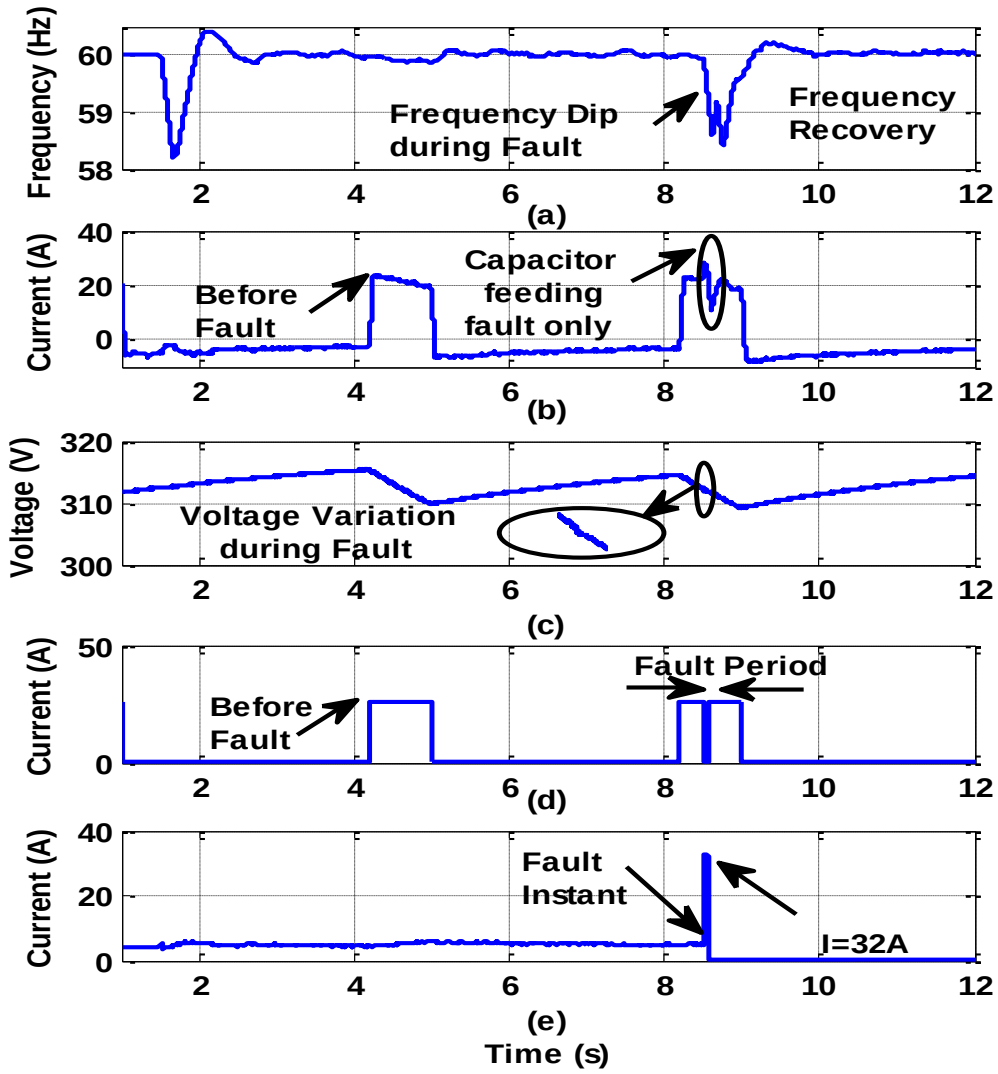

Figure 4.9 System performance during fault at microgrid operation without communication (a) frequency, (b) supercapacitor current, (c) supercapacitor DC voltage, (d) pulse load current, and (e) RMS current in the faulted transmission line

Similarly, in the case of a double-line-to-ground fault (BCG), a decrease in the current drawn from the supercapacitor was observed when the pulse load was disconnected during the fault period (from 78.26% to 13.04% in the 2Ω fault resistance case and from 56.52% to 4.3% in the 3Ω fault resistance case). Therefore, the temporary disconnection of the pulse load, whenever possible, during fault period. That is, when the pulse load is disconnected, the supercapacitor will only be feeding the load. This will not incur any

additional costs on the system to install bigger capacitors than the ones already present to protect the system. It is noted that in the formal two faults, the resources in the microgrid without the supercapacitor were incapable of feeding enough current to the fault for the relays to detect it in case of communication failure. This shows that the developed solution of utilizing a supercapacitor does indeed enhance the reliability of the protection scheme in case of loss of communication. Finally, the AC microgrid generating units were capable of feeding sufficient fault current for fault detection in the case of a single-line-to-ground fault (AG) without assistance from the supercapacitor. This is because the currents produced from this type of faults are usually smaller than the previous fault types. We can see from the table 4.2 that the current drawn from the supercapacitor did not increase in this case.

Table 4.2 Performance of the protection scheme under different types of faults

Fault Type	R_f (Ω)	RS Csae 1	RS Case 2	Case 3			Case 4						I_{PL}(A)	ΔI_c Case 4.1 (%) *	ΔI_c Case 4.2 (%) *
							Case 4.1			Case 4.2					
				I_c(A)	I_m(A)	RS (A)	I_c(A)	I_m(A)	RS (A)	I_c(A)	I_m(A)	RS (A)			
ABCG	2	32	12	20	12	32	45	12	32	27	12	32	23	95.65	17.39
	4	22	10	10	12	22	33	12	22	25	12	22	23	43.47	8.69
BCG	1.8	30	10	15	15	30	41	15	30	26	15	30	23	78.26	13.04
	3	21	8	10	11	21	36	11	21	24	11	21	23	56.52	4.3
AG	0.1	18	8	0	18	18	23	18	18	23	18	18	23	0	0
	1	12	6	0	12	12	23	12	12	23	12	12	23	0	0

4.5.3 Analysis on Sizing and Cost of the Supercapacitor

In order to accommodate for a worst case scenario of having the supercapacitor feed the pulse load (P_{pl} =V_{dc}*I_{pl} =320*23=7.3Kw), as well as the fault current when the pulsed load is turned on, the following criteria was taken into account when sizing the supercapacitor:

The energy supplied by supercapacitor is calculated using the following equation:

$$E = P_{nom} * t_{max} \tag{4.13}$$

Where P_{nom} is the nominal power that can be injected from the supercapacitor at the worst case when the generators and fell cell are not operated and when the pulse load is turned on during the fault at the point that is far from the supercapacitor between buses 5 and 6 in Fig. 1, $(P_{nom} = 40Kw)$. t_{max} is the time that the supercapacitor feeds the pulsed load $(t_{max} = 0.8\ Sec.)$.

$$E = (40\ kw * 0.8)/(60 * 60) = 8.8\ Wh \tag{4.14}$$

According to reference [146], the capacitance of the supercapacitor is determined using equation (14):

$$E = \frac{1}{2} C\ (V_{max} - V_{\min})^2 \tag{4.15}$$

Where Vmax is the maximum voltage of a supercapacitor bank during a pulse load and Vmin is its minimum voltage.

$$8.8 = \frac{1}{2} C\ (314 - 311.5)^2 \tag{4.16}$$

$$C = 2.9F \tag{4.17}$$

It can be noted that this capacitance can feed the fault when the pulsed load is turned on. In order to give more analyses on the cost of the developed algorithm, the cost of the

supercapacitor of this case is added and compared with the case of turning on the pulsed load at the event of a fault.

The commercial price of the supercapacitor Model BMOD0058-E016-B02 manufactured by Maxwell [147], is $122.25. The number of modules that are used are 20 modules. The storage energy per module is 2.1 WH.

The cost of the supercapacitor is 122.25$ * 8.8/2.1=512.28$

When the pulsed load is turned off and a fault happens, the required power that can be injected by the supercapacitor will decrease thus reducing its size and cost consequently.

$$E = (32.7\ kw * 0.8)/(60 * 60) = 7.3\ Wh \tag{4.18}$$

$$7.3 = \frac{1}{2} C\ (314 - 311.5)^2 \tag{4.19}$$

$$C = 2.3F \tag{4.20}$$

The cost of the supercapacitor in this case is 122.25$ * 7.3/2.1=$424.96

Thus, the cost will be reduced by 17.04% and the capacitance of the supercapacitor will also be reduced by 20.68% when the pulse load is turned off during the fault.

4.6 Summary

This chapter gave details on an adaptive protection scheme for AC microgrid systems, which was capable of surviving communication failures by utilizing energy storage devices. This was done using a supercapacitor bank in particular, to contribute enough fault current when the protection relays fail to switch to lower settings. This chapter also give a new design of an autonomous control algorithm for a supercapacitor's AC/DC converter capable of operating when the microgrid is in both grid-connected and islanded

mode. It was shown that the converter's single mode of operation eliminates the reliance on the communicated control command signals to shift the controller between the microgrid's grid-connected and islanded modes of operation. In all simulated cases, the system was able to maintain stable voltage and frequency levels even during extreme cases, such as the occurrence of a fault during a peak pulse load period. Several types of faults were simulated, and the results demonstrated the resiliency of the developed protection algorithms against communication outages. It was also shown that, whenever possible, if the pulse load is disconnected temporarily during the fault period, the supercapacitor will feed only the fault current. Therefore, in these practical situations, no additional costs are incurred in the system, as there will be no need to install larger supercapacitor banks than those already present in the microgrid.

Chapter 5 Utilization of Supercapacitors in Protection Schemes for Resiliency against Communication Outages: A Case Study on Size and Cost Optimization

5.1 Introduction

Microgrids are gaining increasing attention as an important part of the smart grid due to their numerous benefits and their ability to operate both in islanded and in grid-connected modes [148]-[149]. While such a diverse deployment of microgrids provides some important advantages, they introduce key challenges in terms of protection. Microgrids are dynamic entities, where distributed generation, loads, and Energy Storage Devices are constantly connected and disconnected [150]-[151].

For instance, adaptive protection techniques used for a microgrid rely on a stable communication link to and from protective devices, at the PCC, to adjust the settings within these corresponding devices for either a grid-connected or islanded mode of operation. However, during communication outages or in the event of a cyberattack, relays' settings are not changed. Thus adaptive protection schemes are rendered unsuccessful. Due to their fast response, supercapacitors, which are present in the microgrid to feed pulsed loads, could also be utilized to enhance the resiliency of adaptive protection schemes against communication outages. Proper sizing of the supercapacitors is therefore important in order to maintain a stable system operation and the cost of the protection scheme.

This chapter presents a two-level optimization scheme for minimizing the supercapacitor size along with optimizing its controllers' parameters. The latter will lead to a reduction of the supercapacitor fault current contribution and an increase in that of other AC resources in the microgrid in the extreme case of having a fault occurring simultaneously with a

pulsed load. It was also shown that the size of the supercapacitor can be reduced if the pulsed load is temporary disconnected during the transient fault period. Simulation results showed that the resulting supercapacitor size and the optimized controller parameters were feeding enough fault currents for several types of faults in different locations and minimizing the cost of the protection scheme.

In this chapter, an adaptive protection scheme for AC microgrids, which is capable of surviving communication failures by the aid of supercapacitor is developed for enhancing the resiliency of adaptive protection to communication outages. In the normal case, the PCC senses a microgrid's shift to the islanded mode and thus issues a control command to the corresponding relays to shift their settings from high (which is between 6-7 times the rated current value) to low (which is between 1.5-2.5 times the rated current value). However, during communication outages, this process is not possible and thus relay settings remain high in the islanded mode of operation [152].

Therefore in such situations, due to their fast responses, supercapacitor can be utilized to contribute to the fault current and raise this current value to a level, which is sensed by the high relay settings. However, attention must be paid as not to oversize the utilized supercapacitor and therefore incur additional costs on the overall system. As such, this chapter extends our previous chapter by proposing a two-level optimization scheme for minimizing the supercapacitor size along with optimizing its controllers' parameters to reduce its fault current contribution and increase that of other AC resources in the microgrid. In order to ensure that the optimization process will converge to a sufficient supercapacitor size, this chapter addresses the extreme case where a three-phase-to-ground fault occurs during the turn-on period of a pulsed load. The work in this chapter also shows,

in a case study, that the size of the supercapacitor can be reduced if the pulsed load is temporarily disconnected during the transient fault period. All investigated cases, in simulation, showed that the optimization process did indeed reduce both the size and the cost of the supercapacitor bank, as well as maintain stable system operation.

5.2 Hybrid AC/DC microgrid description

Figure 5.1 shows the topology of the hybrid AC/DC microgrid under study. The system has grid connection capabilities and contains two ac generators of 7.5 KVA, 60 HZ, 208 V and 1800 RPM synchronous machines coupled to individual induction motors as prime movers. A three-phase 7.5 KVA Δ/Yg transformer was implemented to feed the AC microgrid with the required rated voltage. The system has a filter located between the transformer and the AC microgrid to filter out the harmonics of the AC grid with the inductance of 4 mH.

Another AC filter was added between the AC and DC parts of the microgrid to improve the performance of converters 1 and 2 and reduce the harmonics of the AC microgrid as well. The supercapacitor bank is 2.9 F with rated voltage of 320 V to feed a 12-Ω DC resistive pulsed load. A DER is also used to inject current to the AC side and helps the generators feed different loads that are connected with circuit breakers at this side. Converter 1 that is connected between the supercapacitor and the AC side is used for charging the supercapacitor in the normal operation. Also, the supercapacitor injects current to the AC side during fault condition in the islanded mode of operation when the communication is not available. Converter 2 is present to allow the DER to support the AC sources in feeding various loads in the microgrid. A relay and circuit breaker is connected

at each end of all transmission lines. CB_11 and CB_12 are connected at the terminals of the DC sources and provide the ability to connect and disconnect these sources.

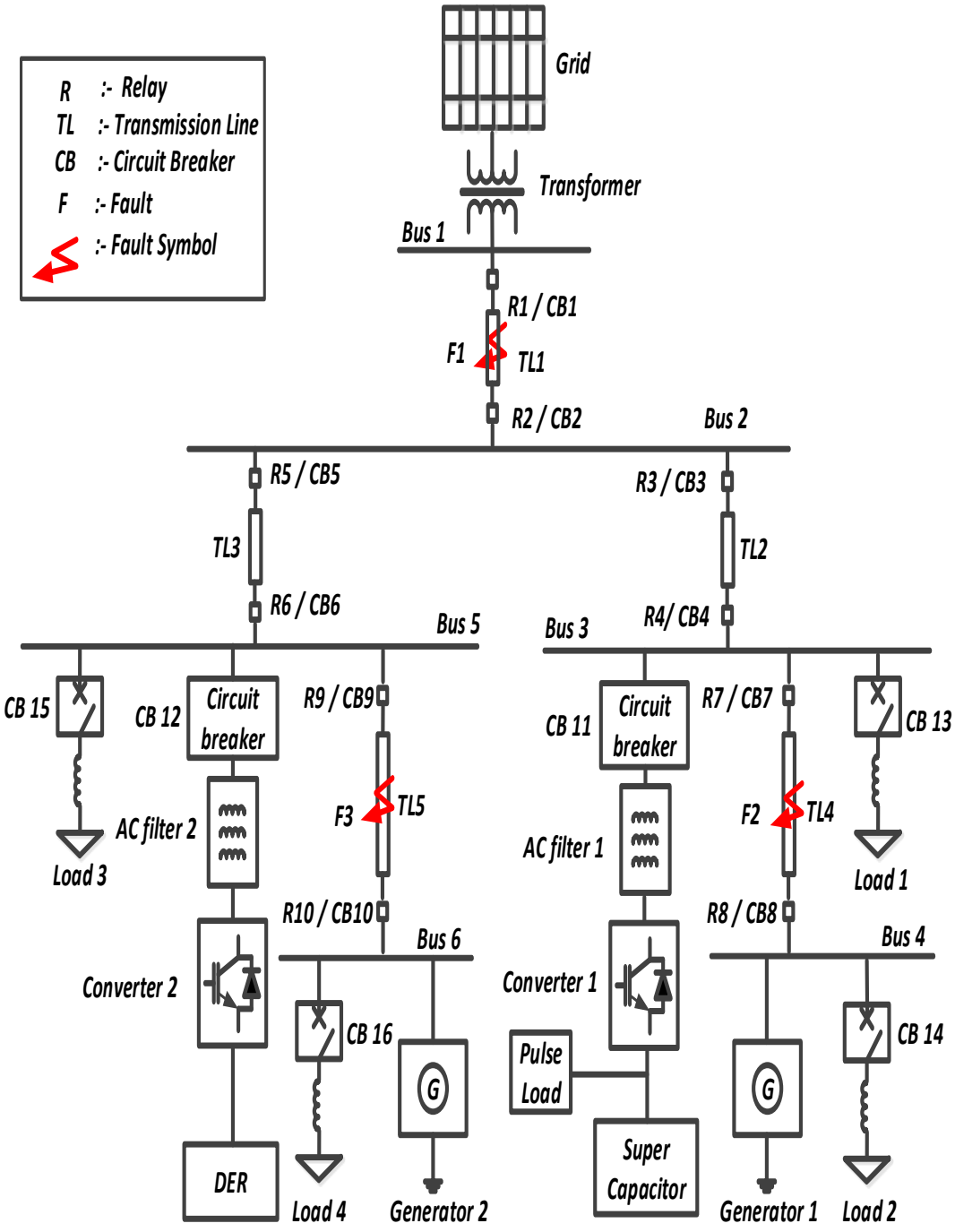

Figure 5.1 Configuration of the microgrid under study.

5.3 Developed Protection Algorithm

The logic algorithm of the relays during the different modes of operation under study, namely grid connected mode, islanded mode with communication, and islanded mode with loss of communication, is shown in Figure 5.2, and can be described in the following equations.

Equation (5.1) gives the operation of the logic circuit of the relay at trigger high (I_TH) that represents high settings, when the system operates at grid connected or at islanded mode with communication failure.

$$I_{TH} = \begin{cases} 1 & (I_f \geq I_G + I_M) + (I_f \geq I_{SC} + I_M) \\ 0 & otherwise \end{cases} \quad (5.1)$$

Where (I_f is the fault current, I_G, I_M and I_{SC} are the current contributions from the grid, microgrid, and supercapacitor, respectively.

Equation (5.2) describes the logic of the relay at the islanded mode of operation when the communication is available in the system.

In this case, the relay will produce (I_TL) and will be adjusted to low settings.

$$I_{TL} = \begin{cases} 1 & (I_f \geq I_m) \,.\, I_c \\ 0 & otherwise \end{cases} \quad (5.2)$$

where I_C is the communication signal issued from the PCC to the relay to adjust its settings. As indicated in equation (5.3), the relay will send a trip signal to the circuit breaker when either (I_TH) or (I_TL) is activated:

$$Trip\ signal = I_{TH} + I_{TL} \quad (5.3)$$

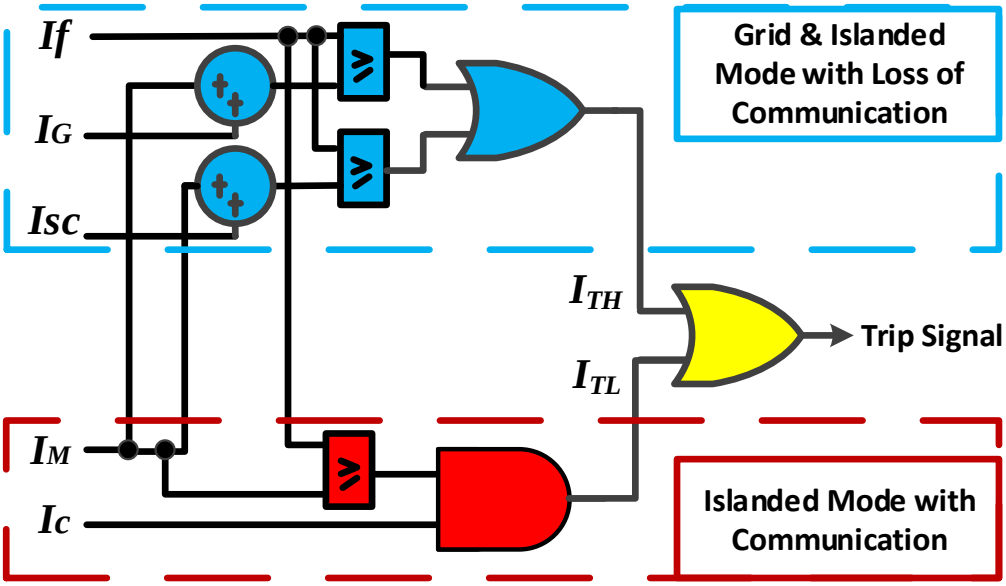

Figure 5.2 The logic diagram of the relay.

5.4 Supercapacitors for Resiliency Enhancement

5.4.1 Supercapacitor Energy Storage

For a microgrid with only one type of energy storage, tasking it to assist in feeding the fault is more complicated. First, a system which only contains a lead acid or lithium ion batteries would be limited to their lifespans. In addition, these batteries are limited by excessive operational currents and particularly temperature. The two most suitable devices, if adequately sized, are the supercapacitor and flywheel, as they provide the greatest balance. The flywheel energy storage provides the highest power density, but has a very high self-discharge rate as a result of friction losses and low energy density. The response time is very fast, limited only by the initial inertia required to start moving the rotating mass. For the maintenance issue that is represented a big problem for the microgrid system, supercapacitor and flywheel are the primarily devices and do not need periodic maintained.

They offer a significant improvement in their capability to source high current as their lifespans are much longer and they have low susceptibility to lifespan issues [153].

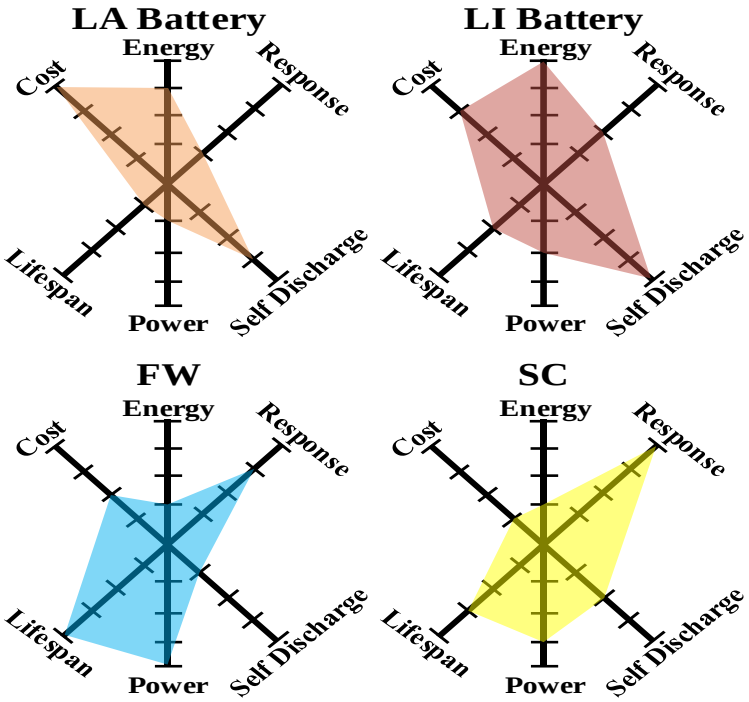

Figure 5.3 Energy Storage Performance Snapshot.

However, the supercapacitor has the best response time of the energy storage types and their construction is chemical in nature, no reaction takes place. This helps to respond extremely fast to a demand heavy current. The capacitance and energy density of a supercapacitor are thousands of times larger than a conventional electrolytic capacitor. A supercapacitor is known to have high power density, low internal resistance, and high life cycle [153]. High power energy storage is commonly used in many systems such as telecommunications, shipboard and spacecraft power systems. In these applications, there are various types of loads that show high instantaneous power requirement but require a relatively low average power. These types of loads are referred to as pulsed loads. The

duration of such loads ranges typically from hundreds of milliseconds to seconds with different power levels. These pulsed loads could be present on ship power systems, which can be electrically treated as islanded microgrids as indicated in [154].

5.4.2 The Supercapacitor's Sizing Process

A two-level optimization process for proper sizing of the supercapacitor in the system under study is developed, as shown in Figure 5.4. In Level 1, the main objective is to reduce the cost of the developed protection scheme by selecting the value of the supercapacitor. In level 2, the main of objective of the optimization process is to minimize the supercapacitor's fault current contribution and maximize that of the distributed generators. This is achieved by optimizing the associated frequency, AC voltage, and DC voltage controllers. Figure 5.4 shows the block diagram of the three PI controllers regulating the frequency, DC voltage and AC voltage of the system. As can be seen in Figure 5.4, the error signals for the frequency and DC voltages (f_{er} and V_{dc_er})) are fed into the first and second PI controllers with parameters k_{p_f}, k_{i_f} and k_{p_vdc}, k_{i_vdc} respectively.

These parameters are used to regulate the direct current component of the system (I_{d_r}), which in its turn regulates the frequency and DC voltage of the supercapacitor bank. Using the AC side frequency as a signature to the active power flow allows the supercapacitor to supply large currents during the fault and contribute to the fault current during loss of communication situations. The AC voltage error signal (V_{ac_er})) is given as input to the third PI controller with k_{p_vac} and k_{i_vac}parameters that used to regulate the quadratic current component of the system I_{q_r}, and regulates the AC voltage.

Based on the inverse Park transformation the reference three phase currents (I_{a_r}), I_{b_r}, and I_{c_r}) are estimated from the dq0 rotating reference frame currents. The angle between the two reference frames and the system frequency are estimated from three-phase Phase Locked Loop block.

The abc reference currents are compared with the actual measured currents and applied to the pulsed width modulation scheme to generate the switching signals of the inverter. The hysteresis band current control is considered in this work because of its simplicity of implementation and fast response current loop. It also doesn't need any knowledge of the load parameters.

The developed algorithm is an iterative one, which is also combined with PSO routine. On the first level, the process first starts by selecting a set of possible values of capacitances, Ci's, such that $C_{min} < C_i < C_{max}$, based on physical constraints of the microgrid under study. A predefined $\Delta C = 0.2\ F$ was selected in our analysis.

It's worth noting that selecting ΔC requires a tradeoff between the optimizations accuracy and the processing time. It was found that $\Delta C = 0.2\ F$ was an adequate value that preserves the optimization's accuracy and does not incur excessive processing time. On the second level, for every capacitance value, C_i the PSO routine is started in order to optimize the associated frequency, AC, and DC voltage controllers.

As mentioned earlier, the controllers in this work are PI controllers, and thus, the parameters to be optimized are the $K_p's$ and $K_i's$ for each controller. For the PSO routine, a search space is randomly generated by defining a population of varying combinations of candidate $K_p's$ and $K_i's$ for the aforementioned controllers.

In order to evaluate the fitness function, the PSO routine was interfaced with a Simulink model of the power microgrid with its controllers to evaluate their response to the different particles in the generated swarm and thus retrieve the capacitor's current fault contribution.

The population generation process is bounded by a vector of LB and UB for each controller. Proper definition of the lower and upper bounds is imperative for the success of the optimization process. Table 5.1, shows the limits of the search space for the parameters to be optimized. During the entire simulation, the solution of the optimization processes is bounded by constraints on the system frequency, AC voltage, and DC voltage in order to ensure stable operation of the microgrid. In fact, two set of constraints were imposed: one during steady state (ss) operation and the other during the pulsed load and fault condition, since the acceptable limits for these constraints are not the same at normal and abnormal conditions as indicated in equations (5.4 to 5.9).

$$f_{min1} < f_{ss} < f_{max1} \tag{5.4}$$

$$f_{min2} < f_{fault} < f_{max12} \tag{5.5}$$

$$Vac_{min1} < Vac_{ss} < Vac_{max1} \tag{5.6}$$

$$Vac_{min2} < Vac_{fault} < Vac_{max2} \tag{5.7}$$

$$Vdc_{min1} < Vdc_{ss} < Vdc_{max1} \tag{5.8}$$

$$Vdc_{min2} < Vdc_{fault} < Vdc_{max2} \tag{5.9}$$

Table 5.1 Lower and Upper Bounds of Optimization Variables

Parameter	Lower Limit	Upper Limit
C	1.5	2.7
Frequency K_p	10	80
Frequency K_i	80	140
AC Voltage K_p	10	50
AC Voltage K_i	100	150
DC Voltage K_p	10	40
DC Voltage K_i	80	160

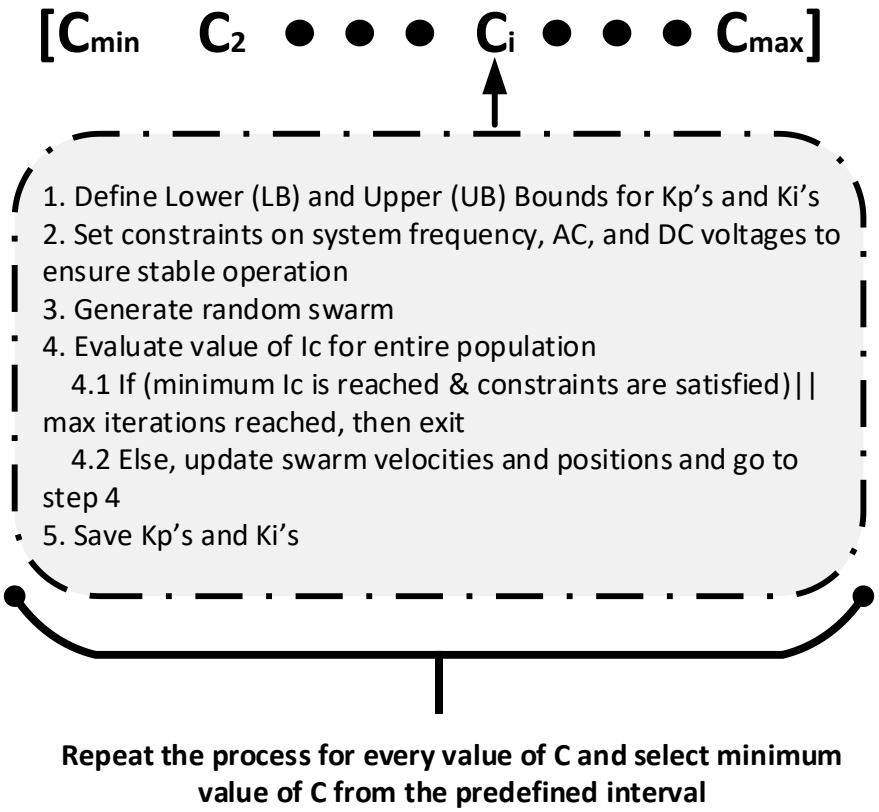

Figure 5.4 The Combined iterative optimization process for supercapacitor sizing

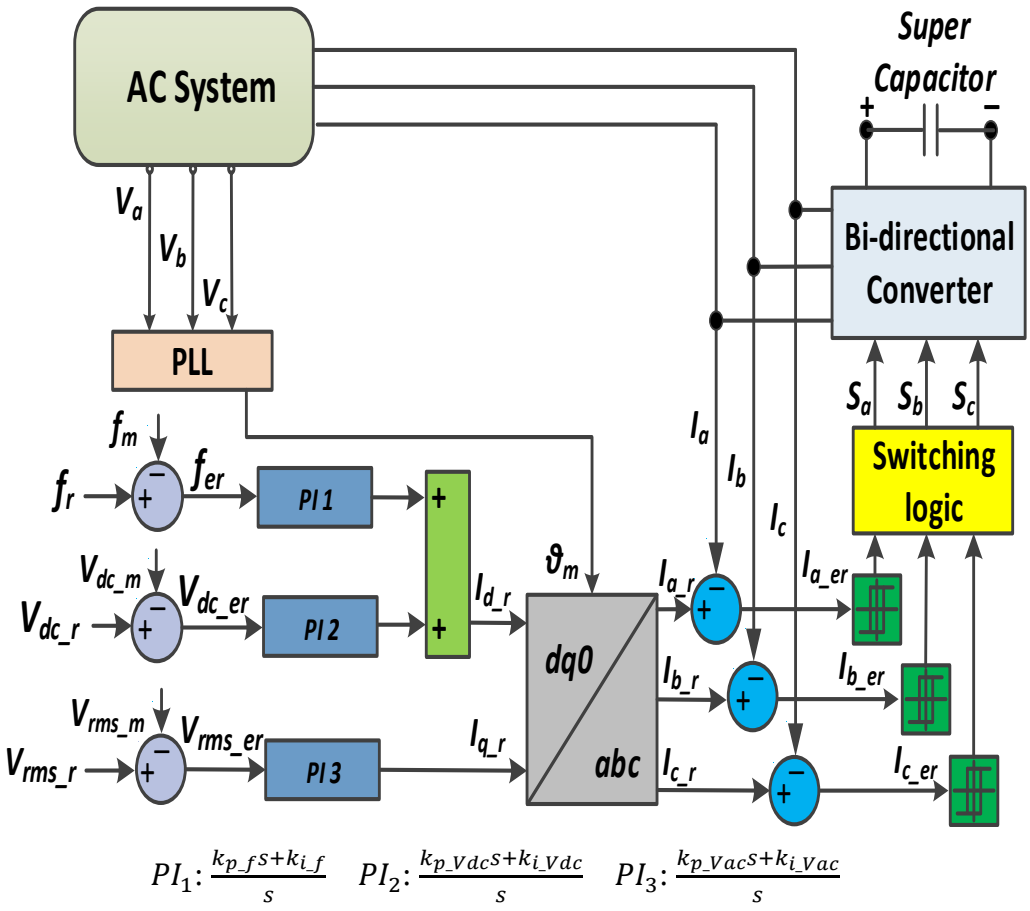

Figure 5.5 Converter control logic block diagram

5.5 Results and Discussion

In this section, multiple case studies were performed in order to investigate the performance of the identified supercapacitor sizing algorithm. The system was first simulated in islanded mode without communication during the extreme case of having a three phase to ground fault and a pulsed load peak period. Next, the system was simulated under the same conditions but using the optimized controller parameters that limits the supercapacitors fault current contribution and the obtained supercapacitor size.

Finally, the case where the pulsed load was temporarily disconnected from the system during the transient fault period was investigated. The supercapacitor's fault current contribution along with the overall system stability was recorded and analyzed in what follows.

5.5.1 Case I: Islanded Mode of Operation without Communication and During Supercapacitor Discharging Period without optimization

A three-phase to ground fault (F_1 in Figure 5.1) has been applied in the transmission line (TL_1) at time t = 1.5 seconds, while the microgrid was in grid connected mode of operation. As a result relay R_1 will send a trip signal to circuit breaker CB_1 to isolate the microgrid. The microgrid successfully shifted to a stable islanded mode by adjusting its overall frequency back to the normal condition after the fault, as shown in Figure 5.6(a). A small disturbance, within acceptable limits, in the output voltages of the sources (V_G, V_{g1}, V_{g2}, V_{inv1} and V_{inv2} representing the voltages at busses 1, 4, 6, 3 and 5, respectively), is noticed in Figure 5.6(b). Figure 5.6(c) and (d) show the supercapacitor-pulsed load microgrid performance which exhibit stable performance during the islanding instant.

It can be seen from Figure 5.6(d) that during the charging of the supercapacitor, the converter 1 allowed 4 Amps of current for the AC side to support the pulsed load.
Finally, Figure 5.6(e) and (f) indicate the minor change in the AC current at both sides of transmission line TL_4 after fault F_1. During the islanded operation, another three-phase-to-ground fault (F_2) occurred at t = 4.5 seconds during the on-time of the pulsed load (i.e. discharging of the supercapacitor) in the middle of transmission line TL_4.

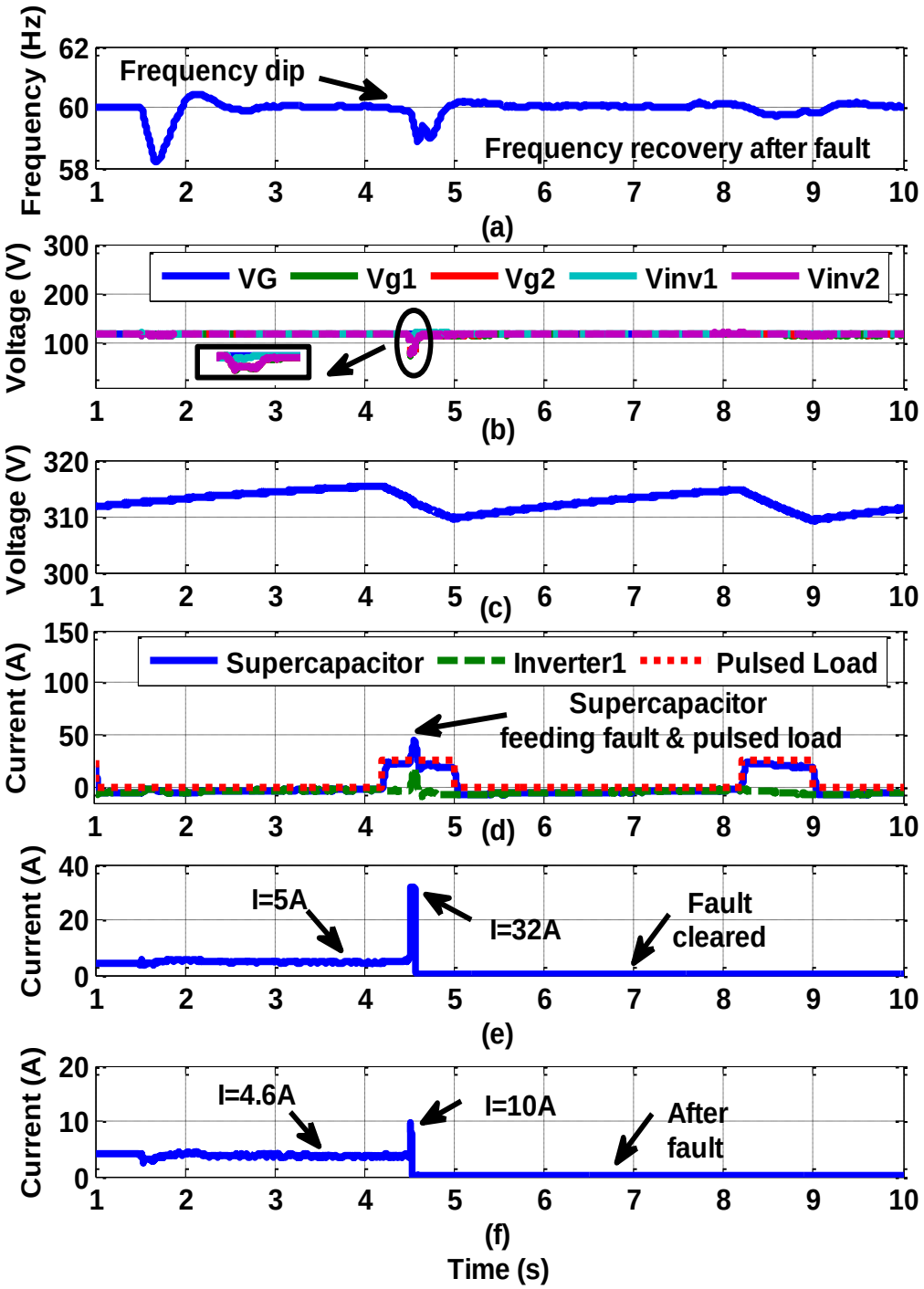

Figure 5.6 System performance during fault at microgrid operation without communication (a) frequency, (b) output voltage of each source, (c) supercapacitor DC voltage, (d) supercapacitor current, and pulsed load current, and inverter1 current (e) RMS current for R7, (f) RMS current for R8.

Due to the assumption of the communication failure, relay R_7 will not be able to switch to the lower settings and the supercapacitor quickly contributed to the fault current while still covering the pulsed load.

Figure 5.6(a) shows the microgrid frequency recovery after the fault incident. As it can be noticed, the system is showing stable performance during and after the fault with disturbances within the specified limits of microgrids operation. The sources voltages V_{g2}, V_{inv1} and V_{inv2} dropped at the fault incident and recovered after clearing the fault, as shown in Figure 5.6(b). As indicated in Figure 5.6(d), the maximum current drawn from the supercapacitor in this case is 43 Amps which is required to feed the fault and the pulsed load simultaneously. As shown in Figure 5.6(d), the current passing through the converter 1 during the normal operation was 4 Apms. However, this current increased to 20 Amps during the fault period. Figure 5.6(e) shows that the fault current drastically increased from 5 Amps to 32 Amps. This resulted in relay R_7 sensing the fault and sending trip signal to CB_7 to isolate the fault. Figure 5.6(f) shows the setting of R_8 that tripped with the help of G_1 to isolate the fault completely.

5.5.2 Case II: System Performance with Optimized Supercapacitor Size

In this case, the optimized frequency, AC, and DC voltages controllers were utilized along with the obtained supercapacitor size of 2.5F (compared with the original 2.9F). Figure 5.7(a) shows a stable system performance, with the new parameters, in terms of its frequency during the first fault (F_1) to isolate the microgrid as well as during the second fault (F_2). It can be noted that the drop of frequency during the second fault is less than the drop without optimized parameters.

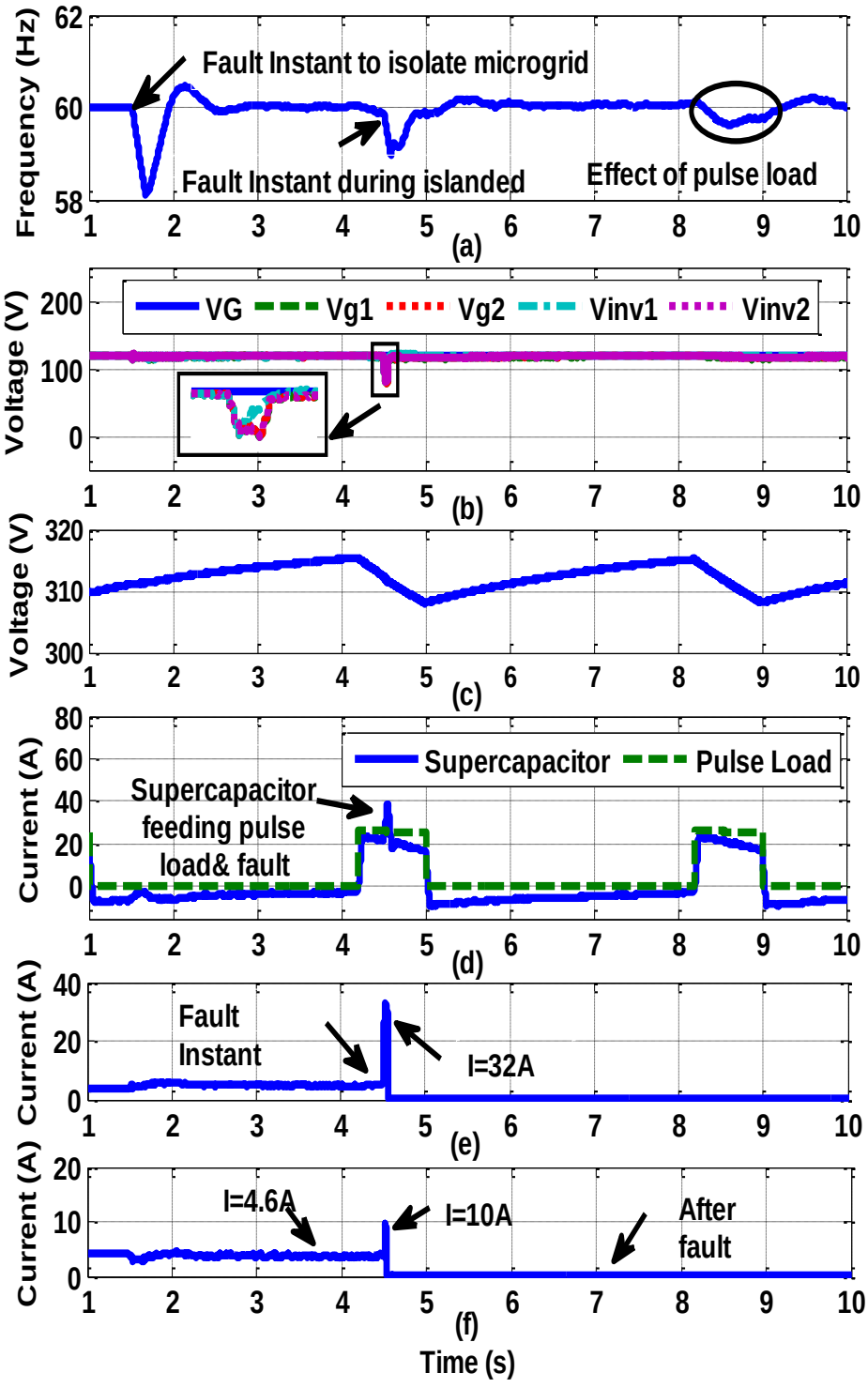

Figure 5.7 System performance during fault at microgrid operation without communication with optimized supercapacitor size (a) frequency, (b) output voltage of each source, (c) supercapacitor DC voltage, (d) supercapacitor current, and pulsed load current, (e) RMS current for R7. (f) RMS current for R8.

Figure 5.7(b) shows that the drop in the sources' voltages (V_G, V_{g1}, V_{g2}, V_{inv1} and V_{inv2}) is within accepted limits during both faults. Figure 5.7(d) shows that the amount of current that was injected by the supercapacitor is reduced to 38 Amps compared to 43 Amps in the previous case. This plays a major role in reducing the size of the supercapacitor and thus it's cost as it will be shown in the next section.

Figure 5.7(e) shows that R_7 reached its high setting value as a result of increasing the amount of current from the AC side even during communication outages. It can be noted that R_8 was tripped to isolate the fault from the other terminal of TL_4 and removed the fault completely from the system.

5.5.3 Case III: Disconnecting the pulsed load during the faulted period

Similar to the previous case, fault F_2 occurred during the on-time period of the pulsed load. It is noticed in Figure 5.8(a) that, due to communication failure, relay R_7 will not switch to the lower settings and the supercapacitor quickly contributed to the fault current. However, in this case, the pulsed load was disconnected for a short period of time during the fault in order to reduce the amount of current drawn from the supercapacitor which reached a maximum of 27 Amps in this case.

To disconnect the pulsed load, the rate of change of the supercapacitor's voltage was monitored to detect a small notch in the DC voltage indicating the fault as shown in Figure 5.8(b) and (c).

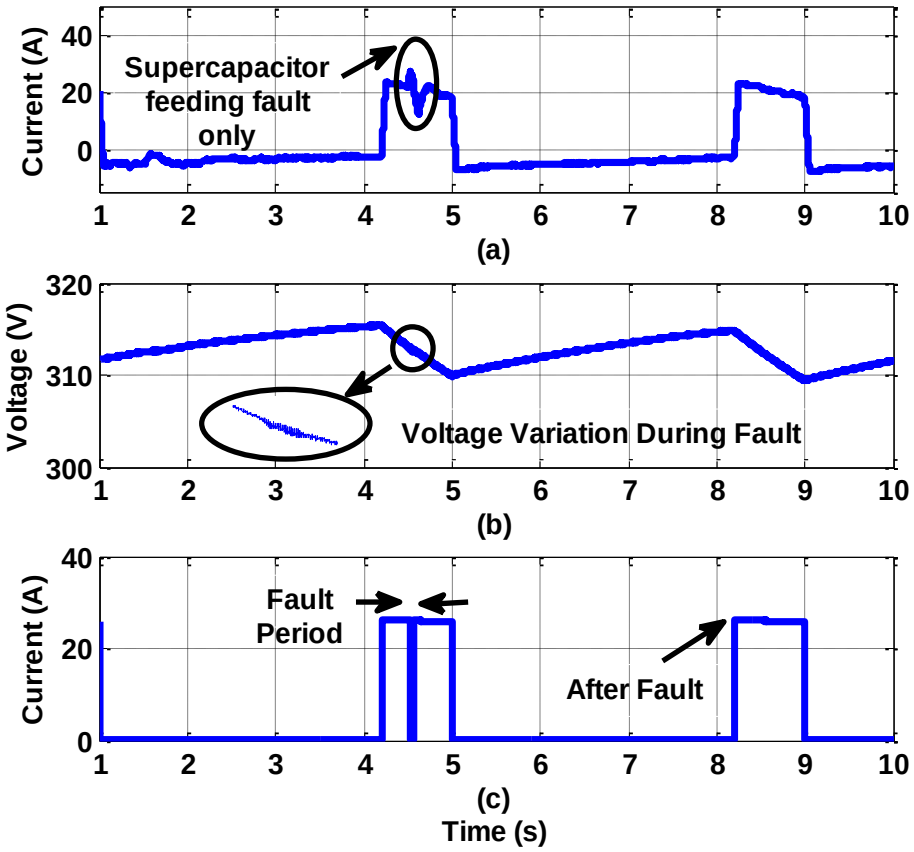

Figure 5.8 System performance during fault at microgrid operation without communication (a) supercapacitor current, (b) supercapacitor DC voltage, (c) pulsed

Table 5.2 shows the operation of the system under several types of faults, applied on different locations (TL_4 and TL_5), for the initial supercapacitor value of 2.9F and the optimized value 2.5F. For a three phase to ground fault (F_2) applied on TL_4 with fault resistance 2Ω, it can be noted that at grid connected mode, the fault current reached 32 Amps that is more than 6 times the rated current which is 5 Amps. For islanded mode of operation, when the communication is available and the relays can adjust its settings from grid mode (6-7 times rated current) to the islanded mode (1.5-2.5 times rated current), the relay R_7 can send a trip signal to the circuit breaker and isolate the fault. During islanded

mode without communication case, the maximum current drawn from the supercapacitor for the initial case with rating 2.9F is 43 Amps which is required to feed the fault and the pulsed load simultaneously. In this case, for complete isolation of the fault, G1 helped R_8 to reach its setting which is 10 Amps. The length of the transmission lines are shown in Table 5.3 and selected such that the sources in the microgrid are enough to help the relays to isolate the fault taking into consideration the current losses due to the voltage drop. However, under the same fault condition, the optimized supercapacitor value (2.5F) and optimized controller parameters, the supercapacitor fault current contribution was 38 Amps. This current is less than the initial supercapacitor case (43 Amps) by 5 Amps, while the contribution from AC microgrid increased to 19 Amps instead of 14 Amps in order to reach to the settings of relay R7 and eventually clear the fault. Thus, the optimized supercapacitor and controller's values can compensate the amount of current that is required to reach to the setting of the relay during discharging the supercapacitor and feed the pulsed load. Similarly, in the case of a double-line-to-ground fault (BCG), the initial supercapacitor and the optimized supercapacitor and controller's values can be sufficient to compensate the amount of current that is needed in islanded mode without communication mode. The AC microgrid generating units were capable of feeing sufficient fault current for fault detection in the case of a single-line-to-ground fault without the need of the supercapacitor.

In this case, the supercapacitor can be used to feed only pulsed load. Also Table 5.2 shows the same fault conditions (F_3) that occurred on TL_5 to investigate the ability of the supercapacitor of feeding the fault current for faults which occur distant from the location of the supercapacitor.

During the grid connected and islanded mode with communication, the fault current setting of relays R_9 and R_{10} were met without interference from the supercapacitor. For the islanded mode without communication, the initial supercapacitor and the optimized one were able to feed the fault current and the pulsed load simultaneously for the three phase to ground and the double line to ground faults. The microgrid resources were enough to feed the single line to ground faults.

Finally, the maximum contribution from the supercapacitor to feed the pulsed load during a three-phase-to-ground fault is 45A in TL_5. It can be noted that the pulsed load at the DC side is supported by little contribution from AC side equivalent to 4 Amps, and from supercapacitor by 23A. The output of supercapacitor which is injected to the AC side is 22A. Therefore, CB_{11} is adjusted at 24A.

Table 5.2 Several types of faults at different locations with the rating of supercapacitor with and without optimization load current.

Fault Type	**R_f (Ω)**	**Relay Setting During Grid Mode (A)**		**Islanded mode with Communication (A)**		**Islanded mode without Communication During Discharging Supercapacitor**								
						Ic		Im		Ipl	RS			
											TL4		TL5	
		R7	R9	R7	R9	R7	R9	R7	R9		R7	R8	R9	R10
ABCG	2	32	31	12	11	43	45	14	15	23	32	10	31	11
BCG	1.8	30	25	10	9	41	42	15	13	23	30	9	25	10
AG	0.1	18	16	8	7	23	23	19	17	23	18	7	16	8

Table 5.3 Lines parameters

TL	**Length**	**R (Ω/km)**	**L (mH/km)**
Line 1	10 km	2.24	0.430
Line 2	8 km	1.41	0.357
Line 3	8 km	1.41	0.357
Line 4	6 km	2.24	0.430
Line 5	6 km	2.24	0.430

5.6 Impact of Reduced Sizing of the Cost of the Supercapacitor Bank

During energy utilization of a supercapacitor bank, its terminal voltage will vary with time. So, the total energy (E_1) that can be delivered by the supercapacitor can be expressed by:

$$E_1 = {}^1\!/_2\, C\, (V_{max} - V_{min})^2 \tag{5.10}$$

Where V_{max} is the maximum voltage of a supercapacitor bank during the pulsed load and V_{min} is its minimum voltage. In the developed hybrid DC microgrid, the maximum acceptable variation of the DC bus voltage is limited to ±5%.

In order to evaluate the economic benefits of the developed optimization method, a financial estimation of the supercapacitor cost is performed. The commercial price of the supercapacitor Model BMOD0058-E016-B02 manufactured by Maxwell, is 122.25$. Table 5.4 shows the optimization results of the cost of the supercapacitor bank, where (E_2) is the stored energy per module, (E_1/E_2) represents the approximate number of required modules.

For the case of the fault on TL_4, it can be noted from the table that the sizing and cost of supercapacitor bank is reduced from 2.9F to 2.5F and the total cost is reduced from $12.155k to $10.47k as a result of the optimization process. Also, in the case where pulsed load was temporarily disconnected during the fault, the supercapacitor's cost was reduced from $12.155k to $6.339k. However, a slightly larger supercapacitor bank was needed for the case of a fault on TL_5. The initial cost was $13.8k and was reduced after the optimization process to $11.5k. For the case of the temporary disconnection of the supercapacitor, the price increase was negligible.

Table 5.4 Cost estimation of the supercapacitor bank

	E1		**E2**	**E1/E2**		**Price (k$)**	
	TL			**TL**		**TL**	
C	4	5	---	4	5	4	5
2.9	208.8	237.5	2.1	99.42	113.1	12.1	13.8
2.5	180	198.4	2.1	85.71	94.5	10.4	11.5
1.8	108.9	110.8	2.1	51.85	52.8	6.3	6.4

Henceforth, the developed sizing algorithm along with optimizing the corresponding controller parameters is suitable feasible and produced excellent results. It is shown that the size and cost of the supercapacitor were minimized, while the system is still meeting the protection and safe operation requirements. This is very beneficial when the system has pulsed loads as these types of loads do not tolerate any interruption during their turned on period. It is important to mention here, that the other identified solution of temporarily disconnecting the pulsed load is suitable for noncritical pulsed loads.

5.7 Summary

This chapter develops two solutions for reducing the size and cost of supercapacitors that are used to compensate for the low-islanded microgrid fault currents during communication outages in adaptive protection schemes. First, for critical pulsed loads, a two-level optimization scheme is presented. In the first level, the goal is to reduce the developed protection scheme's cost by selecting the minimal value of the supercapacitor that maintains the system's stable operation. In level 2, the main of objective is to minimize the supercapacitor's fault current contribution and maximize that of the distributed generators.

The optimized size of the supercapacitor and the associated controllers parameters were investigated under several types of faults in different location in simulation. The results show the ability of the optimized supercapacitor rating to feed different types of faults in order to raise the fault current to the high relay settings and maintain stable system operation during communication outages. Also, the supercapacitor proved effective for faults occurring in distant locations in the microgrid. Finally, temporary disconnection of pulsed loads during the transient fault period proved effective for non-critical pulsed loads as a solution to avoid utilization of oversized supercapacitors.

Chapter 6 Investigation of Protection Strategy for Microgrid System using Lithium-Ion Battery during Islanding

Microgrid protection schemes require a fast, reliable and robust communication system, to adjust relay settings for the appropriate current levels according to the microgrid's operation mode. However, risks of communication link failures and cyber security threats are major challenges for the implementation of protection scheme. This chapter presents a co-simulation platform for microgrid based on MAS when the communication is available in the system. IEC 61850 is used to emulate the developed protection scheme. The DDS middleware is used to link between the hardware and software environments. During islanded mode, the system is capable of riding-through communication failures by the aid of a lithium ion battery. When the communication is attacked, the battery plays an important role and contribute to the fault current for helping the circuit breaker to trip during islanded mode. The design of the control algorithm for the battery's AC/DC converter is developed with single mode operation to eliminate the reliance on communicated control command signals to shift the controller between different modes.

6.1 Introduction

The microgrid is represents a new method of generation and delivery power that contains converter interfaced DERs and loads, energy storage devices, along with traditional rotating machines and DGs. Microgrids can operate in islanded mode or grid-connected mode. One of the main advantages of the microgrids is that it could be fed the loads during islanded mode of operation as shown in Figure 6.1. The main challenge of microgrid

systems is to design an appropriate scheme for protection in different modes of operation. Another problem for the protection of the microgrid is the dynamic change of the configurations in the system [155].

Several research works have addressed adaptive protection scheme using extensive communication to deal with these problems. However the fault current may be significantly smaller in islanded mode of operation as the contribution of the different DERs is limited. As a result, the protection scheme of the system should be designed to be adaptive to shift between the different levels of the short circuit current for both modes of operation. The protection techniques for microgrids are using the communication network, local measurements, or external devices [156].

The communication networks are used to update the relay settings according to the configuration of the system based on the status of DERs (on/off) during the operation. One of the main challenges in designing an adequate protection scheme for microgrids is the ability to integrate cyber and physical systems to update the configuration of the system. Several co-simulation platforms have been discussed to address this concept. In [157], the author used Simulink and Om-net++ to integrate between the dynamic behavior of the physical system and their communication signals. In [158], the authors introduced co-simulation module that linked between OpenDDS and Network Simulator NS2. MATLAB's SimPowerSystems and SimEvents toolboxes were used to represent the co-simulation platform of a low voltage grid based on IEC 61850 in [159].

It can be noted that the previous work presented a vision of how to integrate the physical and cyber components together in power system. However, these works were not implemented the simulation packages over a real communication network.

This chapter introduces a protection scheme for microgrid to isolate the fault at different modes of operation when the communication is available or attacked. A co-simulation platform was installed to validate the concept of using MAS to isolate the fault properly, in case of availability of the real communication architecture. In the event of a physical cyber-attack or loss of communication, a protection scheme would be paralyzed where relays will no longer be capable in adjusting OC limits.

Assuming a physical cyber-attack or communication loss has taken place, relays will now require a much larger full load current setting (high setting) to trip in islanded mode. The developed technique used the installed ion batteries with the help of converter to inject current and raise the fault current to the high relay settings.

The battery is used to feed the pulsed load, which means that the developed method does not add cost to the protection algorithm. It is also worth noting here that the design of the developed controller for the battery's AC/DC converter is capable of operating when the microgrid is in both grid-connected and islanded mode. Utilizing a single mode of operation for the converter will eliminate the reliance on communicated control command signals to shift the controller between different modes. The system, as will be detailed later in the chapter, is also designed to maintain stable voltage and frequency levels.

8.9 System Description

The microgrid under study can be shown in Figure 6.2. It consists of two generators, the primary source of the DER is represented a renewable energy (e.g., photovoltaic source). The battery is connected at DC side to feed the pulsed load. A transformer is used to supply the AC microgrid with the required rated voltage. Two AC filters are used to connect between the AC and DC sides and reduce the harmonics of the AC microgrid.

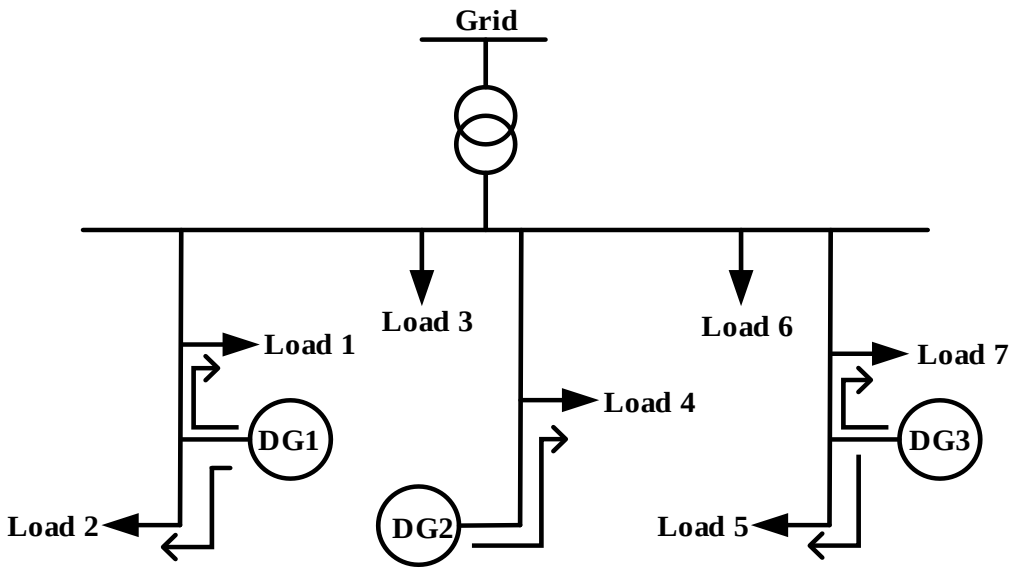

Figure 6.1 Distributed network system.

A bidirectional converter with the battery to allow it to inject current when the communication is not available in the system. F_1 is applied to the system in order to isolate the microgrid from the grid, then another fault F_2, is applied on the islanded microgrid to investigate its performance with and without communication. The AC side also feeds the pulsed load in normal operation when the battery is out of service. DER supplies different loads in the AC side using a unidirectional AC/DC converter in cases where the grid is disconnected from the system and a fault is applied at the AC microgrid. This results in the disconnection of one or more generation units. Specifications of the system components are summarized in Table 6.1. A MAS is defined as a collection of autonomous computational entities (agents), which can be effective in broad applications performing tasks based on goals in an environment that can be difficult to define analytically. Agents are high-level autonomous software abstractions. MAS are distributed and coupled networks of intelligent software agents working in coordination for a global

goal. The focus of this chapter will be on protection of transmission lines in the system using a multi-agent framework.

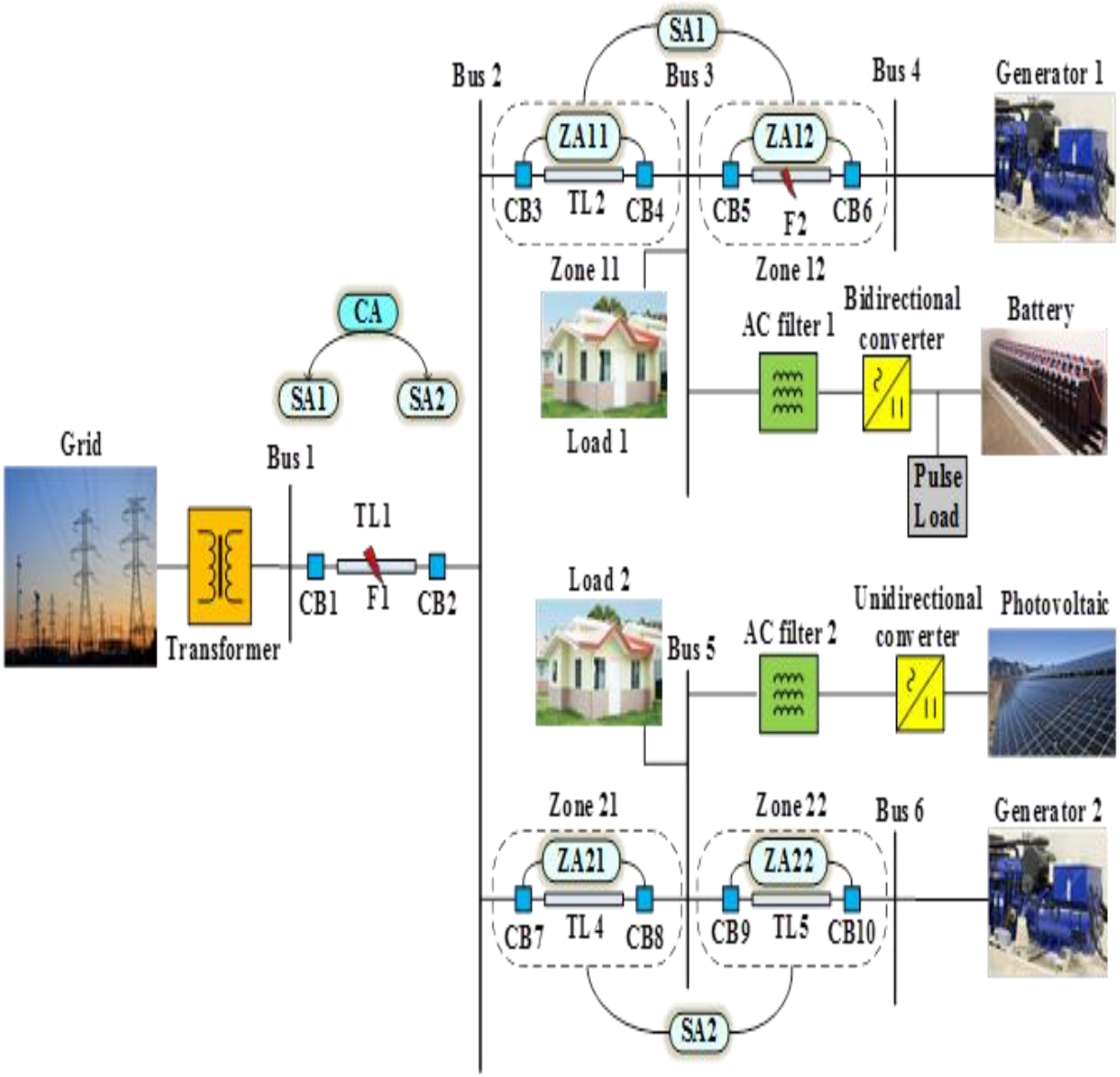

Figure 6.2 Configuration of microgrid.

Table 6.1 System component parameters

Component	Parameter	Specification
Generators 1,2	S_N	7.5 KVA
	V_N	208 V
	F_N	60 Hz
	$X_{L(pu)}$	1.305
Transformer	Connection	Δ/Y_g
	S_N	7.5 KVA
	V_N	208 V
	$R_{eq,}\ X_{eq}$	0.72 Ω, 2.29 mH
Lithium Ion Battery	Number of cells	12
	Nominal voltage	320
	Rated capacity	110 Ah
AC filters 1,2	L_{AF}	12 mH
Transmission Line	$r_{1,}\ r_0$	0.0015 Ω/Km, 0.03 Ω/Km
	$l_{1,}\ l_0$	0.03 mH/Km, 0.1 mH/Km
	$c_{1,}\ c_0$	3 nF/Km, 2nF/Km
Converters 1,2	R_s	1e5 Ω
	R_{on}	1e-3 Ω

8.9 Suggested Multi Agent Information System

Three agents can be used in this chapter for that application as shown in Figure 6.3. A description of the communication between the agents of the system can be shown as follow:-

Central Agent (CA): Operates as a manager of the system and located at PCC. This agent communicates with the different sources in the system (Utility, Generastor1, Generator2, DER) to determine the contribution of each source to the fault current at grid connected mode of operation and islanded mode when the communication is available.

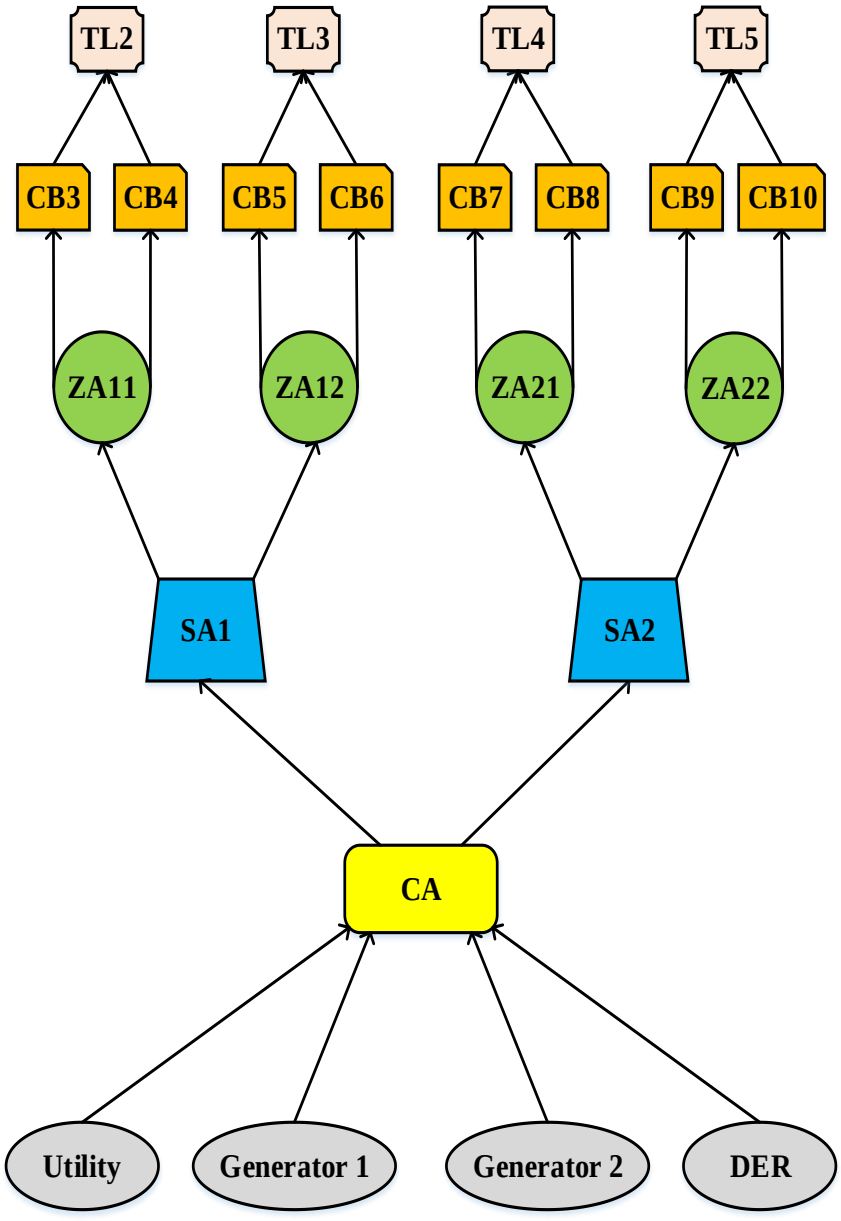

Figure 6.3 Multi Agent Platform.

Section Agent (SA): It can communicate with the central agent to determine the value of the short circuit current to the fault location. During grid connected mode, the fault will be fed by high short circuit current. For the islanded mode of operation and the communication is not attacked, the fault will be fed by low current.

Zone Agent (ZA): This agent receives the signal of the current value from the SA to adjust the relay settings according to the configuration of the system.

It can be noted here that the associate zone will send a trip signal to the circuit breakers at both sides of the unhealthy transmission line to isolate the fault from the system.

8.9 Developed Mutli-Agent Platform

This section explains the integration of the cyber and physical layers of the developed protection scheme.

8.7.3 DDS

In this work, DDS is a protocol for data centric communication middleware from OMG [160]. The DDS is selected by SGIP [161] and for OpenFMB implementation [162] to help the smart grid to perform the interoperability that is defined as the capability of two or more networks, systems, devices, applications, or components to share and readily use information securely and effectively with little or no inconvenience to the user.

The DDS utilizes RTPS mechanism without a message broker scheme which simplifies the communication between different nodes [163]. The DDS is data centric middleware which helps to maintain the focus on the algorithm and control development rather than being concerning with communication and data delivery issues.

The utilization of RTPS as a wire transfer protocol insures the interoperability between different vendors.

For flexible integration with different application DDS provides a standard application programming interface API for support C, C++, Java and .NET. DDS provide reliable peer to peer communication for control agents by avoiding message broker.

The DDS sets the quality of service profiles which enable full control and predictable communication performance for each data type. Unlike other communication schemes which apply QoS policy on the all stream, DDS apply QoS for each individual data type. This feature helps to achieve a predictable network behavior and meets different communication requirements. The QoS policy defines a different set of rules that controls how the data is sent and handled.

8.7.3 Modeling the data in the system

Data Availability: This rule controls the availability of the data for a lately joined subscriber and can be set to a volatile or non-volatile option. It sets to volatile, when any publisher publishes or updates any data.

Then, all current subscribers receive the updated data at the instance of update. Any subscriber who joins the network after the update instance will not be able to receive the last update.

The non-volatile data option forces the DDS infrastructure to make the data available for a lately joined subscriber by storing a local copy of the data. The volatile data option is suitable for periodic data stream, such as voltage measurement.

On the other hand, nonvolatile data is suitable for tracking system statues such as circuit breaker and topology configuration.

Life Span: This rule defines how long the old data will be valid. The infrastructure automatically removes the old non-volatile data which exceeds the defined life span. This QoS rule ensures that the control application does not interact based on old invalid data.

Latency Budget: This rule allows defining the priority for the latency sensitive data. The data with a low latency budget is sent ahead of the data with a higher latency budget.

8.7.3 The Developed Software-Hardware Infrastructure

To validate the developed technique, a co-simulation platform was implemented for an IEC 61850 protocol based protection scheme for microgrid. The microgrid configuration that is shown in Figure 6.2, was modeled on Simulink MATLAB and the suggested protection algorithm was installed on physical IED's. DDS is used to link between the hardware and software environments.

In order to link between the physical merging units and IED's and the simulated model, DDS gateways were implemented at each transmission line. The merging units received the three phase current signals from each terminal of the transmission line and transform them into IEC 61850 SMV messages over Ethernet network.

According to the protection algorithm. ZA sends a GOOSE message to each circuit breaker that is located at each end of the transmission line.

This would isolate the fault from the system at abnormal conditions as shown in Figure 6.4. The merging between DDS and IEC 61850 GOOSE and SMV messages was coded in C with the help of the open source library of IEC 61850 and DDS API from RTI. IDL file is created that contained the measured values and passing through the

publisher/subscriber code generator from RTI. The generated code is then interfaced with routines available from libIEC61850.

The developed codes were downloaded on Odroid C2 SBCs running a real-time Linux kernel. In addition, the automatic code generation for publishers/subscribers based on the data models defined by XML file (to identify the QoS for each application) and/or IDL files simplifies the integration with different data types for other protocols utilized by different IED and remote units' vendors.

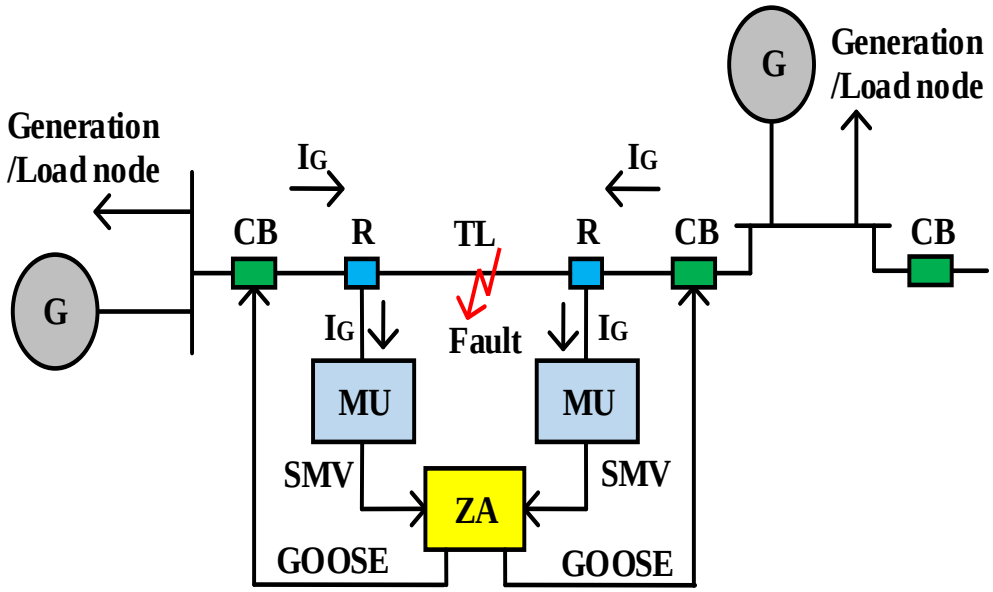

.Figure 6.4 IEC 61850 Messages to Perform the Protection Scheme.

8.9 Protection Scheme Description

The flow chart of the developed protection scheme is shown in Figure 6.5. At grid connected mode and during the normal operation, the battery and AC loads can be fed from the grid, while the pulsed load is supplied mainly from the battery (I_b) with little contribution from grid (I_G). When the fault takes place at microgrid, the relay will send

a trip signal to the circuit breaker when ($I_f \geq I_G + I_m$) and clear the fault from the system. If the fault occurred at PCC, the relay will isolate the fault and the mode of operation changes to be islanded.

The communication network between the main control which located at PCC and the relays plays an important role to identify the relay setting level. When the communication is not available, due to denial of service for example, the relay remains at high settings. In this case and when the fault occurs, the battery can inject high current to the relay and isolate the fault when ($I_f \geq I_m + I_b$).

The stability of the system is tested to ensure the frequency and the voltages at AC and DC sides are changed within accepted values. When the communication is available, the relay can update its settings to lower settings and the fault is cleared at ($I_f \geq I_m$). In this case, the battery can be charged from DERs and the pulsed load can be fed from battery and the generators.

The frequency is measured to check the status of microgrid (grid/islanded) to change the relay settings accordingly.

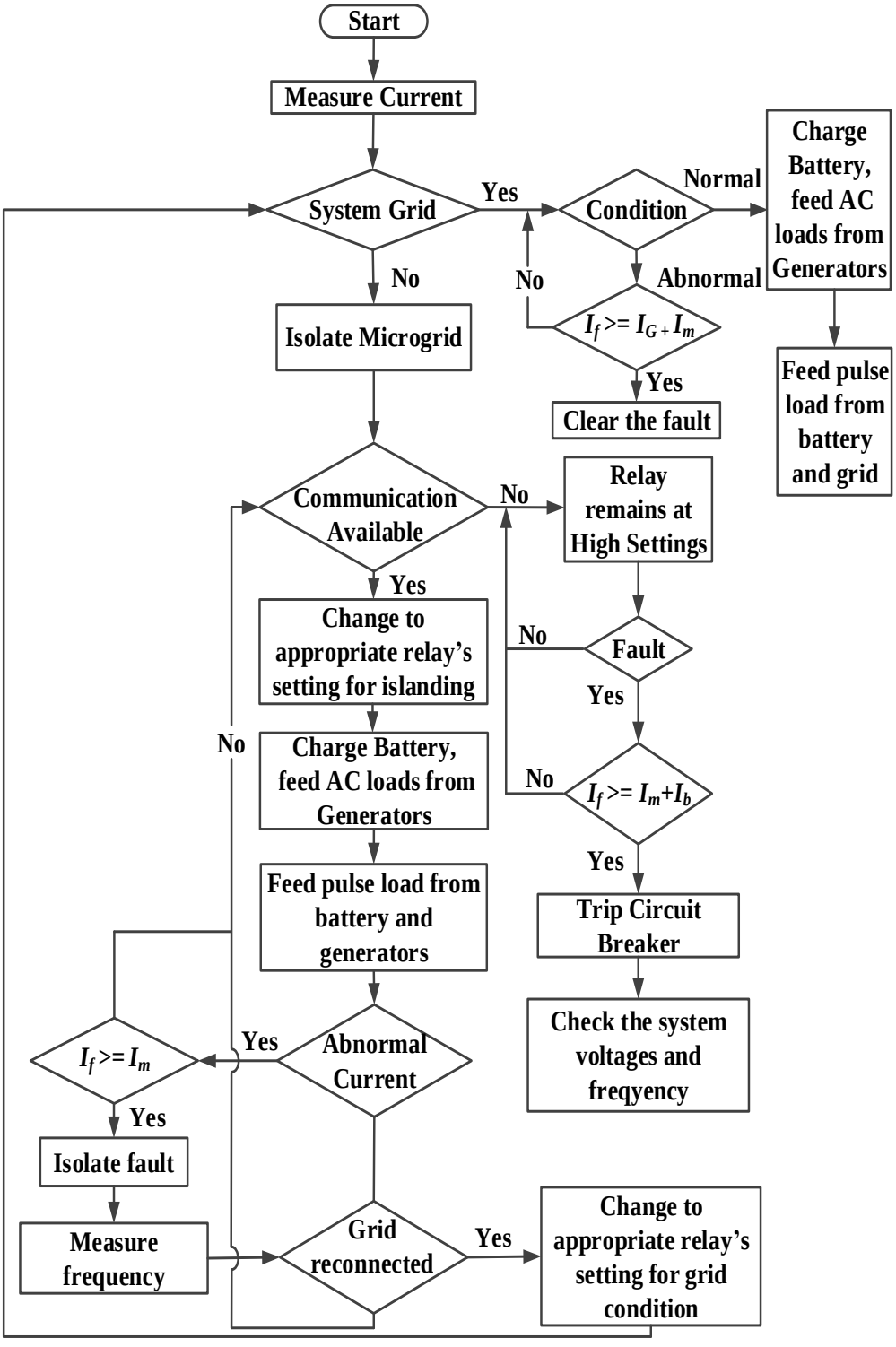

Figure 6.5 Flowchart of the Developed Protection Algorithm

8.9 Control of Battery-Based Microgrid

8.7.3 Lithium Ion Batteries

Lithium ion battery usage has surged in recent years not only in portable electronics, but also in large scale electric vehicles and even grid storage. Advanced lithium ion battery management systems have been demonstrated in microgrid applications for both islanded and grid-connected modes to provide voltage and frequency support. Lithium ion energy storage has been utilized in a wide range of applications, ranging from a few kilowatt hours in residential applications such as rooftop photovoltaic arrays to multi megawatts for grid ancillary services such as frequency regulation and spinning reserve. The anode in lithium ion batteries is made of graphitic carbon while different lithiated metal oxides such as LiCoO2 and LiMO2 can be used as a cathode. When the battery is charged, the cathode is turned into lithium ions and move through the lithium salts electrolyte toward the anode where they combine with external electrons.

This combined with a smaller cell construction allow them to respond faster to a pulsed load which in turn, would also make them suitable in feeding a fault current. Lithium ion batteries have a very high energy density, fast response, and long cyclic life. These advantages led lithium ion batteries to be widely used in portable electronic devices and considered as promising devices in electric and hybrid vehicles. However, the main challenges for their large scale utilization are the high cost due to the requirements of special packaging and internal overcharge protection circuits. These needs are essential to ensure the chemical and mechanical long term reliabilities of lithium ion battery technologies.

8.7.3 AC/DC Converter for Battery

During islanded operation mode, the frequency and AC voltage and DC voltage are changed. The bidirectional AC/DC inverter is used to regulate the active and reactive power by controlling the I_d and I_q, respectively.

The control scheme for the bidirectional AC/DC inverter is shown in Figure 6.6. Two-loop controllers are applied for frequency and DC voltage.

These parameters are used to regulate the direct current component of the system (I_d), which in its turn regulates the frequency and DC voltage of the battery.

Using the AC side frequency as a signature to the active power flow allows the battery to supply large currents during the fault and contribute to the fault current.

To control the voltage amplitude, the error between the measured voltage amplitude and the reference voltage amplitude is sent to a PI controller to generate (I_q) reference.

Equations (6.1) and (6.2) shows the AC side voltage equations of the bidirectional AC/DC inverter in abc and dq coordinates, respectively, where (V_a, V_b, V_c) are the ac-side voltages of the inverter, and (E_a, E_b, E_c) are the voltages of the ac bus. (Δ_a, Δ_b, Δ_c) are the adjusting signals after the Proportional-integral controller (PI) controller in the current-control loop.

$$\boldsymbol{L_{ac}\frac{d}{dt}\begin{bmatrix} i_a \\ i_b \\ i_c \end{bmatrix} + R_{ac}\begin{bmatrix} i_a \\ i_b \\ i_c \end{bmatrix} = \begin{bmatrix} V_a \\ V_b \\ V_c \end{bmatrix} - \begin{bmatrix} E_a \\ E_b \\ E_c \end{bmatrix} + \begin{bmatrix} \Delta_a \\ \Delta_b \\ \Delta_c \end{bmatrix}} \qquad (6.1)$$

$$L_{ac}\frac{d}{dt}\begin{bmatrix} i_d \\ i_q \end{bmatrix} = \begin{bmatrix} -R_{ac} & \omega L_{ac} \\ -\omega L_{ac} & -R_{ac} \end{bmatrix}\begin{bmatrix} i_d \\ i_q \end{bmatrix} + \begin{bmatrix} V_d \\ V_q \end{bmatrix} - \begin{bmatrix} E_d \\ E_q \end{bmatrix} + \begin{bmatrix} \Delta_d \\ \Delta_q \end{bmatrix} \qquad (6.2)$$

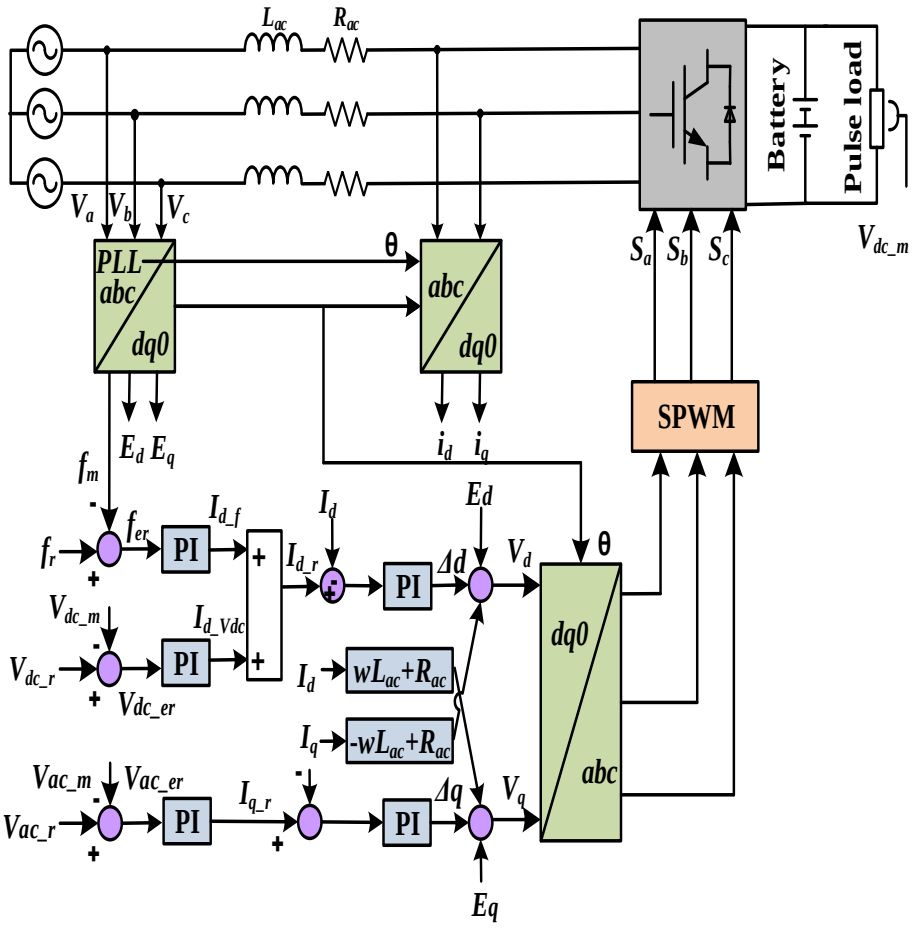

Figure 6.6 Autonomous AC/DC Converter Controller

8.9 Case Studies

8.7.3 Case 1:- Grid Connected Mode of Operation

In this case a three-phase to ground fault (F_2 in Figure 6.2) has been applied in the transmission line between busses 3 and 4 while the microgrid was in grid connected mode of operation. The system performance during this fault is indicated in Figure 6.7 and the fault occurred at t = 6 seconds. Linking modules at both ends of the transmission line 3 reads the current measurements and publishes them as DDS messages. Two physical merging units are subscribing to the published currents from each end of the transmission

line. From this point, the actual IEC 61850 process bus is implemented. These merging units publish the measured current values as SMV packets at a 4,800 Hz publishing rate as set by IEC 61850 for 60 Hz systems. ZA12, which has the protection logic implemented within it, will then subscribe to these SMV message and issue a GOOSE message when the fault current is more than 6 times the rated AC current (drastically increased from 5 Amps to 32 Amps) to control the status of CB5 and CB6 in the simulated microgrid model as shown in Figure 6.7(h). The system frequency was restored to be within the accepted limit after the circuit breakers (CB5 and CB6) opened in response to a GOOSE trip message sent by ZA12. As can be appreciated from the results, the microcontrollers were able to sense, locate, and send trip commands to isolate the fault in the simulated model in a timely manner based on feedback measurements sent to the controllers through the linking modules. Similarly, the simulation model received the correct trip commands from the controllers through the linking modules and opened the appropriate circuit breakers to clear the fault. The cyber part of the system, which was exchanging SMV and GOOSE messages over an Ethernet network, was successfully integrated with the simulation software, in real time. This was recording the dynamics of the system in response to the control actions. This also verifies the ability of the developed framework to accurately capture the relation between the cyber information flow and the physical information flow in power systems. In this case, the utility helped to maintain the system's frequency stable during and after the fault, as shown in Figure 6.7(a). A small disturbance, within acceptable limits, in the output voltages of the sources (V_G, V_{g1}, V_{g2}, V_{inv1} and V_{inv2} representing the voltages at busses 1, 4, 6, 3 and 5, respectively).

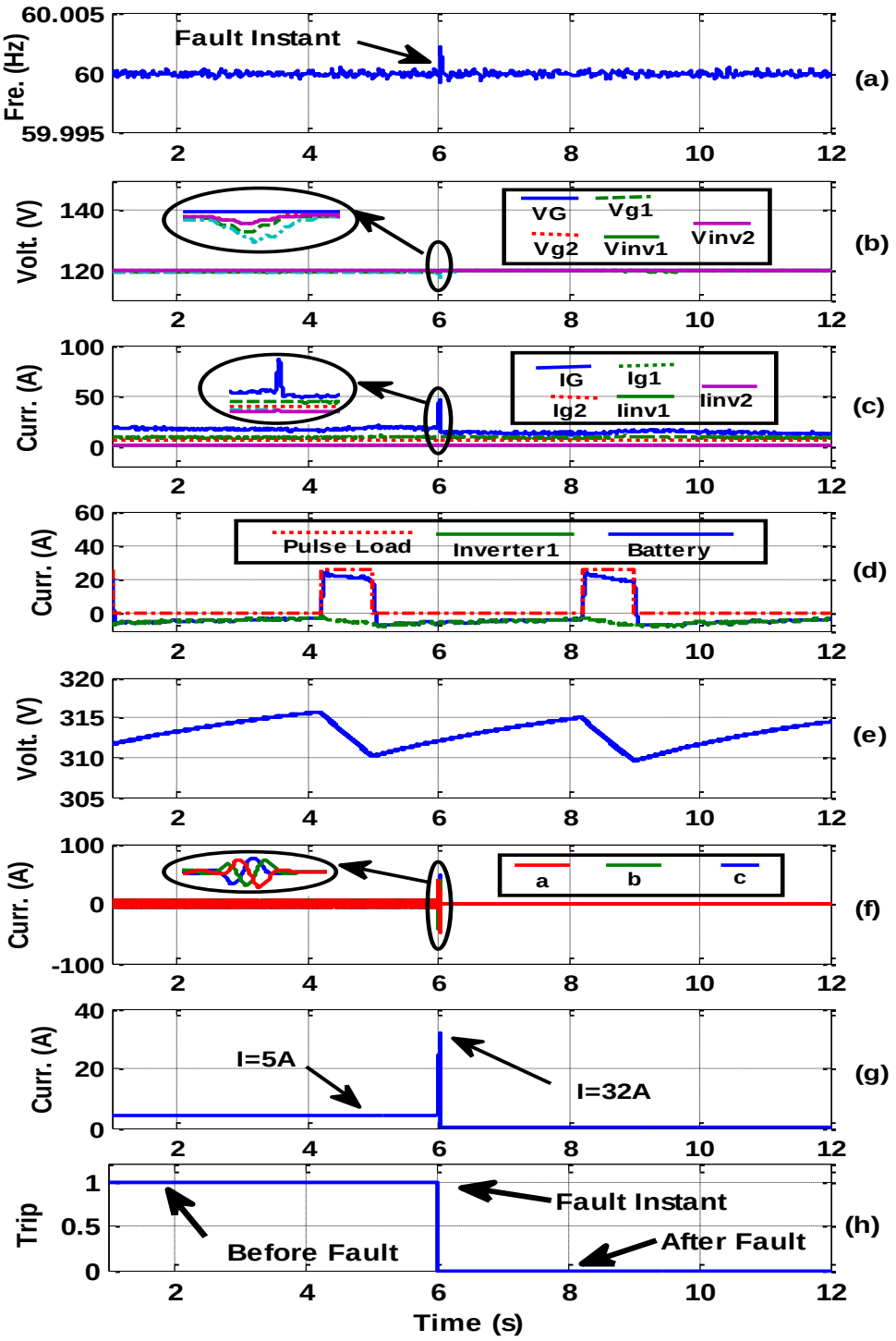

Figure 6.7 System performance during fault at grid connected mode of operation (a) frequency, (b) output voltage of each source, (c) output current of each source, (d) battery current, inverter1 current, and pulsed load current, (e) battery DC voltage, (f) three-phase current in the faulted transmission line, (g) RMS current in the faulted transmission line, and (h) Tripping signal of CBs 5, 6.

Figure 6.7(c) shows a spike in I_G (grid current) due to the fault with a small contribution from other sources (I_{g1}, I_{g2}, I_{inv1} and I_{inv2}) representing the currents of generators 1, 2 and output currents of inverters 1, 2 respectively.

Figure 6.7(d) shows the pulsed load (I_{PL}), battery (I_b), and inverter (I_{inv1}) currents. During the off-time pulsed load, the battery will be charging from the AC side, whereas during the on-time pulsed load the battery will be the major feeder to the pulsed load, as indicated in Figure 6.7(d). The AC side will still be present to feed the pulsed load in case the battery went out of service. Figure 6.7 (e) shows the DC voltage of the battery changes within accepted range $\pm 5\%$ of the rated voltage (320V). Figure 6.7(f) and (g) show the high fault current values of 32 Amps which is mainly being contributed to by the grid.

8.7.3 Case 2:- Islanded Mode of Operation with Communication

In this situation, a three-phase-to-ground fault (fault F_1 in Figure 6.2) occurred at time t = 1.5 seconds, in the transmission line connecting the main grid to the microgrid under study. As a result, relay R_1 will send a trip signal to circuit breaker CB_1 to isolate the microgrid. The microgrid successfully shifted to a stable islanded mode by adjusting its overall frequency back to the normal condition after fault, as shown in Figure 6.8(a). A small disturbance, within acceptable limits, in the output voltages of the sources (V_G, V_g1, V_g2, V_inv1 and V_inv2), is noticed in Figure 6.8(b). Figure 6.8(c) shows a spike in I_G due to the fault and this current drops to zero after clearing the fault by disconnecting the microgrid.

An increase in the generator's currents (I_g1 and I_g2) is noticed in order to compensate for the current which was previously supplied mainly by the grid.

Figure 6.8(d) and (e) show the battery-pulsed load microgrid performance parameters which the exhibit stable performance during the islanding instant. Finally, Figure 6.8(f) and (g) indicate the minor change in the AC current at transmission line connecting busses 3 and 4 after the fault. During the islanded operation, another three-phase-to-ground fault occurred at t = 6 seconds, at zone12. Based on the available communication infrastructure in the system that send the currents of the sources to CA which forward this value to SA12 as the fault is located at the upper section of the system. Then ZA12 sent a GOOSE message to CBs 5 and 6 to trip them, relay R_5 settings is adjusted to the lower setting and thus was capable of detecting the fault and tripping CB_5 accordingly. Figure 6.8(a) shows the microgrid frequency recovery after the fault incident. As it can be noticed, the system is showing stable performance during and after the fault with disturbances within the specified limits of microgrids operation. The sources voltages V_g2, V_inv1 and V_inv2 dropped at the fault incident and recovered after clearing the fault, as shown in Figure 6.8(b).

After the fault was cleared, Figure 6.8(c) shows that I_g1 dropped to zero since generator G_1 was isolated from the system. Current I_g2 increased to feed the loads accordingly. It can be noticed in Figure 6.8(d) and (e) that the battery was not used to feed the fault current due to the adaptation process for R_5 setting to its lower setting. Figure 6.8(f) and (g) show that the AC current in transmission line where fault F_2 occurred increased significantly from 5 to 12 A during the fault instance.

It can be noticed also, that fault current level is less than that appeared in the grid connected mode (32 A) as was discussed earlier.

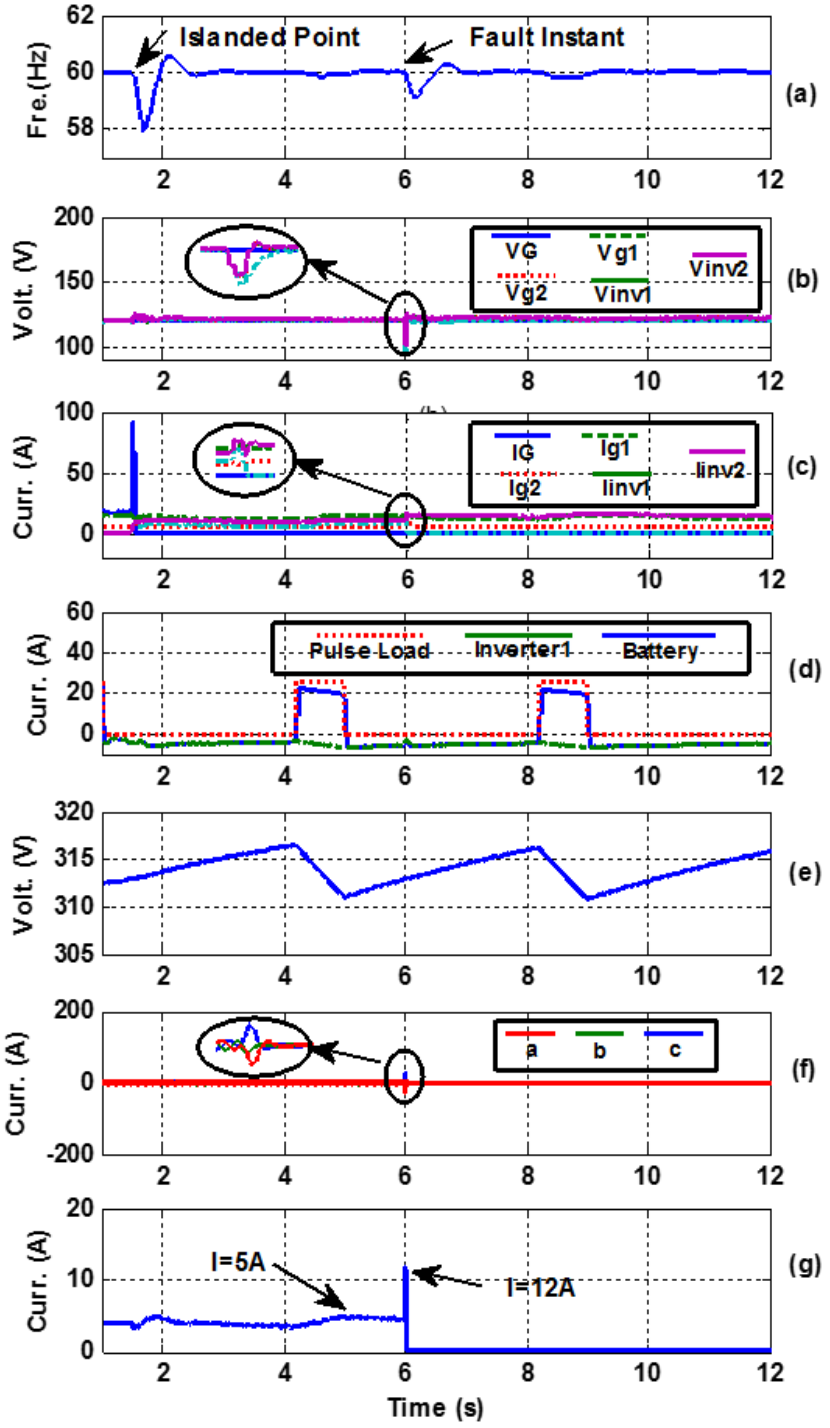

Figure 6.8 System performance during fault at microgrid operation with communication (a) frequency, (b) output voltage of each source, (c) output current of each source, (d) battery current, inverter1 current, and pulsed load current, (e) battery DC voltage, (f) three-phase current in the faulted transmission line, and (g) RMS current in the faulted transmission line

8.7.3 Case 3:- Islanded Mode of Operation without Communication

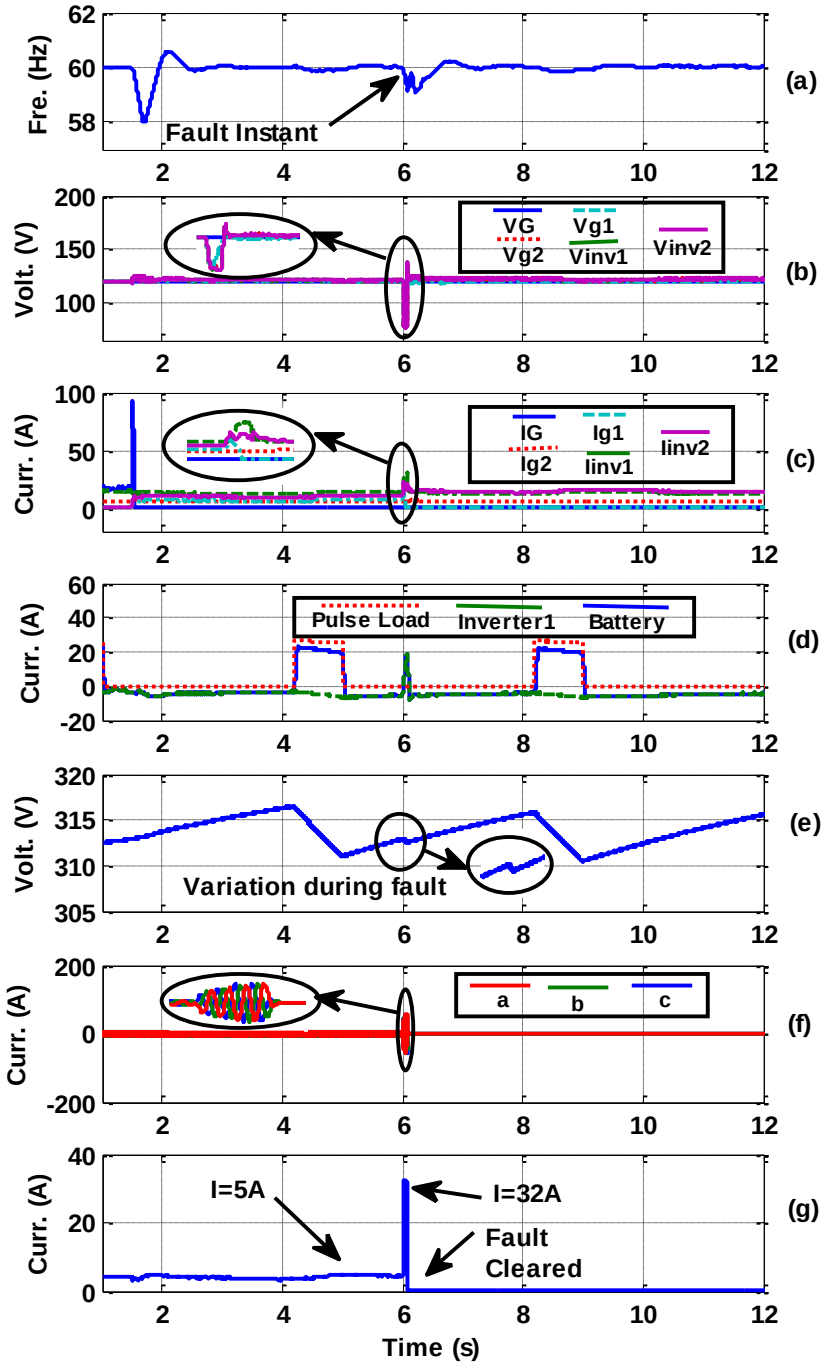

Figure 6.9 System performance during fault at microgrid operation without communication (a) frequency, (b) output voltage of each source, (c) output current of each source, (d) battery current, inverter1 current, and pulsed load current,, (e) battery DC voltage, (f) three-phase cur-rent in the faulted transmission line, and (g) RMS current in the faulted transmission line.

Here the communication infrastructure between the agents was attacked due to DoS. In this case, fault F_2 occurred during the off-time of the pulsed load. Due to the assumption of the communication failure, relay R_5 will not be able to switch to the lower settings. In this case, as shown in Figure 6.9(d), the battery compensate the fault current until it reach to the higher setting of the relay (32 A) as indicated in Figure 6.9(f) and (g).

It can be found a small notch in the DC voltage indicating the fault at AC side as shown in Figure 6.9(e). This resulted in relay R_5 sensing the fault and thus isolating it accordingly. After clearing the faulted region the system restored and shows stable performance as indicated in Figure 6.9 (a), (b) and (c).

8.9 Summary

This chapter presented the developed a co-simulation platform to integrate between the physical-cyber components of a hybrid AC/DC microgrid. The simulated model was interfaced with merging units and microcontrollers over an IEC 61850-based protection scheme. DDS was utilized as a link between the different protocols, hardware, software parts and facilitating the interoperability in the system. The suggested infrastructure used a lithium ion battery to contribute enough fault current for the protection relays to reach it's settings during the islanded mode operation when the communication was not available due to DoS attack. Design of an autonomous control algorithm for the battery's AC/DC converter, which is capable of operating using a single mode for the dynamic operation of the microgrid. It was shown that the converter's single mode of operation eliminates the reliance on communicated command signals requesting a shift by the controller between the microgrid's grid-connected and islanded modes of operation. In all study cases, the system was able to maintain stable voltage and frequency levels.

Chapter 7 A Multi-Agent Based Technique for Fault Location, Isolation and Service Restoration

This chapter gives details on the development of a communication-assisted fault localization, isolation and restoration method for microgrids based on MAS. The developed system comprises distributed agents, located in the middle and at the two ends of a protection section, which will detect a fault through phase angle comparison of current signals at both sides of a given distribution line. The agents then send a trip signal to the corresponding circuit breakers accordingly. The importance of the developed protection technique is twofold: first, it eliminates the use of voltage transformers and thus reduces costs. Second, it does not require transfer of data along long distances which decreases the delay time for fault isolation. Power restoration processes following the fault clearance considering voltage, frequency and power flow constraints in the microgrid under study was also performed.

7.1 Introduction

Communication-assisted microgrid protection schemes are becoming an important research area due to the complex and changing architecture of the contemporary microgrid resulting from dynamically connecting and disconnecting different types of DGs and loads. Thus, it is important to find a suitable communication-assisted protection method between transducers and agents in order to obtain updated fault current values and increase the reliability of the system.

In [164] the authors introduced modeling of a relay and different types of DGs that can be used in a microgrid network. This system can be used to monitor a microgrid over

communication lines and react to dynamic changes of the grid. While such a diverse deployment of microgrids provide important advantages, it possesses key challenges as well. Such systems depend on a MCPU that features complex communication unit due to the different signals from many components in the network, in order to determine the relay that must operate to isolate the fault section from the network.

The authors in [165] developes a protection technique to improve the coordination process of the relay. The relay communicates with DGs and equipment agents in order to obtain a successful coordination. The system was tested by applying it to an agent-based JADE platform.

Multi-agent technology is a powerful new technique for use in many distributed protection systems due to its autonomous, cooperative, and proactive nature. One is based on the use of regional central control; the second uses a regional decentralized peer-to-peer negotiating model in which there are no control centers [166].This work advocates the regional decentralized negotiation approach implemented using agent groups in the microgrid.

The conventional schemes that are used to protect the transmission line face a lot of challenges. The traditional protection techniques use the phasor components of voltage and current to trip circuit breakers. However, these techniques can be affected by the problems of fault resistance and short circuit lines [167].

Current differential line protection schemes have been widely used for detecting and isolating fault sections. However, the operation of these algorithms is based on identifying the vector difference value between the measured currents at both sides of a transmission line. This requires high communication channels bandwidth and thus increases the cost of

communication channels [168]. Also, with the high penetration of distributed generations that are connected through power converters, the short circuit current at different nodes of the microgrid will be close to the nominal current. This leads to a significant source of error for conventional overcurrent protection.

Therefore, a malfunction of these algorithms based on current magnitude measurements is expected to happen due to the difficult task of detecting the branch under fault [169].

The literature shows that the phase differential protection method serves as a better option for transmission line protection due to its simplicity, sensitivity, selectivity and comprehensibility [170]. The work in [166] developes a pilot protection scheme based on the phase jump measured in the current waveform during fault conditions. At each node, the phase jump is registered and used locally to detect changes in the current direction. The change in current direction is determined by the difference between the pre-fault and fault current phase angles. The communication channel requirement and cost of communication equipment can be reduced by considering the phase angle comparison of the positive sequence component of line currents. This leads to an increase in sensitivity and security of the relay or the combination of positive and negative sequence components to give robust discrimination to all types of faults. However, these techniques cannot determine the faulty phase [171].

Complementary to protection, self-healing schemes have been studied in distribution networks. In [172], the authors developed a technique that used a decentralized management and control scheme for distributed microgrids by MAS to achieve resilient self-healing and allow microgrid agents to successfully transition from normal operations to an emergency condition and back again, when conditions have resolved the power

systems. The work in [173] presented a fast FLISR algorithm, which can significantly reduce outage time at the customers' end.

A significant disadvantage to the formal is that they are centralized approaches and depend on a huge amount of data exchange, requiring high communication capabilities and exhaustive computation powers to accomplish power restoration.

Accordingly, this chapter presents a distributed protection technique to locate and determine fault types on distribution lines, which addresses the shortcomings of centralized and resource intensive communication requirements in the surveyed literature.

The main idea behind this work is that the phase angle of the currents of each of the three phases at both terminals of each section in the network is measured using PMU and is communicated to Section Agents (SA) that located in the middle of each section. SAs then calculate the phase angle differences and send trip signal to the circuit breakers (CBs) that are connected at the two ends of the distribution line in case of abnormal operation.

It can be noted here that not all PMUs measure the vector of voltage and current. Some types of PMUs like FNET (Frequency monitoring Network) measures only the voltage component [174].

The FNET/Grid Eye system is currently operated by the Power Information Technology Laboratory at the University of Tennessee (UTK) in Knoxville, TN and Oak Ridge National Laboratory (ORNL) in Oak Ridge, TN. It is possible to design a PMU that only measures the current signal. This means eliminating the voltage measurement which would allow for a low cost PMU.

The advantages of the developed method are:

- The sole dependency on current measurements thus reducing overall costs by eliminating the use of the voltage transducers;
- Current differential protection using a pilot scheme is applied widely on distributed lines as the main protection. Vector difference between the measured currents at the two ends of the transmission line is used for the operation of most current differential relays [168]. The length of the line that can be protected by the pilot wire differential protection is limited by the effect of resistance and capacitance of the pilot wire [175].

  The developed technique presented the phase angle of the current signals to be exchanged between the middle and two ends of the distributed line.

  This means that the communication channels are reduced from 12 to only 6 channels, which reflects on the cost of the protection technique. Also, transferring the data to the middle of the transmission line would limit the effect of resistance and capacitance of the wire;
- Minimized communication delays for fault isolation, as this technique depends on transferring data between two ends of the distribution line and a SA located at the middle length of the line;
- Stable phase comparison techniques by the use of numerical relays and time synchronized measurements which are communicated to relays (synchronization needs to be implement only on SA instead of on the two relays at both sides of each section);
- Protective devices of microgrid are not expected to trip the healthy phases during unbalanced short-circuit. Thus, some utilities and relay manufactures have started contemplating single and double pole tripping for distribution systems [176].

This scheme is able to distinguish the faulty phase reliability and significantly improves the speed of relaying without sacrificing security and enhance the stability;

- Power restoration process: As a result of isolating the fault, some DGs will disconnect from the network and cause loss of power to some loads.

  In order to maintain the reliability of the system, a power sharing operation must be applied to feed these loads through the communications between MAS without the need of supervision from a central point.

8.9 Microgrid Configuration and MAS Framework

The microgrid under study is shown in Figure 7.1. The system consists of two circuits, each having 4-nodes and 2 DGs. DG1 is a 13.8 KVA, 208 V, 60 HZ, and the others are modeled with ratings of 10 KVA, 208 V, 60 HZ. The four loads have a 14.5 Ampere current ratings. Each circuit has one Restoration Agent (RA) and comprises three sections having one SA, two PMUs and two circuit breakers (CBs).

CB is connected between the two circuits and is normally closed to satisfy the synchronization conditions between the generators and enable power flow among the circuits in case of abnormal operation at any section in the system.

A MAS is defined as a collection of autonomous computational entities (agents), which can be effective in broad applications performing tasks based on goals in an environment that can be difficult to define analytically [177].

Agents are high-level autonomous software abstractions. MAS are distributed and coupled networks of intelligent software agents working in coordination for a global goal.

The focus of this chapter will be on the protection of a distributed line and the restoration of the system using a multi-agent framework.

Four types of agents can be used in this chapter: Load Agents (LA), Section Agents (SA), Restoration Agents (RA) and Generator Agents (GA). A description of the communication between the agents of the system can be shown as follow:-

Load Agent (LA): Determine the parameters of voltage, current, frequency, active and reactive power of the connected loads, and transfers these values to other agents to restore the power in case of applying fault in the network.

Section Agent (SA): This agent is located in the middle length of each section. According to the phase angle comparison of currents between both sides of the section, it will send a trip signal to the circuit breakers and isolate the fault section.

Restoration Agent (RA): Operates as a manager of the circuit and can communicates with SAs in the same circuit in order to verify the connection and disconnection areas in the circuit and communicates with other RAs in another circuits to restore the power for the loads.

Generator Agents (GA): Communicates with the RA and determine different parameters of the generator (active and reactive power) to verify the ability to feed the loads in case of applying fault in the system.

Figure 7.2 shows the operation of the developed protection technique. A description of the steps that follow for the protection scheme of the system are as follows:-

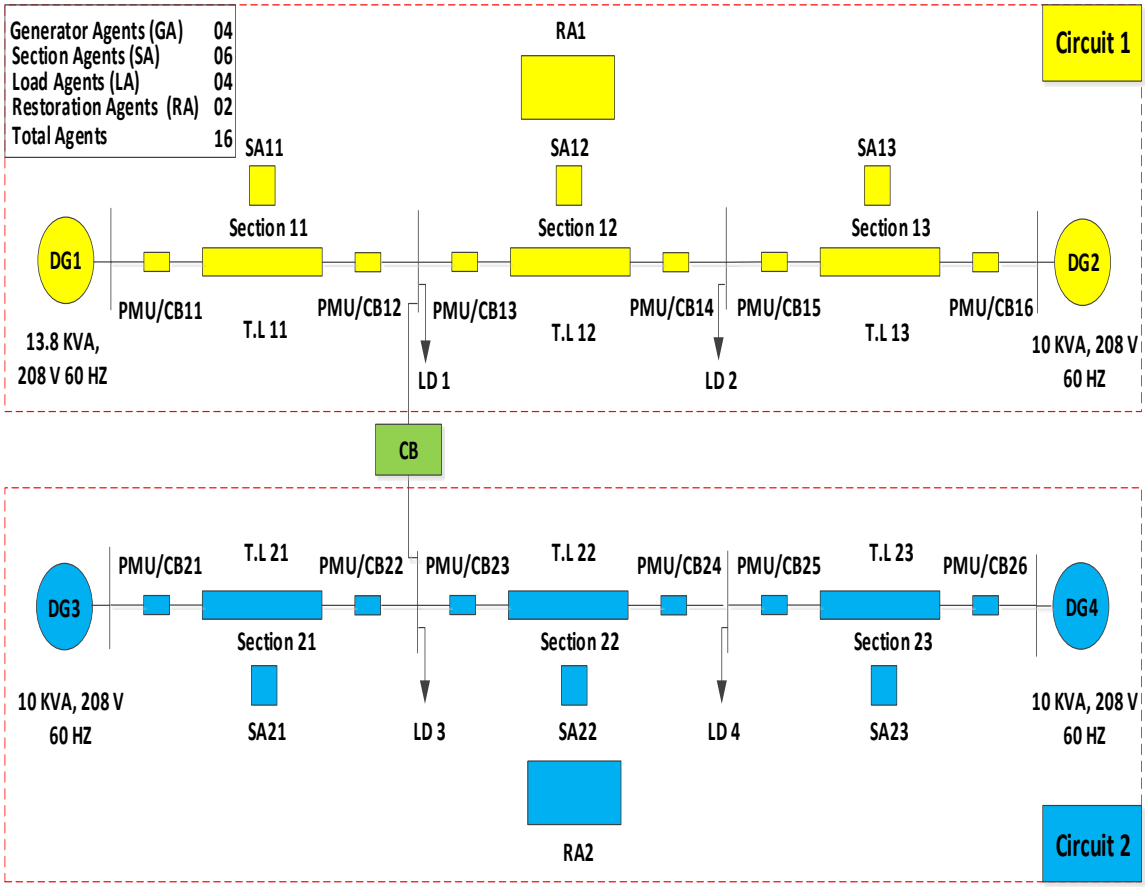

Figure 7.1 The suggested microgrid configuration

Step-I. At normal operation, the current flows in the same direction at both nodes I and j of the distributed line.

After the fault occurred, the current reveres its direction at one side to feed the fault. PMUs at both ends measures the phase angle current signals and forward these values to SA that located at the middle of the protected section.

Step-II. SA receives the data from each side and determine the difference between the phase angles at both ends.

Step-III. If the difference exceeds the threshold value, then SA sends a trip signal to the circuit breakers at both sides of the distributed line.

Figure 7.3 shows the operation of the restoration process. A description of the steps that

follow for the restoration are as follows:-

Step-I. After isolating the fault section from the system as explained in the previous part, LA receives the values of active and reactive power of the load and forward these values to RA.

Step-II. GA receives the amount of capacity of the generator (P_{DG}, Q_{DG}) and forwards these values to RA.

Step-III. RA determine the required power to feed the loads of the system after isolating the fault and send a message to the generators to supply the loads.

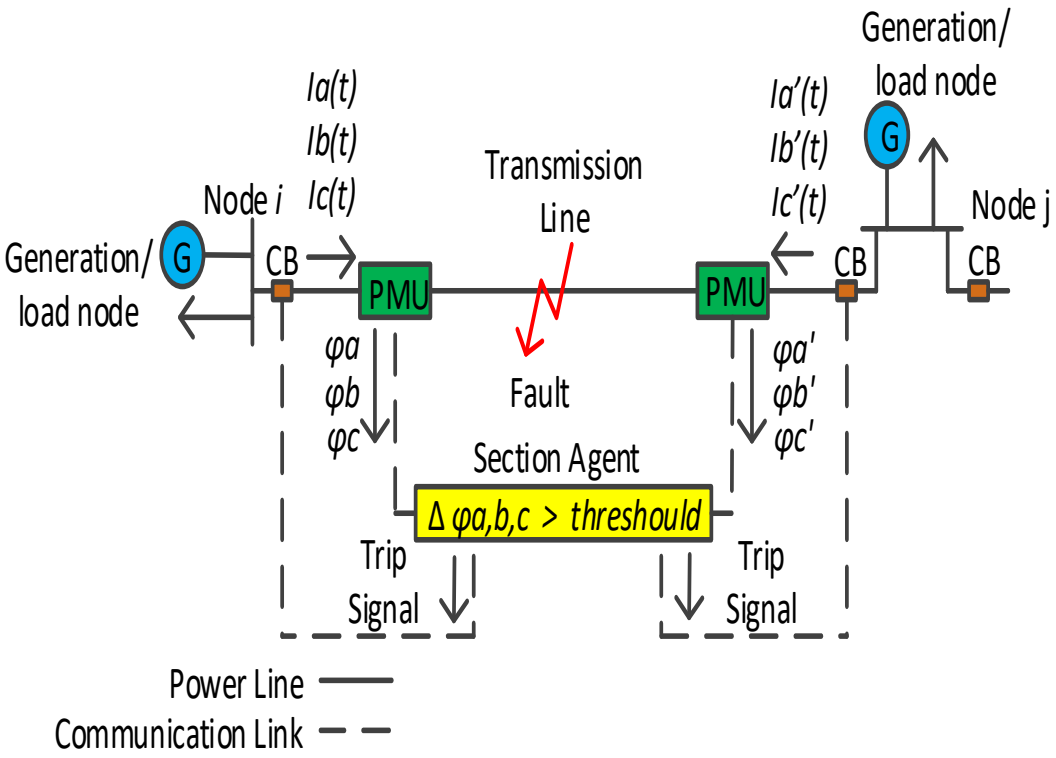

Figure 7.2 Operation of the developed protection scheme

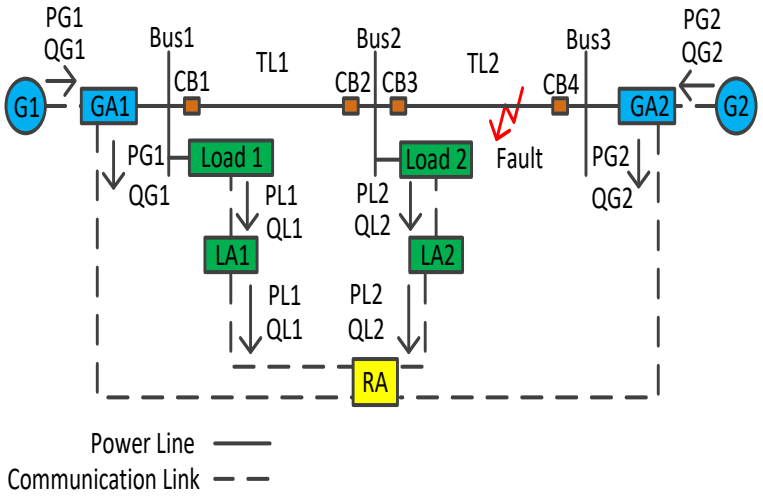

Figure 7.3 Operation of the developed restoration process

8.9 Developed Fault localization Method

The three phase current angle signals at the sending and receiving terminals of each section are measured using PMUs. These measurements are forwarded to SAs. The current at each node is passed to the PMUs at each side of the protected section to obtain the current phase angles (φ^a, φ^b, φ^c). At each terminal, the current phase angle (φ^a) is shifted by 120° from the current phase angle (φ^b) and 240° from the current phase angle (φ^c). For both sides of the section, the phase angle of each terminal (φ^a, φ^b, φ^c) is compared to the phase angle of the other terminal ($\varphi^{a'}$, $\varphi^{b'}$, $\varphi^{c'}$), respectively.

The difference between the phases can be determined as follows:

$$\Delta\varphi^{a,b,c} = \sum_{j=1} [\varphi^{a,b,c}(j) - \varphi^{a',b',c'}(j)] \qquad (7.1)$$

where,

$\Delta\varphi^{a,b,c}$ phase angle difference between the starting and ending terminals of each section;

j index;

$\varphi^{a,b,c}(j)$ phase angle current of phases A, B and C at the sending terminal;

$\varphi^{a',b',c'}(j)$ phase angle current of phases A, B and C at the receiving terminal.

According to the difference $\Delta\varphi^{a,b,c}$, the location and type of the fault can be determined.

For normal operation:

$$\Delta\varphi^{a,b,c} \approx \Delta\varphi_{pre}^{a,b,c} \quad (7.2)$$

For abnormal operation:

$$\Delta\varphi^{a,b,c} \gg \Delta\varphi_{pre}^{a,b,c} \quad (7.3)$$

where "pre" refers to the values in the previous cycle.

The SA of the fault section sends trip signals to both circuit breakers that are located at both sides of this section to isolate the fault from the system.

8.9 Developed Restoration Method

Power restoration is defined as the capability of a system to automatically detect and recover functionality when faced with a single or multiple events. For a power system, this definition is somewhat refined to include the rapid identification of problems, actions to minimize any adverse impacts from casualties, and the prompt recovery of the system to a stable operating state. During restoration, a series of reconfigurations may take place to improve the overall system condition involving breaker manipulations and generation startup or shutdown. Two factors appear to have influenced the recent research direction. First, conglomerating communication, sensory, and control functions in a central manner allows decisions to be made with a global perspective. While it is cumbersome to centralize these functions, this facilitates are the most complete information for decision-making.

The second factor that may have discouraged development of capable distributed multi-agent systems is their difficulty. However, decentralizing decision-making has unique attributes that make it attractive from a resiliency perspective; chiefly because it can avoid the scenario where corruption or failure of the central supervisory node leads to total system collapse [178]. For any system, this definition is somewhat refined to include some constraints in terms of keeping the system stable following the restoration process. The following section explains these constraints with the suggested algorithm to restore the power for the connected loads using MAS.

Mathematically, the restoration problem is formulated as an objective function satisfying the system constraints as indicated in the following conditions:

- Power limit

$$P_{DG} \geq P_{Load} + P_{Loss} \tag{7.4}$$

$$Q_{DG} \geq Q_{Load} + Q_{Loss} \tag{7.5}$$

where P_{DG} and Q_{DG} are the generated active and reactive power of the DGs within the microgrid, $P_{Load}$and Q_{Load} are the load active and reactive power, and P_{Loss} and Q_{Loss} are the active and reactive power losses in lines. As indicated in equations 7.4 and 7.5, generated active and reactive power must supply demand power as shown in Figure 7.4 [179].

- For power line current limits, the maximum current capacity of lines must be lower to prevent overloading [180].

$$I_i \leq I_{max} \tag{7.6}$$

where I (current) is the load current at node i

- Voltage limit

The system must always be within the allowed limits [181].

$$V_{min} \leq V_i \leq V_{\max} \tag{7.7}$$

- Frequency limit

The system frequency must always be within the allowed limits [182].

$$f_{min} \leq f \leq f_{max} \tag{7.8}$$

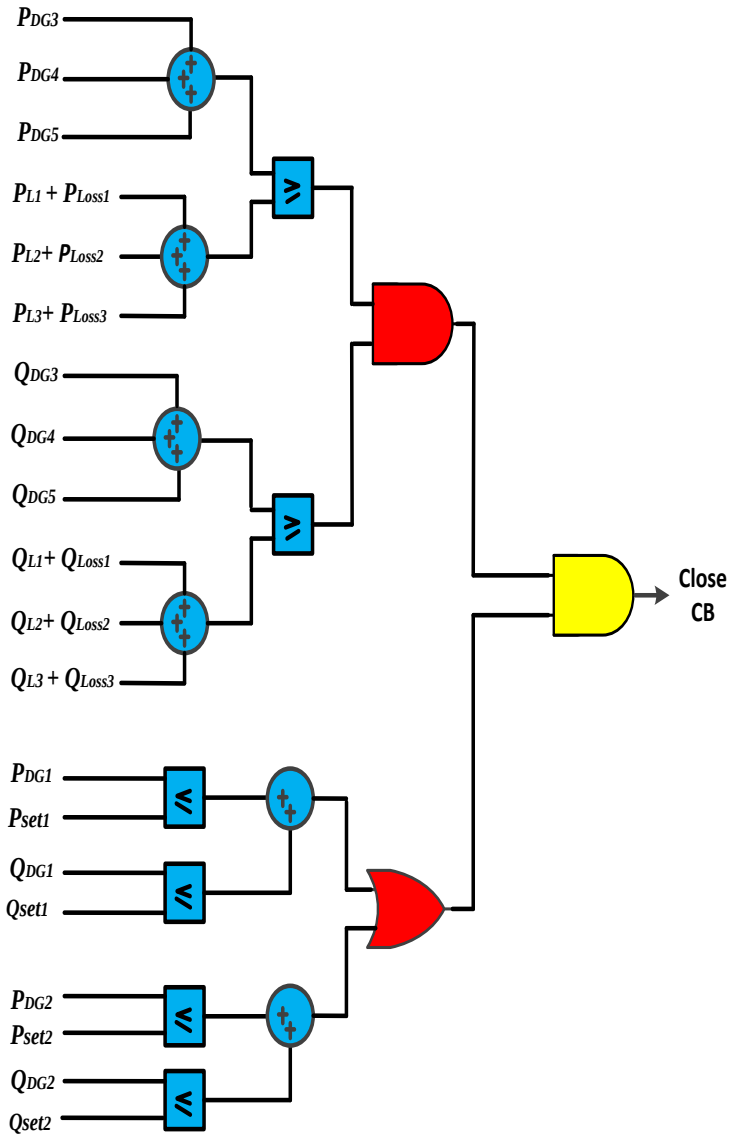

Figure 7.4 Logic Diagram of Circuit agent 2 (CA2)

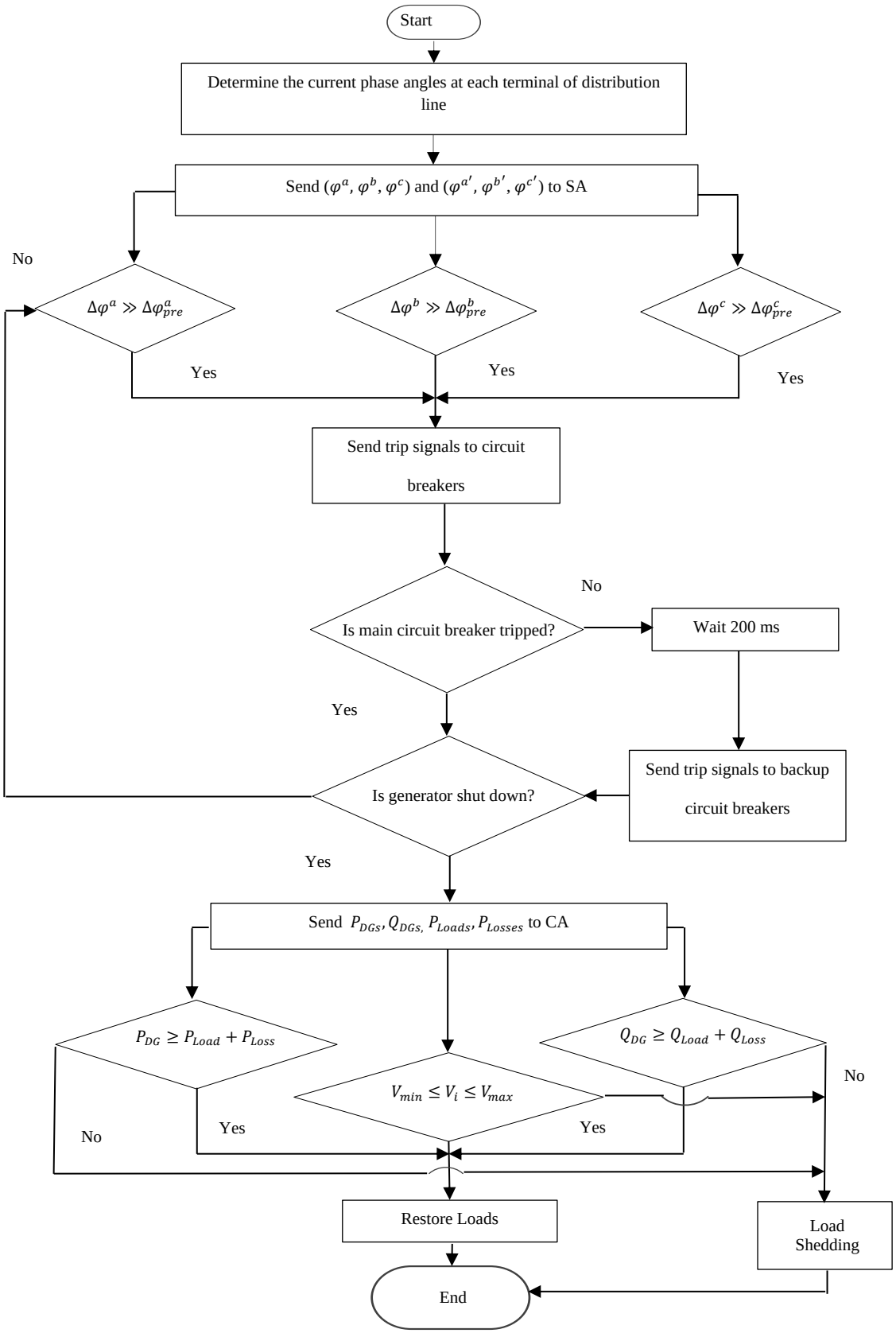

Figure 7.5 Flowchart of the developed protection and restoration algorithm

8.9 Simulation Results

8.7.3 Fault Location, Identification and Isolation Case Study

A single line to ground fault is simulated on phase A, through a 0.5 Ω fault resistance at t = 1.5 seconds on the middle of section 13. The three phase current angle signals at the starting side (φ^a, φ^b, φ^c) and at the ending side ($\varphi^{a'}$, $\varphi^{b'}$, $\varphi^{c'}$) are measured at section 13 using PMU15 and PMU16.

The angle of phase A at each side of section 13 is shifted by 120° (2π/3 Rad) from phase B and 240° (2π/3 Rad) from phase C as shown in Figure 7.6(a), (b) and (c). Deviation phase angles for phases A, B and C for the distribution line at both sides of section 13 are shown in Figure 7.6(d). It can be found that the deviation of phase angle A is greater than the threshold value that is 20°. On the other hand, the deviation phase angle of phases B and C is less than the threshold value. This means that the fault is a single line to ground fault and is located at section 13.

SA13 sends a trip signal to CB15 and CB16 that are connected at each end of section 13 to isolate the fault as shown in Figure 7.6(e).

The phase angle of the three phase current signals are measured using PMU13 and PMU14 at both ends of section 12 during the three phase to ground fault in the middle of this section as shown in Figure 7.6(a), (b) and (c).

The deviation of phase angle for phases A, B and C is greater than the threshold value as shown in Figure 7.6(d).This means that the fault is a three phase to ground fault and located in section 2. SA12 sent trip signals to both CB13 and CB14 at both ends of section 12 as shown in Figure 7.6(e).

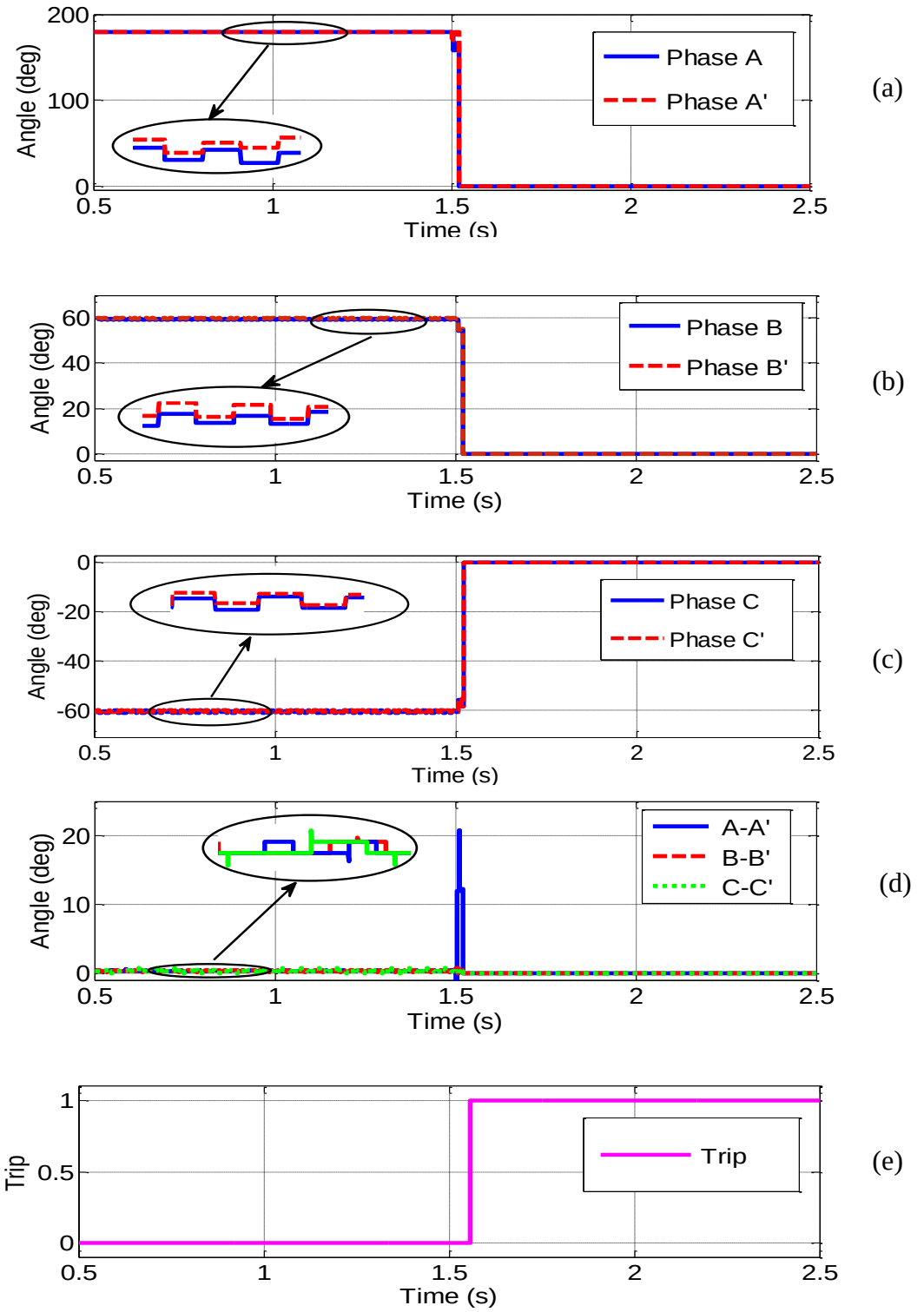

Figure 7.6 Phase angles of starting and ending sides during single line to ground fault on phase A in the middle of section 13. (a) Angles of phases A, A', (b) Angles of phases B, B'. (c) Angles of phases C, C', (d) Deviation angles for phases A, B and C, (e) Tripping signal.

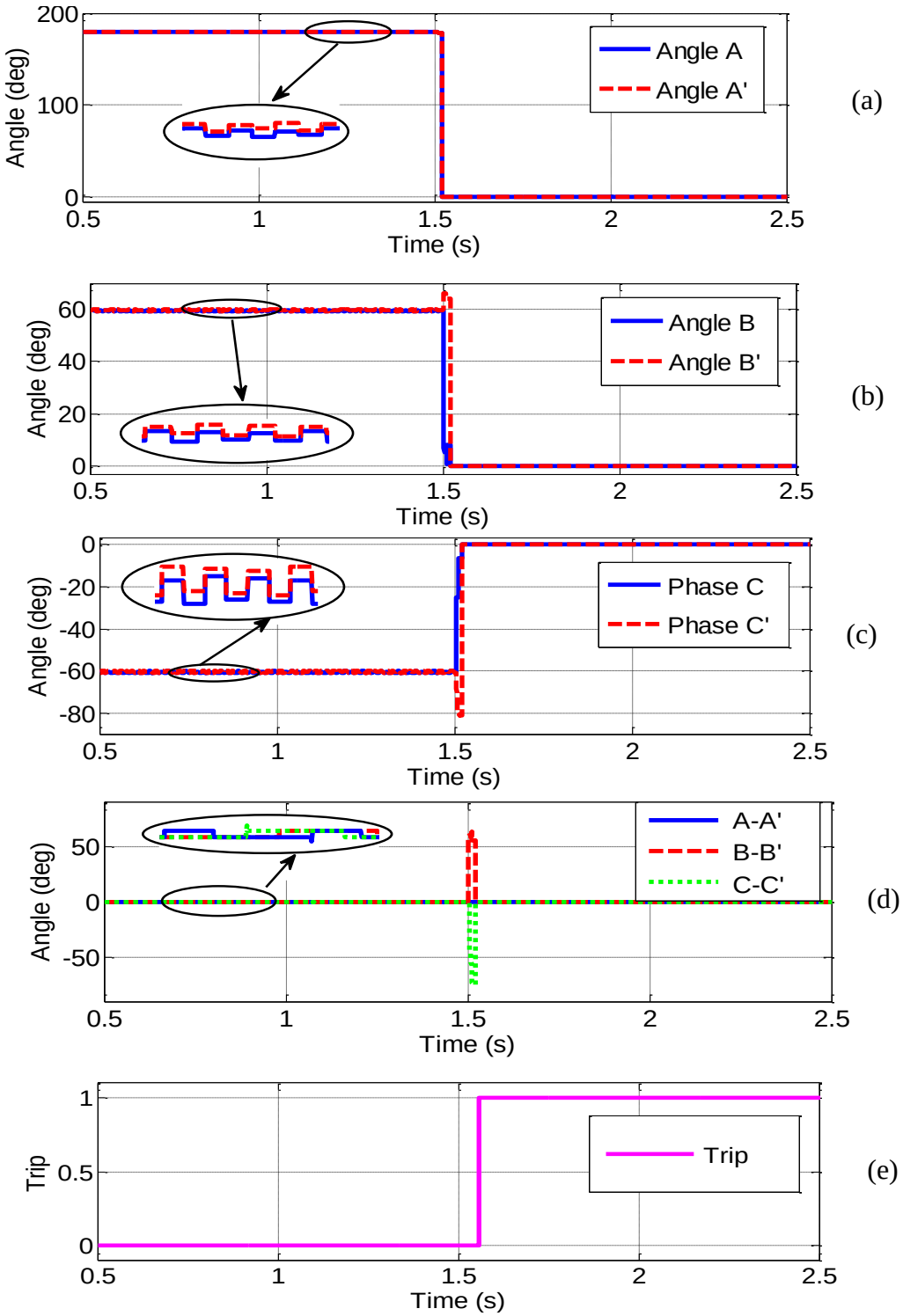

Figure 7.7 Phase angles of starting and ending sides during double line to ground fault on phases B&C in the middle of section 13. (a) Angles of phases A, A', (b) Angles of phases B, B'. (c) Angles of phases C, C' (d) Deviation angles for phases A, B and C, (e) Tripping signal.

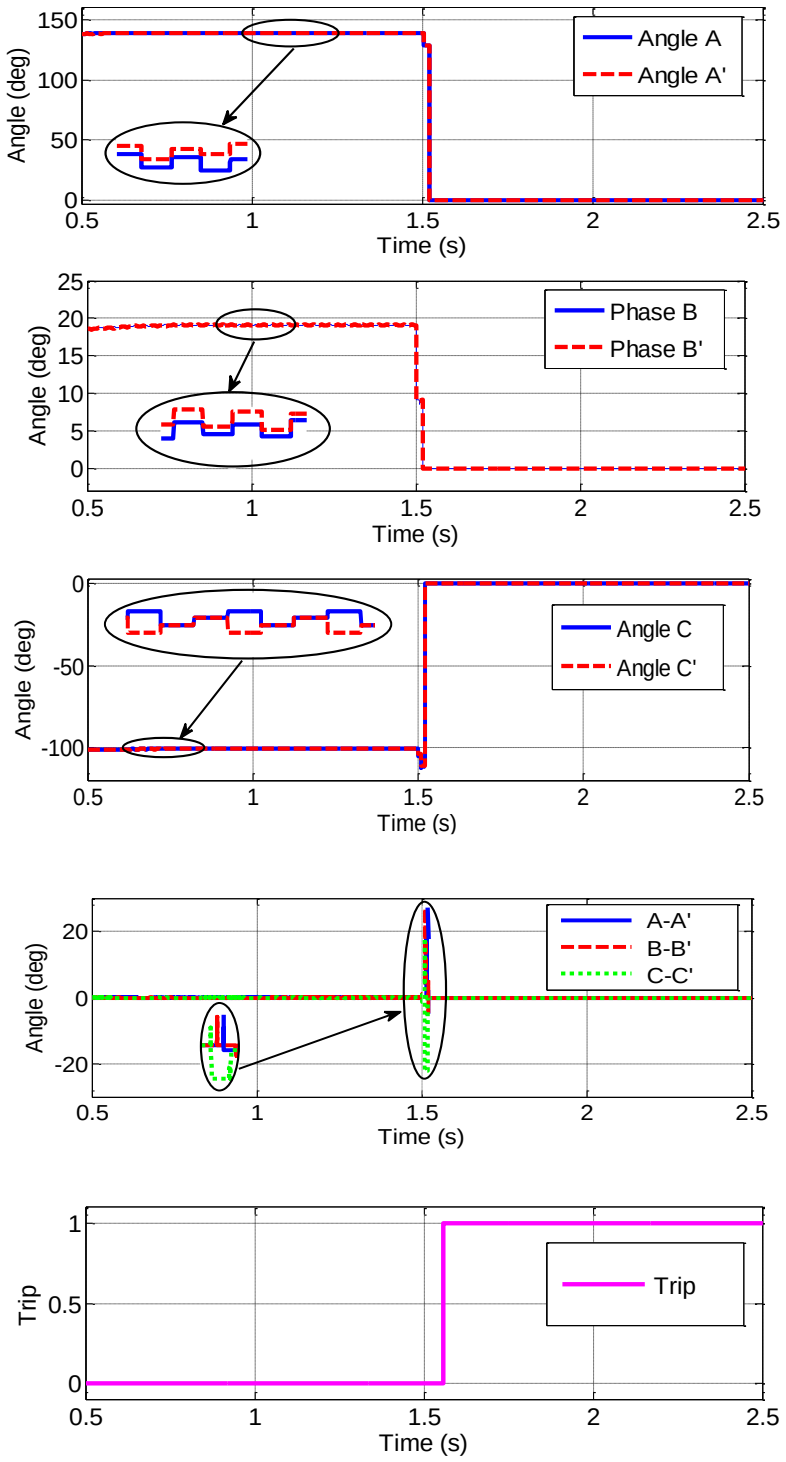

Figure 7.8 Phase angles of starting and ending sides during three phase to ground fault in the middle of section 12. (a) Angles of phases A, A', (b) Angles of phases B, B'. (c) Angles of phases C, C' (d) Deviation angles for phases A, B and C, (e) Tripping signal.

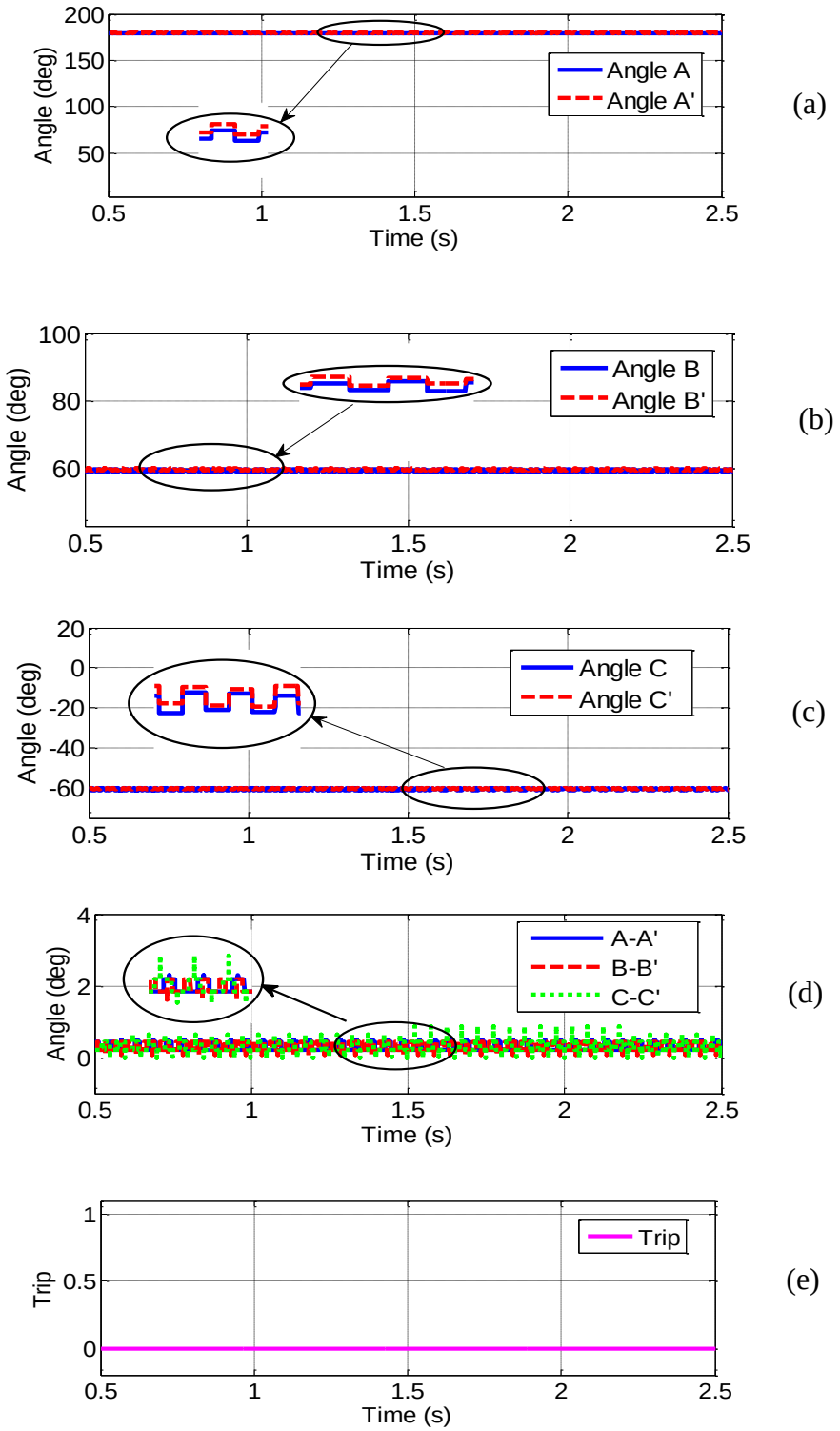

Figure 7.9 Phase angles of starting and ending sides at section 13 during single line to ground fault in the middle of section 12. (a) Angles of phases A, A', (b) Angles of phases B, B'. (c) Angles of phases C, C' (d) Deviation angles for phases A, B and C, (e) Tripping signal.

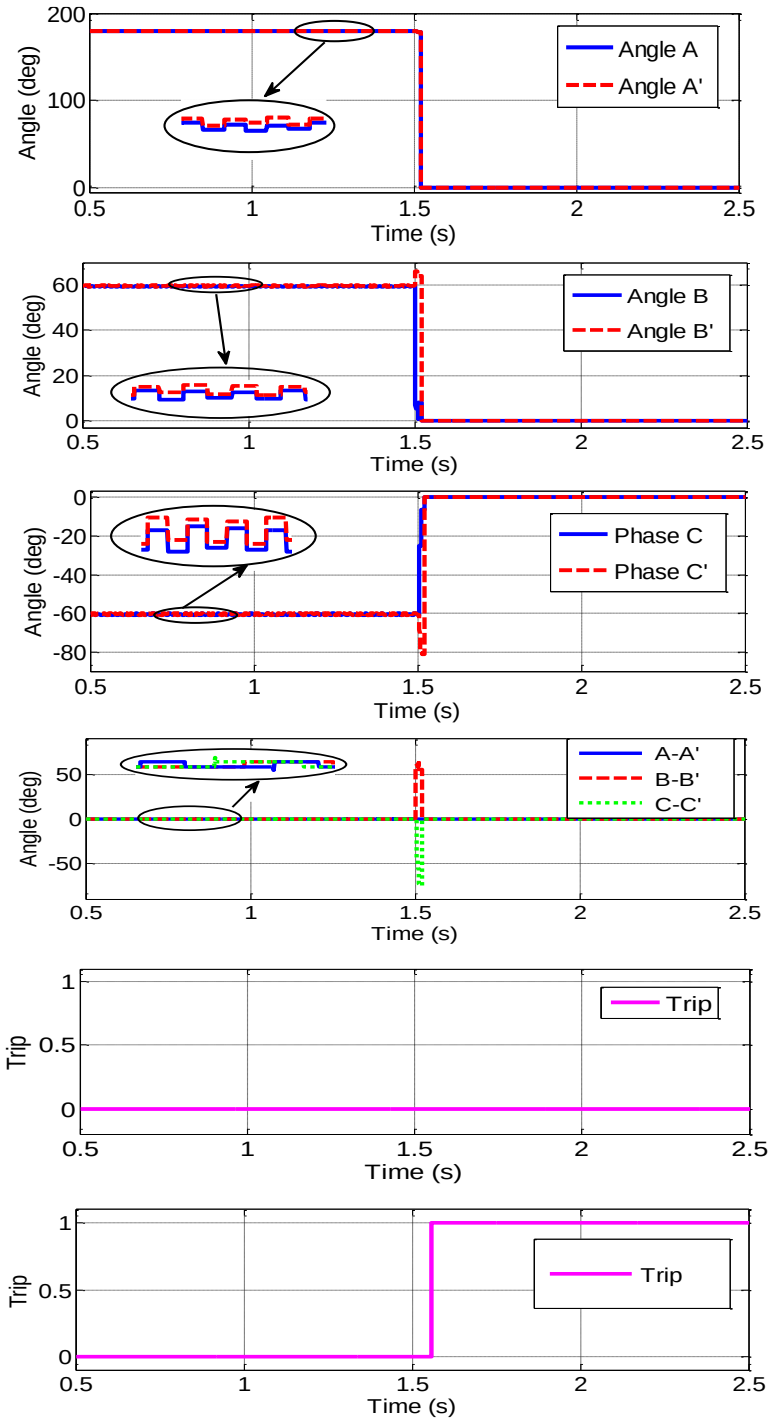

Figure 7.10 Phase angles of starting and ending sides during double line to ground fault on phases B&C in the middle of section 13. (a) Angles of phases A, A', (b) Angles of phases B, B'. (c) Angles of phases C, C' (d) Deviation angles for phases A, B and C, (e) Tripping signal of CBs 5,6, (f) Tripping signal of CBs 4,G2.

The current signals at the sending and receiving ends of section 13 are also measured during single line to ground fault on the middle of section 12 as shown in Fig. 4(a), (b) and (c). The deviation signals for phases A, B, C are shown in Fig. 4(d). The deviation signals for phases A, B, and C are less than threshold value. This means that the fault is external to section 13. Therefore, SA 13 does not send a trip signal to the CB5 and CB6 that are connected on both ends of section 13, as shown in Fig. 4(e).

The three phase current signals are measured at both ends of section 13 for a double line to ground fault on phases B and C on the middle of this section. The phase angles at both sides of section 13 are determined as shown in Fig. 5(a), (b) and (c). The deviation phase angles of Phases B and C are greater than the threshold value while the deviation phase angle of phase A is less than threshold value as shown in Fig. 5(d). SA13 sends a trip signal to CB5 and CB6 at both ends of section 13, but they fail to clear the fault, as shown in Fig. 5(e). After 200 ms the backup breakers, CB4 and CBG2, are activated to isolate the fault from the system, as shown in Fig. 5(f).

The phase angle of the three phase current signals are measured using PMU13 and PMU14 at both ends of section 12 during the three phase to ground fault in the middle of this section as shown in Fig. 6(a), (b) and (c).

The deviation of phase angle for phases A, B and C is greater than the threshold value as shown in Fig. 6(d).

This means that the fault is a three phase to ground fault and located in section 2. SA12 sent trip signals to both CB13 and CB14 at both ends of section 12 as shown in Fig. 6(e).

8.7.3 Power Restoration Case Study

To demonstrate the capability of the suggested microgrid to restore all the loads, a single line to ground fault was applied in section 13.

Using the communication between the SA13, PMU15 and PMU16, the fault can be detected and isolated from the system.

Thus, DG2 gets disconnected from the network scheme by opening the circuit breakers at this section, which affects the required power supplied to loads 1 and 2 in this circuit.

The following explanation is applied to restore power for the connected loads. L1 (is considered as current and voltage transducers connected to merging unit) communicates with LA1 (is assumed to be physical IED communication unit) and sends the values [14.5, 60, 5200, 500] which represented [Load current 1, Frequency, Active power 1, Reactive power 1], respectively.

Similar loading information is sent from [L2, L3, and L4] to [LA2, LA3, LA4] as shown in messages 2, 3 and 4 in Figure 7.11. LA3 and LA4 forwarded the values of L3 and L4 which are [14.5, 14.5], respectively to RA1.

Also, RA2 received messages from LA2 and LA1 with the pre fault information of L1, L2 as seen in messages 7 and 8. DG1 sent the value of its current which is 21 Ampere to RA1. The same messages are sent from DG2, DG3 and DG4 to GA2, GA3 and GA4 as indicated in messages 10, 11, and 12. RA1 communicated with GA3, GA4 to verify the status of DG3, DG4, and receives the data from GA1, GA2 to investigate about the available current of DG1, DG2 to supply L3 and L4 in case of disconnecting DG3 or DG4. Similar data is passed to RA2 from different generator agents as shown in messages 17, 18, 19 and 20. RA2 is informed that DG2 is disconnected, and the output capacity of DG1,

DG3 and DG4, which are [21-20-20], that represented [Current of Distributed Generator 1- Current of Distributed Generator 3- Current of Distributed Generator 4], is enough to supply the connected loads 1, 2, 3 and 4. RA2 sends signals to DG1, DG2 and DG4 in order to supply the loads as shown in messages 21, 22, 23 and 24 as seen in Figure 7.11. A similar decision is taken from RA1 in case of a disconnected DG3 or DG4.

Figure 7.12(a), (b), (c) and (d) shows the three phase currents of all DGs in the microgrid. It can be noted that the current signal of DG1 is increased from 16 A to 21 A. DG3, DG4 are increased from 15 A to 20 A in order to compensate the power losses of disconnecting DG2.

Upon comparison of Figure 7.13(a), (b) with Figure 7.13(c), (d) which show the load currents of 1, 2 and 3, 4 respectively, a higher effect and a faster restoration time can be noted on the former.

After isolating the fault and disconnecting DG2 from the system, loads 1, 2 and 3, 4 were restored after 1.55s and 1.75s respectively.

When a fault occurs in section 12, isolating it from the system using the communication between the SA12, PMU13 and PMU14.

As explained in section II, for circuit one the loads 1 and 2 will be supplied by DGs 1 and 2 respectively.

Generator 3 and 4 will be able to feed the loads 3 and 4 in circuit 2. In this case, we do not need to increase the current from generators, in such a way that the two circuits works independent from each other.

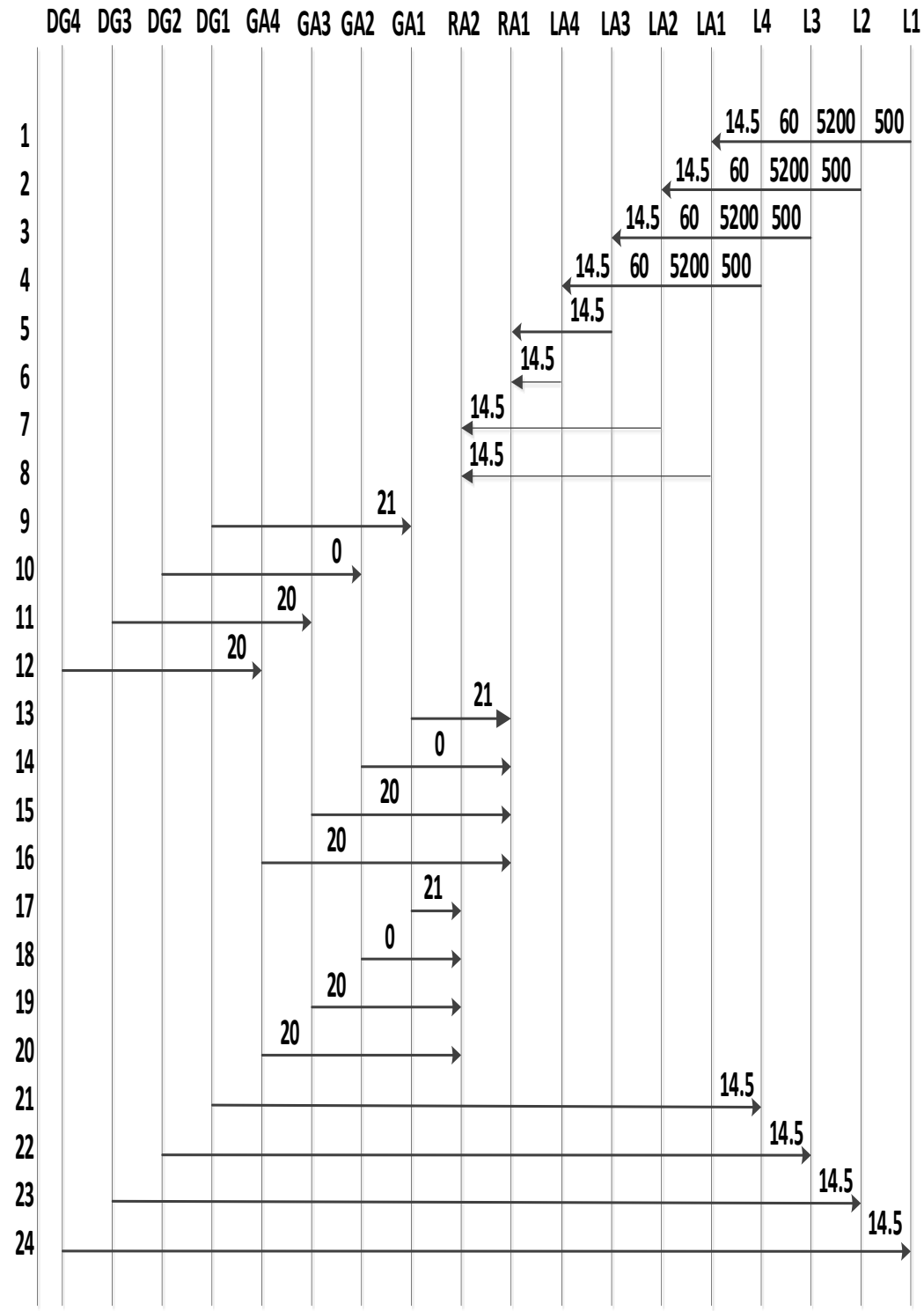

Figure 7.11 Trace of messages between agents for full service restoration.

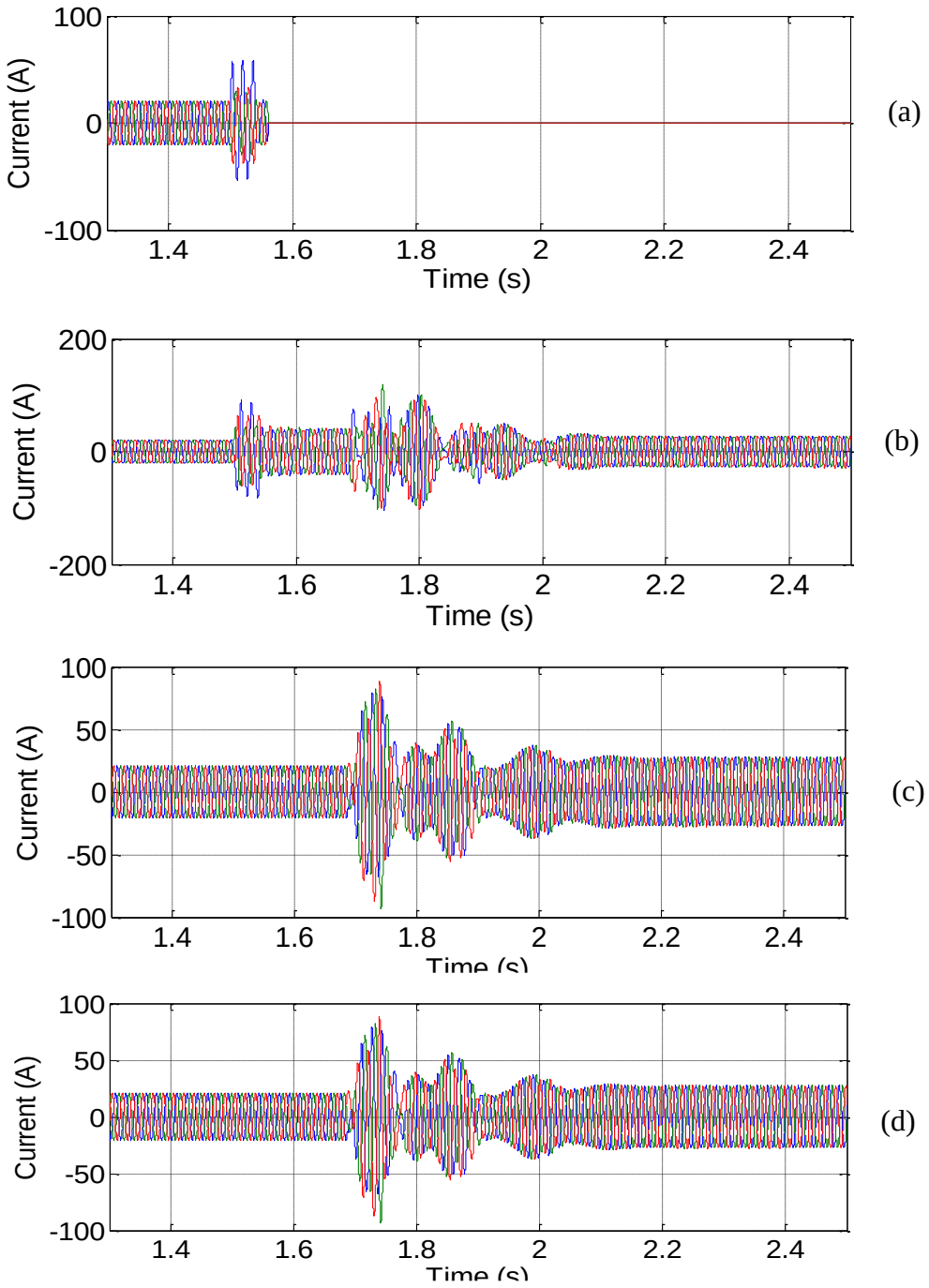

Figure 7.12 The three phase current of DGs during single line to ground fault in the middle of section 13. (a) Current of DG1, (b) Current of DG2, (c) Current of DG3, (d) Current of DG4.

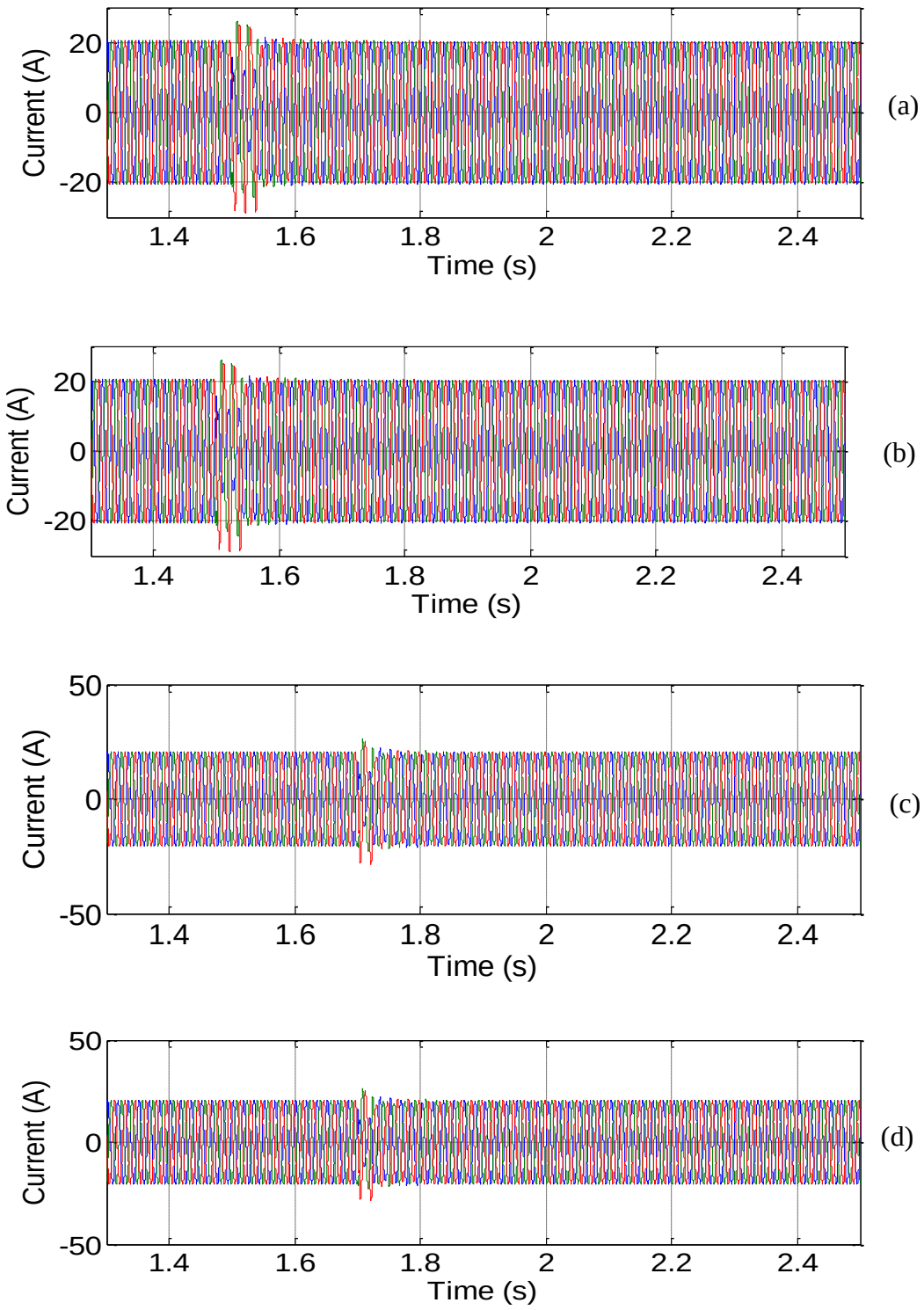

Figure 7.13 The three phase current of the loads during single line to ground fault in the middle of section 13

8.9 Summary

This chapter developed a new distribution line protection methodology utilizing contemporary communication technologies between multi-agents. This technique studied the variation of the phase angle current at both ends of the distribution line to accurate identify and isolate the faulted section in the system. This method did not need voltage transformers and improved the pilot protection scheme. Communication between multi agents was used to restore power for different loads in the system by changing the configuration of the system to maintain its reliability.

Chapter 8 A Multiagent System for Overcurrent Protection of Microgrids with Distributed Generation

The fault current level is different in grid connected and islanded microgrid fault cases for the same relay. Also, the complex architecture of the contemporary microgrid resulting from dynamically connecting and disconnecting DGs is representing serious problems to protect the system. This chapter presents a co-simulation platform for a microgrid based on MAS utilizing a supercapacitor bank to enhance the resiliency of the protection scheme. The simulation software, embedded microcontrollers, and a real communication architecture collectively perform the protection scheme platform. DDS middleware is used to link the hardware and software environments. This method does not need to change the relay settings at different configurations of the microgrid. The developed solution does not incur additional costs to the system studied, as the supercapacitor is already used to feed a pulsed load. The chapter also developes a coordination process between the relays with the help of the supercapacitor. Primary and back-up protection were studied according to IEEE Std C37.112 to isolate the fault properly. This chapter details the fault current that supplied by any DG to any point inside the network. The results showed that the co-simulation infrastructure introduces a high dependability design, analysis, and testing environment for cyber and physical data flow in the system.

8.1 Introduction

Microgrids help in reducing the dependability on conventional generation, thus reducing the emission of greenhouse gases, local energy availability, and good service quality. The renewed interest in distributed generation has resulted in a significant penetration of DGs

in microgrids [165]. One of the major advantages of higher DG penetration is the possibility of operating the distribution system in an islanded mode. The configuration and the number of DG units in a microgrid continually vary depending on the presence or outage of DG units or the installation of new ones [166]. Also, some types of DG units such as solar have an intermitting nature. These kinds of microgrids have a special impact on power flow, voltage regulation, and frequency variation of the network. Microgrids introduce a number of challenges in the protection scheme, fault level, and relay coordination due to the dynamic change of their configuration [168].

This chapter developes a technique of protection for the microgrid to avoid changing the relay settings when the system is connected at different modes of operation to minimize the communication delays for fault isolation using the co-simulation platform that contains simulation soft wares, embedded microcontrollers, and a real communication architecture. During the islanded mode of operation, we will keep the relay at a high setting and raise the current level using the supercapacitor.

The developed solution does not add cost to the protection scheme as the supercapacitor was already used to feed pulsed load at the DC side. This chapter also introduces the coordination between the primary and back-up protective elements with the help of the supercapacitor at the islanded mode of operation.

It is also worth noting here that the design of the developed controller for the supercapacitor's AC/DC converter is capable of operating when the microgrid is in both grid-connected and islanded modes. The study of how to calculate the new fault currents and fault levels for any change occurring in the system is performed in this chapter.

8.9 Microgrid Application System

Figure 8.1 shows the configuration of the microgrid that is used to investigate the developed protection scheme, and the specification of each component can be shown in Tables 8.1, and 8.2. It can be found that the system consists of inverter-based DER to help the other generators feed several loads, which were composed of ten levels of parallel resistive loads from 0 to 3 kW in steps of 300 W and power factor 0.85 at nominal voltage. [2 × 72 Ω + 4 × 144 Ω in each phase] resistance models.

Supercapacitor is connected to the system through the bidirectional converter and filter. The construction of the supercapacitor is chemical in nature; no reaction takes place.

This enables them to respond extremely quickly to a demand, while even under heavy current, their lifetime is virtually unaffected. Moreover, their response time in feeding the required power would be excellent.

A MAS is defined as a collection of autonomous computational entities (agents), which can be effective in broad applications performing tasks based on goals in an environment that can be difficult to define analytically.

Agents are high-level autonomous software abstractions. MAS are distributed and coupled networks of intelligent software agents working in coordination for a global goal. The focus of this chapter will be on the protection of transmission lines in the system using a MAS framework.

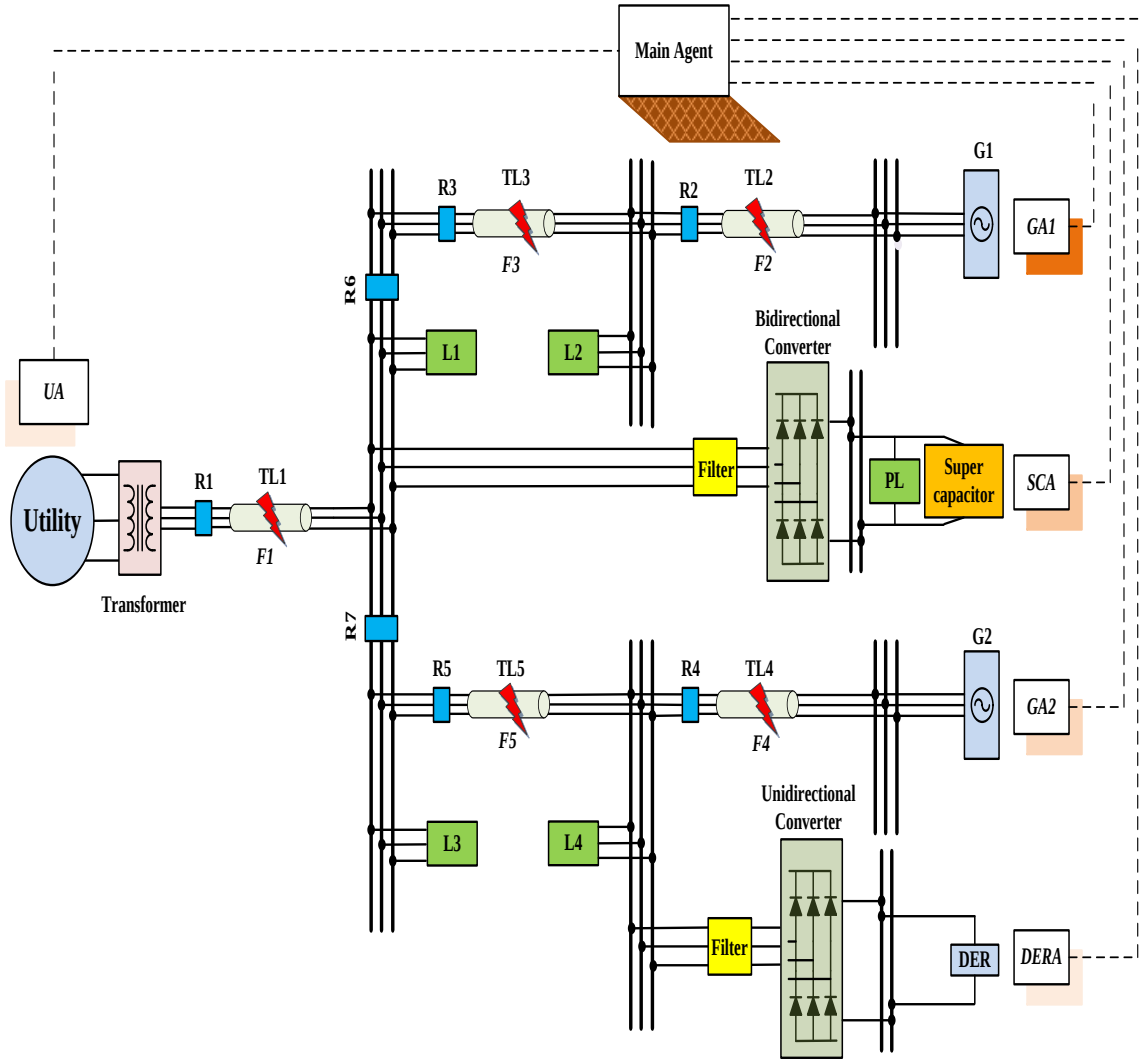

Figure 8.1 Microgrid configuration under study.

Table 8.1 Transmission Lines Parameters

TL	Length	R (Ω/km)	L (mH/km)
Line 1	10 km	2.24	0.430
Line 2	10 km	1.41	0.357
Line 3	6 km	1.41	0.357
Line 4	8 km	2.24	0.430
Line 5	6 km	2.24	0.430

Table 8.2 Specifications of the components

Component	**Parameter**	**Specification**
Generators 1,2	Apparent Power	7.5 kva
	Nominal Voltage	208 V
	Stator Leakage Reactance (X_L)	1.305 pu
	d-axis Synchronous Reactance (X_d)	2.21 pu
	q-axis Synchronous Reactance (X_q)	1.1 pu
	d-axis Transient Time Constant (T_d')	0.014 s
	Frequency (Hz)	60 Hz
Supercapacitor Bank	Number of cells	20
	Nominal voltage	320
	Rated capacity	2.9 F
	R_{SC}	2.1e-3 Ω
	Leakage Current	5.2e-3 A
	Surge Voltage	340 V
	Operating Temperature	25 Celsius
Bidirectional inverter 1	R_s	1e5 Ω
	R_{on}	1e-3 Ω
	Switching Frequency	5 KHz
Pulsed Load	PL	1.66 KW
DER	S_R	4.5 KVA
Load 1,2,3,4	L_1, L_2, L_3, L_4	900, 600, 900, 300 W

Five agents can be used in this chapter for that application. A description of the communication between the agents of the system can be shown as follows:-

Main Agent (MA): Operates as a manager of the circuit and communicates with other agents to determine the contribution of each source to the fault current.

Utility Agent (UA): It can communicate with the utility to determine the value of the short circuit current to the fault location. During grid connected mode, the fault will be fed by a high short circuit current. This level of current is sent to the main agent to identify the required current to isolate the fault.

Generator Agent (GA): This agent determines the contribution of the current from each generator during the fault.

Distributed Energy Resource Agent (DERA): The function of this agent is to identify the status of this source (on/off) and send the fault current value to the main agent.

Super-Capacitor Agent (SCA): This agent is located on the DC side to determine the capability of the supercapacitor to feed the fault during the islanded mode of operation and compensate the difference in the current between grid-connected and islanded modes of operation.

8.9 AC/DC Bidirectional Converter Control

During grid-connected mode, the variation of the AC voltage and frequency values can be ignored, as the ac side can be assumed as an infinite bus. Therefore, the bidirectional ac/dc converter only needs to regulate the dc-bus voltage. Reference I_q is set to be 0 to obtain the unity power factor. Thus, the controller only needs to control the I_d , which

controls the active power flow through the converter. The control block diagram for a bidirectional ac/dc converter in a grid-connected mode is shown in Figure 8.2. A two-loop controller is used to regulate the dc-bus voltage. Based on the error between the dc-bus reference voltage and measured voltage, the outer voltage control loop generates the I_d reference, which is used to regulate I_d in the bidirectional converter. In dq coordinates, I_d is controlled to regulate the active power flow through the inverter, and I_q is controlled to regulate the reactive power flow through the inverter. On the ac side, the active and reactive power flow will influence the frequency and voltage amplitude, respectively [188]. During the islanded operation mode, the frequency, ac voltage and dc voltage are changed. The bidirectional ac/dc inverter is used to regulate the active and reactive power by controlling the I_d and I_q, respectively. The control scheme for the bidirectional AC/DC inverter is shown in Figure 8.3. Two-loop controllers are applied for frequency and dc voltage. These parameters are used to regulate the I_d, which in its turn regulates the frequency and dc voltage of the supercapacitor bank. Using the ac side frequency as a signature to the active power flow allows the supercapacitor to supply large currents during the fault and contribute to the fault current. To control the voltage amplitude, the error between the measured voltage amplitude and the reference voltage amplitude is sent to a PI controller to generate (I_q) reference. Equations (8.1) and (8.2) show the AC side voltage equations of the bidirectional AC/DC inverter in abc and dq coordinates, respectively, where (V_a, V_b, V_c) are the ac-side voltages of the inverter, and (E_a, E_b, E_c) are the voltages of the ac bus. (Δ_a, Δ_b, Δ_c) are the adjusting signals after the PI controller in the current-control loop. The

control scheme is considered in this work because of its simplicity of implementation and fast response current loop.

$$L_{ac}\frac{d}{dt}\begin{bmatrix} i_a \\ i_b \\ i_c \end{bmatrix} + R_{ac}\begin{bmatrix} i_a \\ i_b \\ i_c \end{bmatrix} = \begin{bmatrix} V_a \\ V_b \\ V_c \end{bmatrix} - \begin{bmatrix} E_a \\ E_b \\ E_c \end{bmatrix} + \begin{bmatrix} \Delta_a \\ \Delta_b \\ \Delta_c \end{bmatrix} \tag{8.1}$$

$$L_{ac}\frac{d}{dt}\begin{bmatrix} i_d \\ i_q \end{bmatrix} = \begin{bmatrix} -R_{ac} & \omega L_{ac} \\ -\omega L_{ac} & -R_{ac} \end{bmatrix}\begin{bmatrix} i_d \\ i_q \end{bmatrix} + \begin{bmatrix} V_d \\ V_q \end{bmatrix} - \begin{bmatrix} E_d \\ E_q \end{bmatrix} + \begin{bmatrix} \Delta_d \\ \Delta_q \end{bmatrix} \tag{8.2}$$

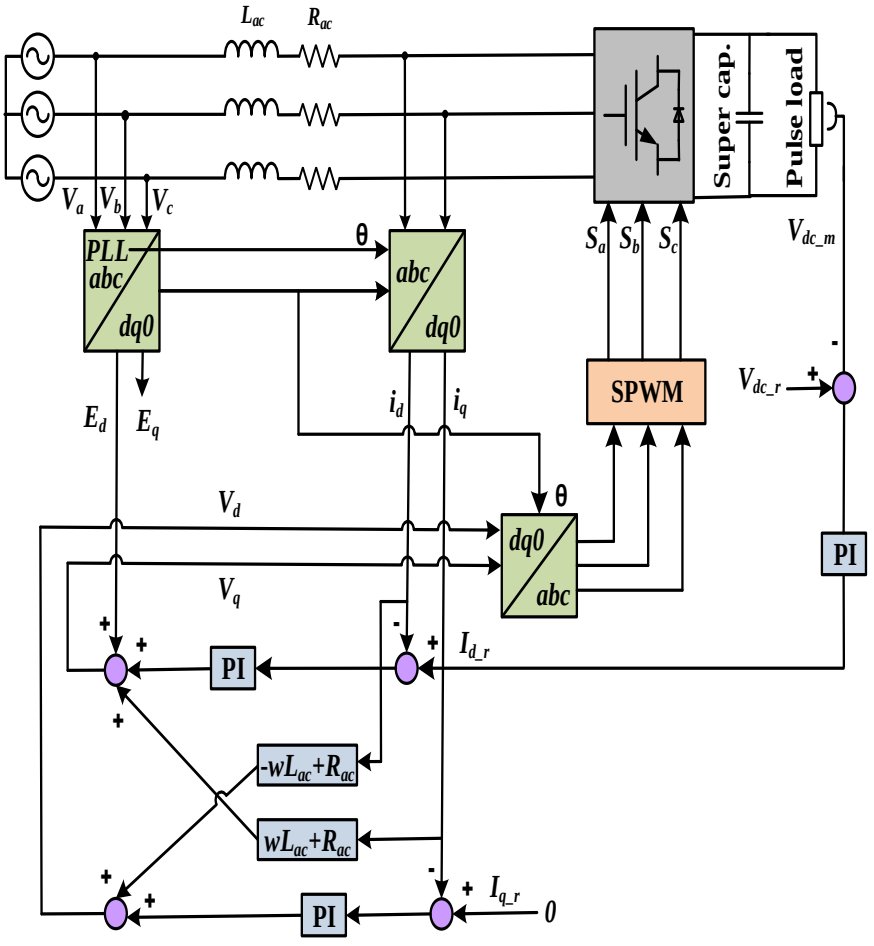

Figure 8.2. Control block diagram for the converter in a grid connected mode.

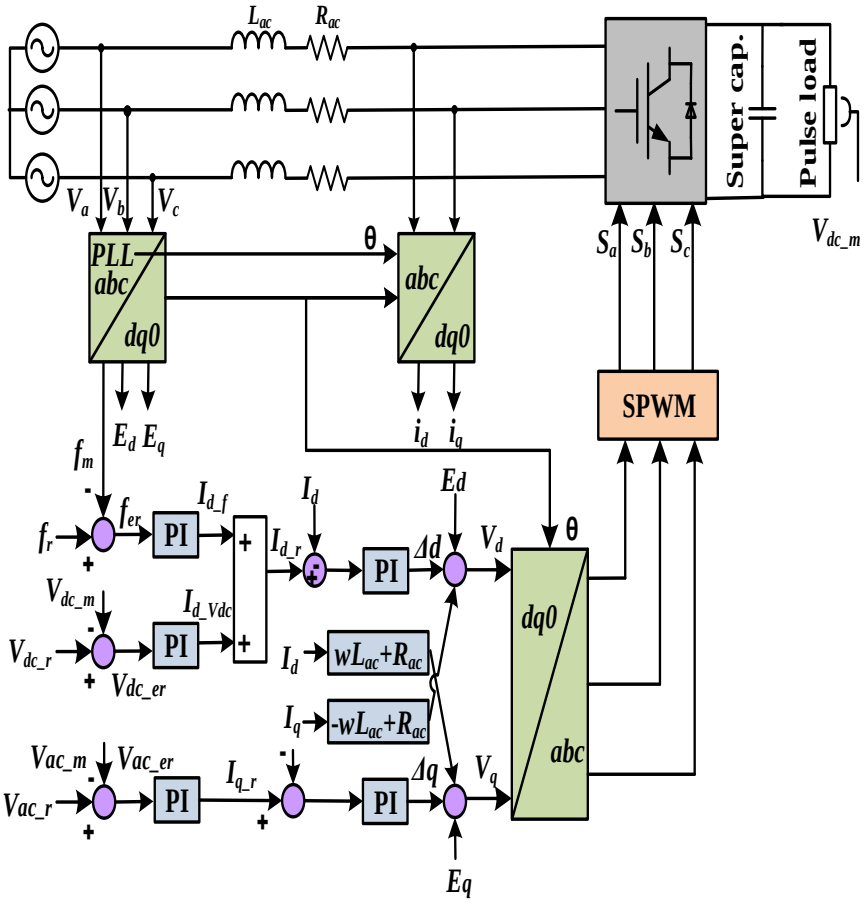

Figure 8.3 Control block diagram for the converter in an islanded mode.

8.9 Formulation of the Protection Coordination Problem

If the primary and back-up relay currents for a given fault are known, their operational characteristics can be calculated by:-

$$t_{primary} = \left[\frac{A}{\left(\frac{I_f}{I_r}\right)^p - 1} + B\right] \times TDS_{primary} \qquad (8.3)$$

$$t_{back\ up} = \left[\frac{A}{\left(\frac{I_f}{I_r}\right)^p - 1} + B\right] \times TDS_{back\ up} \qquad (8.4)$$

Where A, B, and P are constants that represent the inverse, very inverse, and extremely inverse types of over current relay (OCR), respectively. They can be selected based on the related IEEE standard [189]. The values of these constants are shown in Table 8.3. $TDS_{primary}$ and $TDS_{back\ up}$ are considered for the coordination of the primary and back-up relays.

CTI is defined as:-

$$CTI = t_{back\ up} - t_{primary} \tag{8.5}$$

To realize relay coordination, $t_{back\ up}$ should be greater than $t_{primary}$. The acceptable range for CTI is normally a value between o.2 and 0.7 s. The fault current seen by primary and back-up relays changes in case of installation of a new DER unit or the presence of a DER unit with an intermittent nature such as solar. Therefore, tuning the OCRs and their coordination will be lost. For setting the relays, the fault level of the network with DG should be calculated, as shown in the next section. The time dial setting of each relay is designed in such a way that the upstream relay will provide a backup function for the downstream relay. Figure 8.1 shows a microgrid, during islanded mode of operation. It is assumed that the currents that flows in TL2 and TL3 are the currents seen by relays R2 and R3, respectively, for a fault in the transmission line 2. R2 picks up at 50 ms (instantaneous pickup) to clear the fault. If it fails, then R3 picks up at 150ms for the current in TL3. This will give enough time for the instantaneous pickup setting of R2 to pick up and the corresponding circuit breaker to open to clear the fault. If both R2 and R3 fail to pick up, then R6 will pick up at 250 ms to clear the fault from the system. Other relays are similarly

designed. The time dial setting and pickup current for the individual relays in Figure 8.1 are given in Table 8.3.

Table 8.3 Inverse-Time overcurrent relay parameters

Parameter	**Value**	**Remark**
TD1	0.07 s	Time Dial setting of R2
TD2	0.05 s	Time Dial setting of R3
TD3	0.06 s	Time Dial setting of R4, R5
TD4	0.03 s	Time Dial setting of R6, R7
A	3.922	Characteristic parameter
B	0.0982	Characteristic parameter
P	2	Characteristic parameter
I_r	5.34 A	Rated Current

The controller performance was validated through simulation on MATLAB/Simulink. Multiple simulation cases were performed to show the validity of the developed controller.

8.7.3 Calculation of DGs Fault Current

Fault currents supplied by DGs were approximated to 5 times their rated currents whilst fault currents from PE-interfaced DGs were approximated to about 1.5 times their rated current. Then, for a given relay "r" in the network, the operating current is calculated, as in (8.6). This equation considers the grid's and all DGs' fault contribution, including the supercapacitor on that particular relay:-

$$\mathrm{I}_r = I_{f\_G} + I_{f\_DG} + I_{f\_DER} + I_{SC} \tag{8.6}$$

The contribution of the fault grid is calculated, as shown in Figure 8.4, by taking the Thevenin equivalent of the electric network, as in traditional fault current calculations:

$$I_{f_G} = \frac{V_{th}}{Z_{th}} \tag{8.7}$$

Therefore, in the above equation. V_{th} is a constant value while Z_{th} is a function of distance, i.e., $Z_{th}(x)$. In this case, the fault grid contribution also becomes a function of the distance and can be defined as:-

$$I_{f_G} = \frac{V_{th}}{Z_{th(x)}} \times Operation\ Mode \tag{8.8}$$

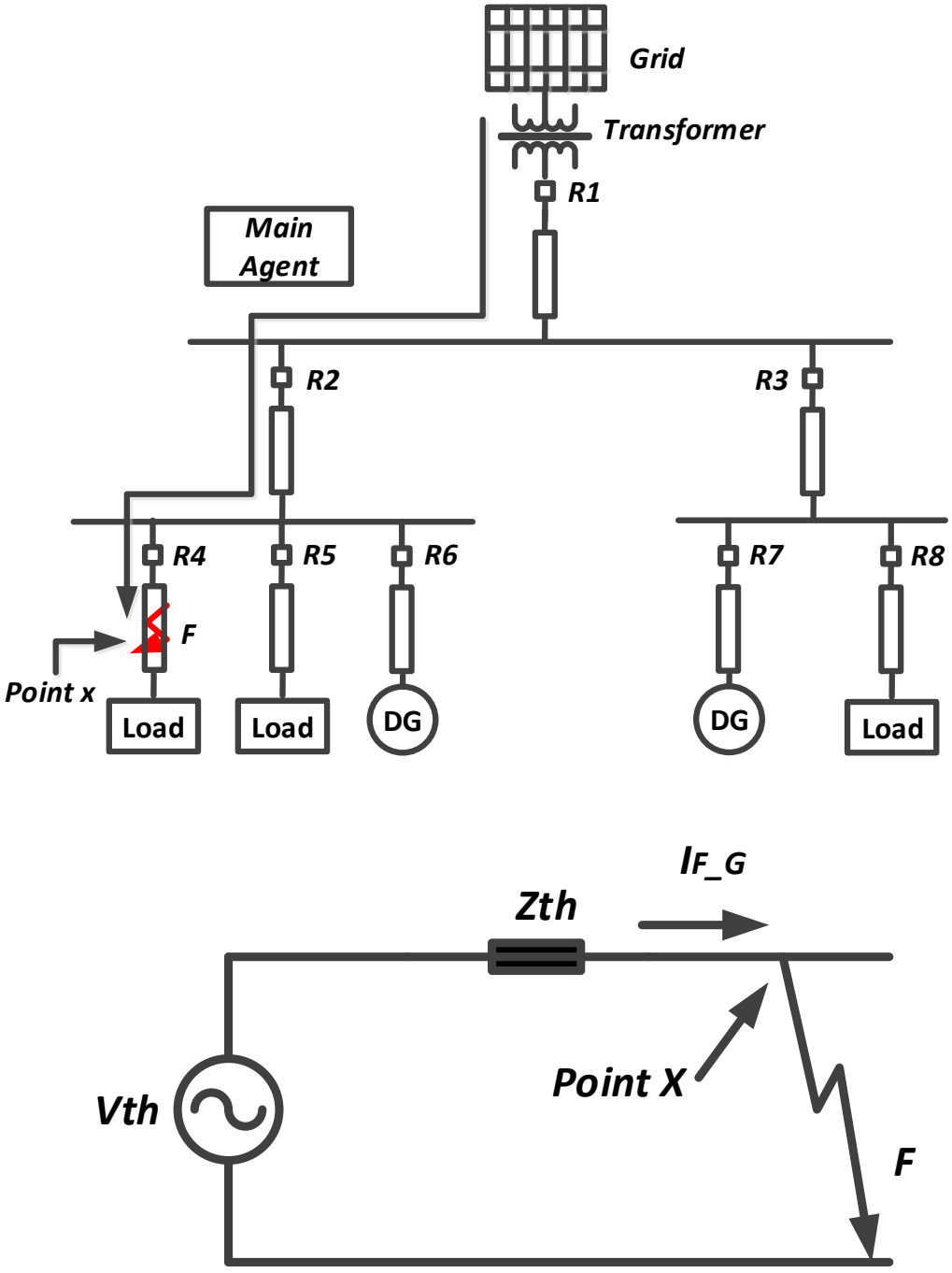

Figure 8.4 Thevenin equivalent circuit taken from point X.

If the microgrid is operating in islanded mode, then the grid's fault contribution will be multiplied by the "Operating Mode" bit, which will be equal to 0.

$$I_{f\_DG} = Av.\times \left(5 \times \sum_{i=1}^{n} \frac{I_{f\_x}}{I_{FM\_DG}} I_{r_{DG}} \times Status_{DG} \right) \tag{8.9}$$

$$I_{f\_DER} = \left(1.5 \times \sum_{j=1}^{m} I_{r_{DER}} \times Status_{DER} \right) \tag{8.10}$$

The signal Status indicates whether that source is in operation or not. Depending on the type of the source, i.e., whether it is inverter interfaced or with rotating machines. In the literature, the fault contribution of the Inverter interfaced DGs is reported to be between 1.2 and 2 [190]. In order to be practical and more realistic, authors selected the coefficient 1.5 since the extreme conditions (where the fault contribution is 1.2 or 2) will not occur as frequently as conditions which require the fault contribution coefficient to be 1.5.

In this case, it considers a capacitor in series with a resistance. The SC model input is the power PSC absorbed/injected from/to the SC [191]. The SC current is defined as follows:-

$$I_{sc} = \frac{Q_{sc}/C_{sc}}{2 \times R_{sc}} - \frac{\sqrt{(Q_{sc}/C_{sc})^2 - 4 \times R_{sc} \times P_{sc}}}{2 \times R_{sc}} \tag{8.11}$$

8.9 Communication Infrastructure of Protection for the Microgrid

In this work, the DDS is a standard for data-centric communication middleware from the OMG. The DDS is selected by SGIP and for open FMB implementation. The DDS utilizes the RTPS mechanism without a message broker scheme, which simplifies the communication between different nodes. The DDS is data-centric middleware, which helps to maintain the focus on the algorithm and control development rather than being

concerned with the communication and data delivery issues. The utilization of RTPS as wire transfer protocol insures the interoperability between different vendors. For flexible integration with different applications, DDS provides standard Application Programming Interface (API) for support C, C++, Java and .NET. DDS provides reliable peer-to-peer communication for control agents by avoiding a message broker. The DDS reach sets quality of service profiles, which enable full control and predictable communication performance for each data type. Unlike other communication schemes, which applies Quality of Service (QoS) policy on the all streams, DDS applies QoS for each individual data type. This feature helps to achieve a predictable network behavior and meet different communication requirements. The QoS policy defines a different set of rules that controls how the data is sent and handled [192].

For this chapter, the simulation model needs to be created to link the components of the co-simulation framework. Then, the measurement points and the DDS gateways should be identified. The Interface Definition Language (IDL) file is used to organize the data structures. In order to identify the quality of service for each application, an XML file is created. For the cyber part, the communication protocol and communication language are identified for the hardware devices. The data mapping table should be developed to manage the interpretation between the data structures of the DDS gateways and the protocol of the hardware devices. DDS domain is used to link the communication software with the hardware devices. That domain creates different topics to link the components of the system. The hardware devices are; Odroid C2 from Hard kernel manufacturer embedded microcontrollers that have the ARM® Cortex®-A53 1.5GHz processor and are running on a real-time Linux Kernel. Also, a dedicated Ethernet switch was used during the study.

Figure 9.5 shows the block diagram that links the cyber and physical layers. It consists of the two generators, DER, supercapacitor bank and utility. The cyber layer is composed of a two-level hierarchy of agents. The lower cyber layer consists of 5 agents, which are responsible for calculating the required current to trip the circuit breaker at an abnormal condition, whereas the upper cyber layer is composed of a Main Agent (MA), which is responsible for gathering the current from the different sources and keeping the coordination between the relays. A communication layer links the physical and cyber layers together through a Global Data Space, which contains four topics: current, frequency, voltage and ON/off States. A DDS gateway is created for every source of the simulated microgrid. On one hand, these gateways will collect and publish the necessary input for the hardware agents.

On the other hand, they will subscribe to the commands issued by the hardware agents and execute them on the simulated microgrid. The main agent receives the frequency signal from the PCC (point of common coupling) access point that links the microgrid to the utility to identify the mode of operation. During the grid connected mode of operation, the main agent receives the required current to trip the circuit breaker from Utility Agent (UA). For the islanded mode of operation, the different sources of the microgrid send their contribution currents to the main agent. According to the Equations (9.9-9.11) the main agent calculates the required current to isolate the fault from the system and asks the Supercapacitor Agent (SCA) to compensate the difference and trip the circuit breaker.

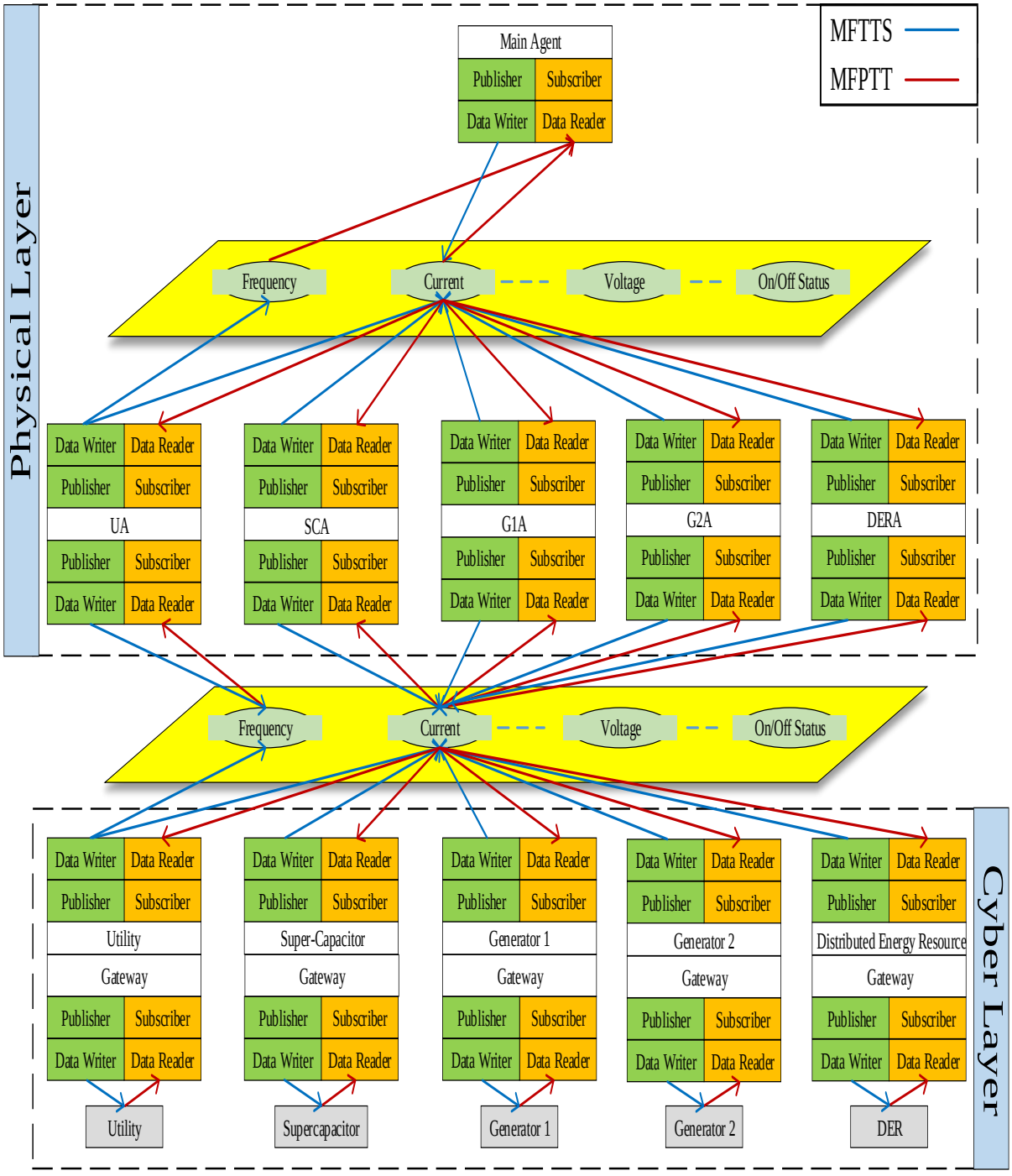

MFTTS:- Message From Topic To Subscriber; MFPTT:- Message From Publisher To Topic

Figure 8.5 DDS network and microgrid logical control hierarchy.

The main agent updates the statues of each source during the operation to adjust the required current from the supercapacitor to inject the required current. Also, the main agent receives the voltage signals from the different sources to ensure that the system is stable after isolating the fault. As it will be seen from the results of this study, the developed framework was successful in providing a smooth link between a multi-agent hardware/software infrastructure and the simulated power system. Through this link, the effect of the control logic, which was implemented in C++, was tested, and the response of the power system to the control logic was investigated.

8.9 Case Studies

8.7.3 Hybrid microgrid performance in a grid-connected mode.

In this case, a three-phase to ground fault (F2 in Figure 8.1) has been applied in transmission line 2. The system performance during this fault is indicated in Figure 8.6. As it can be noticed, the fault occurred at t = 6 seconds and isolated from the system.

In this case, the utility helped to maintain the system's stable frequency during and after the fault, as shown in Figure 8.6(a). Figure 8.6(b) shows the pulsed load (I_{PL}), supercapacitor (I_c), and inverter (I_{inv1}) currents.

During the off-time pulsed load, the supercapacitor will be charging from the AC side, whereas during the on-time pulsed load the supercapacitor will be the major feeder to the pulsed load, as indicated in Figure 8.6(c). The AC side will still be present to feed the pulsed load in case the supercapacitor goes out of service. The different agents that are distributed beside the sources (GA1, GA2, DERA, and UA) sent their contribution currents to MA.

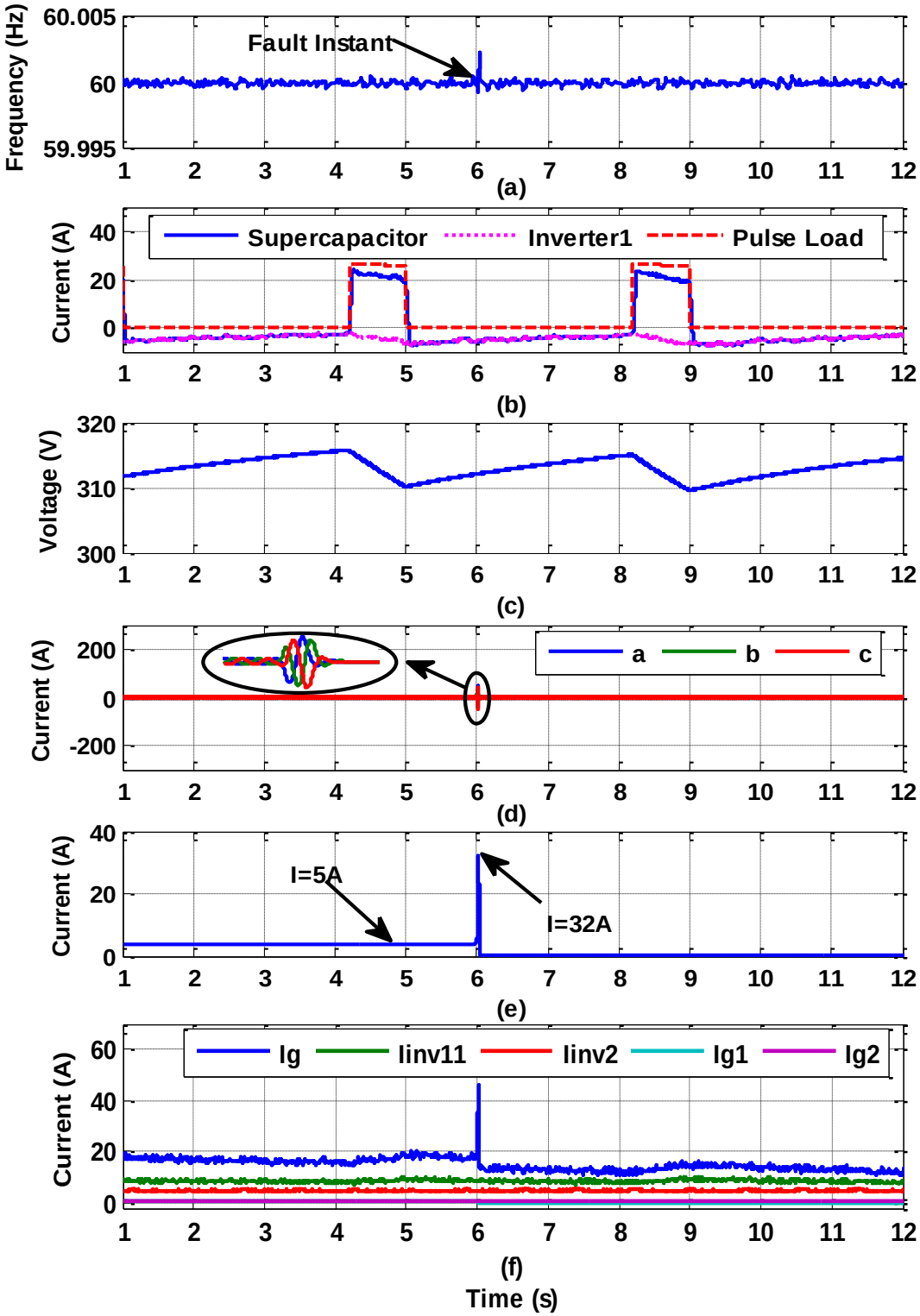

Figure 8.6 System performance during fault at grid connected mode of operation: (a) frequency, (b) supercapacitor current, inverter current, and pulsed load current, (c) supercapacitor DC voltage (d) three-phase currents in the faulted transmission line, (e) RMS current in the faulted transmission line, (f) Source currents.

Figure 8.6(d) and (e) show the high fault current values of 32 Amps which is, mainly, being contributed by the grid. It can be noted here that this setting is saved in MA for that relay (R_2). As anticipated for the grid connected mode, the fault current is almost more than 6 times the rated AC current and thus the protection devices were able to detect and isolate the faults successfully.

This current (32 Amps) will sent to the main agent to identify the required current to isolate the fault during the islanded mode without changing the relay settings.

8.7.3 Hybrid microgrid performance in an islanded mode.

In this case, fault F2 occurs during the islanded mode. The main agent asks DERA, GA1and GA2 to send the value of the contribution from each source, and asks SCA to inject current from SC to avoid changing the setting of R_2. As shown in Figure 8.7(b), the supercapacitor can compensate the fault current with 20 A in order to reach to the high setting of the relay (32 A), as indicated, in Figure 8.7(c). This resulted in relay R_2 sensing the fault and thus isolating it accordingly. After clearing the faulted region, the system restored and showed stable performance, as indicated in Figure 8.7(a).

8.7.3 Islanded mode of operation during supercapacitor discharging.

In this case, the supercapacitor needs to be designed to supply both the pulse load and the fault current requirements. The system performance during a fault F2 at these circumstances is described in Figure 8.8. As indicated in Figure 8.8(b), the fault occurred during the discharging of the supercapacitor phase of the pulse load period. It is noted that the supercapacitor quickly contributed to the fault current while still covering the pulse load. The can be observed as reflected on the pulse load current and the frequency as well

as the DC voltage as changing within the accepted limits (see Figure 8.8(a) and Figure 8.8(c)).The maximum current drawn from the supercapacitor in this case is 45 Amps, which is required to feed the fault and the pulse load simultaneously. Figure 8.8(e) shows that the fault current drastically increased from 5 Amps to 32 Amps. This resulted in relay R_2 sensing the fault and thus isolating it.

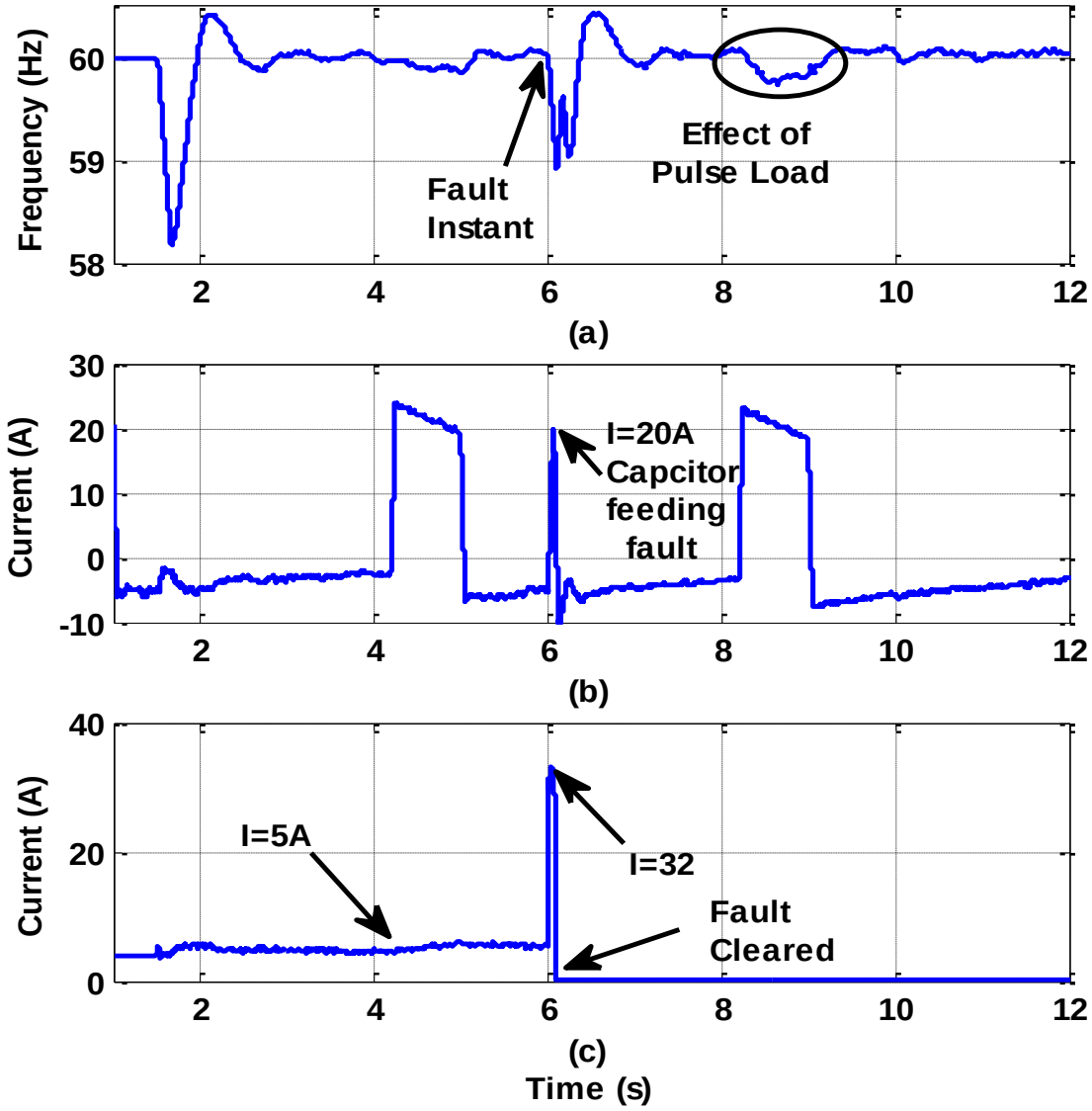

Figure 8.7 System performance during fault at microgrid operation (a) frequency, (b) supercapacitor current, and (c) RMS current in the faulted transmission line

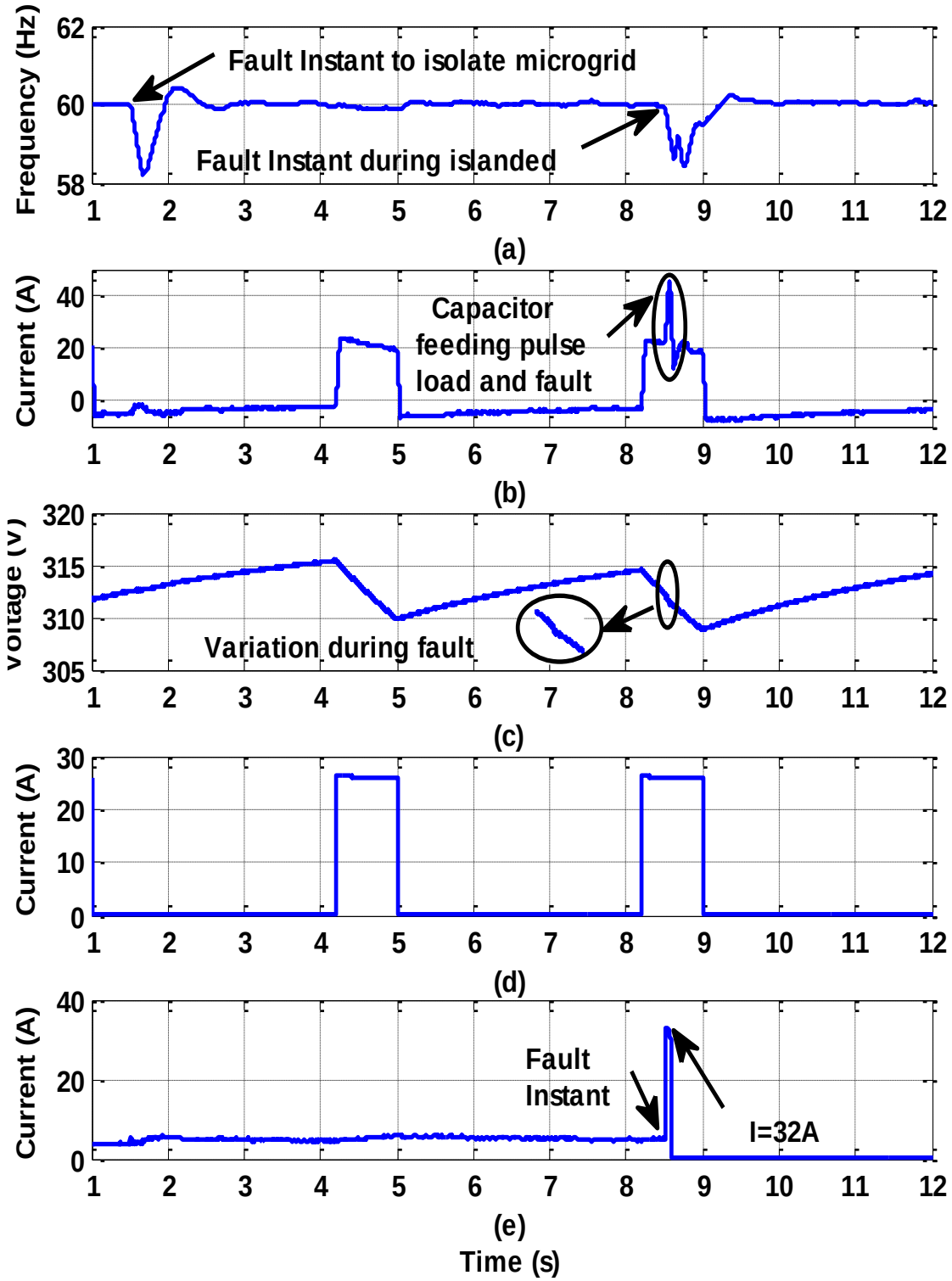

Figure 8.8 System performance during fault at microgrid operation (a) frequency, (b) supercapacitor current, (c) supercapacitor DC voltage, (d) pulse load current, and (e) RMS current in the faulted transmission line

8.9 Results and Discussion for the Coordination between Relays

The communication between MA, and other agents (GA1, GA2, SCA, DERA) at the islanded mode of operation is used to demonstrate the capability of the suggested microgrid to coordinate between the protective relays. The utility gets disconnected from the network scheme by tripping R1.

GA1 communicates with MA and sends the value (I_G1), which represents the current of generator1 during the fault. Similar loading information is sent from (GA2, SCA, DERA) to MA as shown in messages 2, 3 and 4 in Figure 8.9. MA sends a request to SCA to inject current from SC to reach to the settings of the different relays according to the location and the type of the fault (e.g. F2 is the fault at transmission line 2 and R2 is the Main relay, 1st Back up relay R3 and 2nd back up relay (R6)).

The results of the system during the islanded mode of operation for several types of faults in the transmission lines of the system are shown in Table 8.4. The numerical figures in the third row represent the results of different case studies discussed earlier at three phase to ground fault (ABCG) for F2.

The contribution of the different sources is introduced and indicates the important role of the energy storage device (supercapacitor) to help, whether the primary or back up protection devices to reach the required setting and isolate the fault from the system.

For F2 in the transmission line 2, it can be found that the contribution of the SC is represented (63.25%) of the total fault current (32A) to activate R2 (primary protection) and trip the main breaker.

In case the operation of R2 fails, and after the delay time according to the location of R2, as shown in Table 8.2, R3 is activating to isolate the fault. In order to make another back-up for R2, R6 will be activated to isolate the fault from the system. It can be found that the CTI was checked and the selectivity was within the accepted limits. The same results can be shown at the different types of fault (AG and BCG), and the primary and secondary protection elements were performed and verified according to the coordination standard.

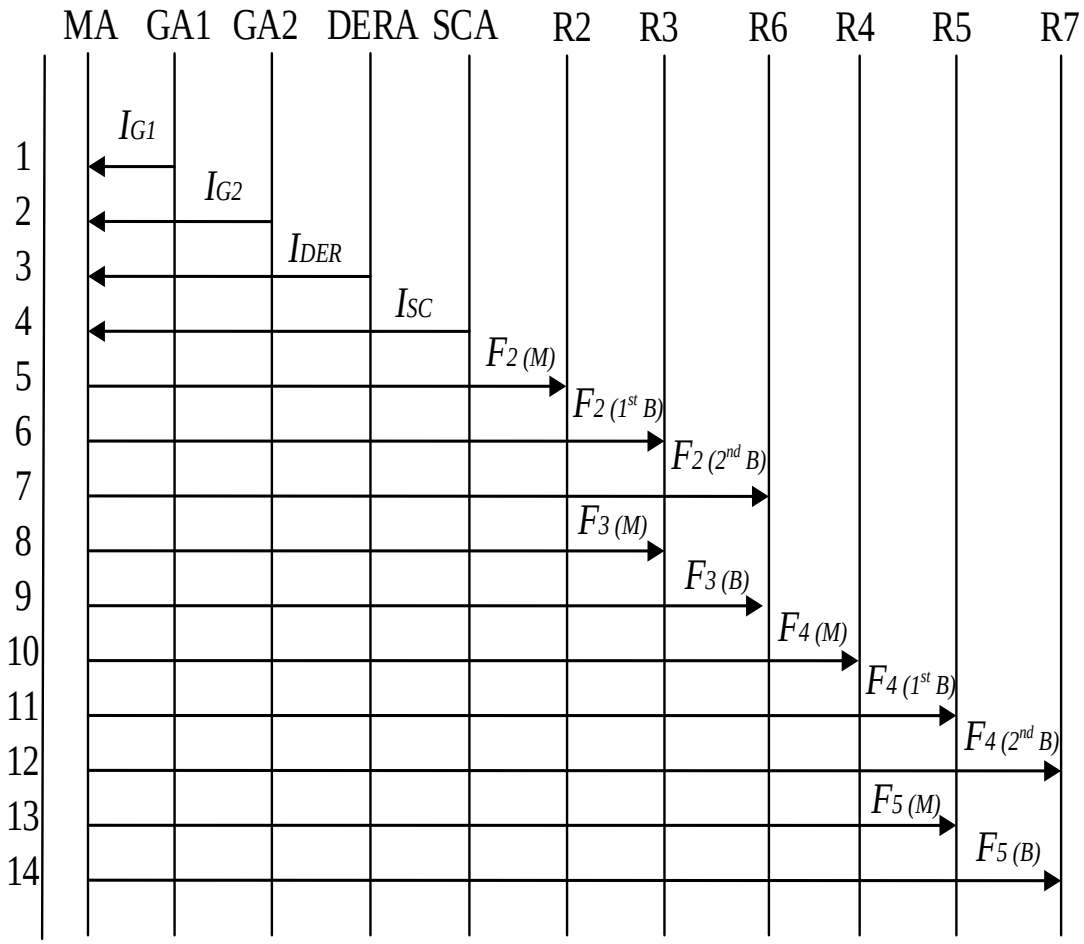

M:- Main protection, B:- Back up, 1st B:- First back up, 2nd B:- Second back up.

Figure 8.9 Trace of messages between agents for full service coordination.

Table 8.4 Primary and back-up protection

Fault Location	Type of fault	Contribution of sources (Amps)				Primary Protection		Back Up Protection		CTI (S)
		DER	G1	G2	SC	Relays	O.T (S)	Relays	O.T (S)	
F2	AG	1.99	4.12	2.50	10.43	R2	0.125	R3	0.769	0.644
								R6	0.775	0.650
	BCG	2.35	4.67	3.21	15.39	R2	0.090	R3	0.589	0.499
								R6	0.625	0.535
	ABCG	2.80	5.11	3.85	20.24	R2	0.095	R3	0.336	0.241
								R6	0.490	0.395
F3	AG	3.87	3.12	2.88	8.89	R3	0.092	R6	0.682	0.590
	BCG	2.21	6.34	3.67	13.22	R3	0.088	R6	0.491	0.403
	ABCG	3.87	7.47	4.13	22.90	R3	0.071	R6	0.359	0.288
F4	AG	1.92	1.04	4.87	7.87	R4	0.140	R5	0.658	0.518
								R7	0.754	0.614
	BCG	2.54	2.58	5.87	10.25	R4	0.112	R5	0.421	0.309
								R7	0.582	0.470
	ABCG	4.77	5.64	9.62	14.87	R4	0.093	R5	0.351	0.258
								R7	0.475	0.382
F5	AG	3.12	3.57	4.88	12.54	R5	0.081	R7	0.645	0.564
	BCG	4.21	5.26	6.96	17.19	R5	0.073	R7	0.428	0.355
	ABCG	5.62	6.73	8.89	23.74	R5	0.069	R7	0.314	0.245

8.9 Summary

This chapter presented details on the development of a hybrid hardware-software co-simulation platform capable of modeling the relation between the cyber and physical parts to provide a protection scheme for the microgrid. The microgrid was simulated on MATLAB/Simulink SimPowerSystems to model the physical system dynamics, whereas all control logic was implemented on embedded microcontrollers communicating over a

real network. The chapter suggested a protection methodology utilizing contemporary communication technologies between multi-agents to protect the microgrid. A supercapacitor is used for enabling the relay to isolate the fault during the islanded mode operation without changing its grid setting. Due to the limited sources of the microgrid during the islanded mode, the super-capacitor bank was implemented to assist the protection elements (primary and back-up) to reach their settings and clear the fault from the network. The contribution from the different sources in the system to feed the fault current was studied. Several cases were conducted to investigate the developed protection technique at different locations in the system.

Chapter 9 Hardware Setup

9.1 Introduction

This chapter introduced the hardware setup of the developed protection schemes that were introduced in the previous sections. One of the main contributions of this dissertation is to create a solution of the communication outages for the protection scheme that is prevent the relyas to trip during the islanded mode operation. To perform this method, we developed a microgrid platform that consists of AC and DC sides and connected through bidirectional converter to all the energy storage device to inject current at this critical case.

We used several programming loads at AC side that were fed by the grid and some synchronous generators at normal operation. For the DC side we selected the supercapacitor to feed pulsed and constant loads at normal operation. The controller of the supercapacitor is adjusted to allow of moving the current from DC to AC side when the communication is not available in the system. The sizing of the supercapacitor was optimized and tested to ensure from the performance of the system at the selected values of the controller.

The results showed an excellent performance to the system and the cost of the protection system was investigated. Another test was performed in Smart Grid Test Bed is the operation of the system when the fault occurred and the need to isolate it and restore the power to the loads using MAS.

9.2 Experimental Verification

The hybrid AC/DC microgrid, used for experimental verification, consists of several types of sources that supply loads with different characteristics, including: AC load, a normal steady-state load, and a heavy pulsed load at DC side. Figure 9.1 shows the experimental test setups of the microgrid. The hardware setup and the control structure for this system and the interconnected AC grid are explained in the following sections.

The two AC generators are mainly supplying different loads which composed of ten levels of parallel resistive loads from 0 to 3 kW in steps of 300 W at nominal voltage. [2 ×72 Ω + 4 × 144 Ω in each phase] resistance models, which can be controlled by PLC, to emulate various load patterns.

This system also includes supervisory control and data acquisition system to monitor the entire system. More details about the AC grid testbed configuration and control can be found in [37], [38]. In addition, a supercapacitor bank was implemented as an energy buffer in our hybrid AC/DC power system laboratory test-bed.

An analog hysteresis protection is designed to ensure that uneven charge distribution, particularly during very fast charges, does not cause the supercapacitor to exceed its maximum voltage limit. This protection unit also provides a backup for the energy control system. If the voltage on any of the supercapacitor arrays exceeds the preset limit, the analog control circuit will open the output of the insulated-gate bipolar transistor (IGBT) switch (sw), as shown in Figure 9.1

The charging path remains open until the supercapacitor is discharged through the bypass diode to the point that its voltage is reduced to the predefined safe threshold.

The detailed parameters of the system are summarized in Table 9.1. For dynamic operation and fault study, the detailed model of the microgrid shown in Figure 9.1 is implemented in our virtual test-bed platform using the MATLAB/Simulink software and executed with the dSPACE 1104 real-time interface to control and adjust the pulsed load and the steady-state load. In order to obtain the optimal values of the PI controllers, the Simulink Response Optimization toolbox was employed [193].

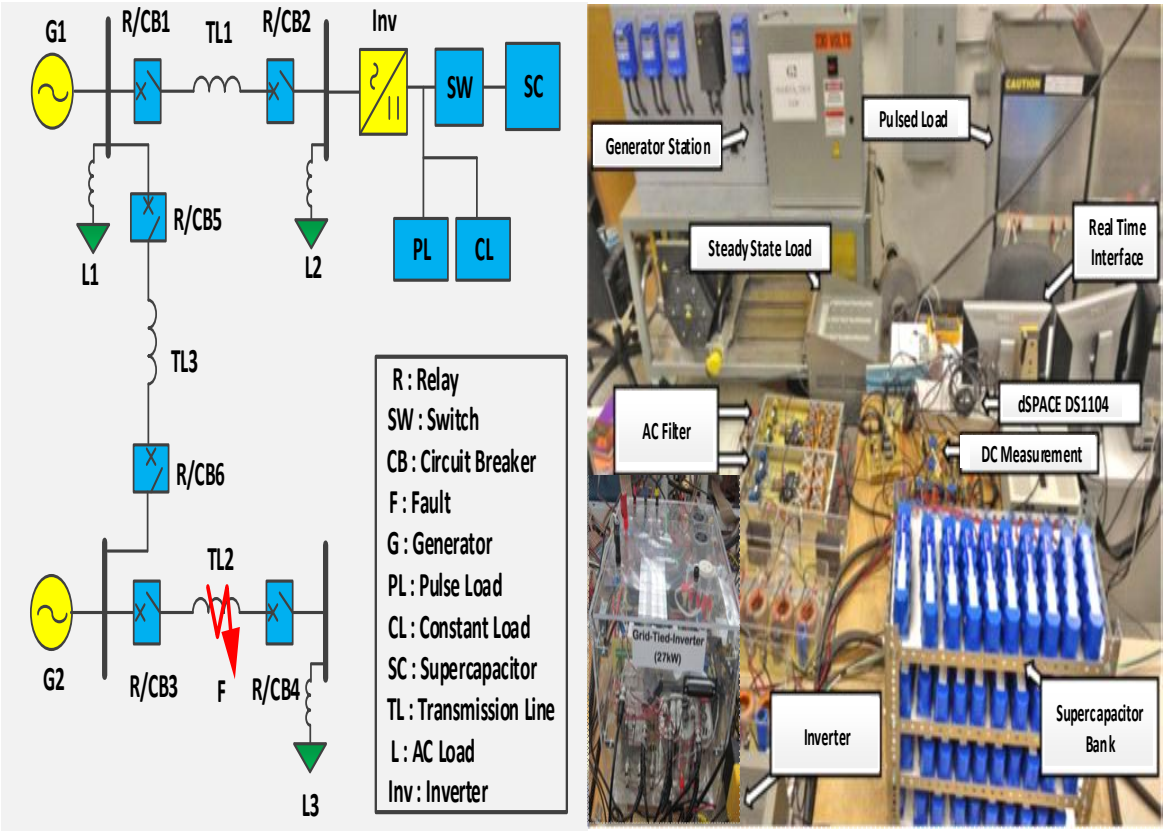

Figure 9.1 General view of the experimental test setup

9.3 Experimental Test Results

The performance of the microgrid at islanded mode of operation was evaluated in three test cases: First, utilizing the original supercapacitor size and controller parameters, then, utilizing the values obtained from the two-level optimization process. Finally, the case in

which the pulsed load is disconnected at fault instant was tested for the developed protection technique.

Figure 9.2 shows the performance of the microgrid using the original supercapacitor value and controllers parameters (C = 2.9 F, k_{p_f}=50, k_{i_f}=100, k_{p_vac}=40, k_{i_vac}=110, k_{p_vdc}=30, and k_{i_vdc}= 100). During the supercapacitor's discharging period between t = 0.94 sec and t = 2.97 sec, the frequency of the system remained at 59.81 Hz and the DC voltage dropped a little from 320 V to 311 V, as shown in Figure 9.2 (a) and (b) respectively.

Also, during the supercapacitor charging period between t = 2.98 sec and t = 5.05 sec, the system frequency was stable at 60 Hz and the DV voltage at 320 V. A three phase to ground fault occurred at t = 6 seconds. This was accompanied by a drop to 59.32 Hz. Figure 9.2(c) shows that during the fault period, the supercapacitor's current increased from 5.21 A to 9.86 A, which indicates that the fault current contribution from the supercapacitor was 4.65 A. Figure 9.2(d) and (e) show that the pulsed load and steady state currents remained stable throughout the experiment. Figure 9.2(f) indicates that the total fault current of R_3 is 7.2 A, thus reaching the high relay settings, which is assumed to be 3 times the normal current (2.4 A). Note that current values in the hardware experimentation were scaled down, compared to those in the simulation, to operate in safe experimental limits in a laboratory environment and the relay settings were adjusted accordingly.

It is important to note that the system maintained it's a stable operation in the experiment. That is, the frequency remained between the acceptable ranges of 59.7 Hz and 60.2 Hz and the AC and DC voltages have a maximum acceptable variation of $\pm$5% of their rated values.

Table 9.1 System Component Ratings

Component	Parameter	Specification
G1, G2	Apparent Power Nominal Voltage Stator Leakage Reactance d-axis Synchronous Reactance q-axis Synchronous Reactance d-axis Transient Time Constant	13.8, 10 KVA 208, 208 V 0.09 0.09 pu 2.21, 2.248 pu 1.1, 1.1 pu 0.014, 0.012 s
Supercapacitor bank	Number of cells Rated voltage Rated capacity Surge voltage Leakage current	20 320 2.9 F 340 5.2 mA
Inverter	R_s R_{on} Switching frequency	1e5 Ω 1e-3 Ω 5 KHz
Transmission Line	$r_{1,}$ r_0 $l_{1,}$ l_0 $c_{1,}$ c_0	0.0015 Ω/Km, 0.03 Ω/Km 0.03 mH/Km, 0.1 mH/Km 3 nF/Km, 2nF/Km
Constant Load	CL	550 W

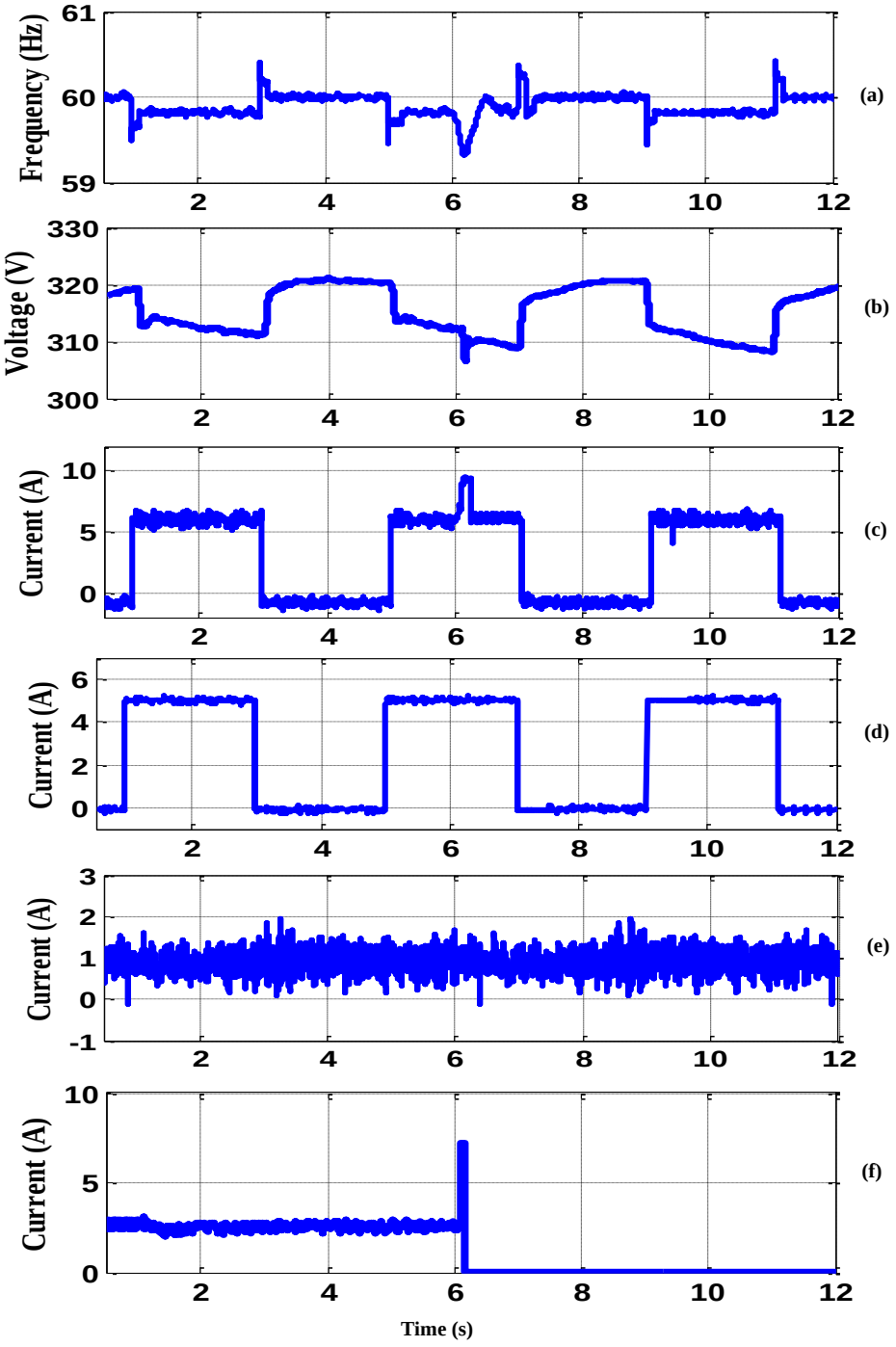

Figure 9.2 Experimental test results during fault at islanded mode of opera-tion without optimized supercapacitor size (a) frequency, (b) superca-pacitor DC voltage, (c) supercapacitor current, (d) pulsed load current, (e) steady state load current, (f) RMS current in the faulted transmission line.

Figure 9.3 shows the performance of the microgrid using the optimized supercapacitor value and controllers parameters (C = 2.5 F, k_{p_f}=65, k_{i_f}=110 , k_{p_vac}=30, k_{i_vac}=115, k_{p_vdc}=40, and k_{i_vdc}=110).

Similar to the previous case, the system operating under the optimized values was capable to maintain its frequency within the acceptable limits.

In fact, during the fault instant at t= 18.8 sec, the frequency dropped to a minimum of 59.61 Hz as shown in Figure 9.3 (a), which is better than the drop to 59.32 Hz of the previous case.

Figure 9.3 (b) shows that during the fault, the supecapictor's current increased from 5.21 A to 7.8 A, which indicates that the fault current contribution of the supercapcitor in this case is 2.59 A.

This corresponds to a 44.3% reduction in the supercapacitor's fault current contribution compared to the previous case.

However, Figure 9.3 (e) shows that the fault current still reached 7.2 A and the relays were activated.

This is because the remaining fault current was supplied by the AC generators as intended from the optimization process.

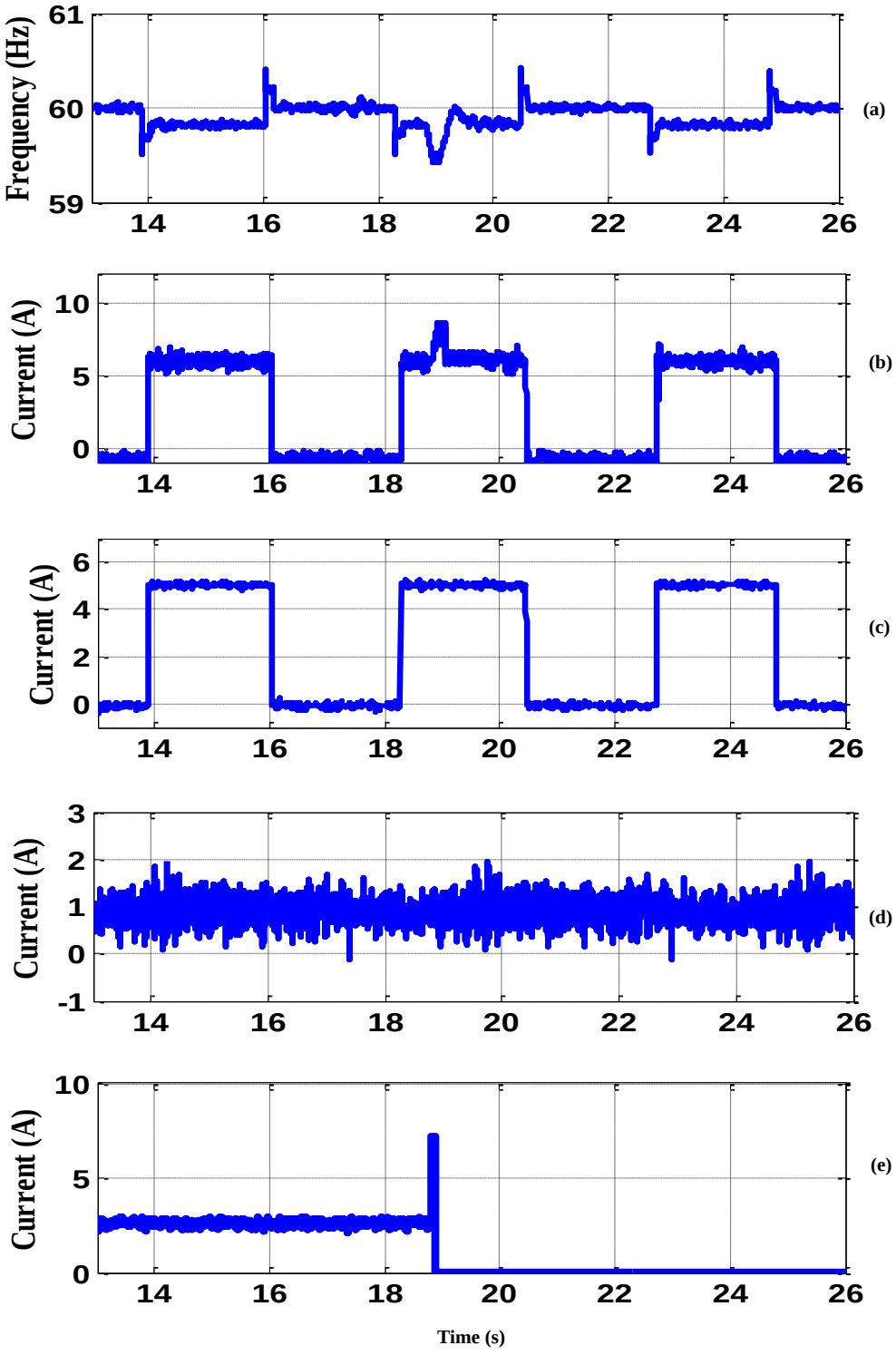

Figure 9.3 Microgrid performance during fault at islanded mode of operation with optimized supercapacitor size (a) frequency, (b) supercapacitor current, (c) pulsed load current, (d) steady state load current, (e) RMS current in the faulted transmission line.

Figure 9.3 (c) and (d) show that the pulsed load and steady state currents remained stable during the experiment.

These results show that the optimization enhanced the operation of the system during normal and fault operations and decreased the size of the supercapacitor (thus reducing its cost) while maintaining enough fault current contribution to trigger the relays in the event of communication loss as explained in the previous section.

Finally, Figure 9.4 presents the performance of the system when uncritical pulsed loads are removed during the fault period.

As mentioned earlier, in this case, a notch in the DC voltage profile indicates a fault and is therefore used as the trigger to disconnect the pulsed load. Figure 9.4(b) shows a notch in the DC voltage at t = 10.2 sec.

At this instant, the pulsed load is disconnected. This is reflected in the pulsed load current in Figure 9.4(c), which drops from 5.2 A to 0 A during the fault period. Figure 9.4(a) shows a decrease in the supercapacitor's current during that period from 5.21 A to 1.03 A, corresponding to a 4.18 A drop.

It is noticeable from Figure 9.4 (b) that the variation of the DC voltage was changed to be between 320 V and 306 V.

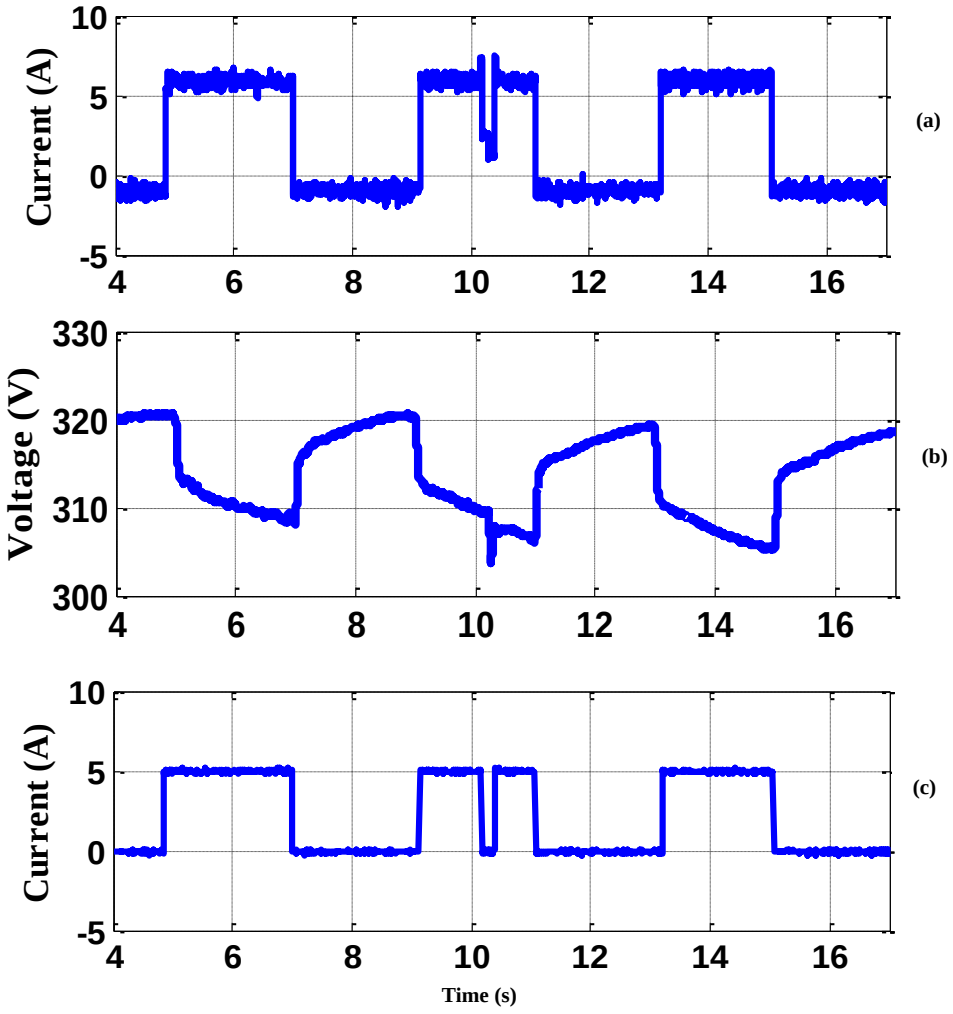

Figure 9.4 Operation test result of the microgrid during fault at islanded mode (a) supercapacitor current, (b) supercapacitor DC voltage, (c) pulsed load current.

9.4 Cyber-Physical Multi-agent Framework

This section briefly explains the hardware, software and the data information model of the multi-agent framework. PMU are located on system buses to enable monitoring and control. The standard IEEE Std. C37.118 includes the data transfer protocol for PMUs for power systems [183]. PMUs using IEEE Std. C37.118 communication protocol were deployed at the connection points. For actual implementation of decentralized control

schemes in power systems, it is imperative to link multi-agent objects to distributed industrial control systems such as PMUs. The required interface is established through a combination of interoperable information data and protocols. The IEEE Std. C37.118 synchro phasor communication provides a standardized information exchange for power systems. However, it is not sufficient to define the behavior of the agents. Therefore, semantics of the exchanged messages should be define using common knowledge representations. The FIPA is an organization which intends to evolve interoperable agent communications with an Agent Communication Language (ACL) [184]-[185]. We implemented the agent framework to run the protection algorithm in real-time using IEEE Std. C37.118 and the FIPA standards as shown in Figure 9.5.

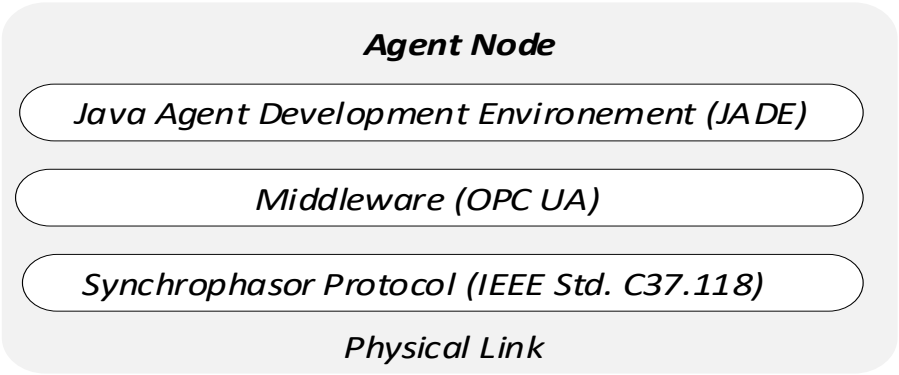

Figure 9.5 Agent node architecture.

ACL messages represent a communicative act or messages (inform, request, refuse etc.) intended to perform some action with precisely defined syntax and semantics. JADE is a software framework to develop agents compliant with FIPA standards with flexible agent behavior methods. OPC UA middleware is used to connect ACL messages and IEEE Std. C37.118 measurements. OPC UA is a platform independent specification with a set of industrial standards for system interconnectivity using publish/subscribe mechanism [186].

In this setup, an off-the-shelf OPC UA server is implemented to acquire IEEE Std. C37.118 measurements. An OPC UA client is embedded in the Java platform to enable JADE to access mapped IEEE Std. C37.118 measurements

9.5 Experimental Setup

The basic structure of the system includes 4 synchronous generators, and loads. The generators are 13.8-kVA and 10-KVA, 60-Hz, 208-V, and 1800-RPM synchronous machines. The prime mover of each of these generators is coupled to one of the available motors which are driven by different frequency drives. All the generators are equipped with AVR in order to maintain an output voltage magnitude. Figure 7.15 shows the overall schematic of Generation Stations and their components. The AVR model is a half-wave phase-controlled thyristor type automatic voltage regulator and forms part of excitation system for brushless generators. Excitation power is derived directly from the generator terminals. The output voltage of generators should be maintained by applying offline parameter settings on AVR module. The frequency drive can be used with 3-phase ac induction motors rated from 1/3 HP up to 7-HP on voltages from 120-V single-phase to 600-V three-phase.

For implementing a smart grid with control, programming via a link with real-time software was performed to control the frequency and change the output active power of generators. The control modes of this drive are “vector speed control” for emulating slack generator and constant frequency-voltage, and “vector torque control” for emulating constant active power-voltage output. Hence, by the proper real-time controller, the whole system generation control can be achieved for wide area control usage. The generators parameters have been presented in Table 7.1. The load module is composed of 10 levels of

parallel resistive loads from 0 – 3 kW in steps of 300 W t nominal voltage. [2 x 72 Ω + 4 x 144 Ω in each phase] resistance models, which can be controlled by PLC, to emulate various load patterns.

Table 9.2 Generation station parameters

Parameter Name	**G1**	**G2-G4**
Apparent Power	13.8 KVA	10 KVA
Nominal Voltage	208 V	208 V
Stator Leakage Reactance (X_L)	0.09 pu	0.09 pu
d-axis Synchronous Reactance (X_d)	2.21 pu	2.248 pu
q-axis Synchronous Reactance (X_q)	1.1 pu	1.117 pu
d-axis Transient Time Constant (T_d')	0.014 s	0.012 s

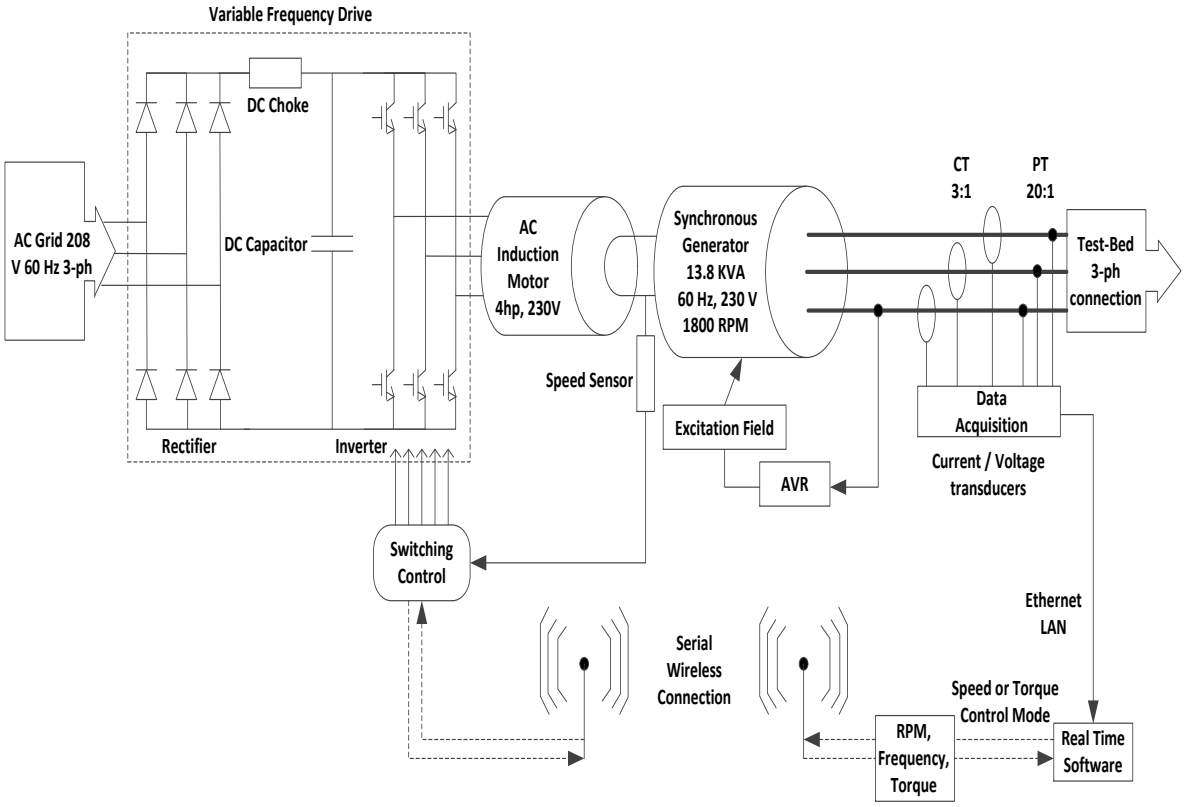

Figure 9.6 Overall schematic of a generator station and its measurements.

9.6 Results and Discussion

This section introduces the real-time experiments to validate the developed multi-agent framework. The developed multi-agent framework is implemented in a reconfigurable small scale power system available at Florida International University, Smart Grid Test Bed as shown in Figure 9.7 [187].

9.6.1 Fault Location and Isolation Operation

Figure 7.18 shows the correspondences exchanged between the agents to perform the operations of fault location, isolation, and restoration in real-time. After applying a fault, PMUs at both sides of each section measure the three phase current angle signals and

forward these signals to their corresponding SA. The SA of the faulted section sends trip signals to both circuit breakers that are located at the both sides of this section to isolate the fault from the system. The type of fault can be identified according to the current phase angle difference between phases A, B and C.

The location of the fault can be determined and the faulty section can be isolated from the system for all types of faults using current phase angle comparison technique. Figure 9.8 shows the difference of the current phase angle between the phases, and it covers the operation before and during the fault. If we applied a single phase to ground fault at section 13, it can be seen from Figure 9.8(a) that at the 131st second the phase angle deviation of (A-A') at both sides of this section is increased above the threshold value, which was adjusted to be 20° and the other deviation phases (B-B') and (C-C') are not changed. Additionally, for a double line to ground fault on phases B and C in the same section, the deviation of these phases increased above the threshold value.

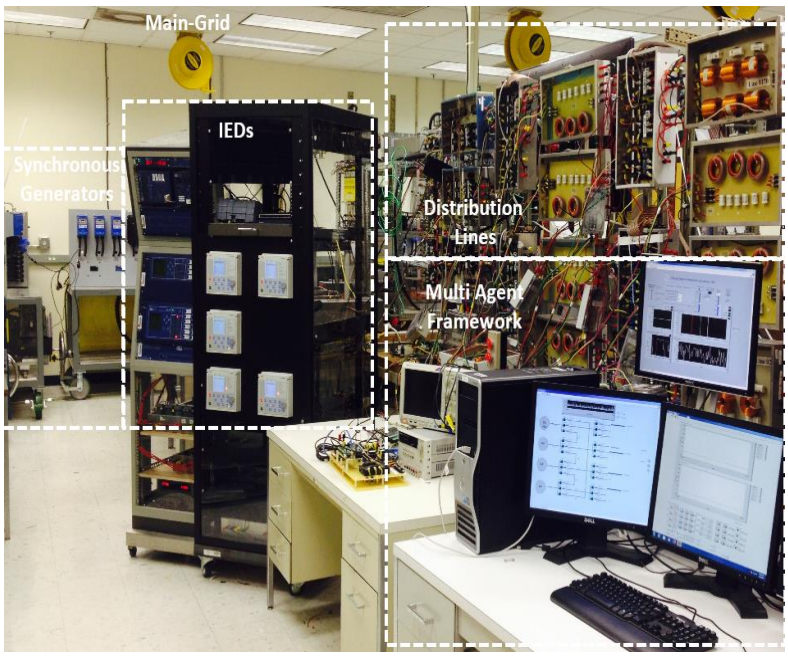

Figure 9.7 Agent platform and laboratory setup

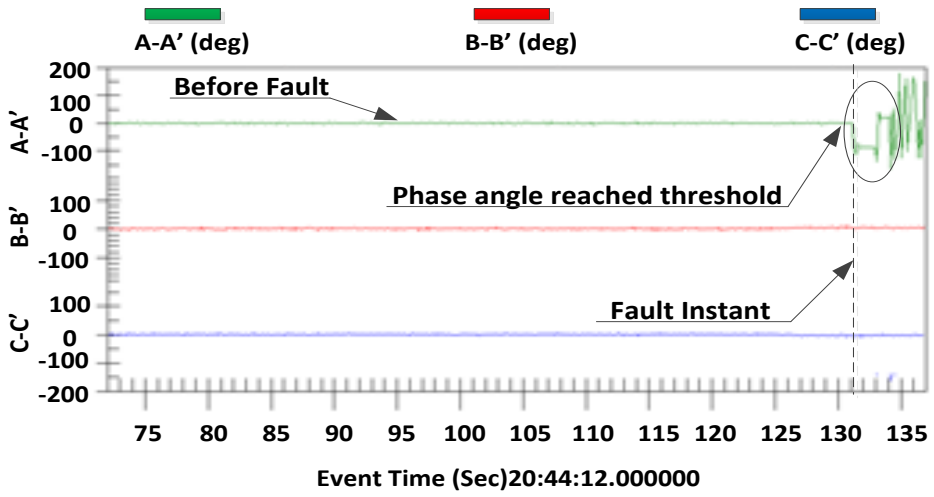

(a)

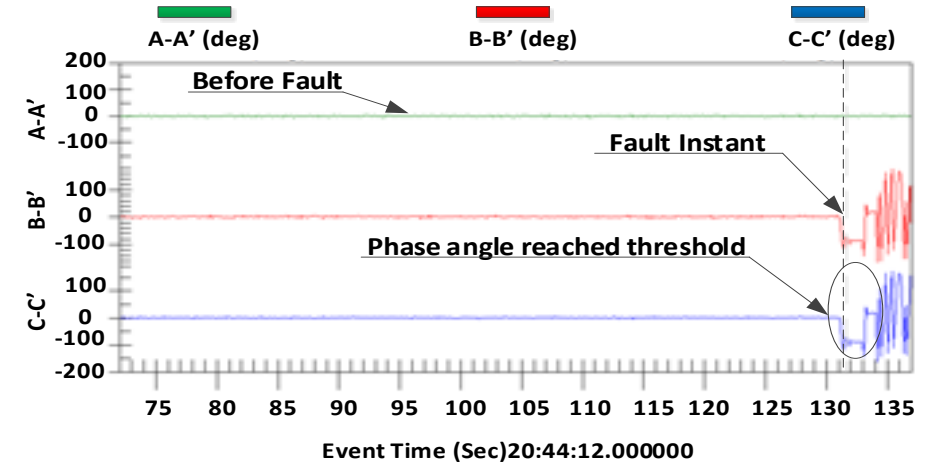

(b)

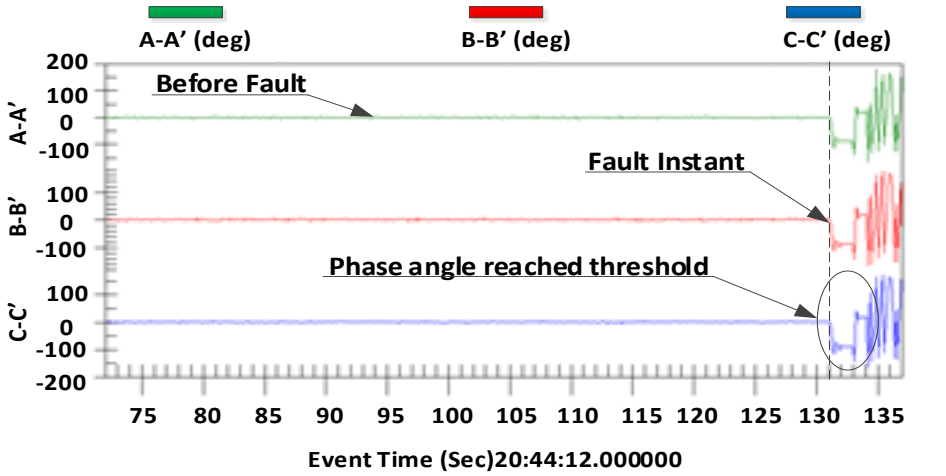

(c)

Figure 9.8 Phase angle difference of starting and ending sides at section 13 during. (a) Single line to ground fault, (b) Double line to ground fault. (c) Three phase to ground fault.

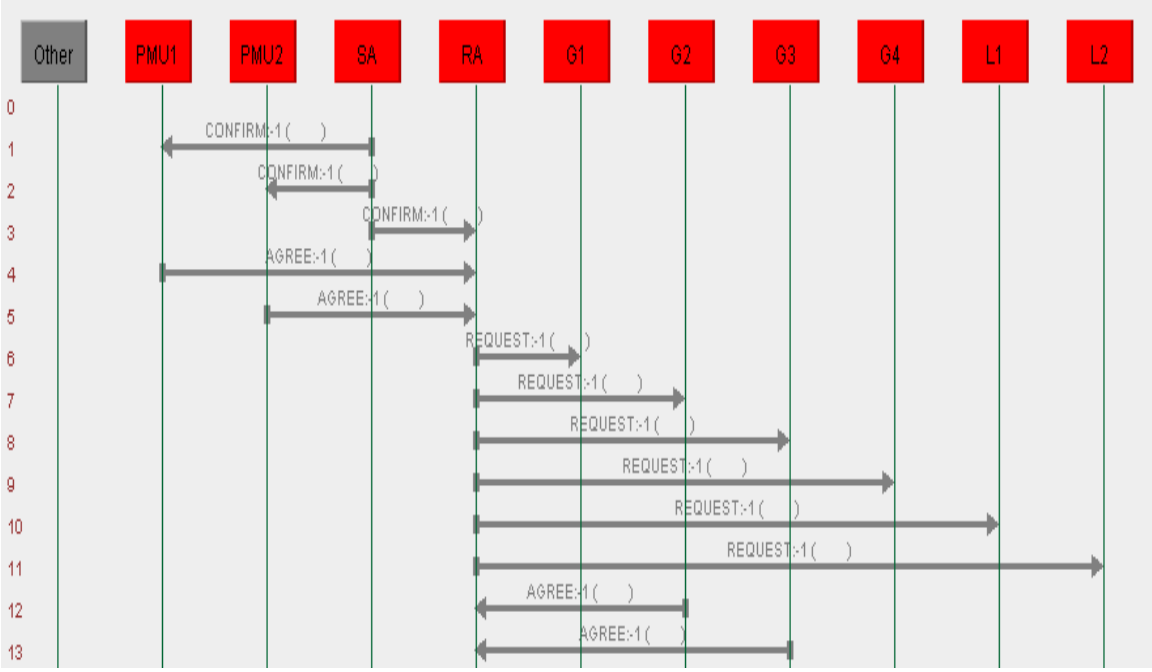

Figure 9.9 Correspondence between multi-agent systems.

On the other hand, the deviation of phase A is not changed as shown in Figure 9.8(b). Finally, a three phase to ground fault is applied to the last section in circuit one and the deviation phase angle of the three phases are increased above the threshold value as shown in Figure 9.8(c).

9.6.2 Restoration Operation

RA is communicating with all the generators in the system. Once the fault occurred in section 13, which is located in circuit 1, RA2 requested from Generator 3 and Generator 4 to inject more power in order to compensate for power losses as a result of disconnecting Generator 2 from the system due to the fault. Figure 9.10 shows the real power of each generator that is connected in the system. From the 70th to the 140th second, all the generators can feed the loads in the system during the normal operation. At the 131st second, the fault occurred and generator 2 is disconnected from the system. For generator 1, the output power is in-creased from 1200w to 1500w after isolating the fault from the

system. Generators 3 and 4 can perform the lower restoration process in order to check the synchronization conditions are satisfied and increased their rating value from 900w to 1200w.

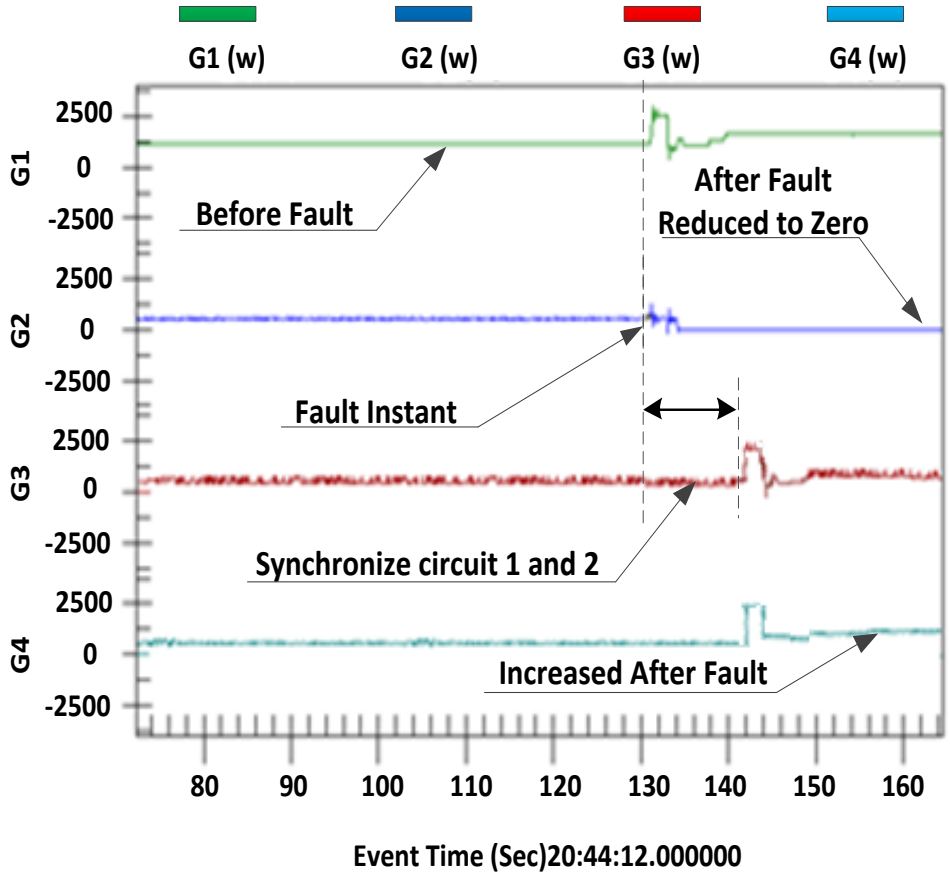

Figure 9.10 The real power of each generator before and after fault at section 13.

9.7 Summary

This chapter developed two solutions for reducing the size and cost of supercapacitors that are used to compensate for the low islanded microgrid fault currents during communication outages in adaptive protection schemes.

First, for critical pulsed loads, a two-level optimization scheme is presented. In the first level, the goal is to reduce the developed protection scheme's cost by selecting the minimal value of the supercapacitor that maintains the system's stable operation. In level 2, the main of objective is to minimize the supercapacitor's fault current contribution and maximize that of the distributed generators. The optimized size of the supercapacitor and the associated controllers parameters were investigated under several types of faults in different location in simulation and were verified experimentally. The results show the ability of the optimized supercapacitor rating to feed different types of faults in order to raise the fault current to the high relay settings and maintain stable system operation during communication outages. Also, the supercapacitor proved effective for faults occurring in distant locations in the microgrid. Finally, temporary disconnection of pulsed loads during the transient fault period proved effective for non-critical pulsed loads as a solution to avoid utilization of oversized supercapacitors.

Also, this chapter introduced the experimental works for fault location, isolation and restoration method base on MAS. The simulation of the developed protection methodology was presented, followed by experimental verification. The experimental results showed excellent agreement with the simulated protection scheme

Chapter 10 Enhancement of Protection Scheme for Distribution System using the Communication Network

One of the main challenges to design a proper protection scheme is the dynamic change in the architecture for the microgrid. The settings of the relays needs to be updated with every configuration in the system to isolate the fault. In this chapter, a centralized control approach is developed to monitor the modes of the microgrid and helping the relays to define the fault location and clear it from the system. The developed technique helps to identify the shortest path from the source to the fault location. MCU is responsible for adjusting the relays settings based on the current topology and the shortest path to the fault point. This technique is investigated on IEEE 14 bus microgrid system for all the possible fault paths. The developed scheme is able to clear the fault by isolating the minimum part of the system and certifying the endurance of the power to supply the different loads in the system.

10.1 Introduction

DERs coupled to a microgrid and its incorporation with the main grid are the objectives in achieving optimum operation of electric power system networks. Decreasing greenhouse gases caused by the conventional energy resources, while increasing the reliability for consumers are some of its foremost advantages. However, along with these benefits, microgrids present several technical challenges for the protection schemes. First, the continuous alterations in the configuration of the system needs observing the status of all DG while automatically modifying their relay settings.

Another issue relate to the protection of the microrgrid is the introduction of bidirectional power flow. The high penetration of DERs based on an interfaced converter reduces the capacity of the short circuit current amount during the islanded mode of operation.

The communication signals plays an important role to update the setting of the relays to accumulate with the current topology of the system, as the microgrid changes the mode of operation between the grid connected and islanded mode with the different connections of the DERs during the latter mode.

This chapter aims to present the helping of the communication system to identify the shortest path from the source location to the fault point. MCU communicates with the different relays that are distributed in the system to adjust their settings with the current configuration of the microgrid.

10.2 Challenges in Microgrid Protection

The following section discusses the different challenges that should be taken into our consideration to design an adequate protection scheme for the microgrid system.

10.2.1 Selectivity and Sensitivity Issues

Two main characteristics that should be found in microgrid system protection devices are selectivity and sensitivity features. First, selectivity refers to the ability of the protection system to locate and classify a fault correctly. OC relays should determine whether the fault is internal or external to its zone. The protection algorithm should be able to distinguish between the main grid and local microgrid fault. During main grid faults, the microgrid needs to be capable of islanding to protect equipment in the system. During microgrid faults, the function of the protection scheme becomes more complicated as it is

required to disconnect the smallest part of the faulty section from the system. It should be noted that the importance of the selectivity feature of the relays is to operate under various faults while isolating the faulty part.

Secondly, sensitivity refers to the fact that OC relays should be able to detect the fault conditions in the system. The fault should be cleared as quickly as possible to maximize safety while minimizing system instability and damage to equipment. The OC relay should quickly arrive at a decision and CBs must function rapidly. The sensitivity of the relays must be adjusted such that a high redundancy can be achieved without affecting selectivity of the protection system [194]-[195].

10.2.2 The Direction of Power Flow

Distribution systems become active systems due to the integration of DERs in the system. The microgrid feeds local loads and can also support power to the grid in the case of excess generation. This operation changes the flow of the power from unidirectional to bidirectional. Bi-directional power flow has effects on the amplitude and direction of the fault current thereby effecting coordination of the protective relays. In this case, the protection system in a typical distribution system is designed accordingly to a time or current coordination principle, in which the relay closest to the fault operates first and in the event of a failure, a backup protective relay operates after a delay time.

However, the effectiveness of this protection requires a radial grid connection, which is no longer the case when DGs are connected to the network. This results in either changing or completely losing coordination between protective devices [196].

The different adverse effects of DG connections on the distribution network protection include false tripping of feeders, blinding of protection, increase or decrease in the fault level with the connection or disconnection of DERs affecting the reach of the OC relay settings [197]- [199].

10.2.3 Dynamic Changes in the Microgrid Architecture

Dynamic changes of the microgrid configuration should be taken into consideration when designing the protection scheme. Some changes include the disconnection of generation units, shutting down some loads during peak hours, or exporting of power to the main grid during excess generation periods for optimum and economic operations [24]. Adaptive protection is required to change the relay settings according to the current microgrid configuration. Prior knowledge of every state in the microgrid as well as online monitoring and calculation of the short circuit fault current is needed for proper operation. As previously discussed, this requires the application of a fast, reliable, and robust communication system.

10.2.4 Faults in Grid-Connected Mode.

For a fault on the main grid during normal operation, the response of the protection devices of individual DERs should not trip before the protection device at the PCC trips, while DERs should continue operation during sensing and switching of the PCC device. To allow this, all DERs should have FRT capability. For a fault within the microgrid during normal operation, the response of line and feeder protection must be to disconnect the faulty portion from the rest of system as quickly as possible and how it is done depends on the features and complexity of the microgrid and the protection strategy used.

There may be some non-fault cases resulting in low voltage at the PCC such as voltage unbalances and non-fault open phases that are difficult to detect and may potentially create hazards for sensitive loads, micro sources, etc. Therefore, some protection mechanisms are needed to avoid such situations.

10.2.5 Faults in Islanded Mode.

The high penetration of DERs based on power electronic inverters interfaced with the microgrid as shown in Figure 10.1 has a great impact on the protection scheme. These systems limit the short circuit current during islanded mode of operation, as they are equipped with a FCL that prevents high OC levels to flow during the fault period. A significant difference exists in the amount of short circuit current that occurs when in grid connected and islanded modes of operation. In grid connected, fault currents of a much higher magnitude (5-10 times the full load current) are available to help conventional OC relays to activate under abnormal operations. However, in islanded mode, the fault current reduces to only about 3 times the full load current. Furthermore, a large integration of connected converter-based DERs further reduces the fault current to only 1.2-1.5 times the full load current. Usually, conventional OC relays are set to operate at 1.2-8 times full load current. Accordingly, the time-current coordination of OC relays and OC devices with extremely inverse characteristics are disturbed.

10.2.6 Sympathetic Tripping

This protection issue causes disconnection of a healthy feeder due to fault on a neighboring feeder. It occurs as a result of reverse power flow from DG units, as indicated in Figure 10.1. When the DG is not connected in the system, a fault current I_{grid} is detected by the

relay at CB3. However, when a DG unit is interfaced to the MG, the current I_{DG} would also contribute to the fault. If I_{DG} is appreciably large, then the relay at CB2 may trip and cause the healthy feeder to isolate.

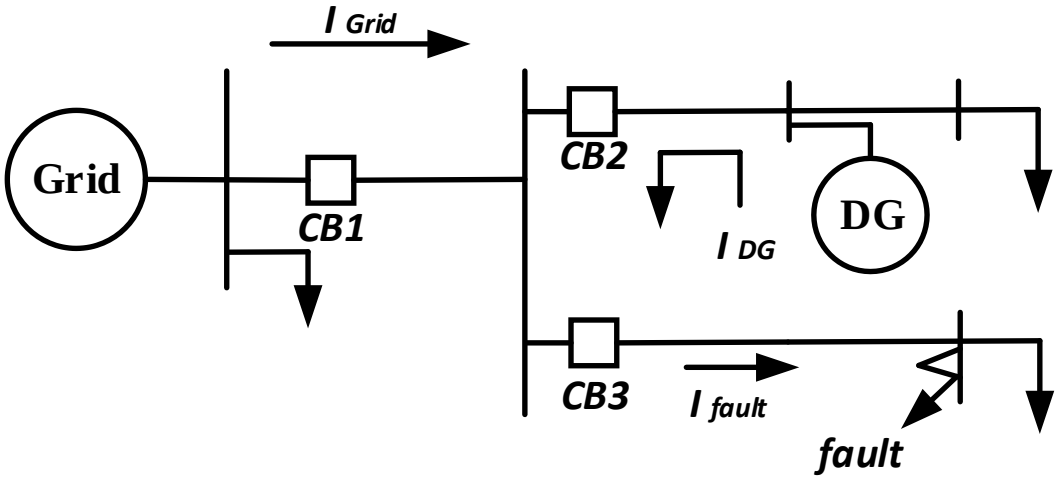

Figure 10.1. Sympathetic tripping in the MG system

10.3 The Fault Current Supplied By DGs

Fault currents supplied by DGs were approximated to 5 times their rated currents whilst fault currents from PE-interfaced DGs were approximated to about 1.5 times their rated current. Then, for a given relay "r" in the network, the operating current is calculated as in (10.1). This equation considers the grid's and all DG's fault contribution including the supercapacitor on that particular relay:-

$$I_r = I_{f\_G} + I_{f\_DG} + I_{f\_PE} + I_{f\_DER} \quad (10.1)$$

During the grid connected mode, the current can be calculated using the Thevenin's equivalent circuit [10] as shown in the following equation (10.2).

$$I_{f_G} = \frac{V_{th}}{Z_{th}} \quad (10.2)$$

To be more accurate, the V_th is the voltage of the Thevines circuit and Z_th is the total impedance that is changed according to the location of the fault. For this case, the fault current by the grid can be represented as a function of the distance and can be shown in the following equation (10.3):-

$$I_{f_G} = \frac{V_{th}}{Z_{th(x)}} \times Operation\ Mode \tag{10.3}$$

During the islanded mode of operation, the fault current that is supplied by the grid is multiplied by the operation Mode, and will be equal to 0.

It can be noted that the contribution to the fault current that is supplied by DGs is approximated 5 times the rated current, while the DGs interfaced inverted is contributed by 1.5 times the rated current.

$$I_{f\_DG} = Av.\times \left(5 \times \sum_{i=1}^{n} \frac{I_{f\_x}}{I_{FM\_DG}} I_{r_{DG}} \times Status_{DG} \right) \tag{10.4}$$

$$I_{f\_PE} = \left(1.5 \times \sum_{j=1}^{m} I_{r_{PE}} \times Status_{PE} \right) \tag{10.5}$$

$$I_{f\_DER} = \left(1.5 \times \sum_{j=1}^{m} I_{r_{DER}} \times Status_{DER} \right) \tag{10.6}$$

The signal Status indicates whether that source is in operation or not. Depending on the type of the source, i.e., whether it is inverter interfaced or with rotating machines. In literature, the fault contributions of the Inverter interfaced DGs is reported to range between 1.2 and 2. In order to be practical and more realistic, authors selected the

coefficient 1.5 since the extreme conditions (where the fault contribution is 1.2 or 2) will not occur as frequent as conditions which require fault contribution coefficient to be 1.5.

In this case, it considers a capacitor in series with a resistance. The SC model input is the power P_{SC} absorbed/injected from/to the SC. The SC current is defined as follow:

$$I_{sc} = \frac{Q_{sc}/C_{sc}}{2 \times R_{sc}} - \frac{\sqrt{(Q_{sc}/C_{sc})^2 - 4 \times R_{sc} \times P_{sc}}}{2 \times R_{sc}} \quad (10.7)$$

The BT model considers a voltage source in series with a resistance. The BT model input is the power P_BT absorbed/injected from/to the BT, being this the output from power splitter control. The BT current is calculated using (10.8):

$$I_{BT} = \left(\frac{V_{OC}\,(SOC_{BT})}{2\,.\,R_{BT}\,(SOC_{BT})} - \frac{\sqrt{(V_{OC})^2\,(SOC_{BT}) - 4\,.\,R_{BT}(SOC_{BT}).P_{BT}}}{2\,.\,R_{BT}(SOC_{BT})} \right) \quad (10.8)$$

being V_{OC} the open circuit voltage and R_{BT} the internal resistance. Both are function of the state of charge SOC_{BT} which is defined as the ratio of the charge present in the battery Q and the nominal charge Q_O.

The SOC_{BT} is subject to a maximum and minimum level constraint. For BT, this is an important constraint since the lifetime strongly depends on the SOC_{BT}-range used. When the SOC_{BT} is lower than 20% both charge-discharge resistances increase rapidly. This is a reason why the minimum SOC_{BT} should be kept above 20% [46].

10.4 Developed Protection Technique

The following section presents the developed technique that used to protect the system for several fault paths from the source to the fault point.

10.4.1 Identification the direction of the fault

Two directional relays are installed in each branch to send the value and the direction of the fault current to MCU. Each relay looks into the value and the direction of the current. If two relays of a branch sense the fault in the same direction, then the fault is outside this branch, but if the relays the direction of the current at two different directions, then the fault identified in this branch. In Figure 10.2, B2 and B3 identified the fault from the right and left sides, then the fault was occurred at this zone.

10.4.2 Identify the shortest path

Figure 10.3 shows the developed protection idea on IEEE 14- bus network. As, it was explained the fault location is identified based on the amplitude and the direction of the fault current. The impedance and the lengths of the different transmission lines of the system are identified, a pre calculation study of this network was prepared in terms of the different values of the impedance and lengths of the transmission lines to identify the shortest path from the grid to the fault location.

Assume that the fault occurred between buses 3 and 4, the possible paths can be illustrated as shown in Figure 10.4 and explained as follows:-

1- B6-B12-B13-B14-B9-B7-B4-B3

2- B6-B13-B14-B9-B7-B4-B3.

3- B6-B11-B10-B9-B7-B4-B3.

4- B6-B5-B4-B3.

5- B6-B2-B4-B3.

Based on these paths, it can be noticed here that the least number of paths is found at paths 4 and 5. However, the best path that may be achieve the minimum time to isolate the fault is path 1 or path 2. The final decision to determine the elected path will be determined according to the length and the impedance of each path as shown in Table 10.1. that should be saved into MCU before the occurrence of the fault. After define the candidate path, MCU send a GOOSE message to the directional relays at both sides of buses 3 and 4 to adjust their settings based on the selected path.

Table 10.1 The length and impedance of the transmission lines

Buses	**Length (m)**	**Impedance (Ω)**
1-2	10	2.24 + J*0.43
2-4	15	8.34+ J*0.87
1-5	12	6.56+ J*0.56
2-5	18	7.54+ J*0.12
4-5	16	5.66+ J*0.54
3-4	13	8.11+ J*0.44
4-7	11	11.84+ J*0.46
5-6	19	7.82+ J*0.13
7-9	25	4.32+ J*0.52
7-8	17	3.56+ J*0.16
9-10	23	2.58+ J*0.43
10-11	14	12.54+ J*0.56
6-11	15	16.14+ J*0.55
9-14	24	18.32+ J*0.87
13-14	19	11.24+ J*0.43
6-13	22	10.40+ J*0.17

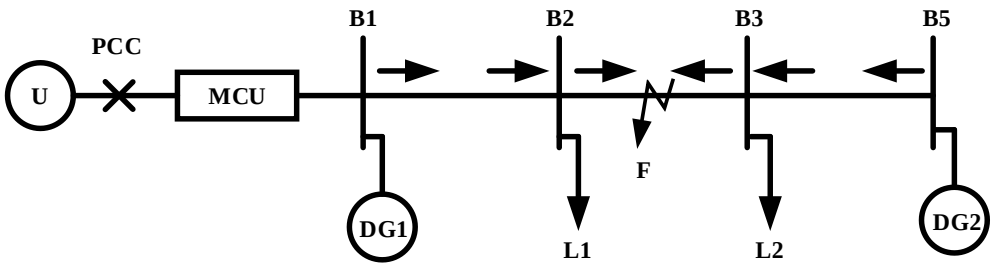

Figure 10.2 Identify the location of the fault

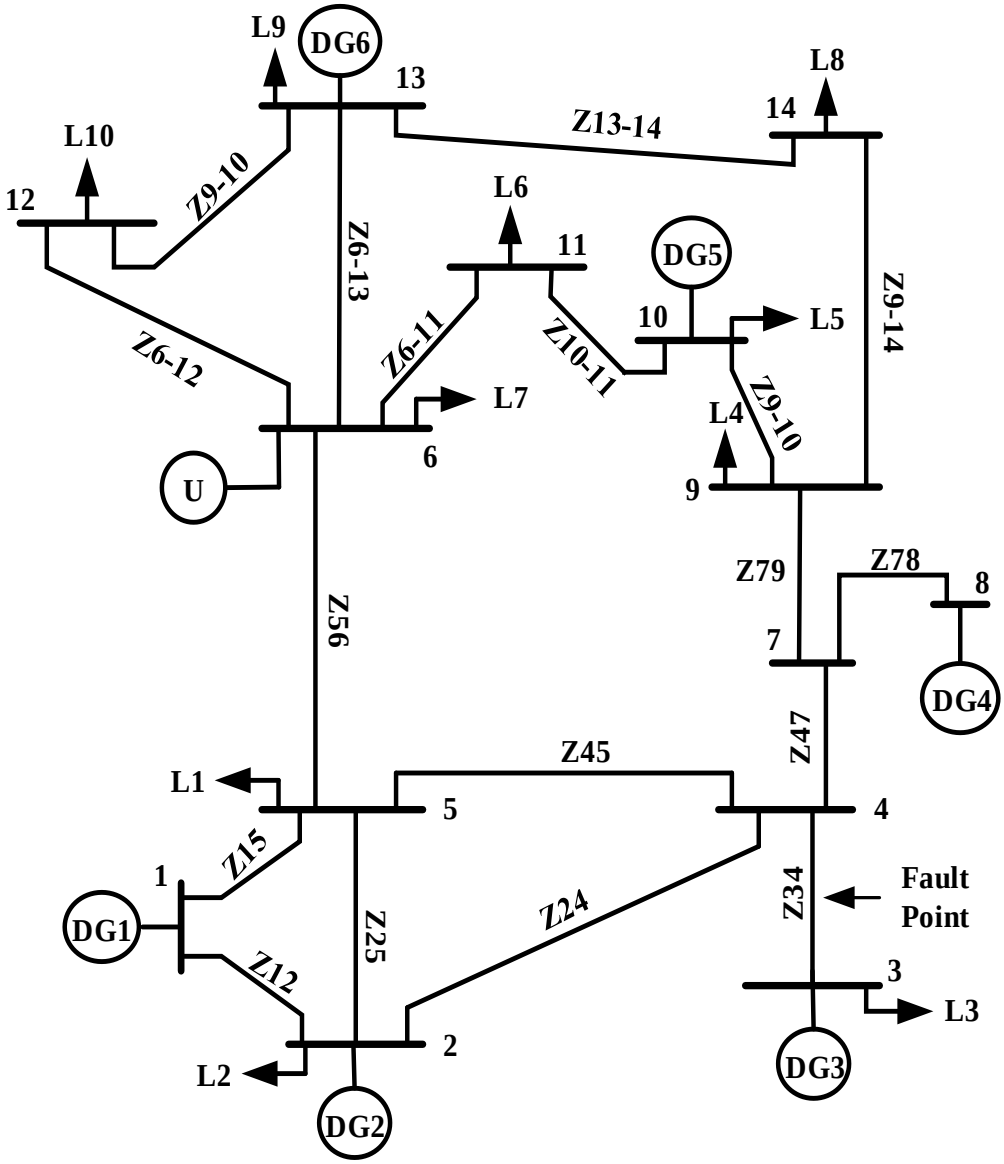

Figure 10.3 Modified IEEE 14 bus system.

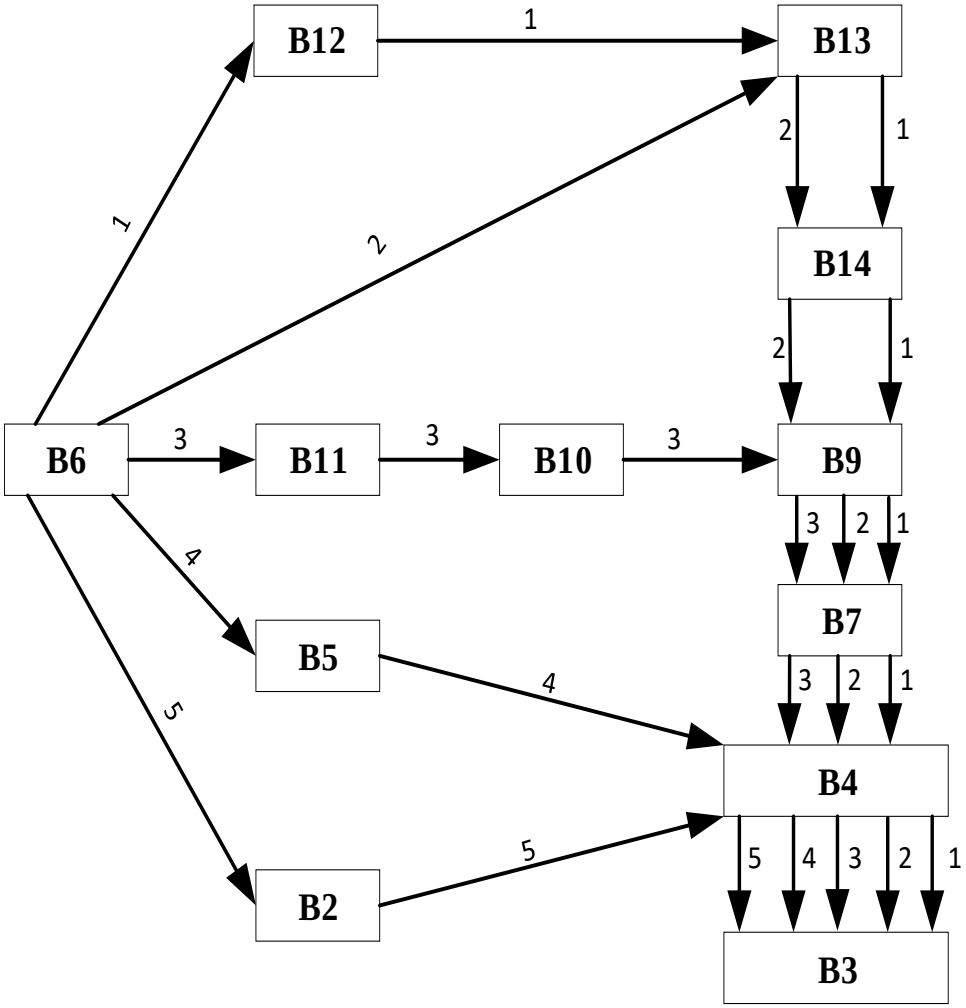

Figure 10.4 Define the possible paths to the fault location.

10.5 Simulation Case Studies

Figure 10.6(a) shows the system performance for the first candidate path, it can be shown that the fault current was tripped at t=3s which represented the longest time period to detect the fault and isolate it from the system. On the other hand, another path was selected to investigate the period time to trip the circuit breaker and that time was improved to be t=2.967s as the number of paths reduced to be 7 buses instead of 8 buses. For the case of 4 buses, the tripped time was reached to t=2.933s, it can be concluded here that the time required to trip the circuit breaker reduced by decreasing the number of buses. The case of

four buses, was studied and the time reduced and reached to t=2.917s as shown in Figure 10.6(d). Finally, the same number of four buses was shown at Figure 10.6 (e) and the trip time became t=2.833s as the total length from the grid to the faulty location is less than the latter case. It can be noted that the required time to trip the circuit breaker was improved between the first and last case study and reduced from t=3s to t=2.833s that helped the system to isolate the system faster and keep the system stable without more disturbance that may be caused by the fault.

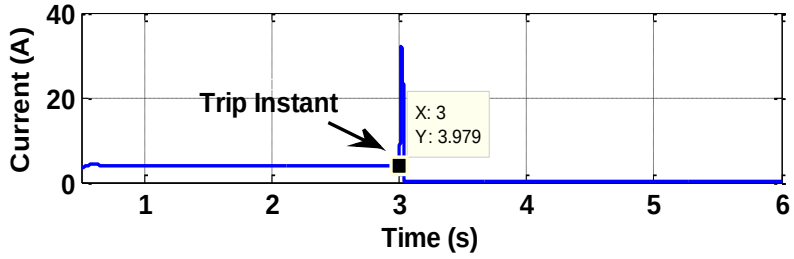

(a)

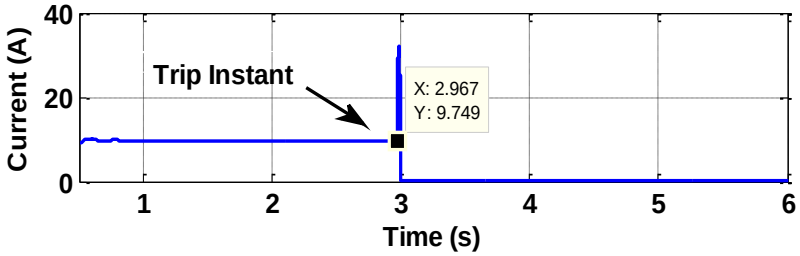

(b)

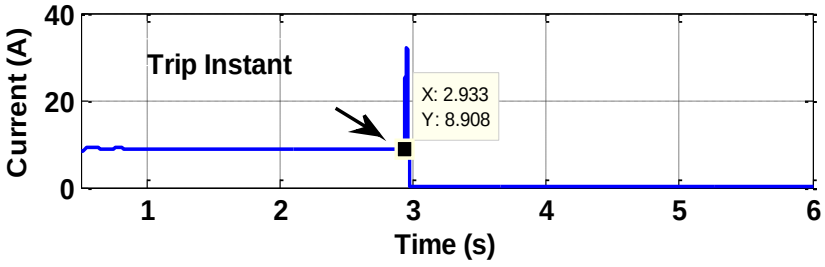

(c)

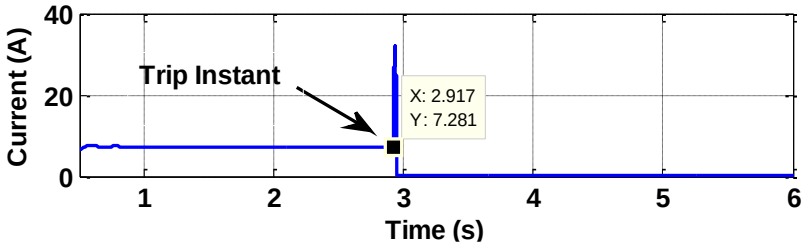

(d)

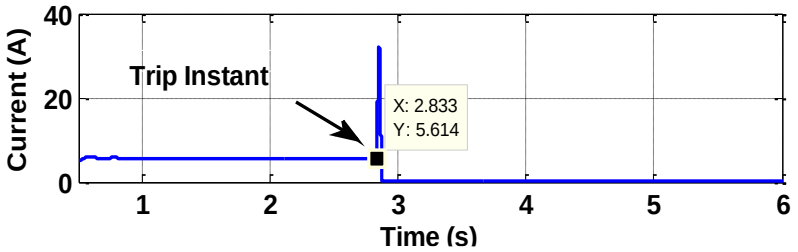

(e)

Figure 10.5. System performance during the fault (a) 1st path, (b) 2nd path, (c) 3rd path, (d) 4th path, and (e) 5th path.

10.6 Summary

The protection of microgrid is represented a challenge due to the continuously change in the architecture of the system. The need to the communication network is necessary to adjust the settings of the relay to be updated with the current topology of the microgrid system. MCU is implemented to monitor the statues of the different sources in the system and identify the location of the fault and isolate it. The developed technique was investigated several paths from the source location to the fault point and selected the shortest path to clear the fault.

Chapter 11 Conclusions and Recommendation for Future Works

11.1 Conclusions

This dissertation presented new techniques for the control, energy management, and protection of wide-area power systems and active distribution networks to improve the performance of the smart grid in terms of efficiency, reliability, communication, aggregation and human/agent participation. Four laboratory-scale hardware/software-based test platforms were developed to experimentally evaluate the contributions of this dissertation.

First of all, a communication-assisted fault localization, isolation and restoration method for microgrids based on MAS was developed. The three phase current angle signals at the sending and receiving terminals of each section of the transmission line were measured using PMUs. These measurements are forwarded to SAs that located at the middle of the protected section. The SA of the fault section send trip signals to both circuit breakers that are located at both sides of this section to isolate the fault from the system when the deviation of the phase angles increases above the threshold limit.

To perform the developed technique, the hardware, software and the data information model of the multi-agent framework was developed. The IEEE Std. C37.118 synchro phasor communication provides a standardized information exchange for power systems. However, it is not sufficient to define the behavior of the agents. Therefore, semantics of the exchanged messages should be define using common knowledge representations. The FIPA is an organization which intends to evolve inter-operable agent communications with an ACL.

We implemented the agent framework to run the protection algorithm in real-time using IEEE Std. C37.118 and the FIPA standards. JADE is a software frame-work to develop agents compliant with FIPA standards with flexible agent behavior methods. OPC UA middleware is used to connect ACL messages and IEEE Std. C37.118 measurements. In this setup, OPC UA server is implemented to acquire IEEE Std. C37.118 measurements. An OPC UA client is embedded in the Java platform to enable JADE to access mapped IEEE Std. C37.118 measurements. We have two main contributions:-: first, it eliminates the use of voltage transformers and thus reduces costs. Second, it does not require transfer of data along long distances which decreases the delay time for fault isolation.

Power restoration processes following the fault clearance considering voltage, frequency and power flow constraints in the microgrid under study was also performed. Simulation of the developed protection methodology was presented followed by experimental verification. The experimental results showed excellent agreement with the simulated protection scheme.

Secondly, cyber-attacks representing a main challenge to design a suitable protection scheme. Here are the main contribution to overcome this problem:-

• Use of energy storages to enhance the resiliency of adaptive microgrid protection schemes against communication failures.

• Design of an autonomous control for a supercapacitor's AC/DC converter capable of operating when the microgrid is in both grid-connected and islanded mode using a single mode of operation. This autonomous control strategy eliminates the need of a communicated control command to shift the controller from grid-connected to islanded modes of operation.

• The ability of the overall system to keep the values of frequency, AC voltage and DC voltage stable during extreme cases such as the occurrence of a fault during a peak pulse load period.

• The developed method was investigated under different fault types. Excellent results were observed using the developed protection scheme.

Another contribution was developed two solutions for reducing the size and cost of supercapacitors that are used to compensate for the low-islanded microgrid fault currents during communication outages in adaptive protection schemes. First, for critical pulsed loads, a two-level optimization scheme is presented. In the first level, the goal is to reduce the developed protection scheme's cost by selecting the minimal value of the supercapacitor that maintains the system's stable operation. In level 2, the main of objective is to minimize the supercapacitor's fault current contribution and maximize that of the distributed generators. The optimized size of the supercapacitor and the associated controllers parameters were investigated under several types of faults in different location in simulation and were verified experimentally. Second, temporary disconnection of pulsed loads during the transient fault period proved effective for non-critical pulsed loads as a solution to avoid utilization of oversized supercapacitors.

Final contribution was presented a hybrid hardware-software co-simulation platform that can be used to model the relation between the cyber and physical parts the microgrid. The microgrid was simulated on MATLAB/Simulink SimPowerSystems to model the physical system dynamics, whereas all control logic was implemented on embedded microcontrollers communicating over a real network. The simulation software, embedded microcontrollers, and a real communication architecture were collected to

perform the protection scheme platform. The Data Distribution Services (DDS) middleware is used to link the hardware and software environments. This method does not need to change the relay settings at different configurations of the microgrid. The developed solution does not incur additional costs to the system studied, as the supercapacitor is already used to feed a pulsed load. The paper also developes a coordination process between the relays with the help of the supercapacitor. Primary and back-up protection were studied according to IEEE Std C37.112 to isolate the fault properly. We also provided details of the fault current that supplied by any DG to any point inside the network. The results showed that the co-simulation infrastructure introduces a high dependability design, analysis, and testing environment for cyber and physical data flow in the system.

As we presented in the previous chapters that the developed protection techniques were verified in Smart Grid Test Bed at FIU and the experimental works were matched with the simulation results. We developed several protection techniques based on energy storage devices and MAS to mitigate the cyber-attacks such as Denial of Service type.

For the experimental part, we tested MAS to isolate and restore the power to the different loads in the system. Also, we developed a non-software method using the energy storage device to inject current and helping the relays to reach the required settings and isolate the fault when the communication is not available in the system.

11.2 Recommendations for Future Work

In this subsection, the new trends on smart grid were highlighted and open research areas were discussed. Comparing the earlier and the current research works, we identified the following trends:

Stability and reliability problems occurred due to integration of renewable energy resources will solve with the FACTs devices like static synchronous compensator (STATCOM), static VAR compensator (SVC), static series synchronous compensator (SSSC) and unified power flow controller (UPFC). Additionally, the harmonics resulting from power circuits will be mitigated by filters integrated these devices. The stability classifications and analysis methods for microgrid. Also researchers compiled available methodologies to improve the micro-grid stability.

Fast static switch, fault current limiter and energy storage devices can be used as external protection devices. Fast static switch provides high-speed isolation for loads when transition from grid-connected to islanded mode.

Different cyber-attacks need to study and investigate the operation of the protective elements to ensure from the cleaning of the faulty part in the system.

Several energy storage devices such as lead acid can be used to be a candidate solution for injection current when the microgrid is not served by the communication networks. The controller of another energy storage devices can be compared with the controller of the supercapacitor bank, also the comparison can be done in terms of the total cost, volume and weight, as well as internal losses and complexity of the control system.

In this dissertation, a new design of the controller for the AC/DC converter is developed to test the capability of the energy storage device to feed the fault at the AC side

when the communication is not available. This technique could be further advanced by using some other artificial and intelligent methods such as Fourier transform to improve the performance of the protection scheme.

List of References

[1] M. A. Haj-ahmed and M. S. Illindala, "Investigation of Protection Schemes for Flexible Distribution of Energy and Storage Resources in an Industrial Microgrid," in IEEE Transactions on Industry Applications, vol. 51, no. 3, pp. 2071-2080, May-June 2015.

[2] O. V. Gnana Swathika and S. Hemamalini, "Prims-Aided Dijkstra Algorithm for Adaptive Protection in Microgrids," in IEEE Journal of Emerging and Selected Topics in Power Electronics, vol. 4, no. 4, pp. 1279-1286, Dec. 2016.

[3] H. F. Habib; T. Yossef; M. Cintuglu; O. Mohammed, "A Multi-Agent Based Technique for Fault Location, Isolation, and Service Restoration," in IEEE Transactions on Industry Applications , vol. no.99, pp.1-1, Feb. 2017.

[4] K. O. Oureilidis and C. S. Demoulias, "A Fault Clearing Method in Converter-Dominated Microgrids With Conventional Protection Means," in IEEE Transactions on Power Electronics, vol. 31, no. 6, pp. 4628-4640, June 2016.

[5] M. A. Haj-ahmed and M. S. Illindala, "The Influence of Inverter-Based DGs and Their Controllers on Distribution Network Protection," in IEEE Transactions on Industry Applications., vol. 50, no. 4, pp. 2928-2937, July-Aug. 2014.

[6] T. S. Ustun et al., “A microgrid protection system with central protection unit and extensive communication,” in 10th Int. Conf. Environment and Electrical Engineering (EEEIC), pp. 1–4, 2011.

[7] H. Wan, K. K. Li and K. P. Wong, "An Adaptive Multiagent Approach to Protection Relay Coordination With Distributed Generators in Industrial Power Distribution System," in IEEE Transactions on Industry Applications, vol. 46, no. 5, pp. 2118-2124, Sept.-Oct. 2010.

[8] Hany F. Habib, T. Youssef, M. H. Cintuglu and O. Mohammed, "A multi-agent based technique for fault location, isolation and service restoration," in IEEE Industry Applications Society Annual Meeting, Portland, OR, pp. 1-8, 2016.

[9] R. Akella, H. Tang, and M.M. Bruce, “Analysis of Information Flow Security in Cyber-Physical System”, in International Journal of Critical Infrastructure Protection, Vol. 3, pp: 157-173, 2010.

[10] J. Hoyos, M. Dehus and T. X. Brown, "Exploiting the GOOSE protocol: A practical attack on cyber-infrastructure," in IEEE Globecom Workshops, Anaheim, CA, pp. 1508-1513, 2012.

[11] M. H. Cintuglu, T. Ma and O. A. Mohammed, "Protection of Autonomous Microgrids Using Agent-Based Distributed Communication," in IEEE Transactions on Power Delivery, vol. 32, no. 1, pp. 351-360, Feb. 2017.

[12] Hany F. Habib, A.A.S. Mohamed, Mohamad El Hariri, Osama A. Mohammed, “Utilizing supercapacitors for resiliency enhancements and adaptive microgrid protection against communication failures,” in Electric Power Systems Research, Vol. 145, pp. 223-233, April 2017.

[13] W.E. Feero, D.C. Dawson, J. Stevens, “Protection Issues of the Microgrid Concept”, White Paper by the Concortium for Electric Reliability Technology Solutions, March 2002.

[14] G. Buigues, A. Dysko, V. Valverde, I. Zamora and E. Fernandez, “Microgrid Protection: Technical Challenges and Existing Techniques,” in International Conference on Renewable Energies and Power Quality, Bilbao (Spain), 20th to 22th March, 2013.

[15] P. Mahat, Z. Chen and B. Bak-Jensen, "Review on islanding operation of distribution system with distributed generation," in IEEE Power and Energy Society General Meeting, San Diego, CA, pp. 1-8, 2011.

[16] N. Schaefer, T. Degner, A. Shustov, T. Keil and J. Jaeger, "Adaptive protection system for distribution networks with distributed energy resources," in 10th IET International Conference on Developments in Power System Protection (DPSP 2010). Managing the Change, Manchester, pp. 1-5, 2010.

[17] S. Chowdhury, S.P. Chowdhury, P. Crossley, “Microgrids and active distribution networks”, in IET Renewable Energy Series 6, The Institution of Engineering and Technology, London, United Kingdom, 2009.

[18] R. Lasseter, et al., “Integration of distributed energy resources”, in The CERTS Microgrid Concept, Lawrence Berkeley National Lab, 2002.

[19] H. Laaksonen, K. Kauhaniemi, S. Voima,” Protection system for future LV Microgrids”, in CIRED 21st International Conference on Electricity Distribution, Frankfurt, 6–9June, 2011.

[20] J. Tang, Y. Gong, N. Schulz, M. Steurer and P. G. McLaren, "Implementation of a Ship-Wide Area Differential Protection Scheme," in IEEE Transactions on Industry Applications, vol. 44, no. 6, pp. 1864-1871, Nov.-Dec. 2008.

[21] A. Oudalav and Antonio Fidigatti ,“Adaptive Network Protection in Microgrids,” in International Journal of Distributed Energy Resources, vol.5, pp. 201-225, 2009.

[22] Y. Han, X. Hu and D. Zhang, "Study of adaptive fault current algorithm for microgrid dominated by inverter based distributed generators," in The 2nd International Symposium on Power Electronics for Distributed Generation Systems, Hefei, China, pp. 852-854, 2010.

[23] M. Dewadasa, A. Ghosh and G. Ledwich, "Protection of microgrids using differential relays," in AUPEC, Brisbane, QLD, pp. 1-6, 2011.

[24] H. F. Habib and O. Mohammed, "Decentralized Multi-Agent System for Protection and the Power Restoration Process in Microgrids," in Ninth Annual IEEE Green Technologies Conference (GreenTech), Denver, CO, pp. 358-364, 2017.

[25] A. Kole, "A review and study on advanced control and automation functions and future control for a modern combined cycle power plant," in International Conference on Intelligent Control Power and Instrumentation (ICICPI), Kolkata, pp. 215-220, 2016.

[26] N. K. Choudhary, S. R. Mohanty and R. K. Singh, "A review on Microgrid protection," in International Electrical Engineering Congress (IEECON), Chonburi, pp. 1-4, 2014.

[27] A. A. Kalage and N. D. Ghawghawe, "A protection scheme for optimum coordination of directional overcurrent relays in presence of distributed generation," in International Conference on Electrical, Electronics, Signals, Communication and Optimization (EESCO), Visakhapatnam, pp. 1-5, 2015.

[28] S. M. Brahma and A. A. Girgis, "Development of adaptive protection scheme for distribution systems with high penetration of distributed generation," in IEEE Transactions on Power Delivery, vol. 19, no. 1, pp. 56-63, Jan. 2004.

[29] A. K. Tiwari, S. R. Mohanty and R. K. Singh, "Review on protection issues with penetration of distributed generation in distribution system," in International Electrical Engineering Congress (IEECON), Chonburi, pp. 1-4, 2014.

[30] M. Baran and I. El-Markabi, "Adaptive over current protection for distribution feeders with distributed generators," in IEEE PES Power Systems Conference and Exposition, pp. 715-719 vol.2. 2004.

[31] S. J. Lee, B. W. Min, K. H. Chung, M. S. Choi, S. H. Hyun and S. H. Kang, "An adaptive optimal protection of a distribution system using a multi-agent system," in Eighth IEE International Conference on Developments in Power System Protection, pp. 611-614 Vol.2, 2004.

[32] Hany. F. Habib, C. R. Lashway and O. A. Mohammed, "On the adaptive protection of microgrids: A review on how to mitigate cyber attacks and communication failures," in IEEE Industry Applications Society Annual Meeting, Cincinnati, OH, USA, pp. 1-8, 2017.

[33] S. Voima, K. Kauhaniemi, H. Laaksonen, “Novel protection approach for MV Microgrid”, in CIRED 21st International Conference on Electricity Distribution, Frankfurt, 6–9 June, 2011.

[34] P. Mahat, Z. Chen, B. Bak-Jensen and C. L. Bak, "A Simple Adaptive Overcurrent Protection of Distribution Systems With Distributed Generation," in IEEE Transactions on Smart Grid, vol. 2, no. 3, pp. 428-437, Sept. 2011.

[35] C. A. Plet, M. Graovac, T. C. Green and R. Iravani, "Fault response of grid-connected inverter dominated networks," in IEEE PES General Meeting, pp. 1-8, Minneapolis, MN, 2010.

[36] H. Laaksonen, K. Kauhaniemi, “Fault type and location detection in islanded Microgrid with different control methods based converters”, in CIRED 19th International Conference on Electricity Distribution, pp. 1–4, 21–24 May, Vienna, 2007.

[37] T. Loix, T. Wijnhoven and G. Deconinck, "Protection of microgrids with a high penetration of inverter-coupled energy sources," in CIGRE/IEEE PES Joint Symposium Integration of Wide-Scale Renewable Resources Into the Power Delivery System, Calgary, AB, pp. 1-6, 2009.

[38] D. Klapp and H. T. Vollkommer, "Application of an Intelligent Static Switch to the Point of Common Coupling to Satisfy IEEE 1547 Compliance," in IEEE Power Engineering Society General Meeting, Tampa, FL, pp. 1-4, 2007.

[39] M. A. Zamani, T. S. Sidhu and A. Yazdani, "A Protection Strategy and Microprocessor-Based Relay for Low-Voltage Microgrids," in IEEE Transactions on Power Delivery, vol. 26, no. 3, pp. 1873-1883, July 2011.

[40] N. Hatziargyriou, “Microgrids: Architectures and Control”, John Wiley & Sons,West Sussex, UK, 2013.

[41] I. Almutairy, "A review of coordination strategies and techniques for overcoming challenges to microgrid protection," in Saudi Arabia Smart Grid (SASG), Jeddah, Saudi Arabia, pp. 1-4, 2016.

[42] H. J. Laaksonen, "Protection Principles for Future Microgrids," in IEEE Transactions on Power Electronics, vol. 25, no. 12, pp. 2910-2918, Dec. 2010.

[43] Taha Selim Ustun, Cagil Ozansoy and Aladin Zayegh, “Fault current coefficient and time delay assignment for microgrid protection system with central protection unit”, in IEEE Transactions on power systems, vol. 28, no. 2, pp. 598-606, 2013.

[44] T. S. Ustun and R. H. Khan, "Multi-terminal Hybrid Protection of Microgrids Over Wireless Communications Network," in IEEE Transactions on Smart Grid, vol. 6, no. 5, pp. 2493-2500, Sept. 2015.

[45] M. Khederzadeh, "Adaptive setting of protective relays in microgrids in grid-connected and autonomous operation," in 11th IET International Conference on Developments in Power Systems Protection (DPSP), Birmingham, UK, pp. 1-4, 2012.

[46] E. Sortomme, S. S. Venkata and J. Mitra, "Microgrid Protection Using Communication-Assisted Digital Relays," in IEEE Transactions on Power Delivery, vol. 25, no. 4, pp. 2789-2796, Oct. 2010.

[47] S. Mirsaeidi, D. M. Said, M. W. Mustafa, M. H. Habibuddin, and Kimia Ghaffari, "An analytical literature review of the available techniques for the protection of micro-grids," in Int. J. Elect. Power Energy Syst., vol. 58, pp. 300-306, Jun. 2014.

[48] D. Linden, T. B. Reddy, “Lead Acid Batteries” in Handbook of Batteries, 3rd ed. New York, NY: McGraw-Hill, ch, 23, 2002.

[49] A. Cooper and P. Moseley, “Progress in the Development of Lead-Acid Batteries for Hybrid Electric Vehicles,” in IEEE Vehicle Power and Propulsion Conference,. VPPC ’06, pp. 1–6, 2006.

[50] Michael Koller, Theodor Borsche, Andreas Ulbig, Göran Andersson, “Review of grid applications with the Zurich 1 MW battery energy storage system”, in Electric Power Systems Research, pp.128-135, 2015.

[51] Maninder Singh, Luiz A.C. Lopes, Nayeem A. Ninad, “Grid forming Battery Energy Storage System (BESS) for a highly unbalanced hybrid mini-grid”, in Electric Power Systems Research, , pp.126-133, 2015.

[52] P. Denholm, E. Ela, B. Kirby, M. Milligan, “The Role of Energy Storage with Renewable Electricity Generation”, in NREL. Golden, CO. NREL/TP-6A2-47187. Jan. 2010.

[53] C. Pillot, “Micro hybrid, HEV, P-HEV and EV market 2012 #x2013;2025 impact on the battery business,” in Electric Vehicle Symposium and Exhibition (EVS27), pp. 1–6, 2013.

[54] E. Wesoff, “Energy Storage at Grid Scale: A123 Gets Li-Ion to Market,” [Online].Available:https://www.greentechmedia.com/articles/read/Energy-Storage-at-Grid-Scale-A123-Gets-Li-Ion-to-Market.[Accessed:10-Feb-2017].

[55] G. Diaz, C. Gonzalez-Moran, J. Gomez-Aleixandre, A. Diez, “Scheduling of droop coefficients for frequency and voltage regulation in isolated microgrids”, in IEEE Trans. Power Syst., vol.25, pp.489–496, 2010.

[56] Z. Miao, L. Xu, V. R. Disfani, L. Fan, “An SOC-Based Battery Management System for Microgrids”, in IEEE Trans. on Smart Grid, vol. 5, no. 2, pp. 966–973, Mar. 2014.

[57] J.-Y. Kim, J.-H. Jeon, S.-K. Kim, C. Cho, J. H. Park, H.-M. Kim, K.-Y. Nam, “Cooperative Control Strategy of Energy Storage System and Microsources for Stabilizing the Microgrid during Islanded Operation”, in IEEE Trans. on Power Electron., vol.25, pp. 3037–3048, 2010.

[58] H. Karimi, H. Nikkhajoei, R. Iravani, “Control of an Electronically-Coupled Distributed Resource Unit Subsequent to an Islanding Event”, in IEEE Trans. on Power Delivery, vol.23, pp. 493–501, 2008.

[59] M. Doyle, J. Newman, A. S. Gozdz, C. N. Schmutz, and J.-M. Tarascon, “Comparison of Modeling Predictions with Experimental Data from Plastic Lithium Ion Cells,” in Journal of the Electrochemical Society, vol. 143, no. 6, pp. 1890–1903, Jun. 1996.

[60] H. F. Habib, A. O. Hariri, A. ElSayed and O. A. Mohammed, "Deployment of electric vehicles in an adaptive protection technique for riding through cyber attack threats in microgrids," in IEEE International Conference on Environment and Electrical Engineering and 2017 IEEE Industrial and Commercial Power Systems Europe (EEEIC / I&CPS Europe), Milan, pp. 1-6, 2017.

[61] B. Sood, M. Osterman, and M. Pecht, “Health monitoring of lithium-ion batteries,” in IEEE Symposium on Product Compliance Engineering (ISPCE), pp. 1–6, 2013.

[62] “Supercapacitor Information – Battery University.” [Online]. Available: http://batteryuniversity.com/learn/article/whats_the_role_of_the_supercapacitor. [Accessed: 10-Feb-2017].

[63] F. Béguin, E. Frąckowiak, and A. Burke, “Testing of Electrochemical Capacitors”, in Supercapacitors, Eds. Wiley-VCH Verlag GmbH & Co. KGaA, pp. 437–471, 2013.

[64] J. P. Kelley, D. A. Wetz, J. A. Reed, I. J. Cohen, G. K. Turner, W. Lee, “The impact of power quality when high power pulsed DC and continuous AC loads are simultaneously operated on a MicroGrid testbed”, in IEEE Electric Ship Tech. Symp., pp. 6–12, 2013.

[65] P. Thounthong, A. Luksanasakul, P. Koseeyaporn, and B. Davat, “Intelligent Model-Based Control of a Standalone Photovoltaic/Fuel Cell Power Plant With Supercapacitor Energy Storage,” in IEEE Transactions on Sustainable Energy, vol. 4, no. 1, pp. 240–249, Jan. 2013.

[66] B. Vural and C. S. Edrington, “Ultra-capacitor based pulse power management in electrical ships”, in IEEE Transportation Electrification Conference and Expo (ITEC), 2012.

[67] J. McGroarty, J. Schmeller, R. Hockney and M. Polimeno, "Flywheel energy storage systems for electric start and an all-electric ship," in IEEE Electric Ship Technologies Symposium, PP. 400-406, 2005.

[68] L. Zhang, L. Li, W. Cui, and S. Li, “Study on improvement of micro-grid’s power quality based on APF and FESS,” in IEEE Innovative Smart Grid Technologies - Asia (ISGT Asia), pp. 1–6, 2012.

[69] C. Xie and C. Zhang, “Research on the Ship Electric Propulsion System Network Power Quality with Flywheel Energy Storage,” in Power and Energy Engineering Conference, Asia-Pacific, pp. 1–3, 2010.

[70] G. O. Suvire and P. E. Mercado, “Improvement of power quality in wind energy applications using a DSTATCOM coupled with a Flywheel Energy Storage System,” in Power Electronics Conference. COBEP ’09. Brazilian, pp. 58–64, 2009.

[71] S. Samineni, B. K. Johnson, H. L. Hess, and J. D. Law, “Modeling and analysis of a flywheel energy storage system for Voltage sag correction,” in IEEE Trans. Ind. Appl., vol. 42, no. 1, pp. 42–52, Jan. 2006.

[72] M. Subkhan and M. Komori, “New Concept for Flywheel Energy Storage System Using SMB and PMB,” in IEEE Trans. Appl. Supercond., vol. 21, no. 3, pp. 1485–1488, Jun. 2011.

[73] I. Lahbib, A. Lahyani, A. Sari and P. Venet, "Performance analysis of a lead-acid battery/supercapacitors hybrid and a battery stand-alone under pulsed loads," in First International Conference on Green Energy ICGE, Sfax, pp. 273-278, 2014.

[74] M. Ibrahim, S. Jemei, G. Wimmer, and D. Hissel, “Nonlinear autoregressive neural network in an energy management strategy for battery/ultra-capacitor hybrid electrical vehicles,” in Electric Power Systems Research, vol. 136, pp. 262–269, Jul. 2016

[75] P. J. Kollmeyer, L. W. Juang, and T. M. Jahns, “Loss optimization and ultracapacitor pack sizing for vehicles with battery/ultracapacitor hybrid energy storage,” in IEEE Transportation Electrification Conference and Expo (ITEC), pp. 1–8, 2014.

[76] B. M. Huhman, J. M. Neri, D. A. Wetz, “Design of a battery intermediate storage system for rep-rated pulsed power loads”, in IEEE Electric Ship Technologies Symp. (ESTS), 2013.

[77] G. L. Kusic, J. M. Heinzel, D. J. Hoffman, “Monitoring pulsed power on ship electrical systems”, in IEEE Electric Ship Technologies Symposium (ESTS), pp. 13–20, 2013.

[78] I. Gyuk et al., “Grid energy storage,” U.S. Dept. Energy, Tech. Rep., 2013 [Online]. Available:http://energy.gov/sites/prod/files/2013/12/f5/Grid%20Energy%20Storage%20December%202013.pdf.

[79] F. Zhang, M. Tokombayev, Y. Song and G. Gross, "Effective flywheel energy storage (FES) offer strategies for frequency regulation service provision," in Power Systems Computation Conference, Wroclaw, pp. 1-7. 2014.

[80] H. Vasconcelos, C. Moreira, A. Madureira, J. P. Lopes and V. Miranda, "Advanced Control Solutions for Operating Isolated Power Systems: Examining the Portuguese islands.," in IEEE Electrification Magazine, vol. 3, no. 1, pp. 25-35, March 2015.

[81] I. Gyuk et al., EPRI-DOE Handbook of Energy Storage for Transmission and Distribution Applications, EPRI, 2003 [Online]. Available: http://www.sandia.gov/ess/publications/ESHB%201001834% 20reduced%20size.pdf

[82] M. H. Ali, B. Wu and R. A. Dougal, "An Overview of SMES Applications in Power and Energy Systems," in IEEE Transactions on Sustainable Energy, vol. 1, no. 1, pp. 38-47, April 2010.

[83] A. Oudalov, D. Chartouni and C. Ohler, "Optimizing a Battery Energy Storage System for Primary Frequency Control," in IEEE Transactions on Power Systems, vol. 22, no. 3, pp. 1259-1266, Aug. 2007.

[84] C. R. Vergara, "Parametric interface for Battery Energy Storage Systems providing ancillary services," in 3rd IEEE PES Innovative Smart Grid Technologies Europe (ISGT Europe), Berlin , pp. 1-7, 2012.

[85] P. F. Frack, M. Martinez, M. G. Molina and P. E. Mercado, "Emulation of Synchronous Generator for Frequency Control of Smart Microgrids," in IEEE Latin America Transactions, vol. 11, no. 1, pp. 486-491, Feb. 2013.

[86] Y. Cho, J. W. Shim, S. J. Kim, S. W. Min and K. Hur, "Enhanced frequency regulation service using Hybrid Energy Storage System against increasing power-load variability," in IEEE Power & Energy Society General Meeting, Vancouver, BC, pp. 1-5, 2013.

[87] L. Zhang and Y. Liu, "Bulk power system low frequency oscillation suppression by FACTS/ESS," in IEEE PES Power Systems Conference and Exposition, pp. 219-226 vol.1, 2004.

[88] M. Heidari-Kapourchali and V. Aravinthan, "Loss allocation control in power distribution system reconfiguration in the presence of distributed generators," in IEEE PES General Meeting Conference & Exposition, National Harbor, MD, pp. 1-5, 2014.

[89] G. Cimuca, S. Breban, M. M. Radulescu, C. Saudemont and B. Robyns, "Design and Control Strategies of an Induction-Machine-Based Flywheel Energy Storage System Associated to a Variable-Speed Wind Generator," in IEEE Transactions on Energy Conversion, vol. 25, no. 2, pp. 526-534, June 2010.

[90] G. Graditi, M. G. Ippolito, E. Telaretti and G. Zizzo, "An Innovative Conversion Device to the Grid Interface of Combined RES-Based Generators and Electric Storage Systems," in IEEE Transactions on Industrial Electronics, vol. 62, no. 4, pp. 2540-2550, April 2015.

[91] M. Yilmaz and P. T. Krein, "Review of the Impact of Vehicle-to-Grid Technologies on Distribution Systems and Utility Interfaces," in IEEE Transactions on Power Electronics, vol. 28, no. 12, pp. 5673-5689, Dec. 2013.

[92] K. Christakou, D. C. Tomozei, M. Bahramipanah, J. Y. Le Boudec and M. Paolone, "Primary Voltage Control in Active Distribution Networks via Broadcast Signals: The Case of Distributed Storage," in IEEE Power and Energy Society General Meeting (PESGM), Boston, MA, pp. 1-1, 2016.

[93] M. Khaterchi, J. Belhadj and M. Elleuch, "DPC for three-phase inverter to improve the integration of wind turbine associated to Flywheel Energy Storage System into the grid," in 6th International Multi-Conference on Systems, Signals and Devices, Djerba, pp. 1-6, 2009.

[94] J. Rocabert, A. Luna, F. Blaabjerg and P. Rodríguez, "Control of Power Converters in AC Microgrids," in IEEE Transactions on Power Electronics, vol. 27, no. 11, pp. 4734-4749, Nov. 2012.

[95] G. Graditi, M. G. Ippolito, E. Telaretti and G. Zizzo, "An Innovative Conversion Device to the Grid Interface of Combined RES-Based Generators and Electric Storage Systems," in IEEE Transactions on Industrial Electronics, vol. 62, no. 4, pp. 2540-2550, April 2015.

[96] W. T. Liu, Y. K. Wu, C. Y. Lee and C. R. Chen, "Effect of Low-Voltage-Ride-Through Technologies on the First Taiwan Offshore Wind Farm Planning," in IEEE Transactions on Sustainable Energy, vol. 2, no. 1, pp. 78-86, Jan. 2011.

[97] C. Abbey and G. Joos, "Supercapacitor Energy Storage for Wind Energy Applications," in IEEE Transactions on Industry Applications, vol. 43, no. 3, pp. 769-776, May-june 2007.

[98] S. I. Gkavanoudis and C. S. Demoulias, "A new Fault Ride-Through control method for full-converter wind turbines employing Supercapacitor Energy Storage System," in 47th International Universities Power Engineering Conference (UPEC), London, pp. 1-6, 2012.

[99] I. A. Gowaid, A. A. Elserougi, A. S. Abdel-Khalik, A. M. Massoud and S. Ahmed, "A series flywheel architecture for power levelling and mitigation of DC voltage transients in multi-terminal HVDC grids," in IET Generation, Transmission & Distribution, vol. 8, no. 12, pp. 1951-1959, Dec., 2014.

[100] R. Arghandeh, M. Pipattanasomporn and S. Rahman, "Flywheel Energy Storage Systems for Ride-through Applications in a Facility Microgrid," in IEEE Transactions on Smart Grid, vol. 3, no. 4, pp. 1955-1962, Dec. 2012.

[101] M. I. Daoud, A. Massoud, S. Ahmed, A. S. Abdel-Khalik and A. Elserougi, "Ride-through capability enhancement of VSC-HVDC based wind farms using low speed flywheel energy storage system," in IEEE Applied Power Electronics Conference and Exposition - APEC, Fort Worth, TX, pp. 2706-2712, 2014.

[102] N. S. Gayathri and N. Senroy, "Wind turbine with flywheel for improved power smoothening and LVRT," in IEEE Power & Energy Society General Meeting, Vancouver, BC, pp. 1-5, 2013.

[103] M. Ahsanul Alam, A. H. M. A. Rahim and M. A. Abido, "Supercapacitor based energy storage system for effective fault ride through of wind generation system," in IEEE International Symposium on Industrial Electronics, Bari, pp. 2481-2486, 2010.

[104] A. Lahyani, P. Venet, A. Guermazi and A. Troudi, "Battery/Supercapacitors Combination in Uninterruptible Power Supply (UPS)," in IEEE Transactions on Power Electronics, vol. 28, no. 4, pp. 1509-1522, April 2013.

[105] J. Jia, Y. Wang, S. Li and G. Wang, "A dynamic discharge structure for ultracapacitor application in the fuel cell UPS," in 10th International Conference on Control, Automation, Robotics and Vision, Hanoi, pp. 2102-2107, 2008.

[106] B. Roberts and J. McDowall, "Commercial successes in power storage," in IEEE Power and Energy Magazine, vol. 3, no. 2, pp. 24-30, March-April 2005.

[107] P. J. Binduhewa, "Uninterruptible power supply for short-time power back-up using ultracapacitors," in 6th International Conference on Industrial and Information Systems, Kandy, pp. 551-556, 2011.

[108] J. M. Crider and S. D. Sudhoff, "Reducing Impact of Pulsed Power Loads on Microgrid Power Systems," in IEEE Transactions on Smart Grid, vol. 1, no. 3, pp. 270-277, Dec. 2010.

[109] M. Falahi, K. L. Butler-Purry and M. Ehsani, "Reactive Power Coordination of Shipboard Power Systems in Presence of Pulsed Loads," in IEEE Transactions on Power Systems, vol. 28, no. 4, pp. 3675-3682, Nov. 2013.

[110] Lijun Gao, R. A. Dougal and Shengyi Liu, "Power enhancement of an actively controlled battery/ultracapacitor hybrid," in IEEE Transactions on Power Electronics, vol. 20, no. 1, pp. 236-243, Jan. 2005.

[111] Hany F. Habib, M. E. Hariri, A. Elsayed and O. Mohammed, "Utilization of supercapacitors in adaptive protection applications for resiliency against communication failures: A size and cost optimization case study," in IEEE Industry Applications Society Annual Meeting, Cincinnati, OH, USA, pp. 1-8, 2017.

[112] N. Jenkins N, “Embedded Generation”, in Power Engineering Journal, vol.9, pp.145-150, 1995.

[113] A. Sachit Gopalan, Victor Sreeram and H.C. Herbert Iu, “A review of coordination strategies and protection schemes for microgrids”, in Renew Sustain Energy Rev., vol.32, pp. 222–228, 2014.

[114] A. Oudalov and A. Fidgatti, “Adaptive network protection in microgrids”, in International Journal of Distributed Energy Resources, vol.5, no.3, pp201-226, 2009.

[115] N. El Halabi a, M. García-Gracia a , J. Borroy a , J.L. Villa, “Current phase comparison pilot scheme for distributed generation networks protection”, in Applied Energy, vol. 88 pp. 4563-4569, 2011.

[116] Ustun, T.S.; Ozansoy, C.; Zayegh, A., "Modeling of a Centralized Microgrid Protection System and Distributed Energy Resources According to IEC 61850-7-420," IEEE Transactions on Power Systems, vol.27, no.3, pp.1560,1567, Aug. 2012.

[117] Najy, W.K.A; Zeineldin, H.H.; Woon, W.L., "Optimal Protection Coordination for Microgrids With Grid Connected and Islanded Capability,", in IEEE Trans, Industrial Electronics , vol.60, no.4, pp.1668,1677, April 2013

[118] Laaksonen, H.; Ishchenko, D.; Oudalov, A, "Adaptive Protection and Microgrid Control Design for Hailuoto Island,", in IEEE Trans. On Smart Grid , vol.5, no.3, pp.1486,1493, May 2014

[119] Y, Han, X Hu, D Zang, " Study of Adaptive Fault Current Algorithm for Migrogrid Dominated by Inverter based Distributed Generators," in 2nd IEEE International Symposium on Power Electronics for Distributed Generation Systems, PEDG, pp. 852-854, 2010.

[120] R.M. Tumilty, M. Brucolit, G.M. Burt and T.C. Greent , " Approaches to Network Protection for Inverter Dominated Electrical Distribution Systems', in the 3rd IET International conference on Power Electronics, Machines and Drives, pp. 622-626, 2006.

[121] H. F. Habib, C. R. Lashway and O. A. Mohammed, "A Review of Communication Failure Impacts on Adaptive Microgrid Protection Schemes and the Use of Energy Storage as a Contingency," in IEEE Transactions on Industry Applications, vol. 54, no. 2, pp. 1194-1207, March-April 2018.

[122] Aushiq Ali Memon, , Kimmo Kauhaniemi, "A critical review of AC Microgrid protection issues and available solutions", in Electric power systems Research, Volume 129, December 2015, Pages 23–31.

[123] Understanding Denial-of-Service Attacks | US-CERT." [Online]. Available: https://www.us-cert.gov/ncas/tips/ST04-015. [Accessed: 08-Mar-2017].

[124] K. Choi, X. Chen, S. Li, M. Kim, K. Chae, JC. Na, "Intrusion Detection of NSM Based DoS Attacks Using Data Mining in Smart Grid," in Energies, pp. 4091-4109, 19 Oct. 2012.

[125] U.-K. Premaratne, J. Samarabandu, T.-S. Sidhu, R. Beresh, and J.-C. Tan, "An Intrusion Detection System for IEC61850 Automated Substations," in IEEE Trans. Power Del., vol. 25, no. 4, pp. 2376-2383, Oct. 2010.

[126] Microsoft TechNet Library, "Common Types of Network Attacks". Accessed on 20 September 2014, [Online]. Available: http://technet.microsoft.com/en-us/library/cc959354.aspx.

[127] Brute-Force Password Cracker." [Online]. Available: http://www.oxid.it/ca_um/topics/brute-force_password_cracker.htm. [Accessed: 08-Mar-2017].

[128] M. T. A. Rashid, S. Yussof, Y. Yusoff and R. Ismail, "A review of security attacks on IEC61850 substation automation system network," in Proceedings of the 6th International Conference on Information Technology and Multimedia, Putrajaya, pp. 5-10, 2014.

[129] N. Kush, E. Ahmed, M. Branagan, E. Foo, “Poisoned GOOSE: Exploiting the GOOSE Protocol,” in Proceedings of the Twelfth Australasian Information Security Conference (AISC). Vol. 149, pp. 17-22, 2014.

[130] S. Malladi, J. Alves-Foss, and R. B. Heckendorn, “On Preventing Replay Attacks on Security Protocols,” [Online]. Available: https://oai.dtic.mil. [Accessed: 08-Mar-2017].

[131] A. Mehrizi-Sani and R. Iravani, “Potential-function based control of a microgrid in islanded and grid-connected modes”, IEEE Trans. Power Syst., vol. 25, no. 4, pp. 1883–1891, Nov. 2010.

[132] M. H. Cintuglu; T. Youssef; O. A. Mohammed, "Development and Application of a Real-Time Testbed for Multiagent System Interoperability: A Case Study on Hierarchical Microgrid Control," in IEEE Transactions on Smart Grid , vol.PP, no.99, pp.1-1, 2016.

[133] A. Cuzzocrea, C. Kittl, D. E. Simos, E. Weippl, and L. Xu, “Availability, Reliability, and Security in Informaiton Systems and HCI”: IFIP WG 8.4, 8.9, TC 5 Internaitonal Cross-Domain Conference, CD-ARES 2013, Rgensbrg, Germany, September 2-6, 2013, Proceedings.

[134] Tarek A. Youssef, Mohamad El Hariri, Nicole Bugay and O. A. Mohammed, “IEC 61850: Technology Standards and Cyber-Security Threats,” in the 16th IEEE International Conference on Environment and Electrical Engineering (EEEIC), Florence, Italy, 7-10 June, 2016.

[135] Mohamad El Hariri, Tarek A. Youssef, Abla Hariri and O. A. Mohammed, “Microgrids on Wheels: Not to Leave Security Behind,” in IEEE Electrification e-Newsletter, June 2016.

[136] M. Ortuzar, J. Moreno, and J. Dixon, “Ultracapacitor-Based Auxiliary Energy System for an Electric Vehicle: Implementation and Evaluation,” in IEEE Trans on Industrial Electronics, vol. 54, no. 4, pp. 2147– 2156, Aug. 2007.

[137] D. Shin, Y. Kim, J. Seo, N. Chang, Y. Wang, M. Pedram, , "Batterysupercapacitor hybrid system for high-rate pulsed load applications," in Design, Automation & Test in Europe Conference & Exhibition (DATE), 2011 , vol., no., pp.1,4, 14-18 March 2011.

[138] P. Bajpai and V. Dash, “Hybrid renewable energy systems for power generation in stand-alone applications: A review,” in Renewable and Sustainable Energy Reviews, vol. 16, no. 5, pp. 2926–2939, Jun. 2012.

[139] M. Farhadi and O. Mohammed, "Energy Storage Technologies for High-Power Applications," in IEEE Transactions on Industry Applications, vol. 52, no. 3, pp. 1953-1961, May-June 2016.

[140] A. Mohamed, V. Salehi, O. Mohammed, "Real-Time Energy Management Algorithm for Mitigation of Pulse Loads in Hybrid Microgrids,", IEEE Transactions on Smart Grid, vol.3, no.4, pp.1911,1922, Dec. 2012.

[141] M. Farhadi and O. A. Mohammed, "Performance Enhancement of Actively Controlled Hybrid DC Microgrid Incorporating Pulsed Load," in IEEE Transactions on Industry Applications, vol. 51, no. 5, pp. 3570-3578, Sept.-Oct. 2015.

[142] R.A.Dougal, Shengyi Liu, R.E. White, "Power and life extension of battery-ultracapacitor hybrids,", IEEE Transactions on Components and Packaging Technologies, vol.25, no.1, pp.120,131, Mar 2002.

[143] T. Ma, M. H. Cintuglu and O. Mohammed, "Control of hybrid AC/DC microgrid involving energy storage, renewable energy and pulsed loads," in Industry Applications Society Annual Meeting, 2015 IEEE, Addison, TX, 2015, pp. 1-8.

[144] T. A. Youssef and O. Mohammed, "Adaptive SRF-PLL with reconfigurable controller for Microgrid in grid-connected and stand-alone modes," in IEEE Power & Energy Society General Meeting, Vancouver, BC, 2013, pp. 1-5.

[145] Z. Jin, G. Sulligoi, R. Cuzner, L. Meng, J. C. Vasquez and J. M. Guerrero, "Next-Generation Shipboard DC Power System: Introduction Smart Grid and dc Microgrid Technologies into Maritime Electrical Netowrks," in IEEE Electrification Magazine, vol. 4, no. 2, pp. 45-57, June 2016.

[146] A. Mohamed, V. Salehi and O. Mohammed, "Real-Time Energy Management Algorithm for Mitigation of Pulse Loads in Hybrid Microgrids," in IEEE Transactions on Smart Grid, vol. 3, no. 4, pp. 1911-1922, Dec. 2012.

[147] Mustafa Farhadi, and Osama A. Mohammed, “Adaptive Energy Mangement in Redundant Hybrid DC Microgrid for Pulse Load Mitigation,” in IEEE Transactions on Smart Grid, Vol. 6, no.1, pp.54-62, Jan. 2015.

[148] Maxwell, 16V small cell module, Model: BMOD0058 E016 B02 (16.2V-58 F), San Diego, CA. Online at: http://www.maxwell.com/images/documents/datasheet_16v_small_cell_module.pdf.

[149] M. Mahmoudian Esfahani, M.H. Cintuglu, O.A. Mohammed, “Optimal real-time congestion management in power markets based on particle swarm optimization”, IEEE Power and Energy Society General Meeting 2017, DOI: 10.1109/PESGM.2017.8274117.

[150] M. Shojaie and H. Mokhtari, "A method for determination of harmonics responsibilities at the point of common coupling using data correlation analysis," in IET Generation, Transmission & Distribution, vol. 8, no. 1, pp. 142-150, Jan. 2014.

[151] H Moradisizkoohi, J Milimonfared, M Taheri, S Salehi, “Duty-cycle-controlled resonant dual-half-bridge converter with multifunctional capacitors for distributed generation applications”, in IET Power Electronics 9 (9), 1873-1884.

[152] H. Moradi Sizkoohi, J. Milimonfared, M. Taheri and S. Salehi, "High step-up soft-switched dual-boost coupled-inductor-based converter integrating multipurpose coupled inductors

with capacitor-diode stages," in IET Power Electronics, vol. 8, no. 9, pp. 1786-1797, 9 2015.

[153] M. Saleh, Y. Esa and A. Mohamed, "Communication Based Control for DC Microgrids," in IEEE Transactions on Smart Grid, vol. PP, no. 99, pp. 1-1.

[154] “Supercapacitor Information – Battery University.” [Online]. Available: http://batteryuniversity.com/learn/article/whats_the_role_of_the_supercapacitor. [Accessed: 10-Feb-2017].

[155] Ahmadi, A., Masouleh, M. S., Janghorbani, M., Manjili, N. Y. G., Sharaf, A. M., & Nezhad, A. E. (2015). Short term multi-objective hydrothermal scheduling. Electric Power Systems Research, 121, 357-367.

[156] T. Ghanbari and E. Farjah, "Unidirectional Fault Current Limiter: An Efficient Interface Between the Microgrid and Main Network," in IEEE Transactions on Power Systems, vol. 28, no. 2, pp. 1591-1598, May 2013.

[157] N. Tummasit, S. Premrudeepreechacharn and N. Tantichayakorn, "Adaptive overcurrent protection considering critical clearing time for a microgrid system," 2015 IEEE Innovative Smart Grid Technologies - Asia (ISGT ASIA), Bangkok, 2015, pp. 1-6.

[158] André N. Albagli, Djalma M. Falcão, José F. de Rezende, Smart grid framework co-simulation using HLA architecture, Electric Power Systems Research, Volume 130, January 2016, Pages 22-33, ISSN 0378-7796.

[159] G. Celli, P. A. Pegoraro, F. Pilo, G. Pisano and S. Sulis, "DMS Cyber-Physical Simulation for Assessing the Impact of State Estimation and Communication Media in Smart Grid Operation," in IEEE Transactions on Power Systems, vol. 29, no. 5, pp. 2436-2446, Sept. 2014.

[160] E. Sharma, C. Chiculita and Y. Besanger, "Co-simulation of a low-voltage utility grid controlled over IEC 61850 protocol," 2015 5th International Conference on Electric Utility Deregulation and Restructuring and Power Technologies (DRPT), Changsha, 2015, pp. 2365-2372.

[161] Object Management Group. Data Distribution Service for Real-time Systems, Version 1.2, OMG, Needham, MA, USA, 2007.

[162] Secure. High-Reliability and High-Performance Scalable Infrastructure. Accessed on Jan. 15, 2016. [Online]. Available: http://www.rti.com/industries/energy.html

[163] Open Field Message Bus (OpenFMB). Accessed on Jan. 15, 2016. [Online]. Available: http://members.sgip.org/apps/ group_public/download.php/6353/2015-03-05%20OFMB%20Kickoff% 20Presentation%20DRAFT.pptx.

[164] G. Pardo-Castellote, “OMG data-distribution service: Architectural overview,” in Proc. 23rd Int. Conf. Distrib. Comput. Syst. Workshops, Providence, RI, USA, 2003, pp. 200–206.

[165] S. H. Horowitz and A. G. Phadke, “Third zone revisited,” in IEEE Transactions on Power Delivery., vol. 21, no. 1, pp. 23–29, Jan. 2006.

[166] L. C. Zhou, B. H. Zhang, L. Y. Cheng, C. G. Wang, A. Klimek, and Z. Q. Bo, “Centralized substation backup protection with high reliability,” in 10th IET International Conference on Developments in Power System Protection, pp. 1–6, 2010.

[167] X. R. Wang, K. M. Hopkinson, J. S. Thorp, R. Giovanini, and K. Birman, “Developing an agent-based backup protection system for transmission networks,” in Power Systems and Communications Infrastructures for the Future, Beijing, China, Sep. 23–27, 2002.

[168] M. Garcia-Gracia, N. E. Halabi, S. Borroy and L. G. De Urtasun, "Phase jump correction factor applied to the differential equation algorithm by an adaptive scheme," in IET Generation, Transmission & Distribution, vol. 5, no. 2, pp. 266-275, February 2011.

[169] K. Abdel-Latif, M. Eissa, A. Ali, O. Malik, "Laboratory Investigation of Using Wi-Fi Protocol for Transmission Line Differential Protection", in IEEE Transactions on Power Delivery, vol. 24, no. 3, pp. 1087-1094, 2009.

[170] Rezaei N, Haghifam M. “Protection scheme for a distribution system with distributed generation using neural networks”, in International journal of Electrical Power & Energy Systems ,30:235–41, 2008.

[171] Trupti P. Hinge, Sanjay S. Dambhare, “Secure Phase Comparison Schemes for Transmission-Line Protection Using Synchrophasors”, in IEEE Transactions on Power Delivery, vol. 30, no. 4, pp. 2045-2054, 2015.

[172] B. Kasztenny and I. Voloh, “Rebirth of the phase comparison line protection principle”, in 59th Annual Conference for Protective Relay Engineers, College Station, TX, USA, 2006.

[173] C. M. Colson, M. H. Nehrir, “Distributed multi-agent microgrids: a decentralized approach to resilient power system self-healing”, in 4th International Symposium on Resilient Control Systems (ISRCS), pp. 83-88, 2011.

[174] P. Parikh; I. Voloh; M. Mahony, “Fault location, isolation, and service restoration (FLISR) technique using IEC 61850 GOOSE”, in IEEE Conference on Power and Energy Society General Meeting (PES), pp. 1-6, 2013.

[175] Available on http://powerit.utk.edu/fnet.html.

[176] M. Yalla, M. Adamiak, A. Apostolov, J. Beatty, S. Borlase, J. Bright, J. Burger, S. Dickson, G. Gresco, W. Hartman, J. Hohn, D. Holstein, A. Kazemi, G. Michael, C. Sufana, J. Tengdin, M. Thompson, and E. Udren, “Application of a peer-to-peer communication for

protective relaying," in IEEE Transactions Power Delivery, vol. 17, no. 2, pp. 446–451, Apr. 2002.

[177] Ali Hooshyar, Ehab F. El-Saadany, Majid Sanaye-Pasand, "Fault Type Classification in Microgrids Including Photovoltaic DGs", in IEEE Transactions on Smart Grid, vol. 99, pp. 1-12, 2015.

[178] J. Solanki, N. Schulz, "A Multi-Agent Solution to Distribution Systems Restoration", in IEEE Transactions on Power System, vol. 22, no. 3, pp. 1026-1034, 2007.

[179] C. M. Colson; M. H. Nehrir; R. W. Gunderson, "Distributed multi-agent microgrids: a decentralized approach to resilient power sys-tem self-healing", in 4th International Symposium on Resilient Control Systems (ISRCS), pp. 83-88, 2011.

[180] T. Nagata, S. Hatakeyama, M. Yasouka and H. Sasaki, "An efficient method for power distribution system restoration based on mathematical programming and operation strategy," in Power International Conference on Power System Technology, Perth, WA, pp. 1545-1550 vol.3, 2000.

[181] Vadivoo, N. S., Slochanal, S. M. R., "Distribution System Restoration Using Genetic Algorithm with Distributed Generation," in CCSE Modern Applied Science, Vol. 3, no. 4, pp. 98–109, April, 2009.

[182] Huo, Limin, Yin, J., and Yu, Y., "Distribution Network Reconfiguration Based on Load Forecasting," in International Conference on Intelligent Computation Technology and Automation (ICICTA), pp. 1039–1043, 2008.

[183] E. M. Carreno, N. Moreira and R. Romero, "Distribution network reconfiguration using an efficient evolutionary algorithm," in IEEE Power Engineering Society General Meeting, pp. 1-6, 2007.

[184] IEEE Standard for Synchrophasor Measurements for Power Systems, IEEE Standard C37.118.1, 2011

[185] R. Belkacemi, A. Feliachi, M. A. Choudhry and J. E. Saymansky, "Multi-Agent systems hardware development and deployment for smart grid control applications," in IEEE Power and Energy Society General Meeting, San Diego, CA, pp. 1-8, 2011.

[186] Dimeas, A.L.; Hatziargyriou, N.D., "Operation of a Multiagent System for Microgrid Control," in IEEE Transactions on Power Systems , vol.20, no.3, pp.1447-1455, Aug. 2005.

[187] Mahnke, Wolfgang, Stefan-Helmut Leitner, and Matthias Damm. "OPC Unified architecture", Springer, 2009.

[188] V. Salehi, A. Mohamed, A. Mazloomzadeh, and O.A. Mohammed, "Laboratory-Based Smart Power System, Part II: Control, Monitoring, and Protection," in IEEE Transactions on Smart Grid, vol.3, no.3, pp.1405- 1417, Sept. 2012.

[189] H. Rahimi-Eichi, U. Ojha, F. Baronti, M. Chow, “Battery ManagementSystem: An Overview of Its Application in the Smart Grid and Electric Vehicles”, Industrial Electronics Magazine, IEEE, vol.7, no.2, pp.4,16, June 2013.

[190] IEEE Standard Inverse-Time Characteristic Equations for Over-current Relays, IEEE Std C37.112-1996, 1996.

[191] B. Hussain et al., “Integration of distributed generation into the grid: Protection challenges and solutions,” in Proc. 10th IET Int. Conf. Developments in Power System Protection (DPSP 2010), pp. 1–5.

[192] V. I. Herrera, A. Saez-de-Ibarra, A. Milo, H. Gaztañaga and H. Camblong, "Optimal energy management of a hybrid electric bus with a battery-supercapacitor storage system using genetic algorithm," 2015 International Conference on Electrical Systems for Aircraft, Railway, Ship Propulsion and Road Vehicles (ESARS), Aachen, 2015, pp. 1-6.

[193] IEC 61850 Stack LibIEC61850 (Research License). Accessed on Jan. 15, 2018. [Online]. Available: http:/libiec61850.com.

[194] Simulink Response Optimization User’s Guide. Natick, MA, USA: The MathWorks Inc., 2004.

[195] P. Elbert, C. Onder, H. J. Gisler, “Capacitors vs. Batteries in a Serial Hybrid Electric Bus”, in Proc. 6th IFAC, Munich, Germany, July, 2010.

[196] L. Xu, F. Yang, M. Hu, J. Li, M. Ouyang, “Comparison of energy management strategies for a range extended electric city bus”, in Proc. 31st Chinese Control Conference, pp. 6866-71, Hefei, China, July, 2012.

[197] Zhu Yongli, Wang Dewen, Wang Yan and Zhao Wenqing, "Study on interoperable exchange of IEC 61850 data model," 2009 4th IEEE Conference on Industrial Electronics and Applications, Xi'an, 2009, pp. 2724-2728.

[198] J. Hoyos, M. Dehus, T.X. Brown, Exploiting the goose protocol: a practical attack on cyber-infrastructure, Globecom Workshops (GC Wkshps), IEEE (2012) 1508–1513.

[199] W. Oliveira and Y. Lopes, "Teleprotection over SONET based on IEC 61850," 2018 Simposio Brasileiro de Sistemas Eletricos (SBSE), Niteroi, 2018, pp. 1-6.

[200] R. E. Mackiewicz, “Overview of IEC 61850 and benefits,” in Proc. Power Syst. Conf. Expo. (PSCE), Atlanta, GA, USA, 2006, pp. 623–630.

VITA

HANY FAWZY HABIB

1985	Born, Cairo, Egypt
2002-2007	B.S., Electrical Engineering Helwan University, Cairo, Egypt
2009-2014	M.S., Electrical Engineering Helwan University, Cairo, Egypt
2016 -2019	Doctoral Candidate, Electrical Engineering Florida International University, Miami, Florida
2019	Award, Dissertation Year Fellowship Florida International University, Miami, Florida

SELECTED PUBLICATIONS AND PRESENTATIONS

[P-1] Hany Fawzy Habib, Tarek Youssef and O. A. Mohammed, "Methods and Techniques for Protection of Microgrid Energy Management System with Distributed Storage," US Patent number US 10269509 B1.

[P-2] M. E. Hariri, Eric Harmon, Hany F. Habib, T. Youssef, O.A. Mohammed, “Content-aware spoofed sensor measurement data detection in microgrids,” (US 10/362,056), United States Patent and Trademark Office (USPTO).

[J-1] H. F. Habib, T. Yossef, and O. Mohammed, “A multi-agent based technique for fault location, isolation, and service restoration,” IEEE Trans. Ind. Appl., vol. 53, no. 3, pp. 1841–1851, May/Jun. 2017.

[J-2] H. F. Habib, A. A. S. Mohamed, M. El Hariri, and O. A. Mohammed, “Utilizing supercapacitors for resiliency enhancements and adaptive microgrid protection against communication failures,” Elect. Power Syst. Res., vol. 145, pp. 223–233, Apr. 2017.

[J-3] H. F. Habib, C. R. Lashway and O. A. Mohammed, "A Review of Communication Failure Impacts on Adaptive Microgrid Protection Schemes and the Use of Energy Storage as a Contingency," in IEEE Transactions on Industry Applications, vol. 45, no. 2, pp. 1194-1207, 2018.

[J-4] H. F. Habib, M. E. Hariri, A. Elsayed and O. A. Mohammed, "Utilization of Supercapacitors in Protection Schemes for Resiliency Against Communication Outages: A Case Study on Size and Cost Optimization," in IEEE Transactions on Industry Applications, vol. 54, no. 4, pp. 3153-3164, July-Aug. 2018.

[J-5] H. F. Habib, M. M. Esfahani and O. A. Mohammed, "Investigation of Protection Strategy for Microgrid System Using Lithium-Ion Battery During Islanding," in IEEE Transactions on Industry Applications, vol. 55, no. 4, pp. 3411-3420, July-Aug. 2019.

[J-6] M El Hariri, E Harmon, T Youssef, M Saleh, H Habib, O Mohammed, “The IEC 61850 Sampled Measured Values Protocol: Analysis, Threat Identification, and Feasibility of Using NN Forecasters to Detect of Spoofed Packets”, Energies 12 (19), 3731, 2019.

[C-1] H. F. Habib, M. E. Hariri, A. Elsayed and O. Mohammed, "Utilization of supercapacitors in adaptive protection applications for resiliency against communication failures: A size and cost optimization case study," 2017 IEEE Industry Applications Society Annual Meeting, Cincinnati, OH, 2017, pp. 1-8.

[C-2] M. E. Hariri, T. A. Youssef, H. F. Habib and O. Mohammed, "Online false data detection and lost packet forecasting system using time series neural networks for IEC 61850 sampled measured values," 2017 IEEE Power & Energy Society Innovative Smart Grid Technologies Conference (ISGT), Washington, DC, 2017, pp. 1-5.

[C-3] H. F. Habib and O. Mohammed, "Decentralized Multi-Agent System for Protection and the Power Restoration Process in Microgrids," 2017 Ninth Annual IEEE Green Technologies Conference (GreenTech), Denver, CO, 2017, pp. 358-364.

[C-4] H. F. Habib, T. Youssef, M. H. Cintuglu and O. Mohammed, "A multi-agent based technique for fault location, isolation and service restoration," 2016 IEEE Industry Applications Society Annual Meeting, Portland, OR, 2016, pp. 1-8.

[C-5] M. E. Hariri, E. Harmon, H. F. Habib, T. Youssef and O. A. Mohammed, "A targeted attack for enhancing resiliency of intelligent intrusion detection modules in energy cyber physical systems," 2017 19th International Conference on Intelligent System Application to Power Systems (ISAP), San Antonio, TX, 2017, pp. 1-6..

[C-6] M. E. Hariri, T. Youssef, H. F. Habib and O. Mohammed, "A Network-in-the-Loop Framework to Analyze Cyber and Physical Information Flow in Smart Grids," 2018 IEEE Innovative Smart Grid Technologies - Asia (ISGT Asia), Singapore, Singapore, 2018, pp. 646-651.

[C-7] H. F. Habib, M. M. Esfahani and O. Mohammed, "Development of Protection Scheme for Active Distribution Systems with Penetration of Distributed Generation," SoutheastCon 2018, St. Petersburg, FL, USA, 2018, pp. 1-7.

[C-8] H. F. Habib and O. Mohammed, "A Multiagent System for Simple Overcurrent Protection of Microgrids with Distributed Generation," 2018 IEEE Industry Applications Society Annual Meeting (IAS), Portland, OR, 2018, pp. 1-8.